STUDIES ON THE RADICAL ENZYMES GLUTAMATE MUTASE AND VIPERIN

by

Gabriel David Román-Meléndez

A dissertation submitted in partial fulfillment
of the requirements for the degree of
Doctor of Philosophy
(Chemistry)
in The University of Michigan
2015

Doctoral Committee:

Professor E. Neil G. Marsh, Chair
Professor Carol A. Fierke
Associate Professor Bruce A. Palfey
Professor Nils G. Walter

DEDICATION

To my loving wife, María, who saved me from the depths of the sea.

ACKNOWLEDGMENTS

I express my deepest appreciation to my advisor and Committee Chair, Professor Neil Marsh, who continually conveyed to me the spirit of adventure in research, scholarship, and teaching. I have always been intrigued by the inner workings of nature, but never had the courage to consider myself a “scientist” until Professor Marsh inspired in me the confidence to think like one. It was my good fortune to coauthor three publications with Professor Marsh. The experience gained in that effort can only be described as the culmination of mentoring combined with the purest form of learning. I consider myself privileged to have been invited to join Professor Marsh’s lab. It is perhaps standard practice to say this, but I cannot over-emphasize that this dissertation would not be possible without his genuine interest, careful supervision and constant help. Professor Marsh taught me not only how to think as a scientist, but how to behave and communicate like one. If graduate school was ever to be fun and exciting, it was only made possible in the laboratory of Professor Neil Marsh. Thank you, Neil, for everything!

I also thank my Committee Members, Professor Carol A. Fierke, Professor Nils G. Walter and Professor Bruce A. Palfey, who demonstrated a deep and sincere concern for my progress as a graduate student. Your discussion, ideas, and feedback have been absolutely invaluable in the shaping of this work. Thanks to Professor Jeremy Harvey, Professor Adrian Mulholland and Dr. Patrick von Glehn for the wonderful collaboration that led to the work discussed in Chapter 2.

Heartfelt thanks to my brother, Ronald, who has always been my friend, even when I felt I had none. The joy you have for life is contagious, embracing all who know you. It has constantly lifted me in times of great need and despair, a hard reality that comes all too frequently in the life of a graduate student. A man like you is very special and I am very proud to have you as my brother. No matter where time may take us, you will always be in my heart. Without you, my success in graduate school would not have been possible. To my cousin and second brother, John Mark, we grew up together, constantly experiencing life through our common prism. A definition of friendship more genuine does not exist. For that, I am grateful to have you in my life.

And to my always-encouraging parents, Eva and David, it is beyond question that I am here today, writing my doctoral thesis, because of the immense sacrifice and support you provided. It is impossible to detail all you have done for me in this limited space. There is nothing I can say other than to thank you for the opportunities you worked so hard to carve for me. I love you both.

TABLE OF CONTENTS

LIST OF TABLES

LIST OF FIGURES

LIST OF APPENDICES

CHAPTER 1*

THE 5'-DEOXYADENOSYL RADICAL IN ADENOSYLCOBALAMIN AND RADICAL SAM MEDIATED CATALYSIS: AN INTRODUCTION

1.1. The 5'-Deoxyadenosyl Radical

Many enzymatic chemical transformations require the abstraction of a non-acidic hydrogen from an alkyl group at some point during their catalytic mechanism. However, the high pKa and weak dipole moment associated with unactivated C-H bonds makes these reactions one of the most difficult to catalyze in biological systems. Invariably, enzymes employ radical chemistry to initiate catalysis by abstraction of a hydrogen atom from their substrates.[1] With a bond dissociation energy of approximately 100 kcal/mol, nature requires a cofactor that can serve as a potent oxidant to activate an otherwise inert C-H bond. Under aerobic conditions, C-H bond activation typically involves oxidizing the carbon atom to an alcohol using a high valent metal-oxygen cofactor. Many enzymes use iron either as cytochrome P450 or a non-heme iron to cleave the di-oxygen bond and generate an iron(IV)-oxo species that can serve as the powerful oxidizing agent. The iron(IV)-oxo species is a strong enough oxidant to

* The work presented in this Chapter 1 is adapted from:

Marsh, E. N. G. and Meléndez, G. D. R. (2012). Adenosylcobalamin enzymes: Theory and experiment begin to converge. Biochimica Et Biophysica Acta (BBA) - Proteins & Proteomics, 1824(11), 1154–1164. doi:10.1016/j.bbapap.2012.03.012

Wang, J., Woldring, R. P., Román-Meléndez, G. D., McClain, A. M., Alzua, B. R. and Marsh, E. N. G. (2014). Recent Advances in Radical SAM Enzymology: New Structures and Mechanisms. ACS Chemical Biology, 9(9), 1929–1938. doi:10.1021/cb5004674

abstract a hydrogen atom from the substrate yielding iron-hydroxyl and substrate radical intermediates. The activated substrate can then undergo hydroxylation by a radical mediated recombination with the iron-hydroxyl species.[1-4]

Whereas nature uses oxygen to generate carbon-based radicals in aerobic environments, the 5'-deoxyadenosyl radical is biology's agent of choice for radical initiation in many obligate anaerobic organisms.[5] Nature has evolved mechanisms to generate the 5'-deoxyadenosyl radical (5'dA•), which is a potent oxidant and participates in a vast array of chemical reactions ranging from complicated DNA repair,[6] cofactor biosynthesis,[7] enzyme activation,[8] RNA modification[9, 10], sulfur insertion[11] and carbon skeleton rearrangements.[12-14]

There are two mechanisms by which enzymes generate 5'dA• (Figure 1). In one, a small group of about twelve known enzymes uses adenosylcobalamin (coenzyme B_{12}, AdoCbl) as a cofactor, which upon thermal homolytic cleavage results in cob(II)alamin and the 5'dA• radical initiator.[15-19] The bond dissociation energy of the Co-C bond in free solution is a relatively low ~30 kcal/mol and, thus, is able to undergo facile homolysis upon substrate binding.[20] A separate, more recently identified yet much larger class of enzymes uses *S-adenosylmethionine* (SAM, AdoMet) as the 5'dA• precursor.[21-25] Radical SAM enzymes typically have a conserved CX_3CX_2C motif, which chelates a [4Fe-4S] cluster's iron through the three cysteine residues; the cluster's free, un-ligated iron is then able to coordinate AdoMet.[26-30] The C-S bond is about twice as strong as the Co-C bond in AdoCbl and, consequently, with a bond dissociation energy ~60 kcal/mol, direct homolytic cleavage is not possible. Instead, single-electron

reduction of AdoMet by the reduced iron–sulfur cluster yields methionine, an oxidized iron–sulfur cluster and the 5'dA• oxidant.[10, 26, 31]

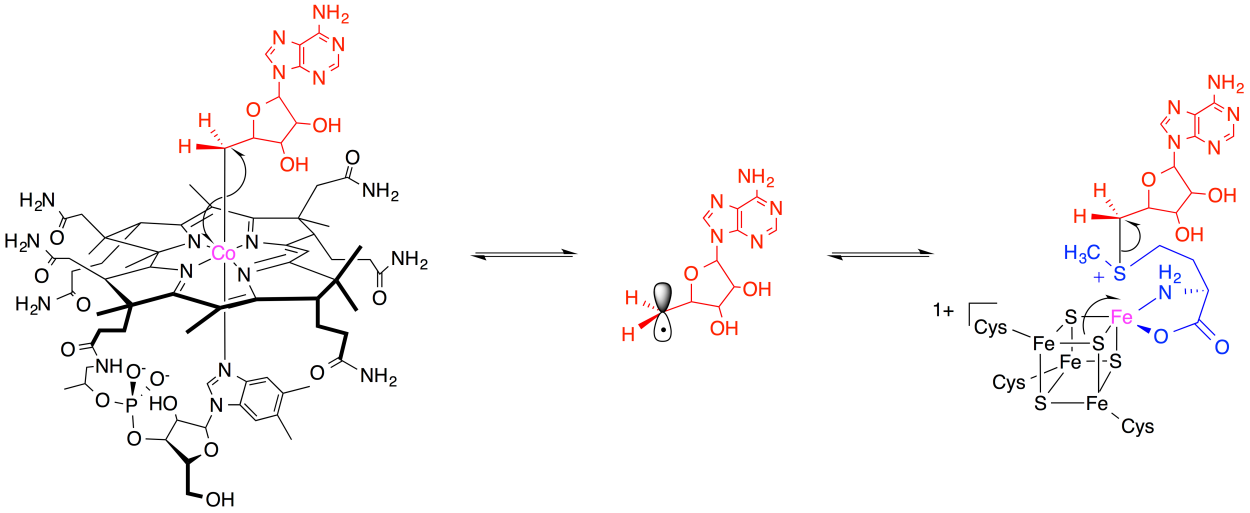

Figure 1. Generation of the 5'-Deoxyadenosyl Radical in AdoCbl-Dependent and Radical SAM Enzymes. Generation of 5'-deoxyadenosyl radical can be accomplished either by homolysis of AdoCbl (left) or reductive cleavage of *S*-adenosylmethionine (right).

How both AdoCbl and SAM-dependent enzymes stabilize highly reactive radical species and harness them towards catalysis is a fundamental question in radical enzymology, as the thermodynamics of generating the Ado• are extremely unfavorable. In free solution, AdoCbl has a homolysis rate of 10^{-9} s^{-1} and yet, in response to substrate binding, AdoCbl readily undergoes homolytic cleavage to such an extent that substrate-based radicals accumulate on the enzyme during turnover, implying the equilibrium constant for homolysis is now close to unity.[20, 32-36] Similarly, reduction of AdoMet to Ado• and methionine is estimated to require a reaction potential of -1.8 V. However, in the radical SAM enzyme lysine-2,3-aminomutase (LAM), the reduction potential of the $[4Fe\text{-}4S]^{+1/+2}$ cluster is greatly reduced to -0.43 V.[37, 38]

It is assumed that AdoCbl-dependent enzymes use substrate binding energy to offset the unfavorable bond dissociation energy and induce a conformational strain on

the coenzyme, which weakens the Co-C bond sufficiently to promote homolysis. However, experiments aimed at substantiating this hypothesis have failed to provide evidence demonstrating significant structural changes to the coenzyme or any changes in the vibrational and electronic modes of the Co-C bond. In contrast, spectroscopic studies on LAM demonstrate the binding of SAM shifts the [4Fe-4S] cluster's redox potential in favor of electron transfer such that ΔE_o is ~ 0.4 V.[39-43]

Both adenosylcobalamin dependent and radical *S-adenosylmethionine* enzymes are able to harness the high reactivity of the 5'dA• intermediate, directing it specifically to its substrate for stereoselective H-abstraction as the first step in their respective catalytic mechanisms.[8, 32, 44-48] The chemistry that occurs after hydrogen abstraction is independent of the cofactor used to generate the substrate radical and can be considered as a separate biochemical process. For instance, lysine-2,3-aminomutase is a well-characterized radical SAM enzyme that shares a requirement for pyridoxal phosphate and catalyzes a rearrangement chemically equivalent to those catalyzed by AdoCbl-dependent lysine and ornithine aminomutases, even though the coenzymes are different. Slight differences between the two classes begin to emerge when considering how they use the 5'dA• radical: AdoCbl always functions as a cofactor, but Ado• generated from SAM is typically consumed during turnover as a co-substrate. Where these enzymes really begin to diverge is in the intolerance for oxygen. AdoCbl enzymes are not especially oxygen sensitive, though they do experience a small degree of oxygen-dependent reactivity, which leads to a gradual accumulation of inactive enzyme during turnover.[49, 50] Presumably, after Co-C bond homolysis, cob(II)alamin is quenched by oxygen during turnover and oxidizes the cofactor to hydroxocobalamin,

which can be detected spectroscopically. In contrast, all radical SAM enzymes studied to date must be handled under rigorous anaerobic conditions to maintain their activity. Reactive oxygen species rapidly oxidize and destroy the iron–sulfur clusters in these enzymes (Figure 2).[51] Surprisingly, the discovery of genes for radical SAM enzymes in aerobic organisms suggests that these enzymes are functional in the microenvironment of a cell even under aerobic conditions.[5]

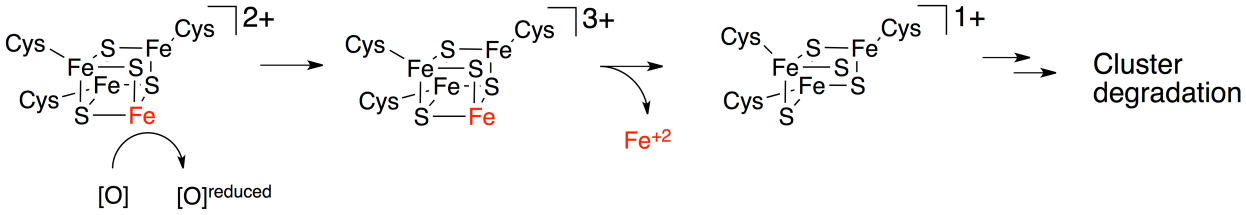

Figure 2. Oxidative Degradation of Iron-Sulfur Clusters. Upon SAM reductive cleavage, the $[4Fe\text{-}4S]^{2+}$ cluster is oxidized to the $[4Fe\text{-}4S]^{3+}$ cluster by oxidants such as molecular oxygen, superoxide, hydrogen peroxide, and peroxynitrite to an inactive $[3Fe\text{-}4S]^{1+}$ cluster, which is susceptible to further decomposition.

1.2. The Reactions Catalyzed by AdoCbl-Dependent Enzymes

The major class of reactions catalyzed by AdoCbl-dependent enzymes is rearrangements (Figure 3).[15, 52] After Co-C bond homolysis, Ado• abstracts a hydrogen atom from the substrate to generate a substrate-based radical and 5′-deoxyadenosine (Ado-H). This activates the substrate toward rearrangement and then the migrating group effectively undergoes a 1,2 rearrangement step to form a product-based radical. The mechanistic details of this step vary dependent upon the identity of the migrating group. Lastly, a hydrogen from the methyl group of Ado-H is re-abstracted by the product-radical to give the final product and regenerate Ado•, which immediately recombines with cob(II)alamin to reform AdoCbl.

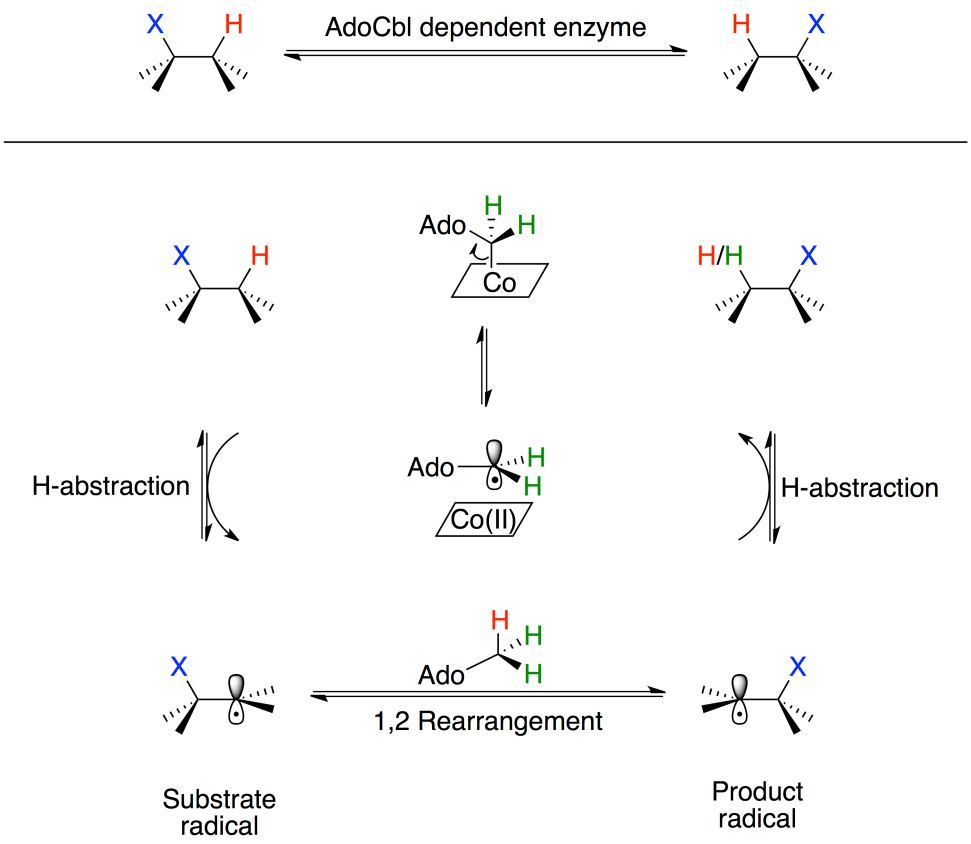

Figure 3. General Mechanistic Scheme Describing the 1,2-Rearrangement Reactions Catalyzed by AdoCbl-Dependent Isomerases. The migrating group -X moves from one carbon to the other to effect the rearrangement. X may be –OH, NH_3^+ or a carbon-containing fragment.

The mechanisms by which the substrate radicals rearrange are dependent on the nature of the migrating chemical group. The twelve known AdoCbl-dependent enzymes can be subdivided into three subgroups based on the nature of the rearrangement step. Carbon-skeleton mutases catalyze the fully reversible interchange of a hydrogen atom on one carbon with a carbon-containing group on an adjacent carbon to effect a skeletal rearrangement (Figure 4). Members of this subclass include glutamate mutase, 2-methyleneglutarate mutase, and methylmalonyl-CoA mutase,[13, 47, 53, 54] the only AdoCbl-dependent enzyme found in animals. Closely related to methylmalonyl-CoA

mutase are isobutyrl-CoA mutase[55] and the recently identified hydroxybutyrl-CoA mutase[56] and ethylmalonyl-CoA mutase[57] enzymes.

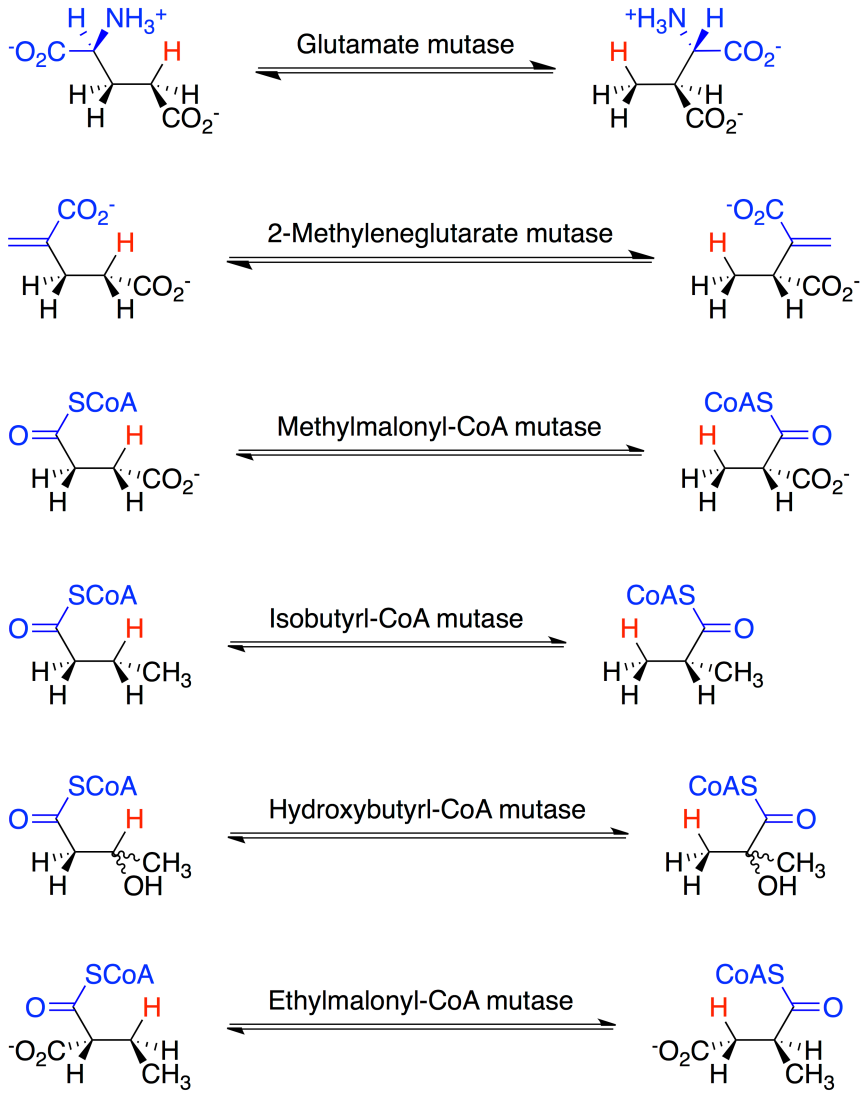

Figure 4. Reactions Catalyzed by AdoCbl-Dependent Carbon Skeleton Mutases. The migrating hydrogen is shown in red and the migrating carbon fragment in blue.

1.2.1. Carbon-Skeleton Mutases. The reactions catalyzed by the carbon-skeleton mutases are fully reversible and appear to employ two distinct mechanisms for the rearrangement step. Model chemical reactions suggest that in 2-methyleneglutarate

mutase, methylmalonyl-CoA mutase and the related acyl-CoA mutases, carbon skeleton rearrangement occurs through a cyclopropylcarbenyl radical intermediate.[58, 59] In contrast, experiments demonstrate the rearrangement catalyzed by glutamate mutase occurs by a fragmentation-recombination step in which the substrate radical fragments to form a capto-dative stabilized glycyl radical and acrylate.[60-62] The glycyl radical can then effect the rearrangement by recombining with acrylate on the adjacent carbon atom to form the methylaspartyl product-radical (Figure 5).

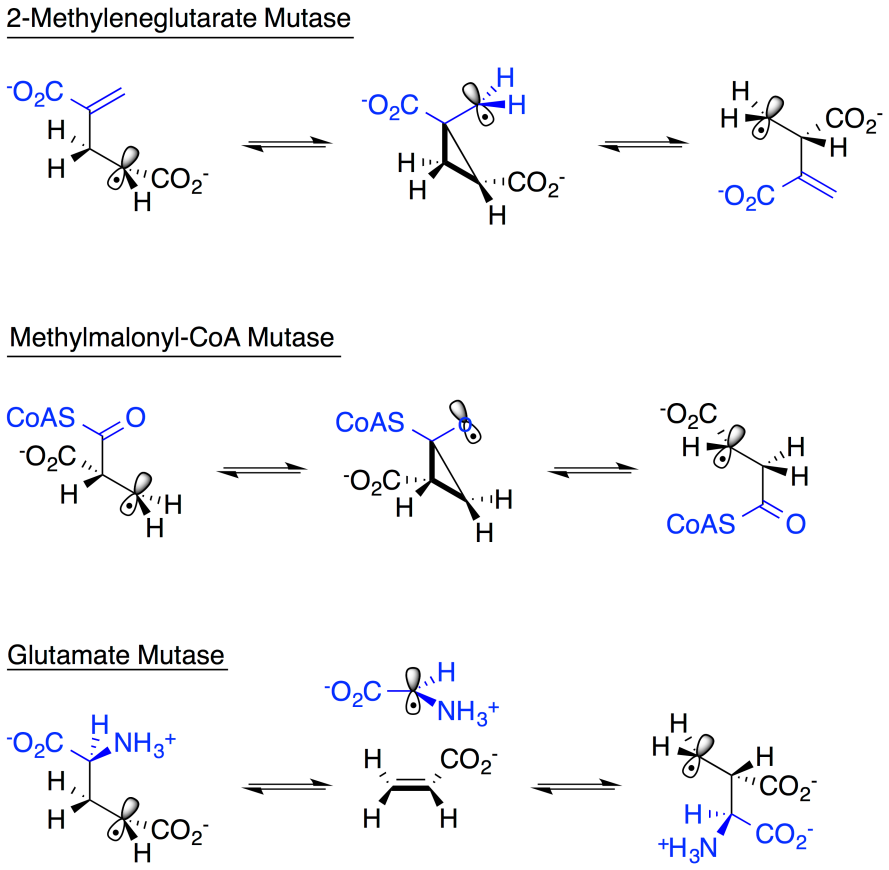

Figure 5. Mechanisms of AdoCbl-Dependent Carbon-Skeleton Rearrangement Reactions. The mechanisms for the carbon skeleton rearrangements catalyzed by methyleneglutarate mutase and the acyl-CoA mutases most likely proceed through an associative addition–elimination mechanism involving a cyclic intermediate, whereas the rearrangement catalyzed by glutamate mutase proceeds through a dissociative fragmentation–recombination mechanism involving a glycyl radical and acrylate as intermediates.

1.2.2. Eliminases. A second subgroup is the AdoCbl-dependent eliminases, which catalyze 1,2-rearrangements of either 1,2-diols to 1,1-diols or 1,2-amino-alcohols to 1,1-amino-alcohols. After the 1,2-migration of –OH or $–NH_3^+$ to form the rearranged product, eliminases go a step further and catalyze an irreversible elimination of water or ammonia from the rearranged product to yield aldehydes as the final product. Members of this subclass include ethanolamine ammonia lyase and the diol and glycerol dehydrases (Figure 6).[63] The charge of the migrating group appears to play an important role for the eliminases. Computational and experimental studies of diol and glycerol dehydrase propose that a migration pathway involving a positively charged cyclic transition state, structure is favored in which calcium serves as a Lewis acid, providing the positive charge (Figure 7).[64-66]

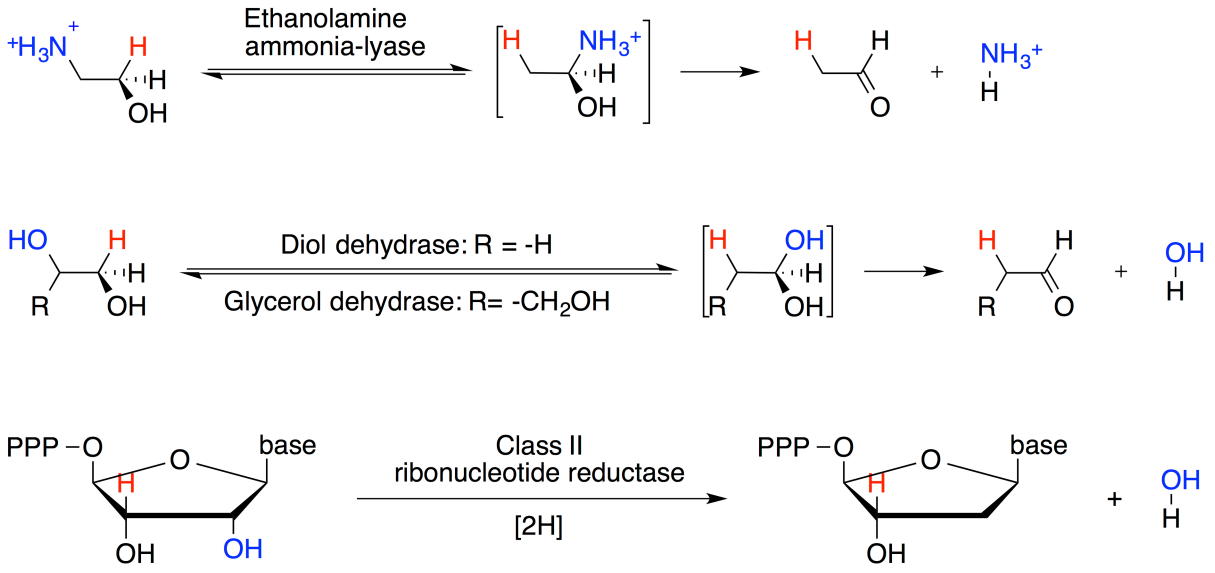

Figure 6. Reactions Catalyzed by AdoCbl-Dependent Eliminases and Class II Ribonucleotide Reductase. The migrating hydrogen is shown in red and the migrating –OH or NH_3^+ groups in blue. After rearrangement, the intermediate amino alcohol or 1,1-diol undergoes enzyme-catalyzed elimination. For ribonucleotide reductase, the C-H bond (red) on the carbon adjacent to the 2′-OH (blue) is transiently cleaved and the 2′-OH eliminated followed by reduction of the 2′-carbon.

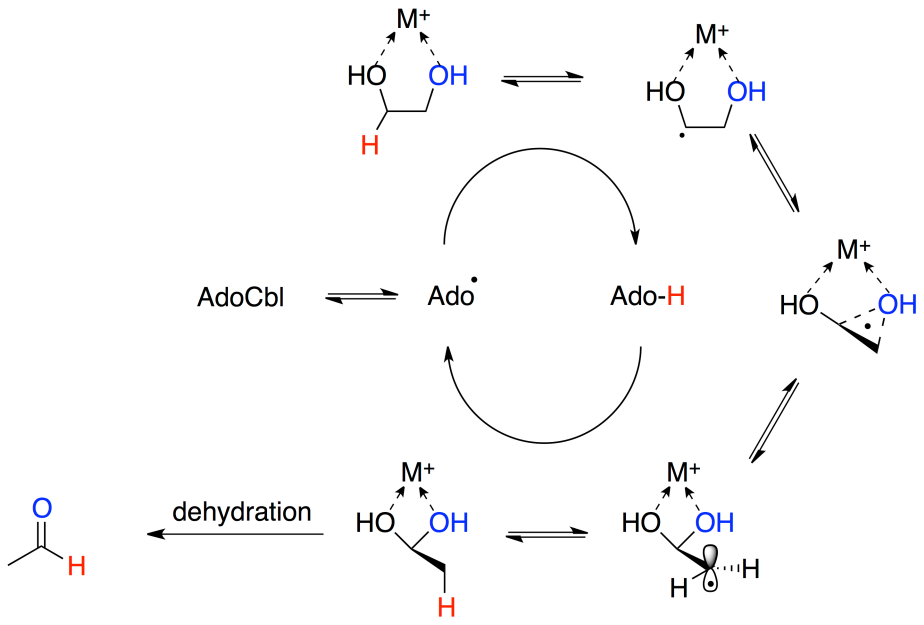

Figure 7. Mechansim of AdoCbl-Dependent Elimination Reactions. The migration of –OH groups catalyzed by diol and glycerol dehydrases involves polarization of the C-O bond by an active site metal ion. Theoretical studies suggest that a migration pathway involving a positively charged cyclic transition state structure is favored.

1.2.3. Class II Ribonucleotide Reductase. Class II ribonucleotide reductase is often classified as an eliminase despite the fact that it catalyzes a reduction instead of a rearrangement-elimination reaction. Although the underlying chemistry is indeed quite different, AdoCbl serves the same function hydrogen abstracting function in this enzyme and the mechanism by which the 2′-OH group is removed parallels the 1,2-migration of –OH catalyzed by diol dehydrase: homolysis of AdoCbl is used to reversibly generate an active site cysteinyl radical which then abstracts the 3′-H adjacent to the site of reduction, activating the 2′-OH for elimination (Figure 8).[67, 68]

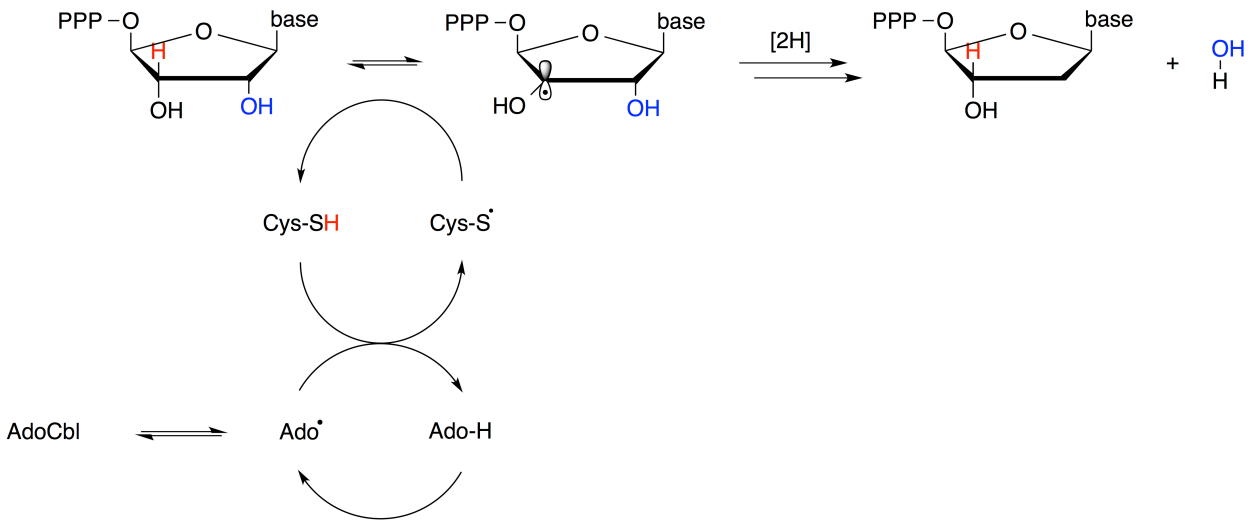

Figure 8. Mechanism of the AdoCbl-Dependent Ribonucleotide Reducatse. The 3′-hydrogen is abstracted through an intermediate cysteinyl radical that activates the substrate towards elimination of the 3′-OH group. Subsequent reduction of the 2′-carbon and replacement of the 3′-hydrogen generates the reduced nucleotide.

1.2.4. Aminomutases. Finally, the last subgroup of AdoCbl-dependent enzymes is the aminomutases. These enzymes catalyze fully reversible 1,2- migrations of amino groups and require pyridoxal phosphate as a cofactor. The two known enzymes that make up this subgroup are ornithine-4,5-aminomutase[69, 70] and lysine-5,6-aminomutase[71, 72] (Figure 9). Site directed mutagenesis and EPR experiments using isotopically labeled substrates, as well as lysine analogues that preferentially stabilize the different radical intermediates produced during rearrangement, have demonstrated that the α-amino group of lysine forms an external aldimine with pyridoxal phosphate. The re-hybridization of the sp^3 amine group to a planar sp^2 configuration allows the 1,2-nitrogen migration to proceed by way of a cyclic azacyclopropylcarbinyl radical intermediate. The nitrogen, being bound to both C-2 and C-3 of lysine, places the unpaired electron on the 4′-carbon of pyridoxal, allowing it to be delocalized through the adjacent π system (Figure 10).[73-76]

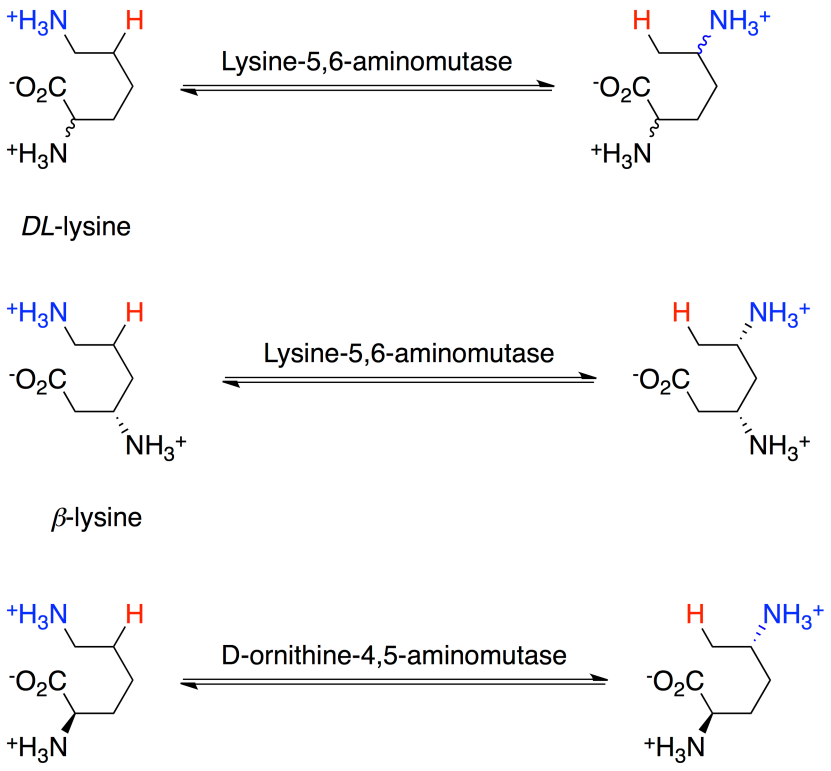

Figure 9. Reactions Catalyzed by AdoCbl-Dependent Aminomutases. The migrating hydrogen is shown in red and the migrating amino group in blue.

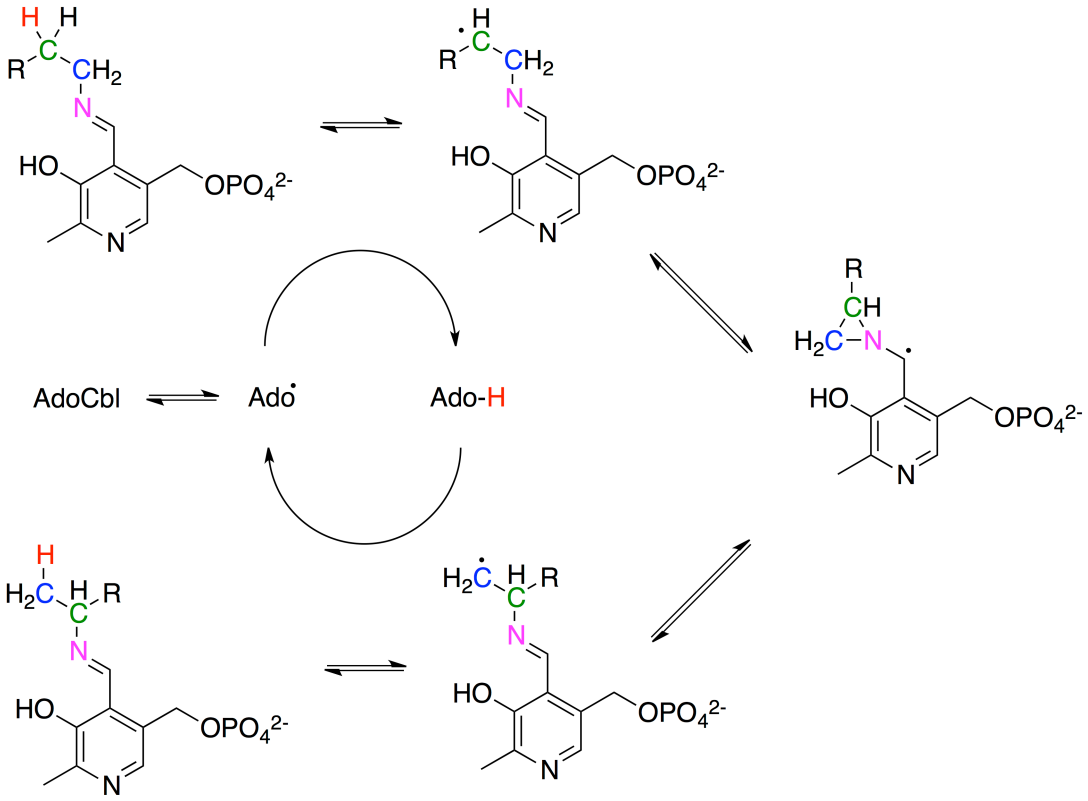

Figure 10. Role of Pyridoxal Phosphate in Facilitating the Rearrangements of Amino Groups in the Aminomutase-Catalyzed Reactions. During the reaction, the α-amino group of lysine forms an external aldimine with pyridoxal phosphate, rendering the nitrogen sp^2-hybridized. This allows the 1,2-nitrogen migration to occur through a cyclic azacyclopropylcarbinyl radical intermediate transition state in which nitrogen is bonded to both C-2 and C-3 of lysine and the unpaired electron is situated on the 4′-carbon of pyridoxal and stabilized by the adjacent π system.

1.3. A Brief Survey of Radical SAM Enzymes

In the early 1970's, lysine 2,3-aminomutase was identified as an enzyme that used SAM to initiate a radical reaction in a manner similar to the AdoCbl-dependent rearrangements.[77] At the time, SAM was only known to react as an alkylating agent. The sulfonium ion allows SAM to serve as an electrophilic methyl donor in a wide variety of cellular methylation reactions such as DNA, hormone, and neurotransmitter alkylations. However, the discovery that SAM is capable of initiating radical reactions

drove a surge of interest into this family of enzymes and, more broadly, into the field of radical enzymology.[73, 78]

Radical initiation by radical SAM enzymes parallels that of AdoCbl-dependent enzymes: reductive cleavage of SAM yields 5'dA• and methionine as the initiating step.[21, 22] Subsequently, the enzyme guides the highly reactive 5'dA• intermediate to react with its substrate, generally stereoselective H-abstraction of a non-acidic hydrogen. This, however, is where the similarities end. Whereas the twelve known AdoCbl-dependent enzymes only catalyze rearrangement reactions, a host of radical SAM enzymes have now been biochemically characterized that use 5'dA• to facilitate a remarkably wide range of reactions, including carbon methylation, sulfur insertion, oxidation, methylthiolation, and complex carbon skeleton rearrangements such as ring formation and isomerization. Bioinformatics methods have played an important role in identifying the existence of thousands of related proteins across all kingdoms of life and the chemistry these enzymes provide play a crucial role in a diverse range of biological functions, including cofactor synthesis, enzyme activation, DNA repair, protein and nucleic acid modification, and primary metabolism.[23] It is now clear that radical SAM enzymes are a cornerstone of biological metabolism and have been designated as a new class of enzymes known as the radical SAM superfamily.[7, 14, 24, 27, 44, 79-81]

The shear breadth and complexity of the reactions catalyzed, along with the technical difficulties associated with working on these highly oxygen-sensitive enzymes, means there is still much that remains to be understood about these enzymes. Many putative radical SAM enzymes have been identified from sequence alignment homology and CX_3CX_2C motif identification but their substrates, the type of reactions they catalyze

and the physiological roles within their host organism are completely unknown. Of the radical SAM enzymes that are known, only a few have had their structure and mechanism characterized. Therefore, a comprehensive introduction into the radical SAM superfamily is beyond the scope of this introduction. Only an overview of selected radical SAM enzymes, for which significant advances in their mechanistic understanding have been made, are presented and categorized broadly by the type of reaction they catalyze.

1.3.1. The Glycyl Radical Activases. Benzylsuccinate synthase (BSS) catalyzes the first step in the anaerobic metabolism of toluene in various denitrifying bacteria allowing them to live on toluene as their sole source of carbon and energy. In the reaction, the methyl group of toluene is added across the double bond of fumarate to yield (*R*)-benzylsuccinate.[82-88] Activity of BSS is strictly dependent on the presence of a radical on a C-terminal glycine residue and belongs to a class of enzymes known as glycyl radical enzymes, of which there are four currently known. Glycyl radical enzymes contain a conserved, active site C-terminal glycyl residue that bears a radical in the active enzyme. The glycine is thought to act as a stable radical reservoir, holding the radical until it is needed for catalysis. At this point, the unpaired electron on the glycine residue is transferred to a conserved, active site cysteine residue. This mediates as a relay between the glycyl and subsequent substrate radical, thereby initiating a catalytic mechanism involving radical intermediates.[87, 89-94]

Pyruvate formate-lyase (PFL) was discovered first and is the best-characterized enzyme in its class. In fact, much of the mechanistic features common to all radical SAM-enzymes were established by experiments on this enzyme. It catalyzes the

conversion of pyruvate to acetyl-CoA and formate during glucose fermentation.[94-97] Under anoxic conditions, *E. coli* will use anaerobic ribonucleotide reductase (anRR) to reduce the ribose sugar in a manner similar to the class II, AdoCbl-dependent reducatse.[97-99] 4-Hydroxyphenylacetate decarboxylase catalyzes the formation of *p*-cresol in various *Clostridia.*[100, 101] Finally, just as the AdoCbl-dependent enzyme, the glycyl radical enzyme glycerol dehydratase catalyzes the conversion of glycerol to 3-hydroxypropanal (Figure 11).[102, 103]

Glycyl radical enzymes require a partner activating enzyme from the radical SAM enzyme family.[104] These activases use a [4Fe-4S] cluster as an electron source in the reductive cleavage of SAM to methionine and a 5'-deoxyadenosyl radical. Indeed, electron paramagnetic resonance (EPR) studies confirm that SAM dependent activases contain a catalytically relevant $[4Fe\text{-}4S]^{+1}$ cluster, which is coordinated to only three peptide cysteine residues of the conserved CX_3CX_2C cluster binding sequence on the activase backbone.[105-108] The fourth free iron binds SAM in the enzyme's active site.[109-111] Consequently, upon reductive cleavage of SAM, the $[4Fe\text{-}4S]^{+1}$ cluster is oxidized to the $[4Fe\text{-}4S]^{+2}$ cluster, which is susceptible to decomposition by oxidants such as oxygen.[51] Thus, strict anaerobic conditions for the activating enzymes are also required. The activating enzyme is then able to harness the high reactivity of the 5'-deoxyadenosyl radical and introduce a radical on the C-terminally located glycine on the partner protein, which in turn uses this glycine residue for chemical catalysis (Figure 12). Interestingly, the activases do not appear to "cross-activate" and are only able to activate their respective partner protein.[5] This allows the activases to essentially function as a post-translational catalytic "on" switch for their cognate enzymes.

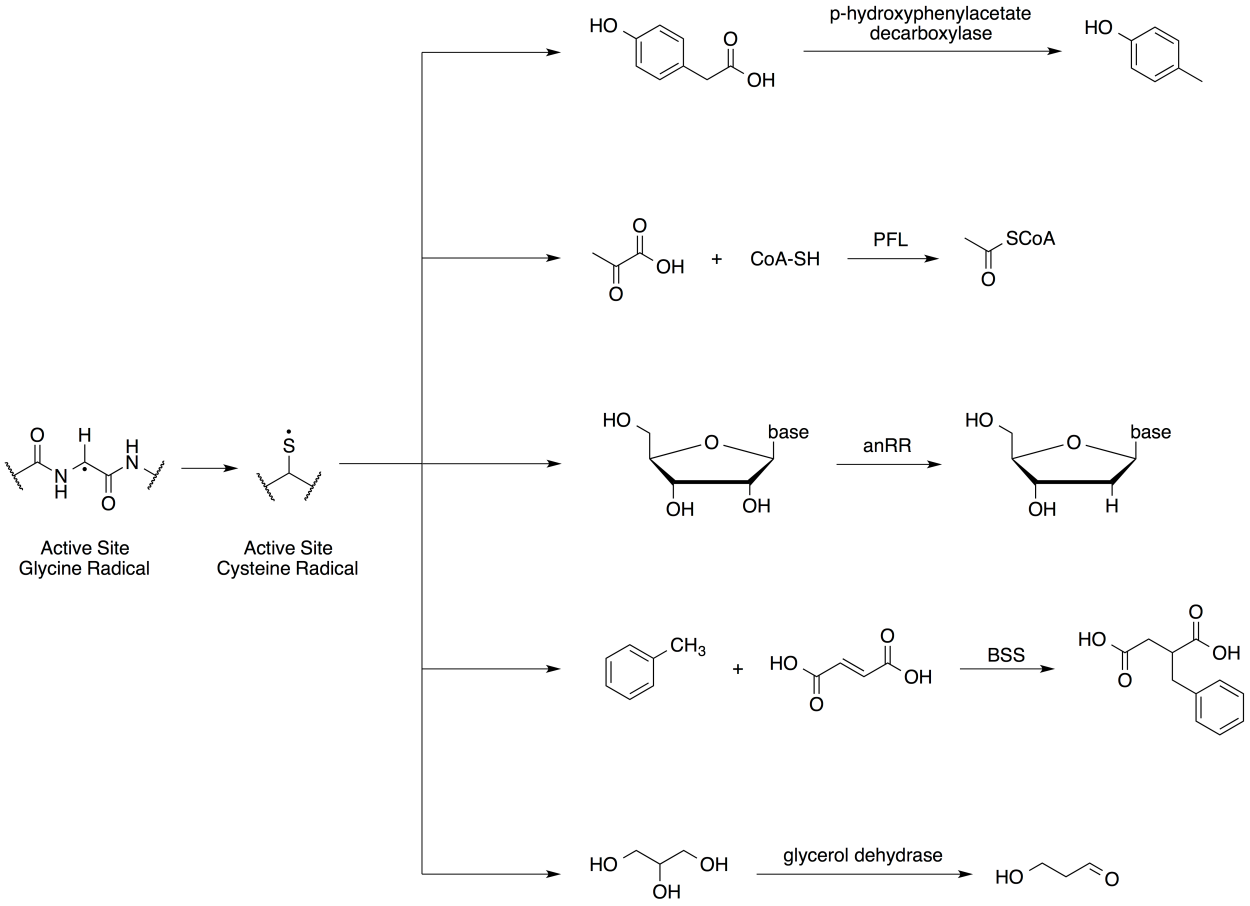

Figure 11. Reactions Catalyzed by the Glycyl Radical Enzymes. Each catalytic enzyme has a partner, radical SAM activating enzyme that installs the glycyl radical on a conserved C-terminal glycine residue.

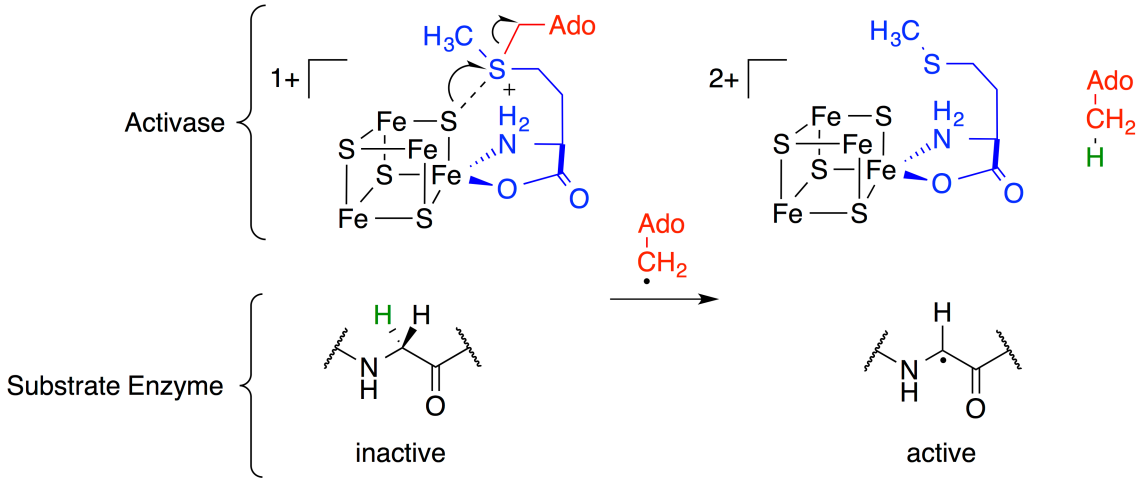

Figure 12. Reaction of a Radical SAM Dependent Activating Enzyme with its Cognate Glycyl Radical Enzyme. The methionine moiety is shown in blue, adenosylmethionine in red, and glycine C_α hydrogens in green. The oxidation numbers correspond to the oxidation state of the Fe-S cluster as a whole and the fish hooks represent the reductive cleavage of SAM. For simplicity, the conserved cysteine motif involved in chelating the three iron atoms of the Fe-S cluster to the peptide backbone is omitted.

1.3.2. The Methylating Enzymes Cfr and RlmN. Most commonly, SAM dependent methylations take advantage of SAM's capability to act as an electrophilic methyl donor and are achieved by SAM-dependent methyltransferases that employ polar chemistry to methylate nucleophillic targets on their substrates. However, recently discovered radical SAM dependent methylations are distinct in that they are found to occur on carbon atoms displaying weak Lewis basicity. These enzymes are able to exploit SAM's dual ability to act as a methyl donor and radical initiator.[112] The best understood radical SAM methylases are the RNA methylating Cfr and RlmN, which methylate the sp^2-hybridized C8 (Cfr) and C2 (RlmN) amidine carbons of A2503 in the bacterial 23S rRNA.[10, 113] Insight into these reactions may provide researchers the ability to create new antibiotics as rRNA methylation seems to play an important role in the ability of certain bacteria to develop antibiotic resistance. These enzymes require two equivalents SAM to methylate their substrate: one equivalent generates the canonical 5'dA• radical while the other acts as the methyl donor.

Mutagenesis studies of two conserved cysteine residues required for *in vivo* function, experiments using isotopically labeled SAM, and the crystal structure of RlmN support a ping-pong type mechanism involving the formation of methylated intermediate on a conserved cysteine residue (Figure 13).

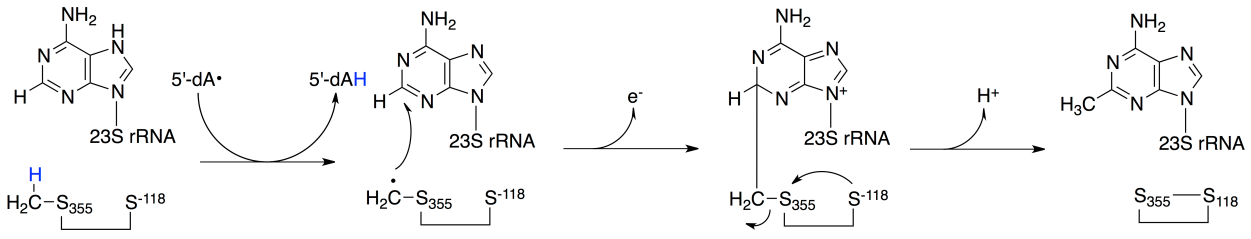

Figure 13. Proposed Mechanism for Carbon-Centered Methylation Catalyzed by RlmN. The enzyme is first methylated on Cys355 by SAM and the reaction is then initiated by hydrogen abstraction from the thiomethyl group by Ado•.

The first SAM equivalent methylates Cys355 on the enzyme. The second equivalent undergoes iron-sulfur cluster-assisted reductive cleavage to produce 5'dA•, which then abstracts a hydrogen atom from the methylated cysteine. This is supported by the fact that when (*methyl-d_3*)-SAM is used, one deuterium is incorporated into Ado-H.[9, 114, 115] The thiomethylene radical then adds to the amidine carbon to form a transient rRNA−protein adduct after a one-electron oxidation and loss of a proton. The covalent adduct is cleaved by attack of a Cys118 to form a disulfide bridge and the methylated rRNA. Isotopic labeling confirms that when deuterated SAM is used, only two deuterium atoms remain in the methyl group and that the third proton originates from the solvent.

1.3.3. The Methylthiotransferase MiaB. MiaB is a tRNA modifying enzyme that introduces a methylthiol group to the modified tRNA base i6A, forming 2-methythio-N-6- isopentenyladenosine (ms2i6A) at position 37 of tRNAs that read codons starting with uridine.[81, 116, 117] It is believed that modification of the nucleotides surrounding tRNA anticodons allows the molecule to maintain fidelity in translational efficiency.[118, 119] Despite this tRNA modification being a well-established process occurring in all organisms, only recently has MiaB been identified as the first tRNA modifying enzyme to contain a [4Fe-4S] cluster.[120]

Not only does MiaB require two equivalents of SAM (as with the radical SAM methylases), it also contains a second [4Fe-4S] cluster.[11, 121-125] Isotopic labeling experiments show that one SAM provides the methyl group yielding SAH as the byproduct, while the other produces 5'dA• to activate the tRNA substrate.[122] It is proposed that 5'dA• generated by the reductive cleavage of SAM initiates catalysis by

abstracting a non-acidic H-atom from C-2 of the i6A37 nucleotide. Interestingly, methyl transfer from SAM to the enzyme does not depend on 5'dA• formation and can proceed in the absence of substrate, suggesting that sulfur insertion may not precede methyl transfer.[116] This eliminates a simpler mechanism in which the second iron-sulfur cluster provides the sulfur required to thiolate the i6A37 followed by a sequential methylation by the second equivalent of SAM to yield the final thiomethylated MeS2i6A37 product.

Treatment of the enzyme with SAM in the absence of a reducing agent followed by acid denaturation resulted in the release of methanethiol, suggesting that the methyl group is transferred to an acid-labile sulfur on the protein.[116] A separate study confirmed that MiaB is able to perform multiple turnovers with exogenous sulfide, as well as demonstrate that sulfur-containing cosubstrates, such as methanethiol, can directly chelate to the second cluster, which 2-dimensional EPR spectroscopy shows remains intact.[11] Furthermore, a recent crystal structure of the related methylthiotransferase RimO (responsible for the post-translational modification of Asp88 of the ribosomal protein S12 in *E. coli*)[126] demonstrates a pentasulfide bridge linking the two unique iron atoms in each of the clusters.[11] These results provide strong evidence that the second cluster remains intact during turnover.

A revised mechanism in which the incorporated sulfur derives from an exogenous source, thus keeping the second cluster intact, begins with accumulation of exogenous sulfide into the pentasulfide bridge between the iron−sulfur clusters (Figure 14). Subsequent cleavage of the sulfide bridge allows SAM to transfer a methyl group and form a methyl-terminated persulfide chain, the details of which remain to be determined, generating the thiomethylating agent. Abstraction of hydrogen from the

substrate by 5'dA• activates the substrate and transfer of the methylthio group to the substrate can now occur. Finally, the substrate can undergo a one-electron oxidation, possibly to the second iron−sulfur cluster, to complete the catalytic cycle.[11, 127]

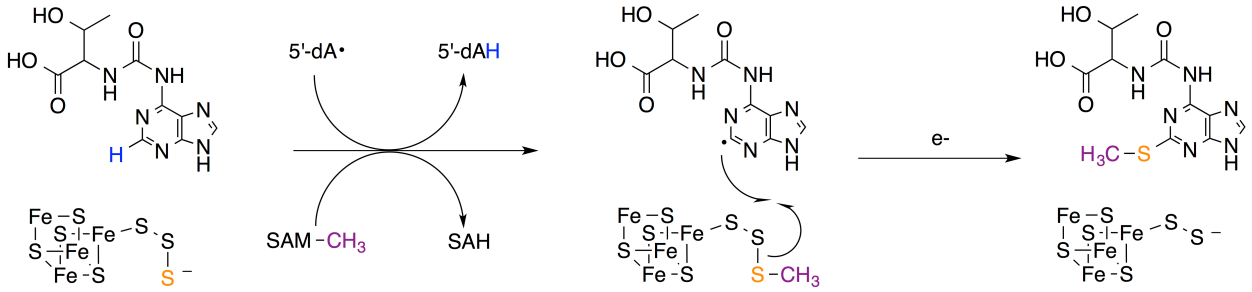

Figure 14. Proposed Mechanism for Methylthiolation Catalyzed by MiaB. Methylation by SAM of a persulfide ion (derived from the pentasulfide bridge) ligated to the unique iron of the auxiliary [4Fe-4S] cluster precedes the radical SAM chemistry to generate 5'dA•, which abstracts hydrogen from the substrate. The substrate radical then adds to the methylated sulfur atom to yield the methythiolated product.

1.3.4. The Carbon-Carbon Bond Forming Tyw1, MqnE, and F_0 Synthase.

Wybutosine (yW) is a tricyclic nucleoside base found at position 37 adjacent to the anticodon of archaeal and eukaryotic $tRNA_{Phe}$.[128] Its large, tricyclic aromatic ring structure is thought to improve fidelity by enhancing codon-anticodon recognition mediated by its strong base-stacking interactions that are able to reduce the flexibility of the tRNA.[129] The enzyme Tyw1 catalyzes the formation of the third aromatic ring found in yW as the second step in its biosynthesis. Despite recent experiments identifying pyruvate as the two carbon donor required for the radical mediated ring closure of N-methylguanosine to 4-demethylwyosine,[130] two plausible mechanisms for how Twy1 activates pyruvate for cleavage remain.[130, 131] Crystallographic data shows, apart from the SAM binding [4Fe-4S] cluster, that the enzyme contains a second, catalytically essential [4Fe-4S] cluster of unknown function.[129] One mechanism involves pyruvate forming a Schiff base to a conserved lysine residue with the second cluster functioning

to either oxidize or reduce the pyruvate carboxylate group - it is not known whether the carboxylate is released as CO_2 or formate. In eukaryotes, the enzyme has an additional flavodoxin domain that may be involved in shuttling electrons to the iron sulfur cluster.[128] Transamination of the Schiff base to the amino-group of N-methylguanosine would then produce the cyclized product. The second mechanism proposes a more active role for the second cluster in which it functions as a Lewis acid to facilitate cyclization and dehydration to form 4-demethylwyosine (Figure 15). Regardless of the manner in which Twy1 uses the second cluster, both mechanistic proposals start with a 5'dA•-mediated hydrogen abstraction from N-methylguanosine to activate the substrate followed by homolytic cleavage of the C1−C2 pyruvate bond.[130, 131]

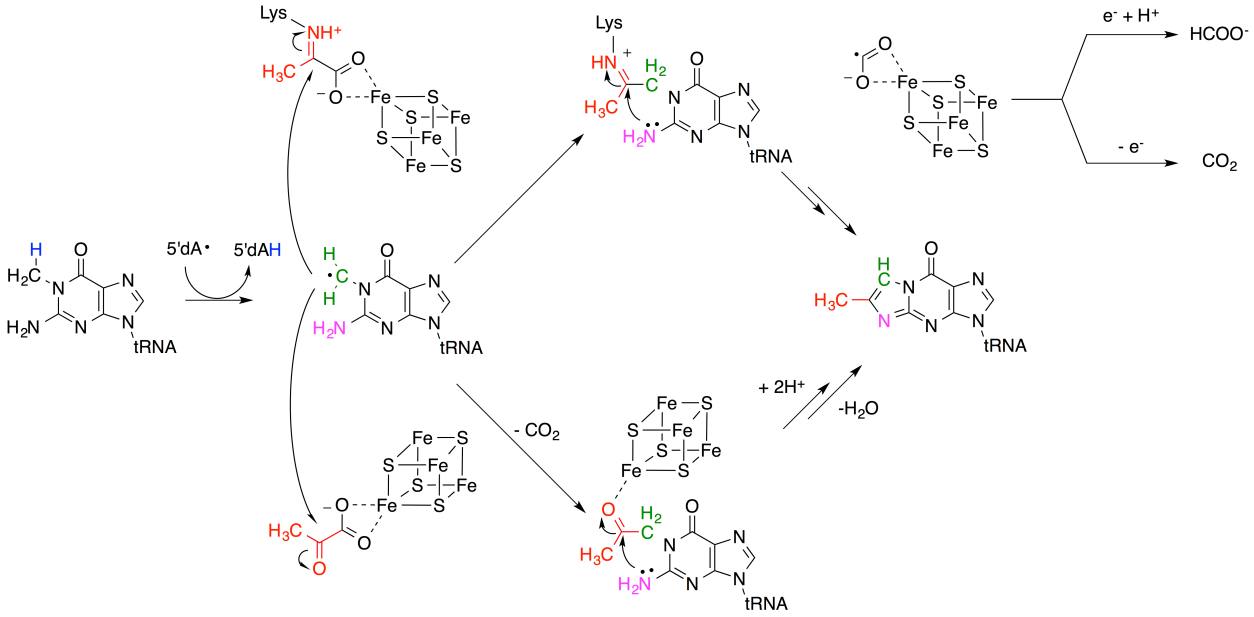

Figure 15. Two Mechanisms Have Been Proposed for the Conversion of N-Methylguanosine to 4-Demethylwyosine Catalyzed by Tyw1. Top: A lysine stabilizes intermediates by forming a Schiff base with pyruvate; the auxiliary cluster functions as a redox center. Bottom: Coordination of the auxiliary cluster promotes the reaction of the substrate radical with pyruvate facilitates cyclization.

Menaquinone (vitamin K) is a lipid-soluble quinone used in place of ubiquinone by some bacteria in their electron transport chain. In mammalian cells, it functions as a coenzyme in glutamate carboxylation reactions important in bone formation and blood clotting. Menaquinone biosynthesis from chorismate and 2-ketoglutarate is well-characterized, but some strains of *Streptomyces* lack the established biosynthetic genes required for menaquinone production suggesting an alternative pathway to vitamin K exists. Indeed, experiments with *S. coelicolor* revealed menaquinone production begins with the conversion of chorismate to 3-[(1-carboxyvinyl)oxy]benzoic acid by MqnA. In the second step, the radical SAM enzyme MqnE catalyzes the conversion of 3-[(1-carboxyvinyl)oxy]benzoic acid to aminofutalosine, releasing methionine and CO_2 as by-products. Surprisingly, unlike all other radical SAM enzymes, MqnE does not use 5'dA• for hydrogen abstraction, but rather incorporates it into the final product (Figure 16). Aminofutalosine is subsequently converted to menaquinone by MqnB, MqnC, MqnD, and other uncharacterized enzymes.[132]

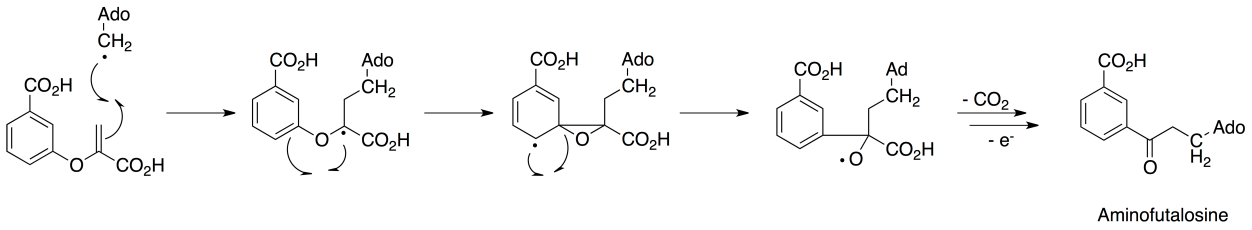

Figure 16. Proposed Mechanism for Aminofutalosine Synthesis Catalyzed by MqnE. The key first step involves a radical Michael addition of 5'dA• to the chorismate-derived cosubstrate; subsequent rearrangement and oxidative decarboxylation produces aminofutalosine.

F_0 is a precursor to F_{420}, a deazaflavin derivative used as an essential cofactor by various enzymes involved in energy metabolism, antibiotic biosynthesis, and DNA repair in both prokaryotes and eukaryotes.[133] Existing as a single large enzyme in

actinobacteria (FbiC), sequence analysis revealed the enzyme possesses two radical SAM domain CX_3CX_2C motifs suggesting the enzyme is able to produce 5'dA• at two separate [4Fe-4S] cluster centers. Interestingly, F_0 synthase from archaea and cyanobacteria is comprised of two subunits (CofG/CofH), each housing one [4Fe-4S] cluster.

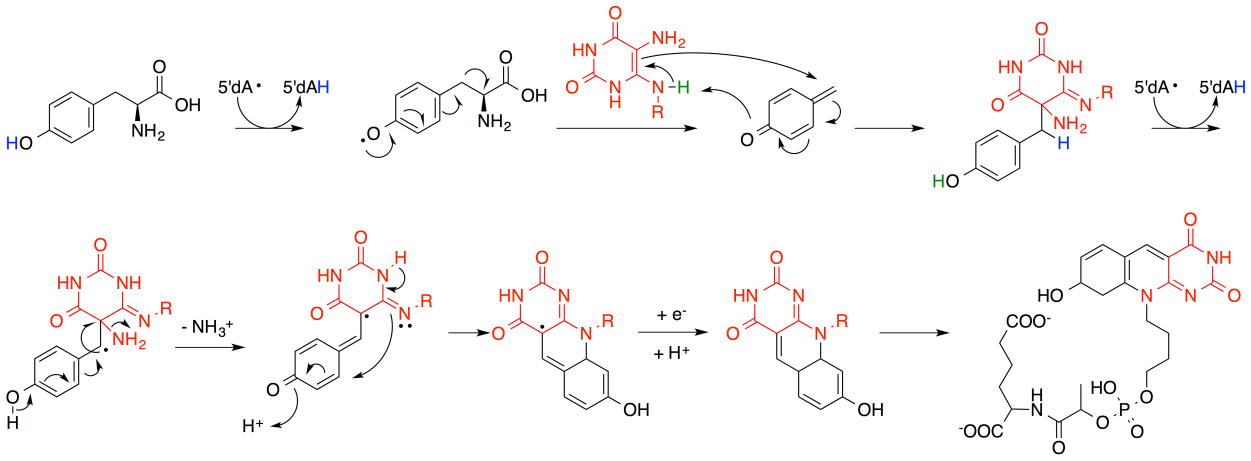

Figure 17. Proposed Mechanism for the Reaction of Tyrosine and Diaminouracil Catalyzed by F_0 Synthase. The mechanism involves the abstraction of hydrogen from tyrosine and the release of a dehydroglycine, producing a reactive 4-oxidobenzyl radical, which adds to diaminouracil. A second round of radical chemistry initiates formation of the tricyclic deazaflavin (F_0) that in further steps is converted to F_{420}.

Experiments using isotopically labeled substrates demonstrate the enzymes responsible for F_0 synthesis show F_0 is formed from the radical SAM mediated oxidative coupling of diaminouracil with tyrosine. It appears synthesis of F_0 occurs in a sequential, two step mechanism as incubation of CofH with diaminouracil, tyrosine, SAM, and reductant yielded a small molecule product that could subsequently be incubated with CofG, SAM, and reductant to yield F_0. Furthermore, consistent with the formation of two molecules of 5'dA•, 2.5 equivalents of 5′-deoxyadenosine were formed for every molecule of F_0 synthesized. Consequently, F_0 synthase FbiC from actinobacteria may serve as bifunctional enzyme catalyzing both reactions. The

originally proposed mechanism includes fragmentation of a tyrosyl radical to generate a glycyl radical and a quinone methide intermediate that can subsequently react with diaminouracil. However, in the light of recent work on hydG (discussed below), we present an equally plausible mechanism involving fragmentation of a tyrosyl radical to give a 4-oxidobenzyl radical (Figure 17).[134] Further experiments will be needed to distinguish between these two possibilities.

1.3.5. Complex Carbon Skeleton Rearrangements Catalyzed by HydG, SPL and MoaA/MoaC. The di-iron-hydrogenase enzyme HydA plays a central role in the metabolism of hydrogen in various anaerobic bacteria. The site of hydrogen generation in the enzyme's active site, known as the H-cluster, is composed of a [4Fe-4S] cluster linked by a cysteine thiolate to a modified [Fe-Fe] cluster. The H-cluster is coordinated by unique ligands not provided by the protein's backbone: CN, CO and dithiolate ligands. Recent studies demonstrate that both the di-iron cluster and non-protein ligands are synthesized separately and then inserted into HydA by the hydrogenase maturation enzymes HydE, HydF and HydG, of which HydE and HydG are radical SAM enzymes.[135] HydG, the better understood enzyme, is responsible for the synthesis of the H-cluster's CN^- and CO ligands. In addition to the 5'dA• generating [4Fe-4S] cluster, the enzyme contains an additional C-terminal [4Fe-4S] cluster that appears to be the site of CN^- and CO production. Disruption of the C-terminal cluster does not affect the enzyme's affinity for SAM but does, however, drastically reduce the affinity for its tyrosine substrate. Furthermore, kinetic analysis of iron−sulfur cluster mutants lacking the protein cysteine ligands indicates the C-terminal cluster is not needed for tyrosine cleavage to p-cresol, but is required for final conversion of the glycyl

fragment into CN^- and CO.[136] EPR spectroscopic studies using various isotopically-labeled tyrosine substrates allowed the identity of several reaction intermediates to be assigned and a detailed reaction mechanism accounting for both clusters is proposed in which heterolytic cleavage of the tyrosine radical, first generated by the phenolic hydrogen abstraction 5'dA•, forms a 4-oxidobenzyl radical and dehydroglycine.[137, 138] While dehydroglycine remains bound to the C-terminal cluster, electron and proton transfers reduce the 4-oxidobenzyl radical to *p*-cresol. In a final step that remains unclear, dehydroglycine is cleaved and dehydrated to give the CN^- and CO ligands, which remain bound to the unique iron of the C-terminal cluster (Figure 18). Stopped-flow FT-IR and electron−nuclear double resonance (ENDOR) spectroscopies suggest that the Fe[CO][CN^-] complex is further modified by HydG to a $Fe[CO]_2[CN^-]$ complex. The entire $Fe[CO]_2[CN^-]$ complex forms the basis for one-half of the H-cluster can then be transferred to apo-HydA, probably through the combined action of HydE and HydF, to ultimately form the mature HydA [FeFe]-hydrogenase.[139]

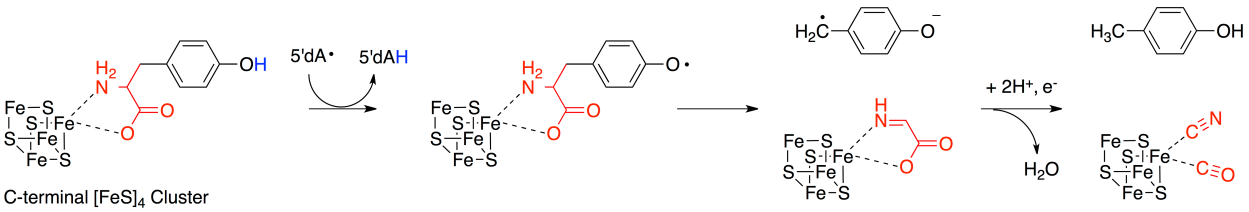

Figure 18. Proposed Mechanism for the Cleavage of Tyrosine by HydG. Tyrosine binds to the auxiliary C-terminal [4Fe-4S] cluster. Ado• generated by N-terminal [4Fe-4S] cluster reacts with tyrosine, producing a tyrosyl radical. Cleavage of the tyrosyl radical results in 4-oxidobenzyl radical and dehydroglycine bound to the auxiliary cluster that is subsequently cleaved to produce CO and CN^- ligands to the H cluster of HydA.

Spore photoproduct lyase (SPL) is a radical SAM enzyme found in bacteria that repairs the dimerization of adjacent thymine bases in DNA as a result of exposure ultraviolet radiation, which if left untreated can have deleterious effects on DNA replication and transcription.[26, 140] In the established mechanism for SPL, the 5'dA•

radical first abstracts a hydrogen atom from C-4 of the dimer's dihydrothymine moiety resulting in a thyminyl radical, which then fragments to restore one thymine residue and generates a methyl-based radical on the second thymine residue. Based on the observation that SAM is required catalytically instead of stoichiometrically, it was thought the thyminyl radical abstracts a hydrogen atom back from Ado-H to regenerate Ado• and the restored second thymine residue.[26] However, a recent study using a dithymine substrate deuterated at the abstractable position revealed that deuterium is not incorporated into the thymine product, suggesting that the initially abstracted hydrogen is not returned to thymine.[141] The crystal structure of SPL revealed the conserved cysteine-140 residue, which is not involved in iron-sulfur cluster ligation but required for enzyme activity, to be closer to the 3′-thymidine residue than SAM suggesting that Cys140 is the true hydrogen atom donor to the thyminyl radical.[140] Indeed, mutation of Cys140 to alanine traps the enzyme before the final step allowing the allylic thyminyl radical to be trapped with dithionite as the thymine sulfinic acid derivative.[6] Despite this advance in mechanistic understanding, the question of how the reaction is catalytic with respect to SAM remains because Ado• must eventually be regenerated. Tyrosine-98, located between Cys140 and SAM in the enzyme's active site, is proposed to act as a hydrogen transfer intermediary: the tyrosine O−H and cysteine S−H have similar bond dissociation energies, indicating that abstraction of a hydrogen atom from Tyr98 by the cysteinyl radical is feasible (Figure 19). However, a caveat remains: the C−H bond dissociation energy is much higher so that regeneration of Ado• by hydrogen abstraction from Ado-H by either a tyrosyl or cysteinyl radical would be unfavorable. Nevertheless, it is thought that this energy difference could be

offset by coupling the abstraction of hydrogen from Ado-H to the regeneration of SAM.[142]

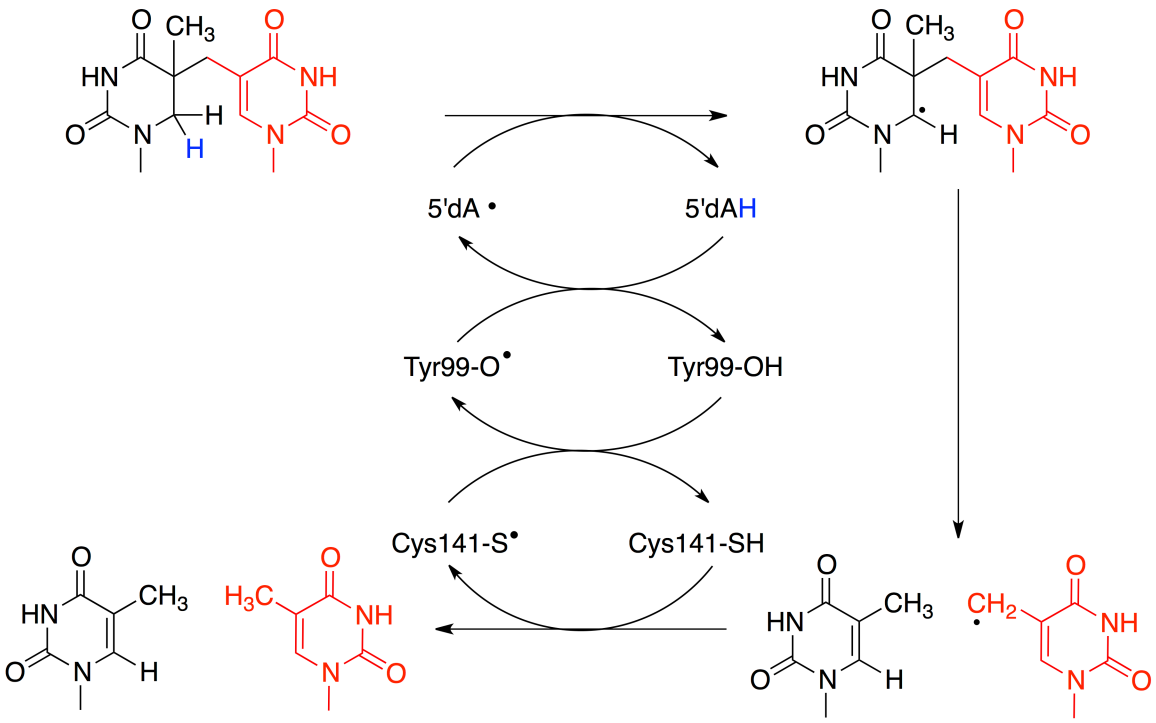

Figure 19. Proposed Mechanism for SPL Accounting for Radical Regeneration by a Hydrogen Atom Transfer Pathway Involving Cys140 and Tyr98. Exposure to ultraviolet radiation results in dimerization of adjacent thymine bases in DNA, which can have deleterious effects on DNA replication and transcription. Spore photoproduct lyase (SPL), a radical SAM enzyme found in bacteria repairs these dimers and, thus, reverses the damage.

The radical SAM enzyme MoaA, along with MoaC, catalyze the first two steps in molybdopterin biosynthesis by converting GTP into a cyclic pyranopterin monophosphate (cPMP) intermediate, composed of a four-linked, six-membered ring system: first, through a complex rearrangement reaction, MoaA mediates the insertion of C8 of GTP between C2′ and C3′ of the ribose to produce 3′,8-cH$_2$GTP which then MoaC modifies to yield cPMP. As a homodimer, MoaA harbors two [4Fe-4S] clusters per subunit and adopts a partial TIM $(\beta/\alpha)_6$ barrel structure with a hydrophilic channel in the center flanked by a [4Fe-4S] cluster on either side. The N-terminal cluster

coordinates SAM and is likely to be responsible for the production of 5'dA• whereas the C-terminal cluster coordinates the N1 of GTP.[143-145] Mass spectrometry of intermediates derived from deuterated substrates demonstrates that the C-3′ H-atom of GTP is abstracted by Ado•.[146, 147] Furthermore, LCMS analysis identified an intermediate containing the bond between the guanine C8 and ribose C3′ when the GTP analogue 2,3-dideoxyGTP was used as a substrate.[148] These results suggest a mechanism in which the C-3′ radical attacks the C8 of guanosine to form a key C−C bond, which after reduction yields the rearranged intermediate 3′,8-cyclo GTP product. Studies under anaerobic conditions demonstrate that MoaA catalysis ends in the formation of 3′,8-cyclo GTP, which can then be isolated and incubated with MoaC to genetrate cPMP (Figure 20).

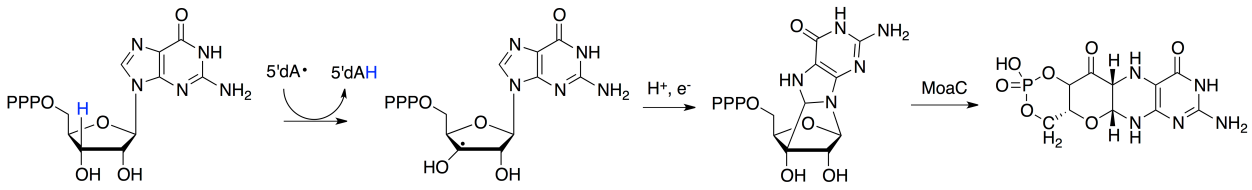

Figure 20. Proposed Mechanism for the Conversion of GTP to 3′,8-cH$_2$GTP by MoaA. In a complex reaction, the first two enzymes in the molybdopterin biosynthetic pathway, MoaA and MoaC, convert GTP into cyclic pyranopterin monophosphate (cPMP).

CHAPTER 2[†]

ROLE OF ACTIVE SITE RESIDUES IN PROMOTING COBALT−CARBON BOND HOMOLYSIS IN ADENOSYLCOBALAMIN-DEPENDENT MUTASES REVEALED THROUGH EXPERIMENT AND COMPUTATION

2.1. Introduction

2.1.1. Mechanism of Adenosyl Radical Formation in Adenosylcobalamin-Dependent Enzymes. Adenosylcobalamin (AdoCbl, coenzyme-B_{12}) is a unique biological cofactor that can function as a stable source of highly reactive free radicals. These are generated by enzymatic homolysis of the cofactor's Co-C bond to yield the carbon-based 5'-deoxyadenosine radical (Ado•) and cob(II)alamin (Figure 1).[15, 16, 18] All AdoCbl-dependent enzymes use Ado• to generate a substrate radical, which initiates a variety of radical-mediated 1,2-rearrangement reactions involving the exchange of a non-acidic hydrogen atom with an electron-withdrawing group (Figure 3). An interesting mechanistic feature of these reactions is that hydrogen abstraction from the substrate by Ado• is closely coupled to Co-C bond cleavage. The homolysis products cob(II)alamin and Ado• are not observed in the *holo*-enzyme indicating that the

[†] The work presented in this Chapter 2 is adapted from:

Román-Meléndez, G. D., Glehn, von, P., Harvey, J. N., Mulholland, A. J., & Marsh, E. N. G. (2014). Role of Active Site Residues in Promoting Cobalt-Carbon Bond Homolysis in Adenosylcobalamin-Dependent Mutases Revealed through Experiment and Computation. Biochemistry, 53(1), 169–177. doi:10.1021/bi4012644

Mutagenesis and kinetic experiments were performed by Román-Mélendez, G. D. and Marsh E. N. G.

Molecular dynamics simulations were performed by von Glehn, P., Harvey, J. N., and Mulholland, A. J.

equilibrium for the homolysis greatly favors geminate recombination. However, it is only during turnover that substrate-based radicals accumulate on the enzyme, implying that the equilibrium constant for homolysis is now close to unity.[17, 149-152] The u.v.–visible spectra associated with AdoCbl's Co(III) core is considerably different than that of the Co(II) present in the cob(II)alamin homolysis product and, accordingly, Co-C cleavage can be followed directly by monitoring the spectral changes associated with the two species.

Pre-steady state stopped-flow experiments have measured the rate of enzymatic Co-C homolysis to be rapid with respect to turnover and, thus, not rate-limiting with $k_{cat} \sim 100\ s^{-1}$. Interestingly, the observed rate of homolysis was found to be significantly slower when deuterated substrates were used to initiate the reaction, even though this is not formally an isotopically sensitive step.[35, 69] This observation was first made for methylmalonyl-CoA mutase, where the use of deuterated methylmalonyl-CoA as substrate decelerated homolysis ~ 20-fold at 25 °C.[153] In glutamate mutase, a very large isotope effect of 28 was observed on cob(II)alamin formation when deuterated *L*-glutamate was used instead of its proteated substrate *L*-glutamate.[33] Similar results were obtained with ethanolamine ammonia lyase.[154] This result can be interpreted by two possible mechanisms. In one, a formally concerted mechanism proposes that Co-C bond homolysis and subsequent substrate hydrogen abstraction occur in a single step, with all bonds formed and broken at the same time. In the other, a kinetically coupled mechanism separates hydrogen abstraction from Co-C hemolysis by proposing a rapid but unfavorable equilibrium between AdoCbl and Ado• is initially established (Figure 1).[155] The more stable substrate-based radical is then generated as Ado• is

siphoned off in a slow and isotopically sensitive step. Regardless, the net result is the same: AdoCbl is consumed at a rate that depends on the rate of hydrogen atom transfer.

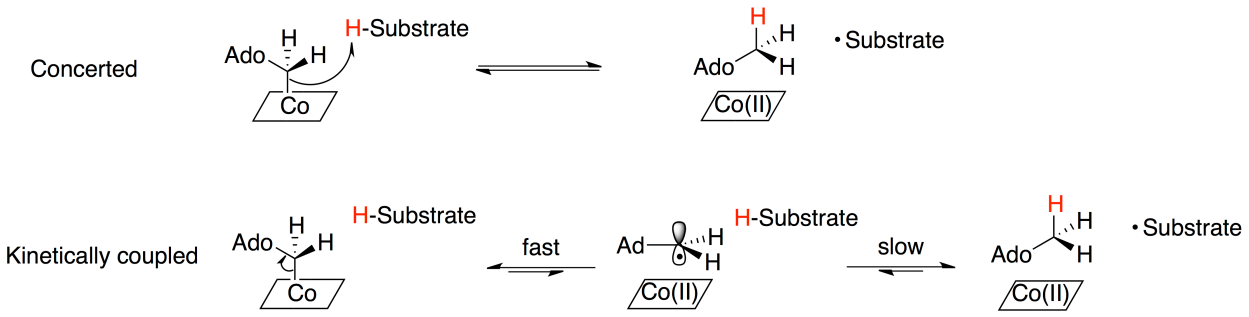

Figure 21. Concerted and Kinetically Coupled Mechanisms in AdoCbl-Dependent Enzymes. Distinction between a concerted mechanism for AdoCbl homolysis and hydrogen transfer from the substrate (top) and a kinetically coupled mechanism for AdoCbl homolysis and hydrogen transfer from the substrate (bottom). In the latter mechanism, an isotope effect on the second, slower step results in a slower apparent rate constant for Co-C bond cleavage in the first step.

Experimentally, it is very hard to distinguish between these two possibilities since both mechanisms predict a kinetic isotope effect. However, other experimental evidence suggests a kinetically coupled mechanism is more likely. EPR[62, 156-163] and crystallographic[71, 164-168] studies on several AdoCbl-dependent enzymes reveal that Ado• must bridge a significant distance of 5-11 Å in order to reach its substrate. Furthermore, crystallographic structures indicate that the distance from the substrate-binding pocket to the 5′-carbon of AdoCbl appears to be too far apart to permit a formally concerted reaction without a major reorganization of the protein′s conformation. Additional support comes from an experiment performed on a catalytically crippled ribonucleotide reductase in which the active cysteine residue responsible for generating the ribosyl radical was mutated. In the presence of an allosteric activator, the inactive

enzyme was still able to epimerize AdoCbl stereospecifically deuterated at the 5′-carbon, providing evidence that Ado• was indeed transiently formed (Figure 22).[169]

Figure 22. Evidence for a Kinetically Coupled Mechanism in AdoCbl Bond Homolysis. Epimerization of stereospecifically deuterated AdoCbl by a catalytically crippled ribonucleotide reductase mutant provides evidence for the transient cleavage of the Co-C bond in the absence of hydrogen transfer.

Finally, as will be discussed further in the next chapter, it seems AdoCbl homolysis may be susceptible to external magnetic fields.[170, 171] The magnetic field affects the rate at which the initially formed singlet radical pair, which can recombine to reform the Co-C bond, converts to the triplet state, which cannot recombine.[172, 173] In ethanolammine ammonia lyase, a significant decrease in catalysis was observed in a static field near 1,200-1,400 Gauss and attributed to change in intersystem crossing rates between the singlet and triplet spin states in the [cob(II)alamin:Ado•] spin-correlated radical pair,[174] which would not exist if Co-C homolysis and substrate H-atom abstraction were concerted.

Kinetic isotope effect (KIE) experiments aimed at studying the transition state of this unusual reaction demonstrate that hydrogen transfer between the substrate and Ado• occurs through quantum tunneling.[175-178] In methylmalonyl-CoA mutase, the deuterium KIE decreases from 50 at 5 °C to 36 at 20 °C. [153, 179] These values are clearly much larger than the semi-classical limit of ~7 and the steep temperature dependence of the KIE indicates a reaction in which tunneling dominates the transfer of protium between substrate and coenzyme whereas the significantly slower deuterium transfer occurs semi-classically.[180, 181] In glutamate mutase, using pre-steady state,

rapid chemical quench techniques, a large inverse *equilibrium* tritium isotope effect of 0.72 was measured suggesting that, despite the 5′-carbon remaining formally sp^3-hybridized, the 5′-Ado-C-H-substrate bonds become significantly stiffer in going from AdoCbl to Ado-H.[182-184] Similarly, a large inverse secondary tritium *kinetic* isotope effect of 0.76 was measured, which in the semi-classical model would be interpreted as a "late" transition state for the observed step.[182] However, when the isotope effect measurements were repeated using deuterated substrate so that Ado-D was formed, the secondary KIE nearly vanished to value of 1.05. Interestingly, the equilibrium secondary isotope effect remained unchanged.[185] In a reaction that involves a large degree of quantum tunneling, these observations are indicative of a transition state in which the 5′-hydrogen atoms adjacent to the hydrogen that is transferred between substrate and coenzyme move in concert (Figure 23).[186]

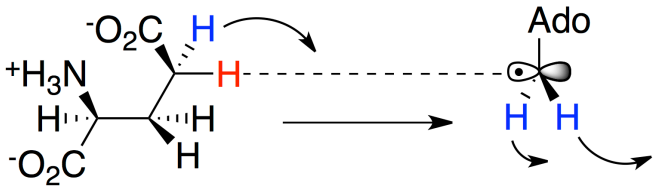

Figure 23. Concerted Motion in the Transition State of the 5′-Hydrogen Atoms Adjacent to the Hydrogen that is Transferred between Substrate and Coenzyme in Glutamate Mutase. Illustration of the coupled motions of primary (red) and secondary (blue) hydrogen atoms involved in the transition state for hydrogen transfer between 5′-Ado radical and glutamate, as deduced from secondary isotope effect measurements.

2.1.2. Computational Studies of Glutamate Mutase. Even though our mechanistic understanding about the pathways these enzymes use in generating their products has grown, a fundamental and important question remains unanswered: How do these enzymes overcome the extremely unfavorable thermodynamics required for Co-C homolysis and harness the resulting highly reactive Ado• radical species towards catalysis? With a Co-C bond dissociation energy of 32 kcal/mol in free solution,

AdoCbl-dependent enzymes facilitate thermolysis of the coenzyme with rate accelerations over the uncatalyzed reaction in free solution of 10^{-9} s^{-1} by 11-12 orders of magnitude.[19, 32, 33, 154] It is generally assumed that, upon substrate binding, a protein-induced distortion of the coenzyme weakens the Co-C bond sufficiently to promote homolysis. However, crystallographic and complementary Raman, u.v.-visible, and magnetic circular dichroism spectroscopies, as well as stopped-flow measurements on cobalamin analogues, have failed to detect a significant distortion of the enzyme bound coenzyme.[39, 41, 42, 187, 188]

Computational studies[189] of these reactions have recently begun to shed light on the origin of such an enormous Co-C homolytic rate enhancement, as well as plausible mechanisms by which the protein is able to achieve such a remarkable stabilization of radical intermediates which, so far, has not been easily addressed by experimentation.[15] Quantum mechanical-molecular dynamics simulations of full enzymatic systems have highlighted the potential role active site residues play in establishing favorable, stabilizing electrostatic interactions with the coenzyme.[190] A detailed study by Jensen and Ryde on glutamate mutase found that in the enzyme, the Co-C bond dissociation energy dropped dramatically to only ~ 4 kcal/mol, compared with an *in vacuo* calculation 34 kcal/mol, which is in good agreement with the solution free value of 32 kcal/mol. When the first step in the reaction was considered (*i.e.*, formation of the 4 glutamyl radical), calculations determined the overall reaction was favorable by ~ 2 kcal/mol, which is also in good agreement with experimental data showing the equilibrium constant for this reaction to be close to unity.[33, 191]

The study was able to separate the energetic contributions made by the protein in lowering the barrier for Co-C homolysis. Some of the contribution was determined to arise from a radical caging effect in which the active site is able to maintain Ado• in close proximity to the corrin ring. Interestingly, the largest effect is attributed to distortion of the coenzyme by the protein, primarily through interactions with the ribosyl moiety that distorts the Co-C5′-C4′ angle, which could not be discerned from the X-ray structure of glutamate mutase as the Co-C bond is cleaved in the structure.[54, 192] However, as discussed below, this effect may not be ruled out as there is not a good structure for the pre-homolysis Michaelis complex and it is unlikely that a crystal structure would trap reactive, strained species if indeed they were formed. Further stabilization is attributed to a preferential stabilization of the cleaved state over the ground state mediated by electrostatic interactions with the ribosyl group that are present only in the Cbl(II) state. Lastly, a minor component contributing to the overall reduction of ~ 30 kcal/mol appears to be the stabilization of the protein structure itself in the cleaved, Cbl(II) state through favorable van der Waals and electrostatic interactions.

Rommel and Kaestner further advanced the idea of electrostatic stabilization in a study that modeled the full glutamate mutase reaction pathway using the complete protein (AdoCbl homolysis was excluded from the calculations since Co-C homolysis is fast compared to the subsequent hydrogen atom transfer reactions).[61] The calculations reveal the hydrogen transfer steps to be rate-limiting in the overall rearrangement with a barrier of 24.2 kcal/mol and qualitatively reproduce the reactions free energy profile determined experimentally.[193] After comparison to the protein-free reaction occurring in water, the model identified several protein residues that appear to significantly alter the

free energy profile of the reaction, mainly though electrostatic effects. Some of these residues had previously been investigated by mutagenesis, allowing the calculations to be compared with experimental data. For example, Glu171, which makes a hydrogen bond with the amino group of the substrate and mutagenesis studies found to be catalytically relevant,[194, 195] was found to assist in catalysis by deprotonating the amino group of the substrate, thereby facilitating the substrate's rearrangement. Other residues of interest are Glu330 and Lys326, which were found to change their hydrogen-bonding pattern to Ado during the hydrogen transfer steps. In particular, hydrogen bonds between Glu330 and the two ribose -OH groups remain stable in simulations that produced the lowest energy barriers. The importance of Glu330 was later demonstrated experimentally by Makins and coworkers when a series of point mutations of this conserved residue in both ornithine 4,5-aminomutase and methylmalonyl-CoA mutase attributed to the weakening of electrostatic interactions between the protein and ribose moiety to an increase in the activation energy barrier for Co−C bond homolysis.[196]

Despite the fact that free radicals are electrically neutral species, experimental and theoretical evidence now points to the importance of electrostatic interactions between the protein, substrate and coenzyme in stabilizing radical intermediates. Since crystallographic[192] and computational[61] studies suggest that the changes in ribose ring conformation is primarily guided by changes in hydrogen bonding to Lys326 and Glu330, we decided to examine the role these two residues play in catalyzing the homolysis of the Co-C bond in glutamate mutase. Specifically, we have combined both computational and experimental approaches to examine the effects of mutating Lys326

and Glu330 on the ability of the enzyme to catalyze homolysis of the Co−C bond and subsequent abstraction of hydrogen from the substrate. This combined approach has allowed changes in the structure and dynamics of the active site, determined computationally, to be correlated with changes in activity determined experimentally.

2.2. Materials and Methods

2.2.1. Materials. The glutamate mutase fusion-protein gene was codon-optimized for expression in *E. coli* with an N-terminal 6x histidine tag and purchased from GenScript subcloned into pET28 expression vector. OptGlmES was expressed and purified by slight modification of the established protocol and assayed as described previously by Barker and coworkers.[197] Point mutations were introduced into the codon-optimized glutamate mutase fusion protein gene (OptGlmES) by William Clay Brown and purified from recombinant *E. coli* as described below for OptGlmES. AdoCbl was purchased from Sigma Chemical Co. Solutions containing AdoCbl were kept in light-proofed vials and handled in dim light so as to avoid photolysis of the coenzyme. *L*-[3,4-^{3}H]-glutamic acid was purchased from Perkin Elmer and unlabeled *L*-glutamic acid from Fisher Scientific. Other materials were purchased from commercial suppliers. Buffers were degassed with nitrogen and allowed to equilibrate in a Coy anaerobic chamber prior to use. Enzyme and AdoCbl stock solutions were made anaerobic by allowing a minimal amount to thaw and equilibrate in the Coy chamber. Radiolabeled glutamic acid stock was made anaerobic by purging with argon.

2.2.2. Heterologous Expression of OptGlmES Mutants. An initial expression screen in which temperature, induction time, and IPTG concentrations were varied was initially performed to establish optimal expression conditions (Figure 24).

Preparation of 1 L culture: 5 mL of sterile LB containing 50 µg/mL kanamycin was inoculated with BL21(DE3) *E. coli* cells containing the OptGlmES appropiate expression vector. The cells were incubated at 37 °C with shaking at 240 rpm overnight. The next morning, the saturated 5 mL overnight was transfered to 1 L of sterile 2xYT media containing 50 µg/mL kanamycin. The 1 L culture was incubated at 37 °C with shaking at 150 rpm until the OD_{600} reached approximately 1.0 (5-6 h). The culture was chilled at 4 °C for 30 min and protein expression was induced by addition of IPTG to a final concentration of 0.1 mM. The culture was further incubated at 18 °C with shaking at 150 rpm overnight (~ 18 h). Cells were harvested by centrifugation at 5,000 rpm for 30 min at 4 °C. Cell pellet was stored at -80 °C until ready for use.

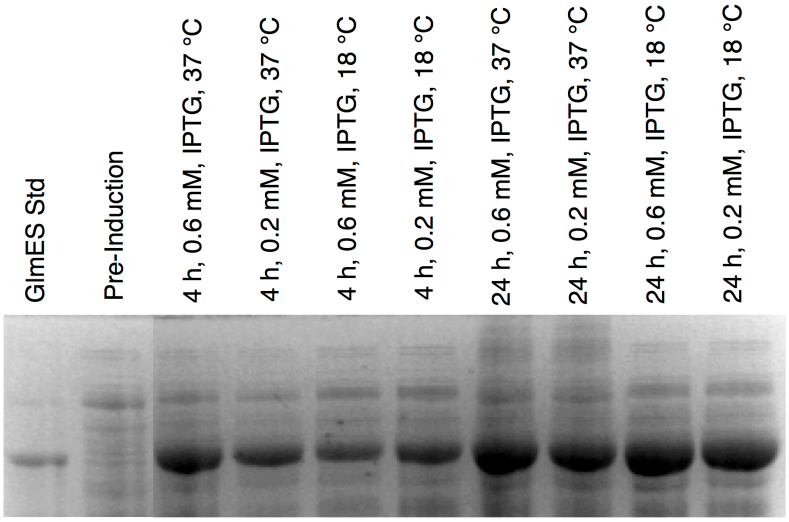

Figure 24. OptGlmES Expression Screen. Mutant expression was similar to that of OptGlmES.

2.2.3. Purification of OptGlmES Mutants. The cell pellet was resuspended in lysis buffer (50 mM Na_2HPO_4, 300 mM NaCl, 5 mM imidazole, 1 mM β-mercaptoethanol, 1 tablet/10 mL complete mini protease inhibitor tablet - *Roche*,

1 mg/mL lysozyme, benzonase nuclease, 1% glycerol, pH 8.0). The suspension was shaken on ice for 30 min and cell lysis completed by sonication. The lysate was centrifuged to remove the cell debris (17,000 rpm, 30 min, 4 °C) and the supernatant loaded onto a 5 mL HIS-Trap (GE) equilibrated in 50 mM Na_2HPO_4, 300 mM NaCl, 5 mM imidazole, 1% glycerol, pH 8.0. The column was washed with 16 column volumes of buffer containing 50 mM Na_2HPO_4, 300 mM NaCl, 20 mM imidazole, 1% glycerol, pH 8.0 and the protein eluted from the resin with 50 mM Na_2HPO_4, 300 mM NaCl, 250 mM imidazole, 1% glycerol, pH 8.0 in approximately six 5 mL fractions (Figure 25).

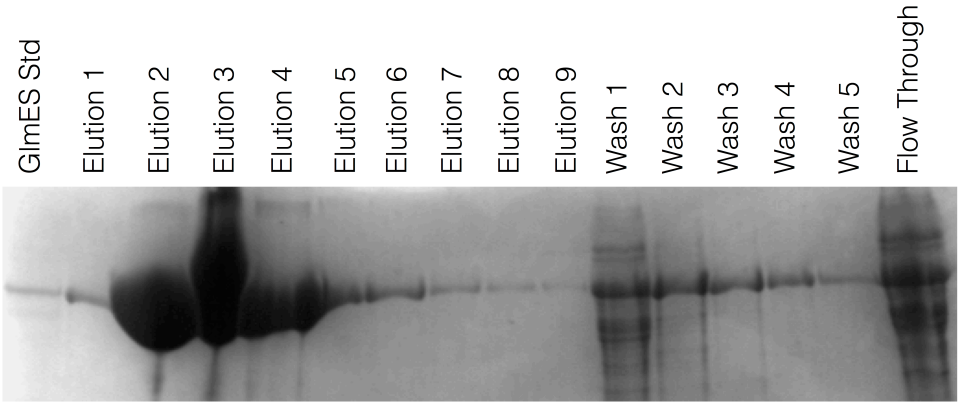

Figure 25. Purification of OptGlmES. Mutant purification was similar to that of OptGlmES.

Fractions containing pure protein (> 95% pure as assessed by SDS-PAGE) were pooled and dialyzed against 10 mM K_2HPO_4, 1% glycerol, pH 8.0 (4x 1 L exchanges over the course of 24 h). The protein was concentrated with a 10 kDa MWCO amicon centrifuge tube and the concentrate diluted with buffered glycerol to make a final concentration of 10 K_2HPO_4, 10% glycerol, pH 8.0. Approximately 80% of the total protein was expressed in soluble form and yielded 90-100 mg/L culture.

2.2.4. Heterologous Expression and Purification of β-methylaspartase.

Preparation of 1 L culture: 5 mL of sterile LB containing 100 µg/mL ampicillin was inoculated with BL21(DE3) *E. coli* cells containing the β-methylaspartase expression vector. The cells were incubated at 37 °C with shaking at 240 rpm overnight. The next morning, the saturated 5 mL overnight was transfered to 1 L of sterile 2xYT media containing 100 µg/mL ampicillin. The 1 L culture was incubated at 37 °C with shaking at 150 rpm until the OD_{600} reached approximately 1.0 (5-6 h). Protein expression was induced by addition of IPTG to a final concentration of 0.6 mM and the culture was further incubated at 37 °C with shaking at 150 rpm for 4-5 h. Cells were harvested by centrifugation at 5,000 rpm for 30 min at 4 °C and the pellet stored at -80 °C until ready for use. Purification was performed in a manner similar to OptGlmES. Approximately 90% of the total protein was expressed in soluble form and yielded approximately 75 mg/L culture.

2.2.5. Spectroscopic Assay of OptGlmES. Enzymatic activity was measured spectroscopically by slight modification of the method described by Barker and coworkers[197] in which the formation of 3-methylaspartate was coupled mesaconate production through the action of methylaspartase. The steady-state kinetics of OptGlmES were determined by varying the final concentration of *L*-glutamate (C_f = 0.25, 0.50, 1.00, 2.50, 10.00 mM) in a final volume of 500 µL containing 0.5 µM enzyme, 50 mM K_2HPO_4, pH 7.0, 10 mM KCl, 1 mM $MgCl_2$, and 2 units coupling enzyme. For each range of substrate concentrations, adenosylcobalamin was varied to final concentrations of 25, 15, 10, and 6 µM. Assays were started by the addition of

substrate and carried out at room temperature. After an initial lag phase the rate was linear for several minutes.

2.2.6. Spectroscopic Assay of OptGlmES Mutants. Initially, the mutants seemed to be unstable in the original assay buffer and would precipitate upon addition of $MgCl_2$. A buffer system containing 10 mM tris-HCl, pH 8.0, 10 mM KCl, 1 mM $MgCl_2$, and 10% glycerol was found to be optimal for the mutant enzymes as no precipitation was observed over 24 h at room temperature. The enzyme's stability was confirmed by monitoring the absorbance at A_{280}. No significant change in absorbance was observed over 24 h. Assays were conducted in 500 µL at room temperature, initiated by the addition of B_{12} (C_f = 5 µM AdoCbl) and contained: 5 µM enzyme, 5 mM *L*-glutamate, 10 mM tris, pH 8.0, 10 mM KCl, 1 mM MgCl2, 10% glycerol, 10 units coupling enzyme.

2.2.7. Equilibrium Ultrafiltration Measurements. AdoCbl (50 µM) was mixed with protein (50 µM) in 10 mM tris-HCl buffer and 10% glycerol (pH 8.0) in a total volume of 500 µL. After incubation for 15 min at 37 °C, the sample was spin-filtered through a Microcon-30 filter until 75 µL had passed through the filter. The absorbance at 522 nm was recorded for the retentate and filtrate. K_d values were calculated assuming the ultrafiltrate absorbance represents the concentration of free AdoCbl and the retentate absorbance represents free and enzyme-bound AdoCbl.

2.2.8. Enzymatic Synthesis of 5'-^{3}H-AdoCbl. Exchange of tritium from glutamate into the 5'-adenosyl carbon of unlabeled AdoCbl was achieved by modification of a previously reported method.[198] Reagents were used in final concentrations of 10 mM tris-HCl at pH 8, 10% glycerol, 50 µM enzyme, 250 µM AdoCbl, 100 µM unlabeled *L*-glutamic acid, 75 µCi/mL [3,4-^{3}H]-glutamic acid (specific

activity of 184 Ci/mol at the exchangeable position) in a total volume of 1.2 mL. Assay mixtures were prepared in the dark inside a Coy anaerobic chamber to minimize exposure to oxygen and deter hydroxocobalamin formation. The reaction was started by addition of 100 µL radiolabeled glutamic acid using a Hamilton syringe and allowed to age at 37 °C. Over the course of ~ 4 h, 100 µL aliquots were extracted using a Hamilton syringe and quenched on ice with 25 µL of 500 mM HCl to make a final quench volume of 125 µL. Aliquots were frozen in liquid nitrogen and stored at -20 °C until ready to recover AdoCbl by reverse-phase HPLC. No protein precipitation was observed during the course of the assay.

2.2.9. Purification of AdoCbl. AdoCbl was purified by HPLC on a Vydac 201SP54 250 x 4.6 mm C18 reverse-phase column with a 5 µ particle size. Quenched time points were centrifuged to remove any precipitation and 100 µL injected onto the column (pre-equilibrated in 0.1% TFA / 5% acetonitrile) using a 100 µL injection loop. AdoCbl was eluted using a gradient of 0-5 min, 0% B; 5-20 min, 0-70% B; 20-30 min, 70-95% B, 30-40 min, 95-0% B at a flow rate of 1 mL/min. AdoCbl was detected by monitoring absorbance at 360 nm (Solvent A = 0.1% TFA / 5% acetonitrile in water, Solvent B = 0.1% TFA in acetonitrile).

2.2.10. Analysis of Radiolabeled AdoCbl. Radiolabeled AdoCbl was recovered from reaction mixtures by HPLC as described above and the entire AdoCbl-containing peak collected into scintillation vials. The absolute tritium content in decays per minute (DPM) of the isolated AdoCbl was then determined using the LS6500 Beckman liquid scintillation counter's factory installed quench curve.

2.3. Results

2.3.1. Choice of K326 and E330D Mutants. The high-resolution X-ray structure of active glutamate mutase reported by Gruber and coworkers[192] provides insight into how these enzymes safely guide the highly reactive Ado• from cobalt to the substrate while avoiding potentially harmful side reactions. It is proposed that the anchoring of the purine ring coupled to the constrained ribose pseudo-rotation allow for a highly controlled trajectory which can safely guide the highly reactive 5'-deoxyadenosine radical from cobalt to substrate without any pernicious side reactions by either forming stronger hydrogen bonds with the ribose ring or by forming an increased number of hydrogen bonds.[190, 191] Even though the enzyme was crystallized solely in the presence of AdoCbl and glutamate, the electron density demonstrated a 30% to 70% mixture of glutamate and the methylaspartate product suggesting the enzyme had turned over during the crystallization process. Similarly, the ribose ring of the adenosyl moiety exists in two distinct conformations already dissociated from the corrin's cobalt atom. In one, species A (40% of the electron density), the 5'-carbon is directed toward the cobalt atom at a distance of 3.2 Å and shows the ribose moiety in a C2'-endo conformation. The other, species B (60% of the electron density), is in a ribose C3'-endo conformation and, thus, has the 5'-carbon at an increased distance of 4.2 Å from the cobalt atom. The difference between the ribose conformers shows a net displacement of the 5'-carbon from the cobalt atom toward the substrate, positioning it well within van der Waals distance of the *pro*-S hydrogen of glutamate (Figure 26).

The spatial orientation and hydrogen-bonding pattern (inferred by analyzing the geometry of the chemical environment)[199, 200] of the purine ring is nearly identical in both

conformations: N6 hydrogen bonds to the backbone carbonyl oxygen atom of Gly68 and Asn123 while N7 is hydrogen bonded to one of the corrin's acetamide side-chains (N40). However, the interactions of the ribose ring vary significantly between both conformers. Species A is stabilized by a hydrogen bond between the ribose O2' and the O28 on a corrin side-chain amide. It is also stabilized by a hydrogen bond between O3' and Lys326, as well as O3' and Glu330. Species B has rotated about the glycosidic bond by ~ 25° and now has strong hydrogen bonds exclusively between both the ribose O2' and O3' hydroxyl groups and Glu330.

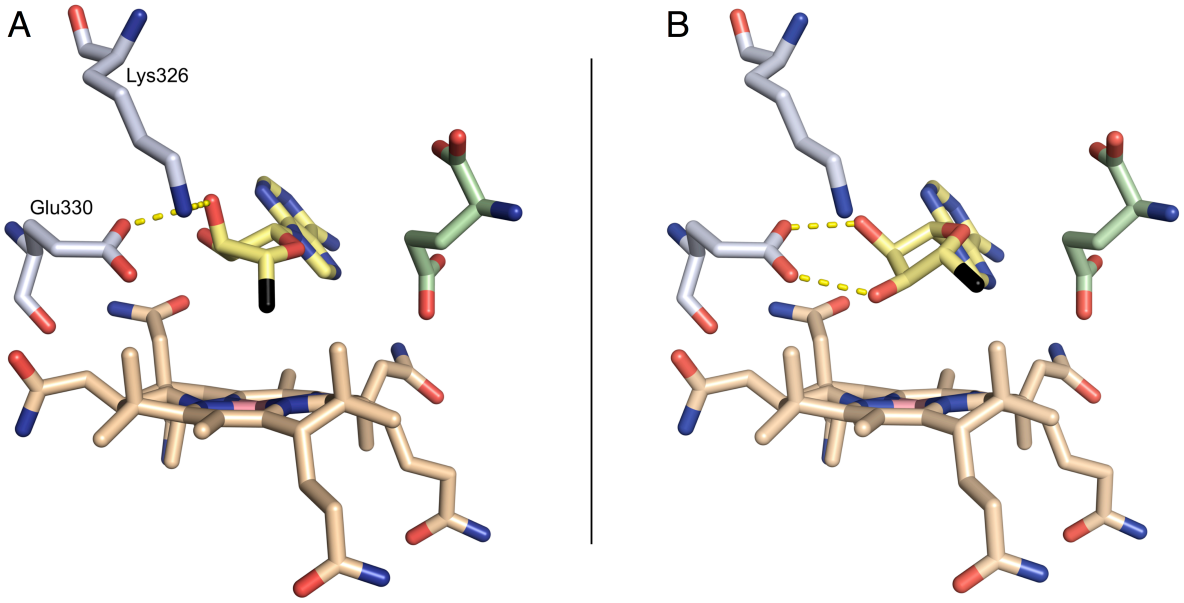

Figure 26. Key Interactions in the Active Site of Glutamate Mutase. Hydrogen bonding interactions are shown as yellow-dotted lines. Residues that interact with the Ado (yellow) moiety are shown in grey. The corrin ring is shown in wheat with the cobalt center in magenta. The corrin's dimethylbenzimidazole tail has been omitted for clarity. The AdoCbl 5'-carbon atom is shown in black, nitrogen atoms in blue, and oxygen atoms in red. As referred to throughout the text, species A is labeled "A" and species B is labeled "B" in the figure above.

Glu330 is conserved in the structures of AdoCbl-dependent mutases,[164, 192, 196, 201] indicating that this residue plays an important role in the mechanism of homolysis. Glu330 has been proposed to facilitate homolysis by stabilizing the dissociated state, either by forming stronger hydrogen bonds with the ribose ring or by forming an increased number of hydrogen bonds. However, it could also be important for

positioning the ribose ring to facilitate abstraction of hydrogen from the substrate. Lys326 is not conserved, but is the only other side-chain to directly interact with the ribose group, suggesting it is also important for catalysis. To test these proposals, we constructed a series of enzyme variants at Lys326 and Glu330 and determined their effect on catalysis *in vitro* and on the structure and dynamics of the active site *in silico*. We then examined whether the experimentally determined changes in activity correlate with changes observed in various structural parameters derived computationally.

As the overall position of the ribose ring is dictated by the interactions it makes with the K326 and E330 side-chains, five mutations were introduced into OptGlmES – K326Q, K326M and E330D, E330A, E330Q – in order to examine how these residues interact with the ribose ring and the role they play in Co-C bond homolysis. The Lys326Met mutation was chosen because the hydrophobic side-chain of methionine mimics that of lysine, but removes the hydrogen bonding interaction with the O2' oxygen on the ribose ring. The Lys326Gln mutation reduces the side-chain length and removes the positive charge, but the amide nitrogen retains the potential to act as a hydrogen bond donor to the 2′-hydroxyl group. Lysine to arginine, which would have arguably been the most conservative mutation, was omitted because using the proteins crystal structure to model in the mutation seemed to create destabilizing steric clashes in the protein's active site. The glutamate to aspartate mutation represents the most conservative mutation of the set. Despite it being one carbon atom shorter (moves the carboxylate ~ 1 Å from the ribose hydroxyl groups), aspartate retains the negative charge of glutamate and is still able to hydrogen bond with both O2' and O3' hydroxyl groups. Apart from being isosteric with glutamate, Glu330Gln was chosen because

while removing the side-chain's negative charge, glutamine still retains the ability to act as a hydrogen bond donor and acceptor. The glutamate to alanine mutation can probe the removal of this residue altogether by removing the possibility of hydrogen bonding, thus serving as a "loss of function" mutation.

2.3.2. Initial Mutant Activity Assays. The first goal was to establish kinetic constants for the OptGlmES mutants. Since the two subunits of the active *holo*-enzyme assemble in a kinetically complex process, the mutations were incorporated into the "single-subunit" glutamate mutase (OptGlmES) which has the S and E subunits genetically fused by an 11 amino acid $(Gly\text{-}Gln)_5$-Gly linker (Figure 27).[40]

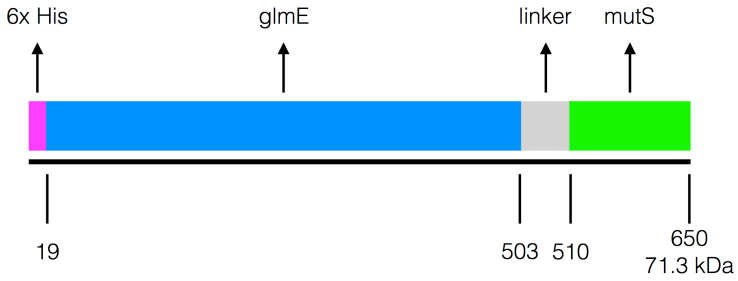

Figure 27. Design of OptGlmES Construct. To facilitate mechanistic and structural studies of glutamate mutase, the *mut*S subunit gene from *C. tetanomorphum* was genetically fused to the C-terminus of the *glm*E subunit gene from *C. chochlearium* through an 11 amino acid $(Gly\text{-}Gln)_5$-Gly linker segment.

This avoids the complications associated with concentration-dependent dissociation of the protein subunits making the kinetic interpretations more straightforward. Characterization of codon-optimized, N-terminally HIS-tagged OptGlmES showed it behaves similarly to the two-subunit wild-type[197] and the non-tagged GlmES[40] enzymes (Figure 28, Table 1).

[AdoCbl] (μM)	$k_{cat}(s^{-1})$	K_M(mM)
25	1.84±0.05	0.47±0.04
15	1.74±0.02	0.39±0.02
10	1.45±0.02	0.49±0.03
6	1.13±0.06	0.35±0.07

Table 1. OptGlmES Kinetic Parameters. Kinetic parameters were obtained by fitting the rate data to the Michaelis-Menton equation $v_0 = V_{max}*[S]/(K_M+[S])$. The error associated with the data is reported as its standard error.

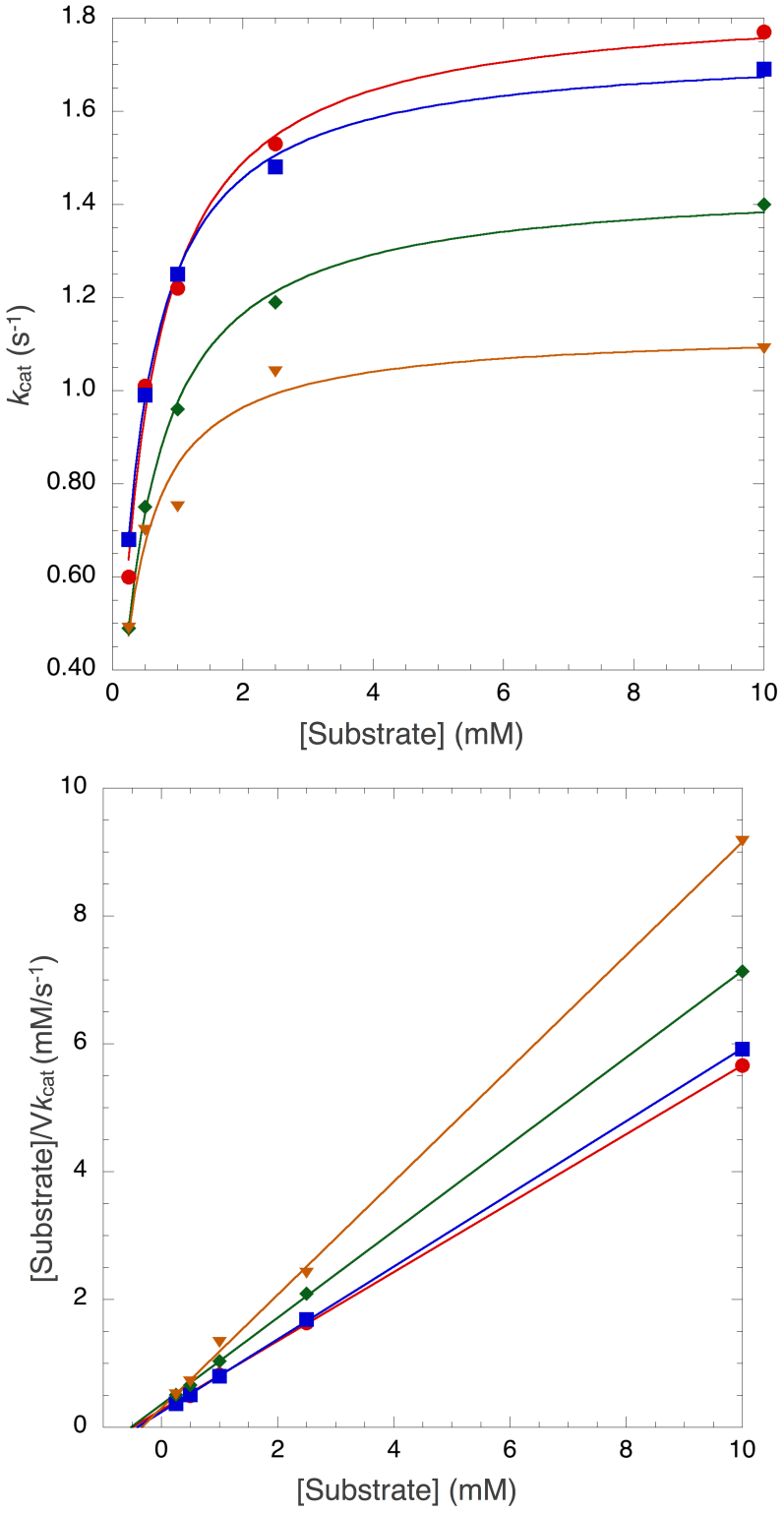

Figure 28. OptGlmES Steady-State Kinetics. Michaelis-Menten (top) and Hanes Plots (bottomt) for OptGlmES at varying concentrations of AdoCbl. Michaelis-Menten plot was derived by fitting the individual initial rates for each concentration of AdoCbl to $v_0 = V_{max}*[S]/(K_M+[S])$. Hanes plot was derived by fitting the individual initial rates for each concentration of AdoCbl to $[S]/v_0 = [S]/V_{max}+K_M/V_{max}$. Similar to the previous charactetrization of the original GlmES fusion protein, the pattern lines intersecting the X-axis indicates that binding of *L*-glutamate does not alter the affinity of the enzyme for AdoCbl for the N-terminally tagged 6x His OptGlmES. [AdoCbl] (μM): 25 (●), 15 (■), 10 (◆), 6 (▼).

Glutamate mutase was assayed using the spectroscopic assay described by Barker and coworkers,[197] in which the reaction is made irreversible by coupling the formation of 3-methylaspartate to the production of mesaconate using 3-methylasparatase as coupling enzyme. The reaction is followed in real time by monitoring the increase in absorbance at 240 nm corresponding to the formation of mesaconate (Figure 29). Under the assay conditions of 5 μM enzyme, 5 μM AdoCbl, 10 mM tris, pH 8.0, 10 mM KCl, 1 mM $MgCl_2$, 10% glycerol, 1 μM coupling enzyme, and 10 mM glutamate, none of the OptGlmES mutants showed any detectable signs of activity (Figure 30). After various conditions were examined, the concentrations of OptGlmES and AdoCbl were empirically chosen so as to have the largest amount of enzymes present in the assay without saturating the detector's response at 240 nm, while keeping AdoCbl at least equimolar. Nevertheless, the introduction of these mutations proved to be highly deleterious for activity. It was concluded that the mutant enzymes possess significantly less than 1% of the OptGlmES activity.

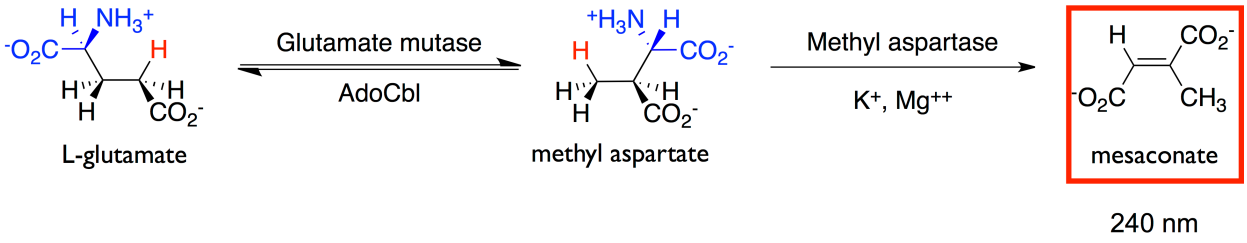

Figure 29. Design of OptGlmES Spectroscopic Assay. The reaction catalyzed by glutamate mutase is coupled to the formation of mesaconate by methyl aspartate and is followed in real time by monitoring the formation of mesaconate at 240 nm.

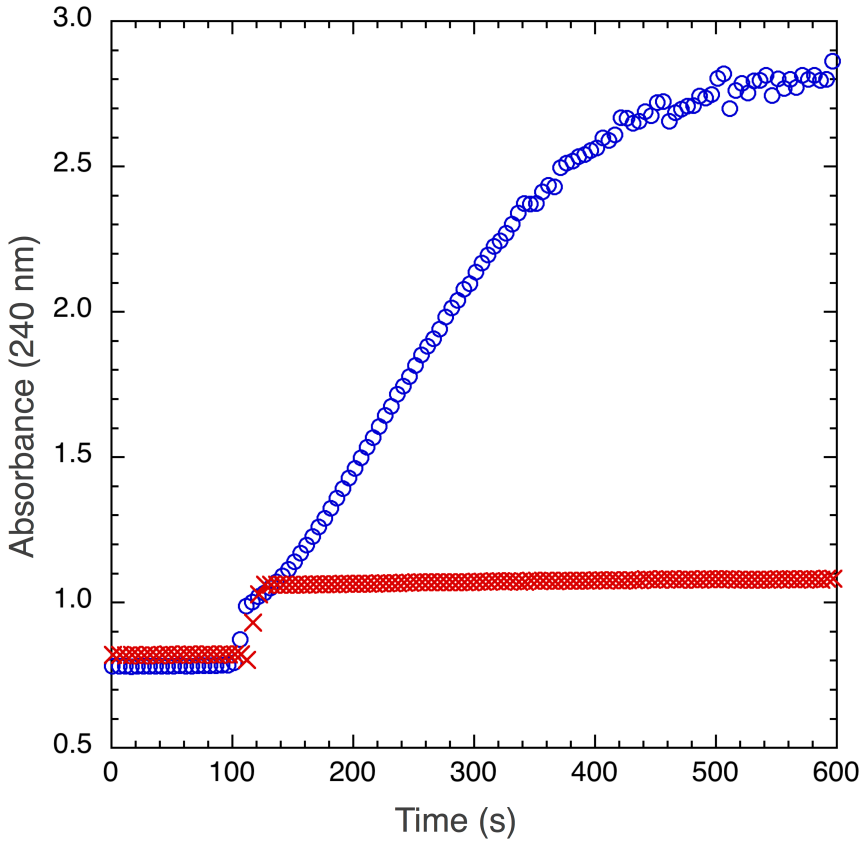

Figure 30. Spectroscopic Assay of the OptGlmES Mutant Enzymes. Representative traces of OptGlmES (o) and the K326Q (x) mutant enzyme. The first ~ 100 s represent the assay background rate. The reaction was initiated by the addition of AdoCbl as evidenced by the break in the trace and a corresponding increase in absorbance due to the cofactor. Similar results obtained with the other mutant enzymes and possess significantly less than 1% of the wild-type activity.

2.3.3. Formation of Cob(II)alamin as an Indicator of Co-C Bond Cleavage.

As AdoCbl undergoes homolysis of the Co-C bond, the cobalt atom is formally reduced from Co(III) to Co(II) and the spectral differences between cob(III) and cob(II)alamin are well-characterized by a concomitant 520 nm decrease and 420 nm increase in absorbance.[36] Figure 31 shows the absorption spectrum for AdoCbl bound to OptGlmES following substrate induced homolysis under anaerobic conditions. The distinct isosbestic points at 395 and 585 nm indicate a clean conversion of AdoCbl to cob(II)alamin over the time it takes to add the substrate without signs of side reactions

to form hydroxocobalamin (see below). Since glutamate mutase only builds up a detectable amount of cob(II)alamin during steady-state turnover, the formation of cob(II)alamin can be used as a proxy for activity by monitoring these spectral changes.

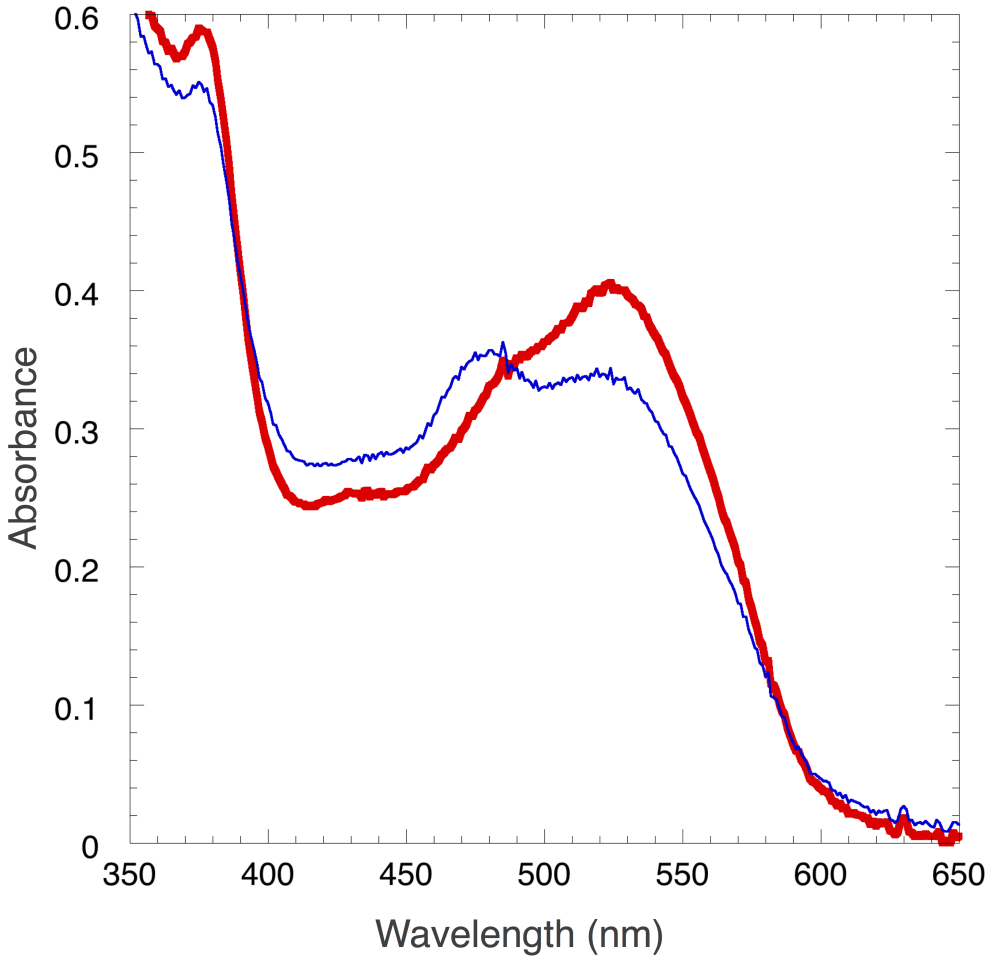

Figure 31. U.V.-Visible Spectra Showing the Formation of Cbl(II) on OptGlmES. Sample was prepared in a Coy anaerobic chamber and spectra taken using a cuvette fitted with septa. The red trace shows 25 μM *holo*-enzyme prior to addition of substrate, blue trace shows 25 μM *holo*-enzyme after the addition of glutamate to 10 mM. Cob(II) is already formed within the time it takes to add the substrate, mix, and re-record the spectra.

Figure 32 shows the spectra of 50 μM K326Q mutant incubated with 75 μM AdoCbl in 10 mM tris-HCl, 10% glycerol, pH 8.0 before and after the addition of 10 mM glutamate under anaerobic conditions over the course of 1 h at 37 °C. The spectra

show that addition of substrate does not lead to any significant spectral changes indicating that cob(II)alamin, if formed, must be present at very low concentrations. Similar results were obtained for the other mutant enzymes and are consistent with the prediction that Glu330 and Lys326 stabilize the homolytic state.

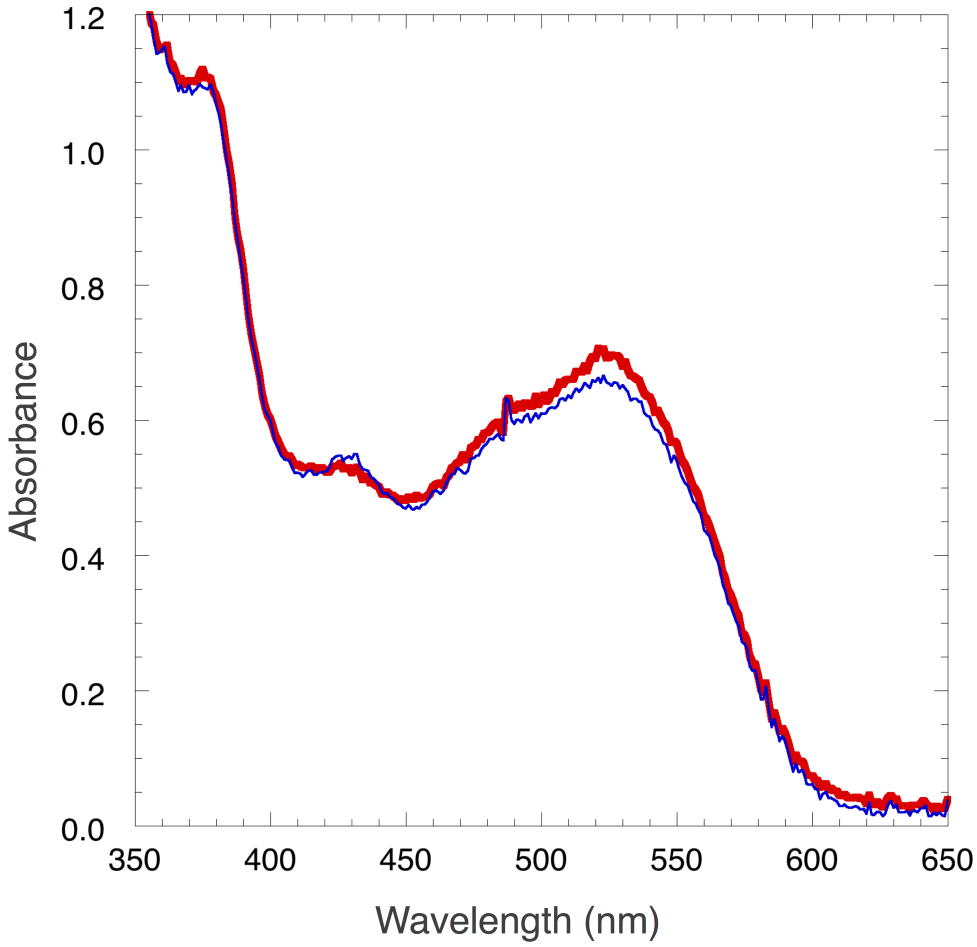

Figure 32. UV-Visible Spectra Probing the Formation of Cbl(II) on the K326Q Mutant at 37 °C. Sample was prepared in a Coy anaerobic chamber and spectra taken using a cuvette fitted with septa. The red trace shows 50 μM *holo*-enzyme prior to addition of substrate, blue trace shows 50 μM *holo*-enzyme after the addition of glutamate to 10 mM over the course of 45 min. Similar results were obtained with the other mutants.

2.3.4. Formation of HOCbl as a Proxy for Co-C Bond Cleavage. During aerobic turnover, a portion of the AdoCbl is irreversibly degraded to hydroxocobalamin (HOCbl) in a slow, oxidative side reaction of cob(II)alamin (Figure 33).[202] This

degradation can be monitored spectroscopically by following the changes in spectral properties associated with the two distinct species, even if Cbl(II) is formed only at low steady-state concentrations: specifically an increase in absorbance of the prominent peak at 340 nm that occurs as AdoCbl is oxidized to HOCbl (Figure 34).

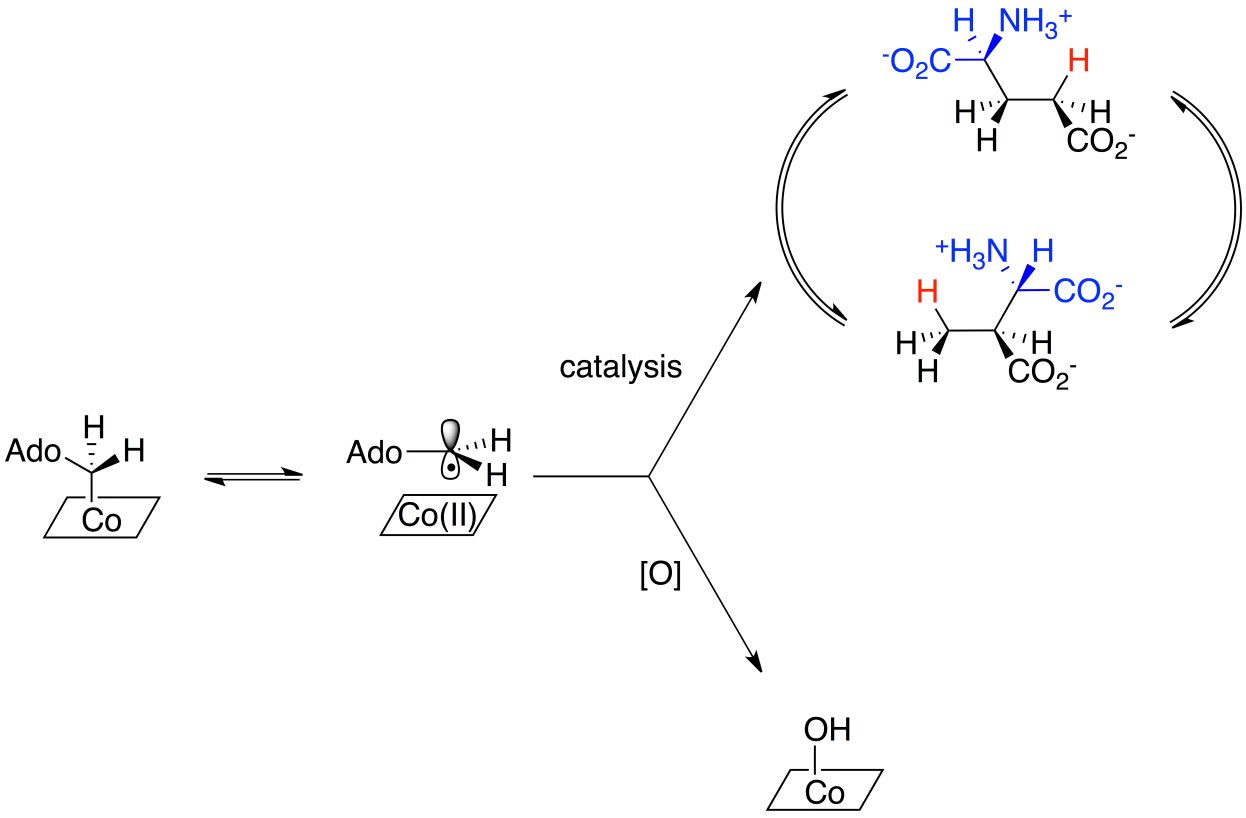

Figure 33. Oxidation of AdoCbl to HOCbl during OptGlmES Turnover. As the reaction proceeds, cob(II)alamin builds up on the enzyme and a portion gets oxidized to HOCbl.

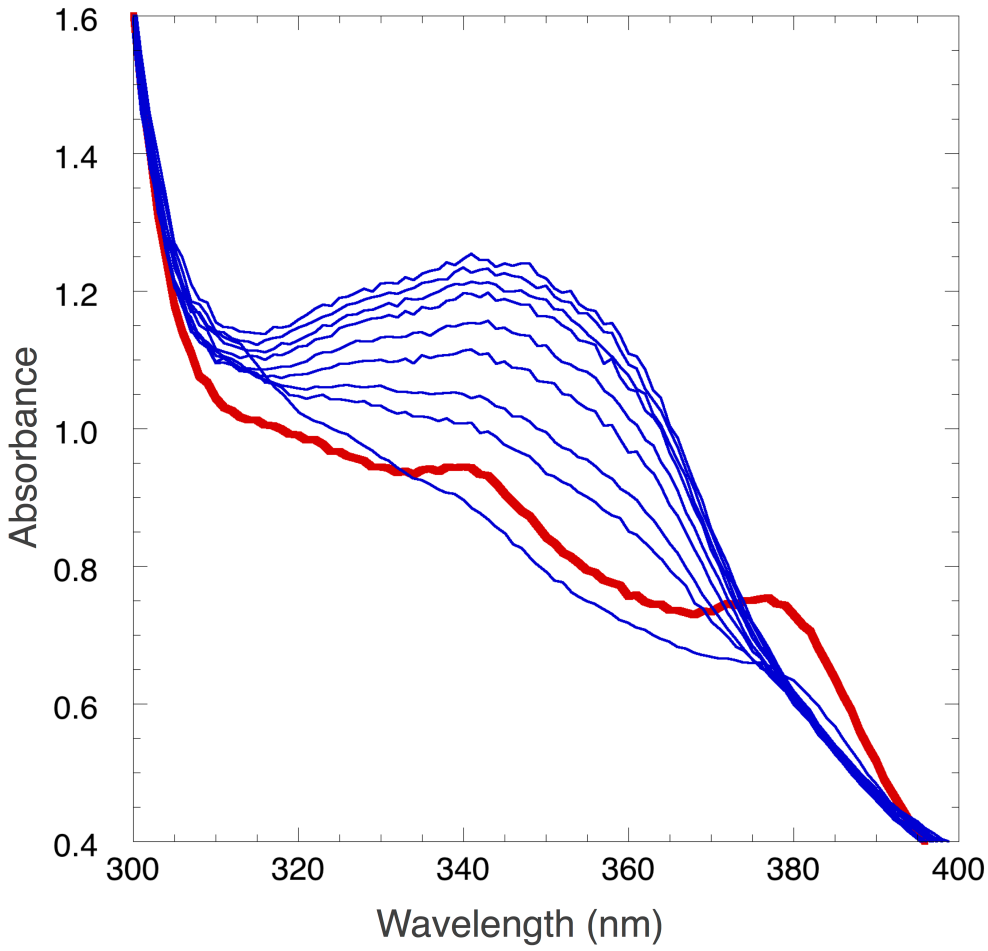

Figure 34. Oxidation of AdoCbl to HOCbl in OptGlmES. Time course showing the enzymatic oxidation of AdoCbl to HOCbl. The red trace shows 50 μM GlmES *holo*-enzyme prior to the addition of substrate. Blue traces show the formation of HOCbl over 8 min after the addition of substrate to 50 mM.

Since this side reaction is strictly enzyme-dependent, formation of HOCbl can be used as a proxy for enzyme activity. Figure 35 shows the spectra of 25 μM E330D mutant aerobically incubated with 50 μM AdoCbl in 10 mM tris, 10% glycerol, pH 8.0 before and after the addition of 50 mM *L*-glutamate over the course of 24 h at room temperature. No HOCbl could be detected as evidenced by the lack of an absorbance change at 340 nm after 24 h upon incubation of the mutant with substrate (similar results were obtained for the other mutant enzymes). However, HOCbl formation was evident after

several minutes upon incubation of wild-type *holo*-glutamate mutase under similar conditions.

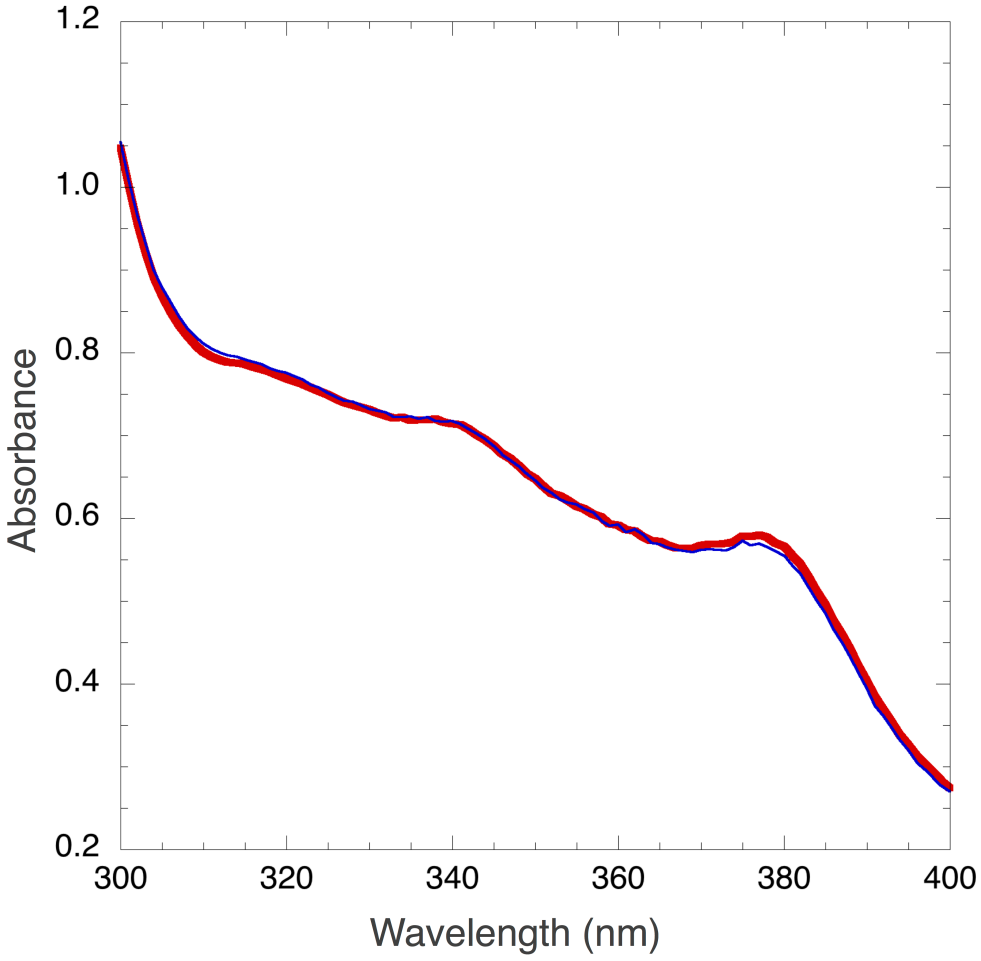

Figure 35. Oxidation AdoCbl to HOCbl in OptGlmES Mutants. Time course showing the first 2 h (blue trace) for the enzymatic-dependent oxidation of AdoCbl to HOCbl by the E330D mutant. Further incubation over 24 h still showed no evidence of HOCbl formation. *Holo*-enzyme is represented by the red trace. Similar results were obtained with the other mutants.

2.3.5. Experimental Design of a Tritium Exchange Assay between Glutamate and AdoCbl. In light of the mutant proteins not displaying any activity using the spectroscopic methods described thus far, a much more sensitive activity assay was developed based on the exchange of tritium from substrate to AdoCbl with the goal of being able to correlate the rate at which AdoCbl incorporates tritium to the rate of Co-C

homolysis and subsequent hydrogen abstraction. During the mechanism of AdoCbl-dependent isomerizations, the hydrogen abstracted from the substrate and the hydrogen atoms at the 5′-position of AdoCbl can exchange positions (Figure 36).[198]

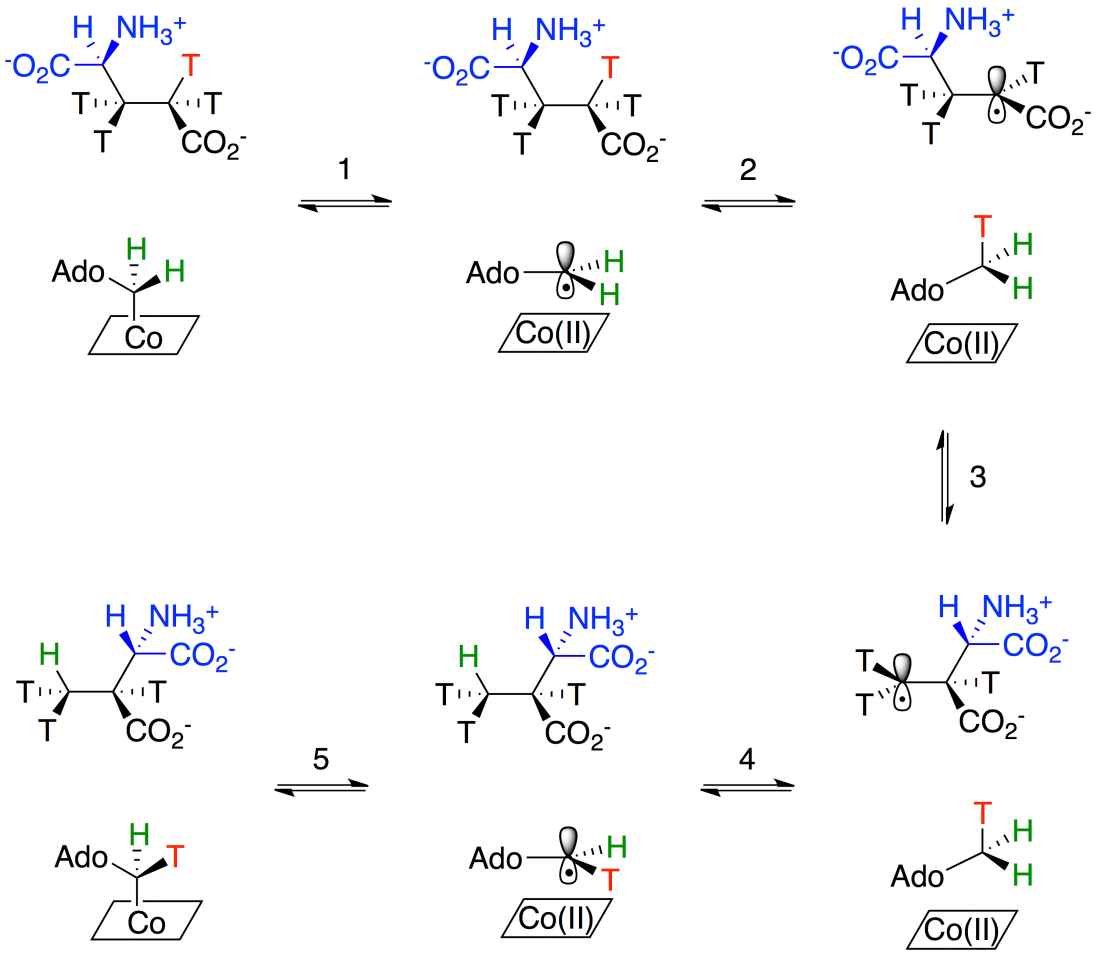

Figure 36. Mechanistic Scheme of the Exchange of Tritium between Substrate and AdoCbl in Glutamate Mutase. The transfer of tritium between AdoCbl and substrate in the reaction catalyzed by glutamate mutase was examined to investigate the activity of the OptGlmES mutants.

Measurements of deuterium and tritium kinetic isotope effects on wild-type glutamate mutase indicate that AdoCbl homolysis and hydrogen abstraction are kinetically coupled[33] in the enzyme and that these steps are partially rate-determining for protium and substantially rate-determining for tritium.[193] The failure to detect any

significant concentration of Cbl(II) in the experiments noted above implies that the mutations destabilize the dissociated coenzyme and, thus, recombination must be much faster than homolysis in the mutant enzymes. Under these conditions, provided that the exchange reaction does not approach equilibrium, the initial rate of incorporation of tritium into AdoCbl reflects the rate of homolysis and hydrogen abstraction.

The glutamate used in our experiment is tritiated at carbons 3 and 4 and, therefore, has the potential to exchange tritium at three of the four tritiated positions as the reaction approaches equilibrium. To make the assumption that one Co-C bond-breaking event correlates to an AdoCbl tritium incorporation event, we must ensure the reaction only proceeds in the forward direction to prevent tritium from making multiple passages through the enzyme. At equilibrium, the specific activity of AdoCbl will approach that of the starting glutamate and, thus, comparison of the two provides a way to probe the extent of the reaction. Initial experiments using 50 μM *holo*-mutant, 100 μM carrier *L*-glutamate and 50 μCi/mL [3,4-^{3}H]-*L*-glutamate at 0.5 Ci/mmol in 10 mM tris-HCl, 10% glycerol, pH 8.0 demonstrated that AdoCbl incorporated at most 4% of the tritium atoms in the substrate's exchangeable position establishing the reaction to be far from equilibrium (Table 2).

	Rate (k_T)					
Mutant	DPM/min	nM/min	$s^{-1}(x10^{-3})$	*WT/Mutant	Δ Δ G‡ (kcal/mol)	%Tritium Incorporated
E330Q	1,509±78	37±2	50±2	100	3	4.0
E330D	564±53	14±1	20±1	250	3	0.9
K326M	290±3	7.0±0.1	8.0±0.1	625	4	0.9
E330A	29±1	0.70±0.03	0.90±0.04	5,556	5	0.1
K326Q	24±1	0.60±0.02	0.70±0.02	7,143	5	0.1

Table 2. Apparent Rate Constants of Tritium Exchange (k_T) by OptGlmES Mutants. Wild-type k_T is calculated to be 5,000±100 s^{-1} from Chih, H.-W., and Marsh, E. N. G. (2001) Biochemistry 40, 13060−13067.

This indicates that the exchange of tritium back to glutamate remained negligible and thus, the requirement that the measurement reflect the initial rate of tritium incorporation is met. Finally, the experiments used high concentrations of enzyme (50 μM) and coenzyme (250 μM) in order to minimize possible complications resulting from AdoCbl dissociating from the enzyme. The effective concentration of 50 μM *holo*-enzyme is 25-fold higher than the wild-type[198, 203] K_d of 2 μM for AdoCbl (as well as in OptGlmES, see section 2.3.8) and exchange of AdoCbl is known to be similar in GlmES.[40] Thus, dissociation of AdoCbl from the mutants is unlikely to contribute to the kinetics of tritium incorporation.

2.3.6. Rates of Tritium Exchange into AdoCbl. Exchange of tritium into AdoCbl from [3,4-^{3}H]-*L*-glutamate was accomplished as described in the methods section and the absolute AdoCbl tritium content for each quenched time point determined by liquid scintillation counting using the factory installed tritium quench curve. The rate at which tritium is incorporated into AdoCbl was then determined by plotting the absolute DPM as a function of time for each quenched time point and fitting the data using Kaleidagraph's linear fit tool. Figure 37 shows AdoCbl tritium incorporation is clearly linear with time up to several hours and demonstrates that, despite being unable to detect turnover using standard spectroscopic methods, the mutant enzymes are indeed able to labilize the Co-C bond. The rates in decays per minute per minute (DPM/min) obtained from the linear fit are shown in Table 2. The results demonstrate that the mutants are severely crippled as AdoCbl incorporated at best 4% of the total tritium atoms in the substrate's exchangeable position over the course of several hours.

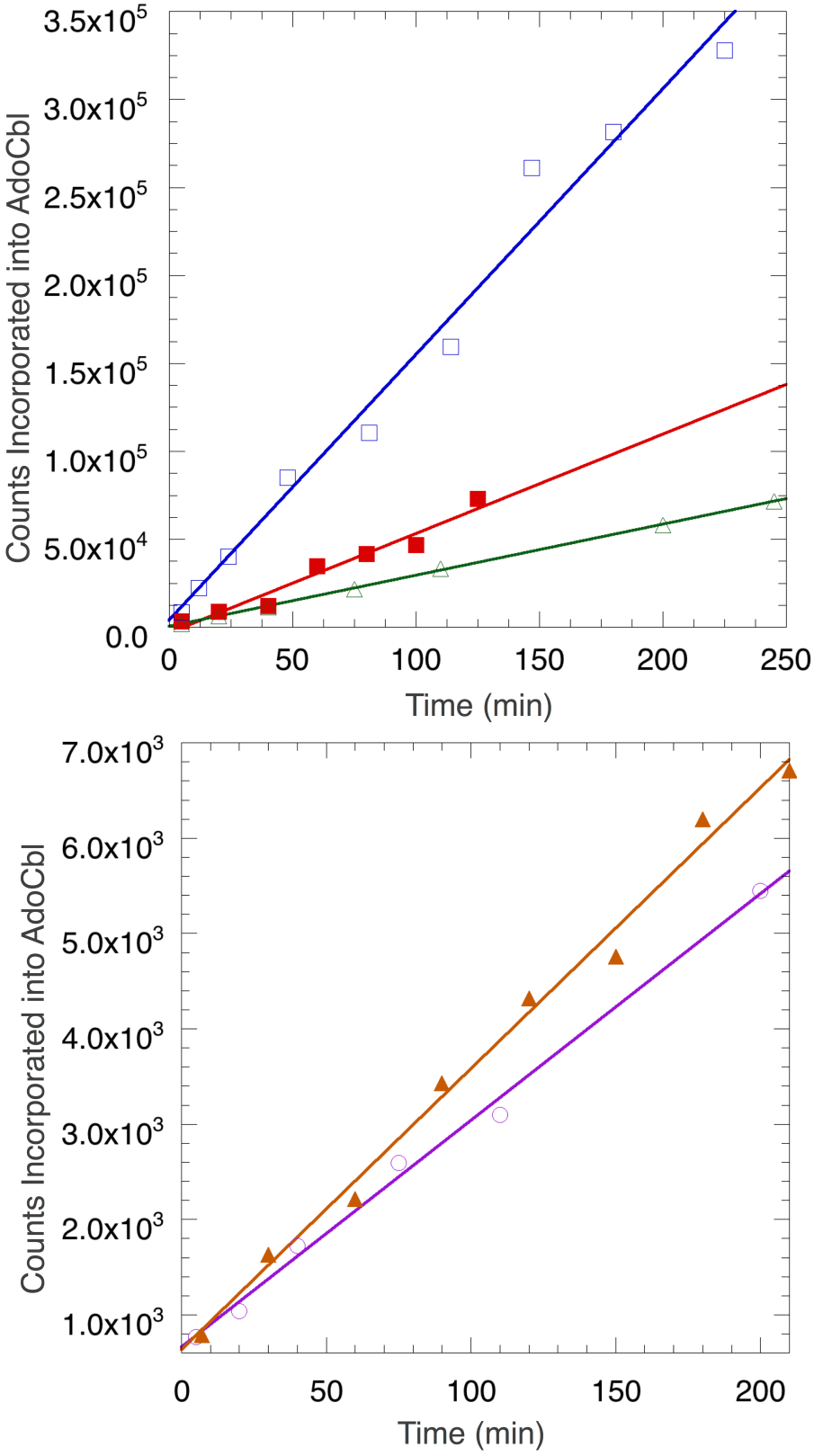

Figure 37. Rates of Tritium Incorporation into AdoCbl by OptGlmES Mutant Enzymes. Glu330Gln (□), Glu330Asp (■), Glu330Ala (▲), Lys326Met (△), and Lys326Gln (○).

In contrast, wild-type achieves incorporation of ~ 50% within 30 min.[198] Control experiments, which omitted enzyme, ruled out the non-enzymatic exchange of tritium into AdoCbl. Therefore, the results obtained can be directly correlated to the rate at which the Co-C bond is being leaved and successfully validate the extreme sensitivity of the assay. The relative activities of the mutants span two orders of magnitude and are summarized as follows: Glu330Gln > Glu330Asp > Lys326Met > Glu330Ala > Lys326Gln.

2.3.7. Rates of Co-C Bond Homolysis. From the tritium counting, the exchange rate in nM/min of tritiated AdoCbl was determined by dividing the AdoCbl DPM by the known specific activity of the starting glutamate and the HPLC injection volume. From this, the rate constant for tritium exchange, k_T, was calculated in units of s^{-1} from the known amount of enzyme injected onto the HPLC and the results listed in Table 2.2. To facilitate comparisons with the wild-type enzyme (GlmES),[33] for which the rate of homolysis and hydrogen transfer has been measured using pre-steady-state methods, k_T was corrected assuming a kinetic isotope effect of 20 (a value that has been previously measured for the transfer of tritium between glutamate and AdoCbl).[193] Comparing the rates obtained for Co-C homolysis to that previously reported for GlmES, the mutants are less active by a factor of 100-fold to 7,143-fold. Assuming a change of 1.4 kcal/mol in activation energy corresponds to a 10-fold change in rate,[204] the mutants seem to have an increased barrier of activation for Co-C homolysis of 3 - 5 kcal/mol.

Interestingly, Glu330Asp is a more deleterious mutation than Glu330Gln, and Lys326Met is far less deleterious than Glu330Ala. To facilitate comparisons with the wild-type enzyme, for which the rate of homolysis and hydrogen transfer has been

measured using pre-steady-state methods, k_T was corrected assuming a kinetic isotope effect of 20, a value that has been previously measured for the transfer of tritium between glutamate and AdoCbl. Although this assumption may not be entirely valid, because the mutations may affect the value of the intrinsic KIE, it is very unlikely that changes in the KIE would significantly contribute to the difference in the rates measured for the enzyme variants, which span four orders of magnitude. As an example, a recent study by Kohen and coworkers examining the effect of active site mutations designed to change the distance for the transfer of hydride between donor and acceptor atoms in dihydrofolate reductase found that intrinsic KIE were increased by no more than 50% at 37 °C in the mutant enzymes.[205]

2.3.8. Binding of AdoCbl to Glutamate Mutase Mutants.

In order to establish that the drastic decrease in activity was not due to a severe change in the enzyme-coenzyme interactions, the binding of AdoCbl to the mutant proteins was qualitatively assessed by the method of equilibrium ultrafiltration.[206, 207] AdoCbl (50 μM) was mixed with protein (50 μM) in 10 mM tris-HCl, 10% glycerol, pH 8.0 in a total volume of 500 μL. After incubation for 15 min at 37 °C, 75 μL was passed through the Microcon-30 filter by centrifugation and the absorbance at 522 nm recorded for both the retained and ultrafiltered solutions (Figure 38). Binding assessments were conducted at a single concentration of AdoCbl and, thus, K_d values are representative of a single data point. However, these measurements can provide an adequate estimate of the mutant's affinity for AdoCbl relative to that of OptGlmES. The dissociation constants for the mutant enzymes (shown in Table 3) were obtained assuming a simple ligand-acceptor association model in which enzyme and AdoCbl

bind in a single step to form the enzyme-coenzyme complex and compared to that of OptGlmES and calculated from

$$K_d = ([L]*[A])/[LA] = ([L]_{Total}-[LA])*([A]_{Total}-[LA])/[LA]$$

where $[LA] = [AdoCbl]_{retentate} - [AdoCbl]_{ultrafiltrate}$. This provided an estimate of ~ 13 μM for non-mutated OptGlmES. Despite this value being ~ 7-fold larger than the established value of 2 μM (possibly due to mass action effects resulting from concentrating the protein), the conditions used were consistent over several trials to within 5% error and could thus be used as a qualitative assessment of AdoCbl binding to the mutant proteins relative to the wild-type OptGlmES enzyme. Control experiments in which AdoCbl was incubated without enzyme resulted in statistically the same concentration for both retentate and ultrafiltrate. The binding data suggests that the mutants binding of AdoCbl is slightly altered, which is not surprising considering similar changes in binding were obtained with other active site mutants.[36] However, these changes represent at most a 5-fold reduction in affinity relative to OptGlmES and, thus, cannot account for the drastic two to four orders of magnitude decrease in activity displayed by the mutants. Furthermore, the K_d for AdoCbl of the wild-type and fusion GlmES enzyme is 2 μM,[40, 198, 203] whereas the activity measurements were conducted with 5 μM mutant enzyme and up to 50 μM AdoCbl. Additionally, Chen and Marsh examined the binding of the AdoCbl, MeCbl, and cob(II)alamin to the GlmES fusion protein and found that each bound with similar affinity which suggests that interactions between the enzyme and the ribose ring do not play a large role in binding the coenzyme.[40] It is therefore highly unlikely that the lack of activity results from the inability of the mutant enzymes to bind AdoCbl.

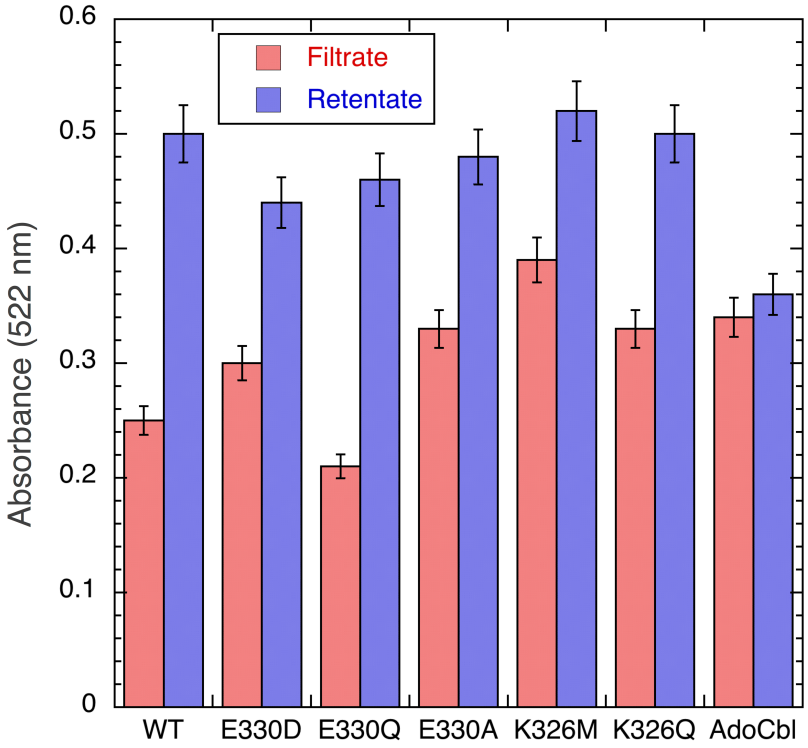

Figure 38. Assessment of AdoCbl Binding in OptGlmES and Mutants by Spectroscopic Equilibrium Ultrafiltration Measurements. K_d values were calculated assuming the ultrafiltrate absorbance represents the concentration of free AdoCbl and the retentate absorbance represents free and enzyme-bound AdoCbl.

Enzyme	K_d (±5%)
WT	13
E330D	64
E330Q	11
E330A	55
K326M	66
K326Q	37

Table 3. Binding Constants for OptGlmES and Mutant Enzymes. Qualitative estimates of dissociation constant for OptGlmES and mutants establish the mutations bound AdoCbl with an affinity similar to or slightly lower than that of wild-type glutamate mutase.

2.3.9. Molecular Dynamics Simulations. The lack of significant change in the AdoCbl binding constant for the mutant enzymes suggests the changes in rate (*i.e.*, lack of AdoCbl homolysis) are indicative of an underlying fundamental change in catalysis. As described above, previous computational modeling suggests that electrostatic interactions between the enzyme's active site and the adenosyl's ribose ring help stabilize the dissociated state over the bound state through an increase in hydrogen bonding interactions.[190, 191] The active site residues also likely play an important role in optimally positioning the 5′-carbon of the adenosyl radical for the

abstraction of hydrogen from the substrate. To gain further insight into how the Glu300 and Lys326 mutations modulate homolysis and subsequent hydrogen abstraction, a collaboration was formed with Patrick von Glehn, Jeremy N. Harvey and Adrian J. Mulholland, from the Centre for Computational Chemistry, School of Chemistry at the University of Bristol, U.K., who performed molecular dynamics simulations on the wild-type and mutant enzymes using the enzyme-AdoCbl-substrate crystal structure as a starting point (PDB ID 1I9C).[192] The AdoCbl was modeled in both the pre-homolysis, Co(III) state with the Co-C bond formed (associated state) and the cleaved Co(II) state with the Co-C bond broken (dissociated state). Representative structures of the wild-type and Glu330Asp mutant obtained from MD simulations are shown in Figure 39. It is important to note that in the crystal structure, the Co-C bond is not formed. However, force field energy minimization included a term for the Co-C bond and careful equilibration produced a satisfactory starting structure for the associated state. Molecular dynamics were performed over an 18-nanosecond timescale with a 2-femtosecond time step and produced no significant changes to the enzyme's backbone as demonstrated by an α-carbon root mean-square deviation (RMSD) value of 1.3 Å for the dissociated state and 1.6 Å for the associated state when compared to the crystal structure. This shows that the protein structure is well-modeled by the force field used and that the overall conformational state of the protein is similar in the associated and dissociated states. To further validate the model used, RMSD were calculated for only the backbone α-carbons of residues in the active site region (all residues within 6 Å of the adenosyl moiety) and values fell within 1 - 1.6 Å for wild-type and mutant enzymes. This indicates that changes to the active site introduced by the

mutations are minimal. The RMSD values obtained are shown in Table 4 and overlays of wild-type and mutant active site average structures obtained from simulation are shown in Figure 40.

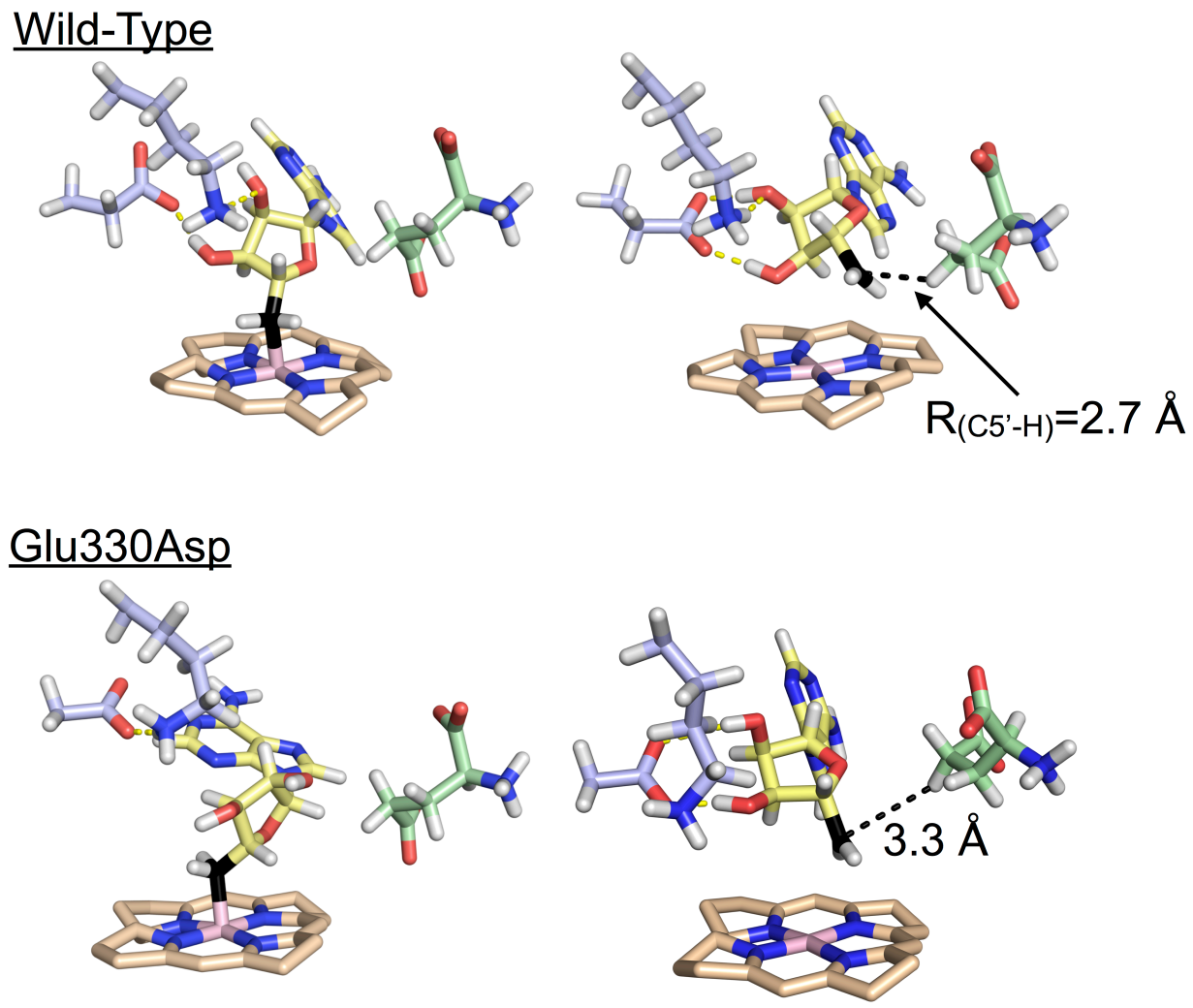

Figure 39. Molecular Dynamics Simulation Structures of Glutamate Mutase and the Glu330Asp Mutant. Representative structures of the wild-type enzyme and of the Glu330Asp mutant obtained from molecular dynamics (MD) simulations of the associated (left) and dissociated (right) states of AdoCbl in glutamate mutase. The substrate (glutamate) is colored green and the 5′-carbon of adenosine is colored black.

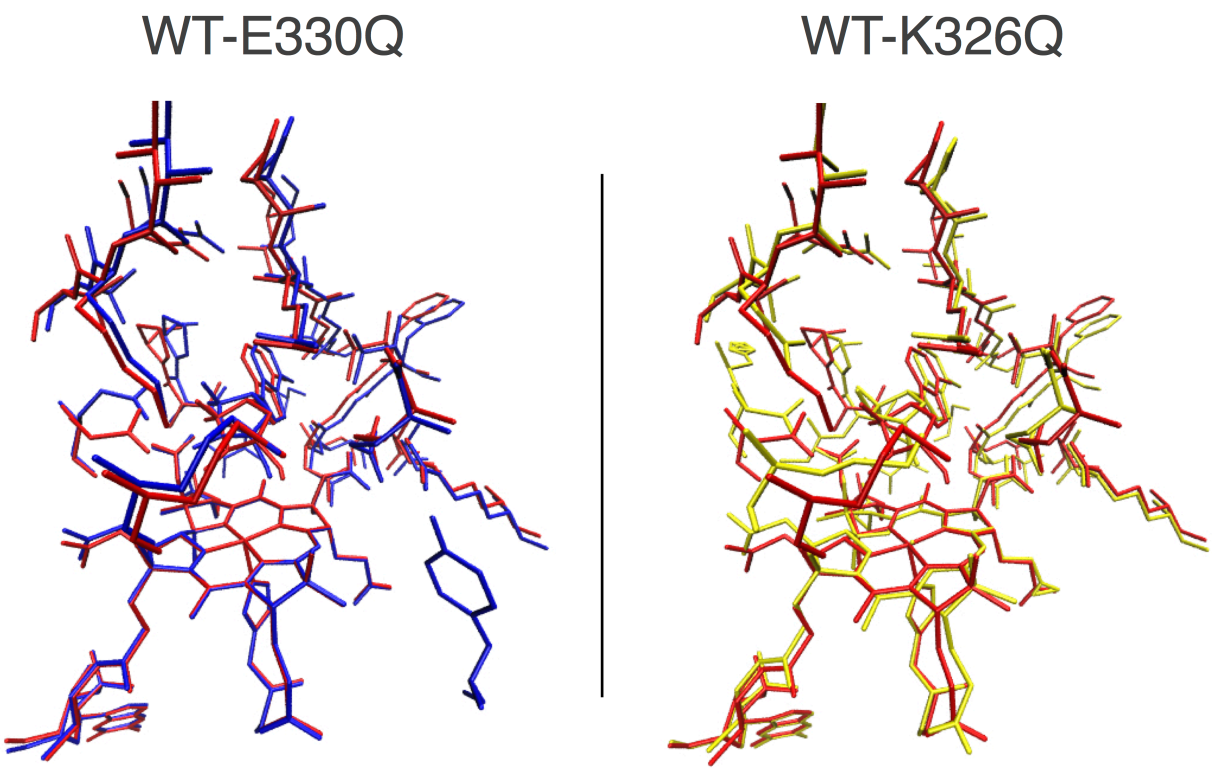

Figure 40. Overlays of the Structures Obtained from MD Simulations for Wild-Type and Mutant Glutamate Mutase Enzymes. Left: wild-type and E330Q mutant; Right: wild-type and K326Q mutant.

	Mean RMSD of All C_α Atoms (Å)		Mean RMSD C_α Atoms < 6 Å from the Adenosyl Moiety (Å)	
	Associated State	Dissociated State	Associated State	Dissociated State
Wild-Type	1.55	1.29	1.16	1.01
E330Q	2.42	1.44	1.44	1.19
E330D	1.81	1.54	1.25	1.08
K326M	1.92	1.76	1.51	1.23
E330A	1.55	1.50	1.16	1.20
K326Q	1.82	1.97	1.59	1.35

Table 4. Average Root Mean Square Deviations (RMSD) of C_α Atoms for Wild-Type and Mutant Enzymes. Mean RMSD were determined over the course of the molecular dynamics simulations relative to the crystal structure for all backbone α-carbons and those with at least one atom within 6 Å of the adenosyl group (active site). Values fell within a narrow range of 1−1.6 Å, indicating that no large changes to the active site were introduced by any of the mutations.

Tunneling is an important contributing factor to the chemistry of AdoCbl-dependent enzymes. Since the distance between reacting species is a crucial parameter for tunneling to occur, the simulations were analyzed to calculate the average distance, $R_{(C5'\text{-}H)}$, between the 5'-carbon of the adenosyl moiety - the location of the adenosyl radical - and the abstractable hydrogen of the substrate in the dissociated state *(see Figure 39 arrow)*. Distances extracted from the simulations were binned and fit to the gamma probability density function

$$f(x) = s\frac{1}{(\kappa-1)!\,\theta^{\kappa}}(x-x_0)^{\kappa-1}e^{-\frac{(x-x_0)}{\theta}}$$

where the variables κ and θ are shape and scale parameters respectively, *s* is a scaling parameter and x_o is the off-set of distribution from zero. The mean distance, $R_{(C5'-H)}$, was then calculated from the resulting fit (see Appendix A.2 for the parameters obtained from the fits). The binned distance distributions and associated fits for the wild-type and mutant enzymes are shown in Figure 41. The average distances are listed in Table 5.

The wild-type enzyme displayed the shortest mean distance (2.67 Å) of the group, as well as the narrowest distribution (standard deviation) of distances. When compared to the most active mutant, Glu330Gln, $R_{(C5'-H)}$ has increased to 2.85 Å and the distribution of interatomic distances is somewhat broader. At the other end of the activity spectrum, the least active mutants Glu330Ala and Lys326Gln show an even longer $R_{(C5'-H)}$ to 3.61 and 3.43 Å, respectively. Their distribution of interatomic distances becomes much broader as well.

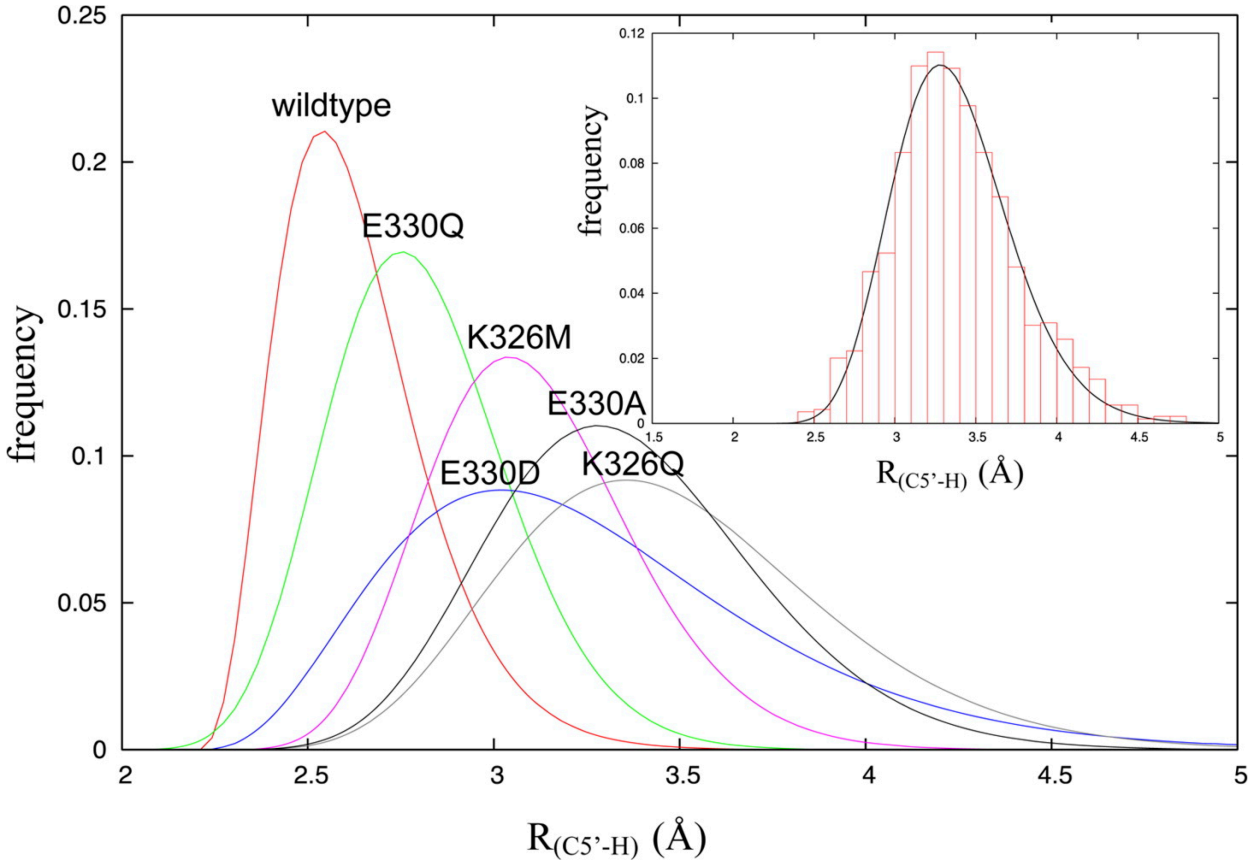

Figure 41. Gamma Distribution Plots of Distances between the 5′-Carbon of the Adenosyl Radical and the Abstractable Hydrogen of Glutamate, $R_{(C5'-H)}$, for Wild-Type and Mutant Enzymes. The inset shows a representative fit of the binned data from MD simulations for the E330Q mutant. Fits for all other enzymes are found in Appendix A.4.

Enzyme	$R_{(C5'-H)}$ (Å)	-Log (k_T)
WT	2.67±0.18	0
E330Q	2.85±0.23	-2.0
E330D	3.27±0.44	-2.4
K326M	3.30±0.62	-2.8
E330A	3.61±0.56	-3.7
K326Q	3.43±0.39	-3.9

Table 5. Mean Distance between the 5′-Carbon of the Adenosyl Radical and the Abstractable Hydrogen of the Substrate in the Dissociated State. Log(k_T) (relative to that of the wildetype) is included for comparison and was found to correlate well with $R_{(C5'-H)}$ (see section 2.4). *Value calculated from Chih, H.-W., and Marsh, E. N. G. (2001) Biochemistry 40, 13060−13067.

It is interesting to note that the most conservative mutation, Glu330Asp, is not the most active mutant. In fact, the $R_{(C5'-H)}$ of 3.27 Å is significantly longer than that of the wild-type, which might explain why it is unexpectedly less active than the Glu330Gln mutant. These results suggest that both residues are important for positioning the adenosyl radical optimally for the abstraction of hydrogen from the substrate.

The simulations were also analyzed for the occurrence of hydrogen bonding interactions between the ribose -OH groups and Glu330 and Lys326 in order to quantify how hydrogen bonding affects homolysis. A simple geometric approach was used to establish the presence of a hydrogen bond and was defined as any instantaneous configuration during the MD simulations in which any donor−acceptor distance was < 3.5 Å and the donor−hydrogen−acceptor angle was > 135°. Previous work has shown that simple geometric criteria for hydrogen bonding (as used here) yield good agreement with more elaborate energy-based criteria.[208] Table 6 shows the average number of hydrogen bonds that met the defined criteria over the length of each simulation for the associated and dissociated states. Furthermore, the average H-bond donor-acceptor distances were also extracted from the simulations by averaging the distances over only the structures in which the donor-acceptor distance was less than 3.5 Å in order to asses not only the number of hydrogen bonds, but also the strength of the interaction (Table 7).

	Associated AdoCbl			Dissociated AdoCbl			
Enzyme	Ado-330	Ado-326	Total	Ado-330	Ado-326	Total	# H-bond (dissociated-associated)
WT	0.90	0.26	1.16	2.03	0.41	2.44	1.28
E330Q	0.15	0.14	0.29	1.04	0.43	1.47	1.18
E330D	0.14	0.23	0.37	1.64	0.13	1.77	1.4
K326M	0.38	0.00	0.38	1.57	0.00	1.57	1.19
E330A	0.00	0.16	0.16	0.00	0.09	0.09	-0.07
K326Q	0.06	0.57	0.63	1.53	0.15	1.68	1.05

Table 6. Hydrogen Bond Counts between Adenosyl Hydroxyl Groups and Side-Chains at Positions 326 and 330 in the Coenzyme Associated and Dissociated Configurations of Glutamate Mutase. A hydrogen bond was considered to be present at any instantaneous configuration during the MD simulations if any donor−acceptor distance was < 3.5 Å and the donor−hydrogen−acceptor angle was > 135°.

	Associated AdoCbl		Dissociated AdoCbl	
Enzyme	Ado-330	Ado-326	Ado-330	Ado-326
WT	2.77	3.04	2.72	3.11
E330Q	3.24	3.08	3.12	3.03
E330D	2.90	3.04	2.87	3.10
K326M	2.92	-	2.81	-
E330A	-	3.09	-	2.99
K326Q	2.96	2.98	2.86	3.25

Table 7. Mean Hydrogen Bond Donor-Acceptor Distance for Wild-Type and Mutant Glutamate Mutase Enzymes. Distances in angstroms were averaged over only those structures for which a hydrogen bond was judged to be present (those in which the donor–acceptor distance was less than 3.5 Å).

It is interesting that out of all the enzymes, the wild-type enzyme is able to form both more and shorter (*i.e.*, stronger) H-bonds with the adenosyl-OH groups in both the associated and dissociated state than any of the mutants. In particular, with the exception of the E330A mutant, because it cannot hydrogen bond, Glu330 forms far more and stronger H-bonds with the adenosyl -OH in the dissociated state over the associated state. In the case of Glu330Ala, water molecules enter the active site to fill the void created by the mutation. These results highlight the important role the active site Glu330 residue plays in facilitating catalysis by the hydrogen bonding interactions it makes with the coenzyme.

In contrast to Glu330, hydrogen bonding between Lys326 and the ribose moiety seems to be less important. For the benchmark wild-type enzyme, the total number of H-bonds between between Lys326 and the adenosyl -OH is smaller and less differentiated between the associated and dissociated state. Except for K326M which cannot H-bond, there is no clear correlation between mutation and the number or strength of hydrogen bonds established with the ribose. However, despite H-bonding between Lys326 and the ribose hydroxyl groups appearing to be less important, mutation of Lys326 does appear to impair the ability of Glu330 to form its hydrogen

bonds with the ribose moiety. Furthermore, in Lys326 mutants, the 5′-carbon is much less well-positioned for hydrogen abstraction. Taken together, the low activity of the Lys326Met and Lys326Gln mutants suggests that Lys326 plays an important role in positioning Glu330 to effectively hydrogen bond with the ribose group.

2.4. Discussion: Correlation between Simulation and Experiment

The fundamental principles by which AdoCbl-dependent enzymes accelerate coenzyme homolysis and stabilize the resulting reactive free radical intermediates remain the most poorly understood aspect of these enzymes. In this work, we sought to gain insight into the mechanism of radical generation in AdoCbl-dependent enzymes by a coordinated approach employing both computation and experiment. By themselves, the rate data measured experimentally provides little insight into *how* the enzyme is able to labilize the Co-C bond; we simply know that mutation of Glu330 and Lys326 severely impairs the enzyme's ability to do so. Only when the experimental data is studied in light of the molecular dynamics simulations can an answer begin to emerge. To support the idea that the changes in active site H-bonding patterns identified through the simulations were, in fact, contributing to the kinetics measured experimentally, the data was examined for a correlation between the computationally derived parameters and the experimentally derived tritium exchange rate k_T. As shown in Figure 42, $-\log k_T$ demonstrates a good linear relationship with $R_{(C5'\text{-}H)}$, the mean distance of the adensoyl 5'-carbon and the substrate's abstractable hydrogen (r = 0.93, and r^2 = 0.86). However, changes in hydrogen bond number or strength between the associated and dissociated state demonstrate no identifiable relationship. This is not to say that changes in the hydrogen bonding network is not important, as the wild-type enzyme shows a much

lower H-bond sampling population as demonstrated by a narrower gamma probability distribution, but the fact that mutation affects changes in the position of the adenosyl radical in the active site as well, seems to mask any obvious trend from being established.

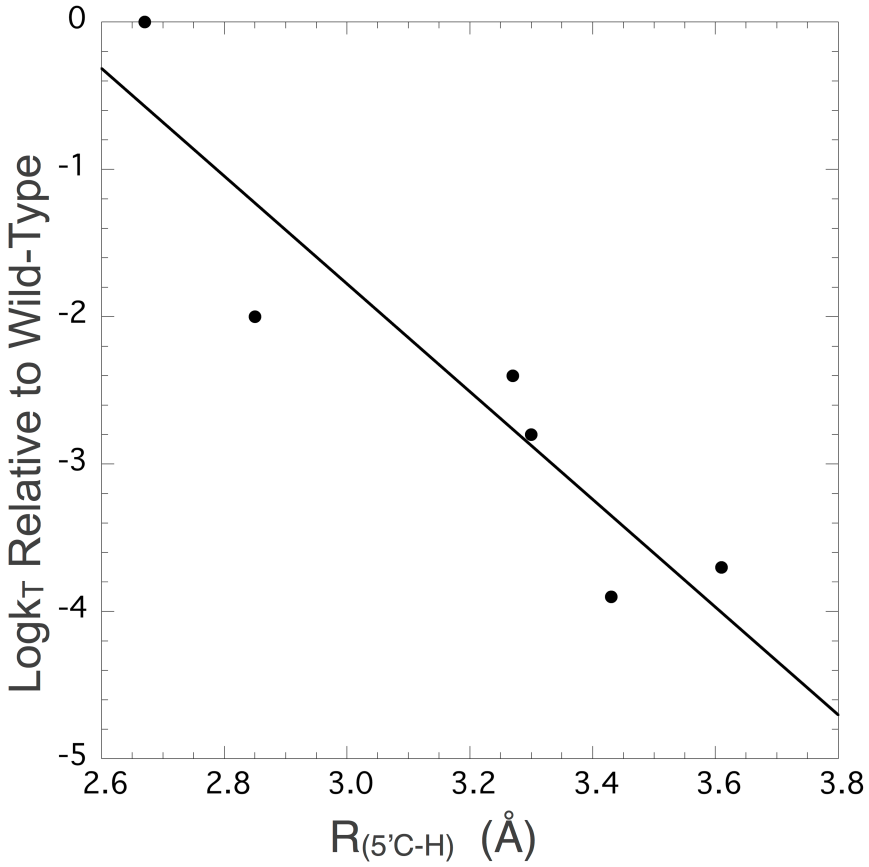

Figure 42. Correlation between $R_{(C5'-H)}$ Determined from MD Simulations and Logk_T Determined by Experiment. $R_{(C5'-H)}$ exhibited a good linear correlation with $-\log k_T$ ($r = 0.93$ and $r^2 = 0.86$) and demonstrates the important role that Lys326 and Glu330 residues play in positioning the adenosyl radical relative to the substrate.

The crystal structure of glutamate mutase,[192] as well as the computations done by Rommel and Kaestner,[61] suggests that Glu330 and Lys326 play an important role in catalyzing homolysis of the coenzyme in glutamate mutase. Indeed, the results highlight the role that Glu330 and Lys326 play in positioning the adenosyl radical

relative to the substrate. By developing a highly sensitive assay for homolysis and hydrogen abstraction, the activities of mutant enzymes that are slower by two to four orders of magnitude than the wild-type enzyme were successfully measured. This wide range of activities allowed to examine whether changes in the structure and dynamics of the active site identified by MD simulations correlated with changes in activity. This strategy has provided a powerful approach for gaining new atomic-level insights into the reaction mechanism that would have been unavailable from either experimental observation or computation alone.

AdoCbl enzymes involve tunneling with respect to hydrogen transfer between the substrate and the coenzyme and this step is known to be rate limiting.[153, 175, 179, 185] Therefore, it is not surprising that the position of the adenosyl radical with respect to the substrate is of critical importance for catalysis. However, up until now, there is no experimental data to support this claim. These experiments demonstrate that Lys326 and Glu330 position the adenosyl radical closer to the substrate's abstractable hydrogen in the wild-type enzyme and samples a much narrower standard deviation than any of the mutants. This suggests that the wild-type enzyme samples many fewer conformations as the 5'-carbon of the adenosyl radical moves toward the substrate and is therefore optimized for hydrogen atom abstraction. Importantly, since the experimentally measured $-\log k_T$ directly reflects the changes in activation energy for the transfer of tritium between the substrate and coenzyme, a correlation between $-\log k_T$ and $R_{(C5'-H)}$ extracted from MD simulations provides strong support for the idea that optimizing the distance between the 5′-carbon and the abstractable substrate hydrogen is vital for efficient catalysis in glutamate mutase and other AdoCbl mutases.

The results presented support the existing hypothesis that H-bonding interactions are important for efficient catalysis.[190, 191] However, they also show that mere changes in electrostatic interactions among the protein and co-enzyme between the associated and dissociated state alone cannot fully explain the difference in activity between wild-type and mutant enzymes. Even though the MD simulations do not quantify the catalytic contribution that hydrogen bonding makes, they do indicate that the extent of hydrogen bonding is significantly increased between Glu330 and ribose in the dissociated state for wild-type glutamate mutase. However, these changes in electrostatics appear to be insufficient to fully explain the difference in activity between wild-type and mutant enzymes, as the mutants also show increased numbers of hydrogen bonds in the dissociated state relative to the associated state, albeit by forming fewer hydrogen bonds in total. For instance, the Glu330Asp mutant is less active than Glu330Gln despite Glu330Asp forming well-defined hydrogen bonds with the ribose -OH groups in the dissociated state. If electrostatics were the only contributing factor to catalysis, one would expect Glu330Gln to be less active as the neutral glutamine side-chain should form weaker hydrogen bonds with the ribose ring than the negatively charged aspartate carboxylate side-chain. However, this is not the case. The analysis presented here resolves this discrepancy by showing that hydrogen bonding between the ribose and the shorter aspartate causes the 5'-adenosyl carbon to be 0.42 Å farther from the substrate than the glutamine mutant. Interestingly, this same activity trend was observed in ornithine aminomutase and methylmalonyl-CoA mutase when the equivalent glutamate residues were mutated to glutamine and aspartate.[196]

Therefore, it is not only favorable electrostatics between the enzyme and the ribosyl moiety of the coenzyme that contribute to the lability of the Co-C bond in AdoCbl-dependent enzymes, but also the precise positioning transiently formed adenosyl radical by the active site residues. As has been proposed previously,[192] precise control of the radicals trajectory is not surprising feature as these enzymes require a mechanism to harness the high reactivity of their radical intermediates and their reactions are heavily influenced by large tunneling contributions. Nevertheless, this work represents the first study to examine in atomistic detail the structural features of AdoCbl-dependent enzyme's active site that are fundamental to its catalytic requirements. Finally, since none of the mutant enzymes accumulated detectable amounts of cob(II)alamin during catalysis, indicating that they do not stabilize the dissociated state as well as the wild-type, it is concluded that two factors must contribute to the high levels of coenzyme homolysis observed in AdoCbl enzymes. First, favorable electrostatic interactions, as previously proposed by Sharma and coworkers,[190] between the dissociated coenzyme and protein are necessary to offset part of the enthalpic cost of radical generation. Second, precise positioning of the transiently formed adenosyl radical by the enzyme, a feature that has not been widely discussed previously, facilitates the rapid transfer of hydrogen from the substrate to coenzyme, to generate the substrate radical that is further stabilized by electronic effects.

CHAPTER 3

MAGNETIC FIELD EFFECT STUDIES ON THE ADENOSYLCOBALAMIN-DEPENDENT ENZYME GLUTAMATE MUTASE

3.1. Introduction

A magnetic field may in principle alter the rate of an enzymatic reaction in which there are unpaired electrons produced as intermediates.[172, 209-214] The explanation to this is borne out of consequence to the Pauli exclusion principle, which states that electrons, being indistinguishable particles, must be anti-symmetrical with respect to exchange. In order to satisfy the exclusion principle, electrons are attributed a property known as *spin* which, as discussed below, is the property that makes an electron susceptible to external magnetic fields.

3.1.1. The Physical Chemistry of an Electron Pair and the Pauli Exclusion Principle.

Electrons have an intrinsic angular momentum component known as *spin*, for which the only allowed value is $s = 1/2$ (spin quantum number). The term spin can be misleading because quantum mechanically, the electron is not a localized object spinning about its axis. Nevertheless, the idea of a spinning motion can be useful for discussion purposes. The electron's spin can only exist in two different states or "directions" with respect to a specified axis: $m_s = +1/2$ or $m_s = -1/2$ (Figure 43).

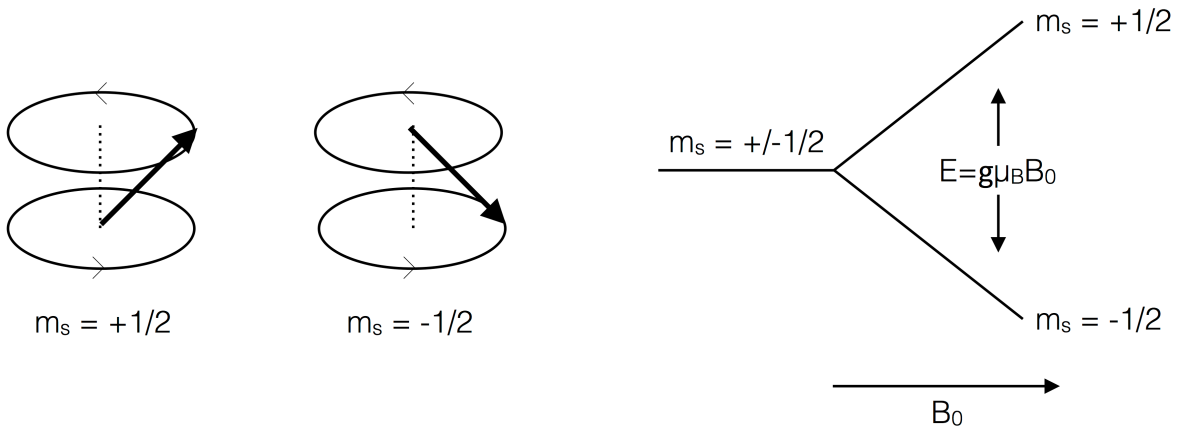

Figure 43. Properties of Electron Spin. The angular momentum of an electrons spin can only take on the value of *s* = 1/2 and its vector can only point in one of two directions with respect to a specified axis. A "spin up" electron is designed by its magnetic quantum number m_s = +1/2. A "spin down" electron is designed by its magnetic quantum number m_s = -1/2. In an external magnetic field, the degeneracy between the two states is removed (Zeeman effect) and separated in magnitude proportional to the strength of the applied field. The m_s = +1/2 state moves up in energy by an amount $1/2g\mu_B B_0$ and the m_s = -1/2 state will move down by $1/2g\mu_B B_0$. If the electron is then exposed to microwave radiation of frequency *v*, the system will "resonate" if the frequency satisfies the condition: $\hbar v = g\mu_B B_0$, where g, known as the electron's *g*-value, is a proportionality constant arising from the electron's interaction with the electromagnetic fluctuations of its environment (spin-orbit coupling). At resonance, the electron is able to readily absorb the microwave radiation and will transition between the spin up and spin down states.

For two electrons to share the same bonding molecular orbital, the net angular momentum must be zero. In other words, since no two electrons can occupy the same spatial coordinates (exclusion principle), one electron must be "spin up" and the other "spin down." This spin pairing points the spin vectors of the two electrons in opposite directions and, from a wave mechanical point of view, are 180 degrees out of phase. This spin state in which the net angular momentum is zero is known as a singlet state (S_0) (Figure 44). If an electron is promoted to a separate molecular orbital as occurs in the homolysis of a covalent bond, the two resulting electrons could still have their spins paired (singlet) but a configuration in which their spins are parallel is energetically more favorable. This is because unpaired electrons prefer to be as far away from each other since they have the same negative charge, and a parallel spin configuration ensures this (Hund's rule). In a triplet state ($T_{0,\pm1}$), the two electron spin vectors point in the same direction and the sum of their phase angles yields a total spin of one (Figure 44).

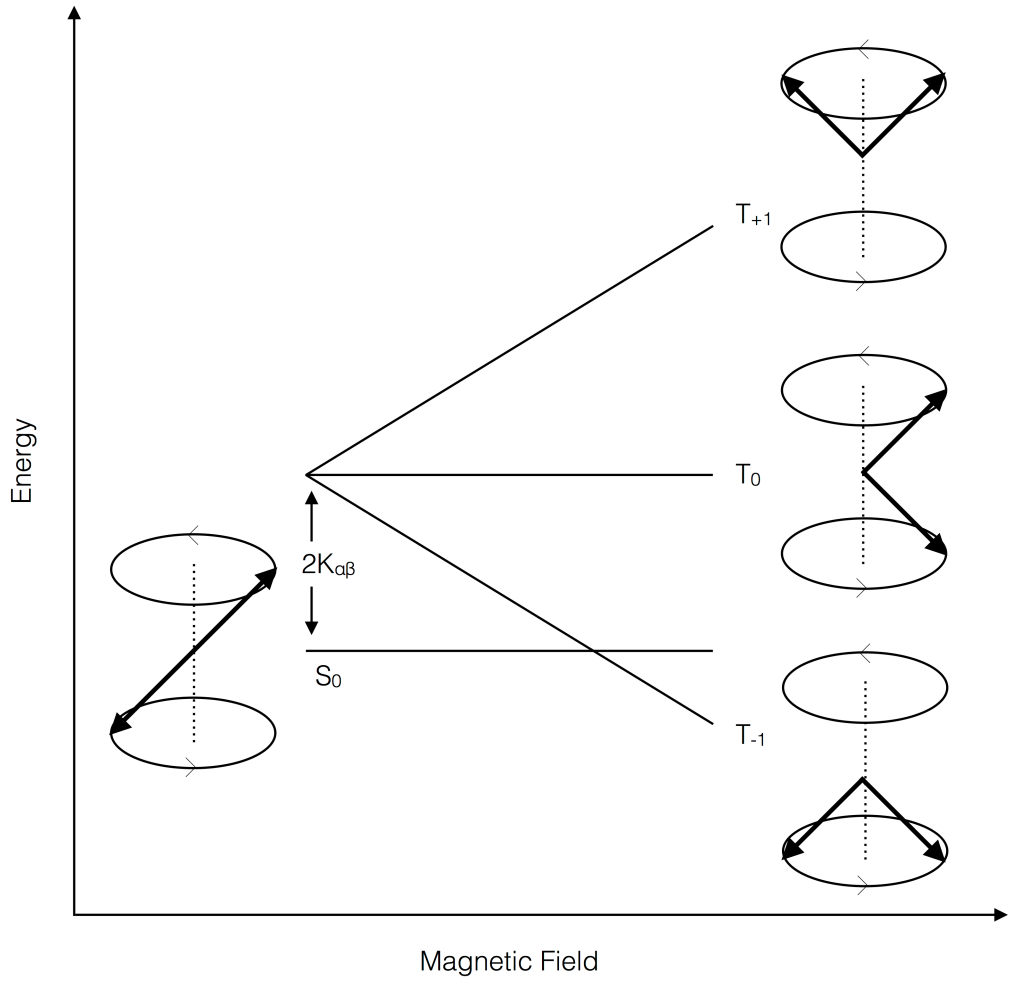

Figure 44. Magnetic Field Dependence of the Spin States for an Electron Pair. Hyperfine induced intersystem crossing can promote S_0 to all three degenerate $T_{0,\pm1}$ states in the absence of a magnetic field. An external magnetic field will split the degenerate triplet states into three energetically separate configurations (Zeeman effect) with T_{+1} and T_{-1} split to higher and lower energy from S_0 and T_0. Under these conditions, hyperfine coupling can only promote S_0 to T_0, diminishing the population of the $T_{\pm1}$ states.

The energy of two electrons α and β in the singlet and triplet state is:

$$E_{singlet} = E_\alpha + E_\beta + J_{\alpha\beta} + K_{\alpha\beta}$$

and

$$E_{triplet} = E_\alpha + E_\beta + J_{\alpha\beta} - K_{\alpha\beta}$$

where $E_\alpha + E_\beta$ are the energies of the electrons and $J_{\alpha\beta}$ represents the Coulomb repulsions between the electrons. Since the wave function of fermion particles must be anti-symmetrical with respect to spatial exchange, $K_{\alpha\beta}$ accounts for the electron's

indistinguishability by exchanging their spatial coordinates between the two product terms that make up $K_{\alpha\beta}$: $K_{\alpha\beta} = (e^2/8\pi\varepsilon)\ [\sigma(\alpha)\sigma(\beta)] * (r_{\alpha\beta})^{-1} * [\sigma(\beta)\sigma(\alpha)]\ d\tau_\alpha d\tau_\beta$. The exchange of the individual electron's wave function in $K_{\alpha\beta}$ ensures the total wave function for the singlet or triplet state represents a superposition of both electrons that satisfies the Pauli exclusion principle. Spin-correlation describes this inherent connection between two electrons in a given configuration. This relationship is deemed coherent because it is retained despite any conversion between the singlet and triplet spin states and is modulated by the exchange interaction ($K_{\alpha\beta}$). Note the energy difference relative to the two electrons is $J_{\alpha\beta} + K_{\alpha\beta}$ for the singlet state and $J_{\alpha\beta} - K_{\alpha\beta}$ for the triplet state. It can be shown that both $J_{\alpha\beta} + K_{\alpha\beta}$ are always positive and, thus, the two states differ in energy by $2K_{\alpha\beta}$ (Figure 44).

The Wigner spin conservation rule states that for both radiative and non-radiative transitions, transitions between terms of the same multiplicity are spin-allowed, while transitions between terms of different multiplicity are spin-forbidden. Therefore, immediately after the Co-C bond undergoes thermolysis, the newly-formed [cob(II)alamin-AdoCH$_2$•] radical pair maintains the spin correlation of the original bond's spin state. By the exclusion principle, the ground state sigma bond is in a spin paired singlet state and, thus, the product radical pair will also be a singlet. Similarly, if a ground state electron is promoted to a higher energy orbital, the spin-paired excited singlet state will rapidly decay to the more stable, parallel-spin triplet state. When this bond undergoes homolysis, the resulting radical pair will be in a triplet spin state (Figure 45).

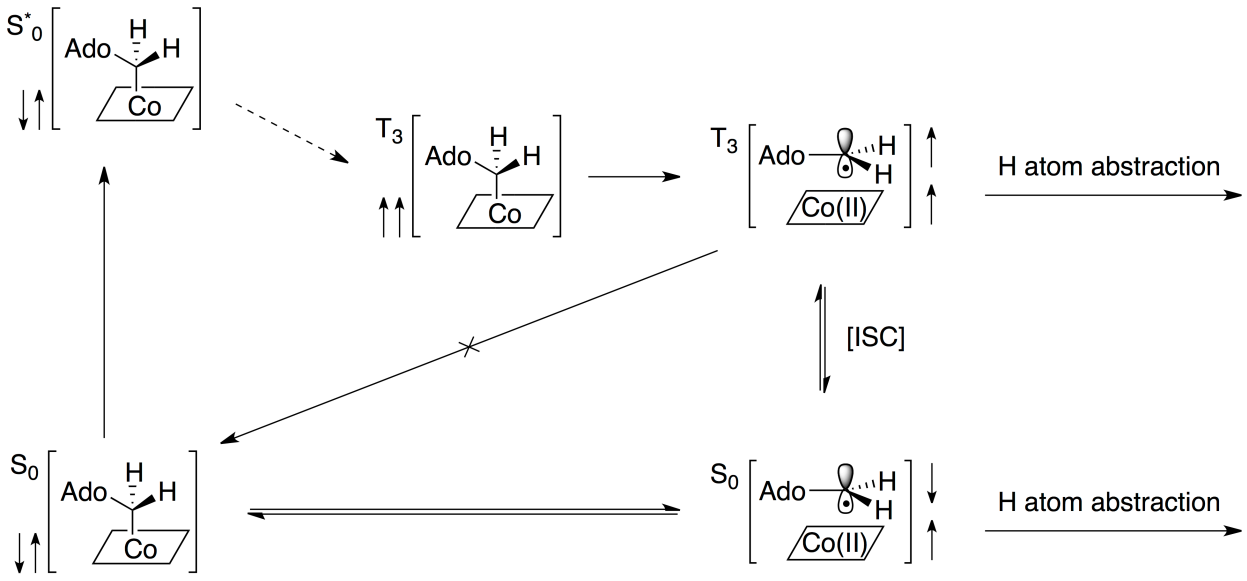

Figure 45. Proposed Mechanism for the Radical Pair Recombination of AdoCbl. The exclusion principle dictates the two electrons in the ground state Co-C σ bond must be spin-paired. Immediately after thermolysis, the [5'dA radical-cob(II)alamin] radical-pair maintains a singlet state spin correlation. The radical pair can recombine to reform the cofactor or continue forward to abstract a hydrogen atom from the substrate. If held in close proximity for sufficient time (1 ns to 10 μs), the singlet radical pair can undergo intersystem crossing to the triplet state. Recombination from the triplet state is forbidden by the exclusion principle and, thus, the only option is for the reaction to proceed forward onto hydrogen abstraction. This effectively decreases the recombination rate back to adenosylcobalamin and may result in an observed rate of change with respect to product formation.

Once the bond breaks, $K_{\alpha\beta}$ becomes very small and the radical pair can oscillate between a singlet and triplet state by way of intersystem crossing (ISC); the singular solution to the configuration's wavefunction vanishes and the radical pair is now described by superposition of the individual wavefunctions representing the individual singlet and triplet states. This is because the exchange energy that ensures that the exclusion principle is met within the close confines of a chemical bond is now less significant as the electrons are spatially separated. The equilibria of singlet and triplet populations are dependent upon having a small enough energy gap between the spin states so that the hyperfine interaction between a neighboring nucleus and the unpaired electron is able to promote intersystem crossing (ISC).[209, 214, 215]

3.1.2. Nuclear Hyperfine Coupling. In order to understand the origin of the hyperfine interaction (HFI), consider a simple C-H bond with the unpaired electron in a π orbital on the carbon atom. Since an *s* orbital has a non-zero probability of finding the electron at the nucleus, the small amount of current generated by the electron spin can interact with the magnetic field generated by the proton spin (Fermi contact). As fermions, protons also have a nuclear spin of $I = 1/2$ and, thus, also follow the Pauli exclusion principle. Therefore, the electron in a hydrogen atom's *s* orbital will pair its spin to that of the nucleus proton (Figure 46).

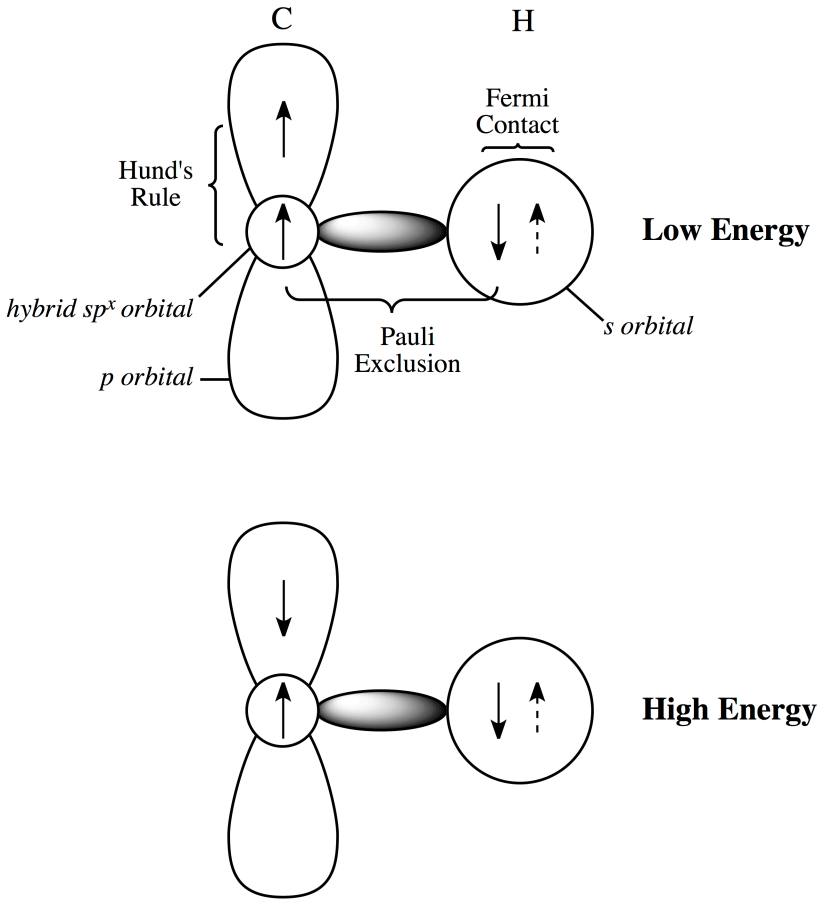

Figure 46. Origin of the Hyperine Interaction. Since an *s* electron has a non-zero probability of being found at the nucleus, the Pauli exclusion principle dictates that the Fermi contact between an *s* electron and the proton it orbits be spin-paired. This chemically induces the spin polarization of the electron in the adjacent sp^x nucleus, ultimately influencing the spin of the unpaired *p* orbital electron.

In order to satisfy the exclusion principle, the electron in carbon's sp^x orbital will also pair its spin to the hydrogen electron. Therefore, the bonding system will be slightly lower in energy if the unpaired electron in carbon's *p* orbital satisfies Hund's rule and it has its spin parallel to the sp^x electron. This effect is referred to as chemically-induced dynamic spin polarization (CIDEP) because the unpaired electron can sense the nuclear spin indirectly by maintaining its spin correlation to the sp^x electron. This hyperfine interaction can induce a circular motion of the electron and provide enough energy to promote the flipping of its spin. Hyperfine induced intersystem crossing is a central mechanism in radical pair recombination because it drives the coherent interconversion between the singlet and triplet state of a radical pair and, consequently, establish population differences between them.[209, 216, 217]

3.1.3. The Radical Pair Mechanism. Since radical pair recombination reactions are sensitive to the unpaired electron's spin, CIDEP can lead to changes in recombination rate, as well as product distribution.[218] For example, homolysis of the Co-C bond yields a [cob(II)alamin-AdoCH_2•] radical pair in the singlet state.[174, 209] This correlated pair has two choices: (1) it can non-productively recombine to reform AdoCbl, retarding the reactions leading to forward catalysis, or (2) the AdoCH_2• radical can proceed through the next step of the catalytic cycle and abstract a hydrogen from the substrate. If the [cob(II)alamin-AdoCH_2•] radical pair remains in close coordination for 10^{-10} to 10^{-6} s, hyperfine interactions can promote ISC to the parallel triplet state. Recombination from the triplet state is energetically unfavored by the exclusion principle creating a net decrease in recombination.[209] However, forward catalysis to hydrogen

abstraction can still proceed and, thus, funneling the reaction through the triplet state will increase the catalytic flux in the forward direction onto product (Figure 45).

When an external magnetic field is applied, the degeneracy of the three triplet energy states – both spin up, both spin down, parallel spin up/spin down – is removed (Zeeman effect). The Zeeman splitting, whose magnitude is proportional to the strength of the applied field, causes the T_{+1} and T_{-1} states to separate from T_0 with equal and opposite sign. This causes the HFI-induced ISC between the S_0 and $T_{\pm1}$ states to be decreased. Consequently, the equilibrium between S_0 and T_0 is enriched resulting in an increase in the recombination rate. Therefore, if the rate of electron recombination is kinetically significant, one may expect to see an influence on the rate of an enzyme-catalyzed reaction when a magnetic field is applied, a phenomenon that has been observed in organic and enzymatic photochemical reactions.[170, 171, 174, 209, 213, 218-224]

Harkins and Grissom demonstrated the steady-state kinetic parameter V_{max}/K_M in the catalyzed reaction of the AdoCbl-dependent ethanol ammine ammonia lyase (EAL) was decreased up to 25% (reaching its minimal value at 1,000 Gauss) and as well as unambiguously showed that non-productive [cob(II)alamin-AdoCH$_2$•] recombination to be the magnetically sensitive step in EAL.[174, 225] Furthermore, since isotopic substitution is capable of modulating the extent of hyperfine induced ISC,[216, 219] V_{max}/K_M was further decreased up to 60% (reaching its minimal value at 1,500 Gauss) using perdeuterated substrate. Since publication, Taoka and coworkers, in collaboration with the original authors, confirmed the original results and attempted to extend his findings to another AdoCbl-dependent enzyme: methylmalonyl CoA mutase (MMCM).[221] However, despite similarities in reaction mechanism (*i.e.*, AdoCbl homolysis followed by

H-atom abstraction as initial steps), Taoka and coworkers reported V_{max}/K_M for the human and bacterial mutase to be invariant up to 2,500 Gauss. Interestingly, Jones and coworkers were not able to reproduce the sizeable field effect observed by Harkins and coworkers on ethanolamine ammonia lyase and there seems to be no obvious explanation for the experiment's irreproducibility.[171] None the less, with an established precedent for field effects on EAL, as well as successful experiments on modulating the photolytic recombination rate of both enzyme bound and free solution AdoCbl,[170, 213, 220] as well as its methylcobalamin analogue (in free solution),[218, 220] the kinetic parameters of the glutamate mutase reaction were probed for magnetic field effects.

3.2. Materials and Methods

3.2.1. Materials. OptGlmES was expressed and purified as described in Chapter 2. AdoCbl was purchased from Sigma Chemical Co. Solutions containing AdoCbl were kept in light-proof vials and handled in dim light so as to avoid photolysis of the coenzyme. (2,3,3,4,4-d_5)-*L*-glutamic acid was purchased from Perkin Elmer and unlabeled *L*-glutamic acid from Fisher Scientific. Other materials were purchased from commercial suppliers. Nickel-plated neodynium (N42 grade, 1.25x0.25 inch diameter) disk magnets were purchased from K&J Magnetics, Inc.

3.2.2. Deuterium Kinetic Isotope Effect Measurements. The activity of glutamate mutase was coupled to methyl aspartase and monitored spectroscopically by following the production of mesaconate, indicated by an increase at 240 nm.[197] Reactions were conducted in the dark to prevent AdoCbl Co-C bond photolysis at room temperature and contained a final concentration of: 100 mM potassium phosphate, 10 mM KCl, 1 mM MgCl2, 25 μM AdoCl, 10 units of methyl aspartase, and 0.5 μM

OptGlmES, in a total volume of 500 µL. For V_{max} studies, 6 mM deuterated or deuterated *L*-glutamic acid was used. Studies under k_{cat}/K_M conditions used 0.2 mM deuterated or deuterated *L*-glutamic acid. The pH was varied from 6 to 8 depending on the nature of the experiment. A stock solution, including all reagents except substrate, was prepared in advance, kept dark and incubated for approximately 10 min. Then, 490 µL reagent stock was aliquoted into a cuvette and the assay started by addition of 10 µL substrate. This assay setup minimizes any contributions from pipetting error.

3.2.3. Magnetic Field Effect Studies on V_{max} and k_{cat}/K_M. Measurements of magnetic field effects on V_{max} *and* k_{cat}/K_M were performed using a Hewlett Packard diode array spectrophotometer in which all metal from the cuvette holder was removed (cuvette was held in place with a cardboard shim). A magnetic field was generated by placing two N42 grade 1.25 x 0.25 inch neodynium magnets across the cuvette holder with the center around the cuvette. This generates a 25 mm gap across the magnets, generating a field in the range of 1,400 Gauss. A Gauss meter established the field was homogeneous up to ~ 15% within the assay volume (despite a considerably large error, this results in a magnetic field strength well within the range in which Harkins and coworkers observed a magnetic field effect on EAL).[174]

3.3. Results

3.3.1. Effect of pH on the V_{max} Kinetic Deuterium Isotope Effect Measurements. Harkins and coworkers observed the kinetic parameter k_{cat}/K_M for the AdoCbl-dependent ethanlamine ammonia lyase for unlabeled and perdeuterated for ethanolammine by was decreased by 25% and 60%, respectively.[174] The authors reported V_{max} to be invariant with magnetic field flux density up to 2,500 Gauss.

However, Taoka and coworkers reported that neither the human nor the bacterial methylmalonyl-CoA mutase from *Propionibacterium shermanii*, another AdoCbl-dependent enzyme, exhibited no magnetic field effect within the 0 - 2,500 Gauss range used by Harkins. Taoka and coworkers noted that if there indeed was an effect, it could be no greater than 15% after taking into account the experimental error in their measurements. Therefore, in order to enhance the spectroscopic assay measurement sensitivity to magnetic fields, the effect of pH on the V_{max} deuterium kinetic isotope effect ($^{D}V_{max}$) was measured first. The pH providing the greatest magnitude in $^{D}V_{max}$ would then provide the best assay sensitivity to magnetic field effects. Isotope effect measurements were determined using 6 mM substrate, 10 times higher than the K_M for *L*-glutamate, and ensure steady-state conditions were met. Under the conditions of the assay, the coupled formation of mesaconate was linear with time up to 1.5 min (total assay time) under all three pH conditions. Less than 2% of the substrate was consumed. Each assay was repeated at least 9 times in order to minimize random error. A representative assay of each condition is shown in Figure 47.

The isotope effect on V_{max} was measured by first individually measuring the rates of *L*-glutamate and d_5-*L*-glutamate. The amount of mesaconate formed as a function of time was determined by monitoring the change in absorbance at 240 nm and assuming an extinction coefficient of 3,850 $M^{-1}cm^{-1}$.[40, 197] The rate obtained was then divided by the amount of enzyme used in the assay to obtain k_{cat} in units of s^{-1}. $^{D}V_{max}$ was calculated simply by taking the ratio of the rates of reaction of proteated and deuterated substrates (Figure 48). The results are shown in Table 8. Despite the k_{cat} being greatly affected by pH, the $^{D}V_{max}$ isotope effect was similar under all three conditions of pH

(Table 8). Since the isotope effect apparently did not change, further experiments were conducted at pH 8, the pH that provided the fastest k_{cat}.

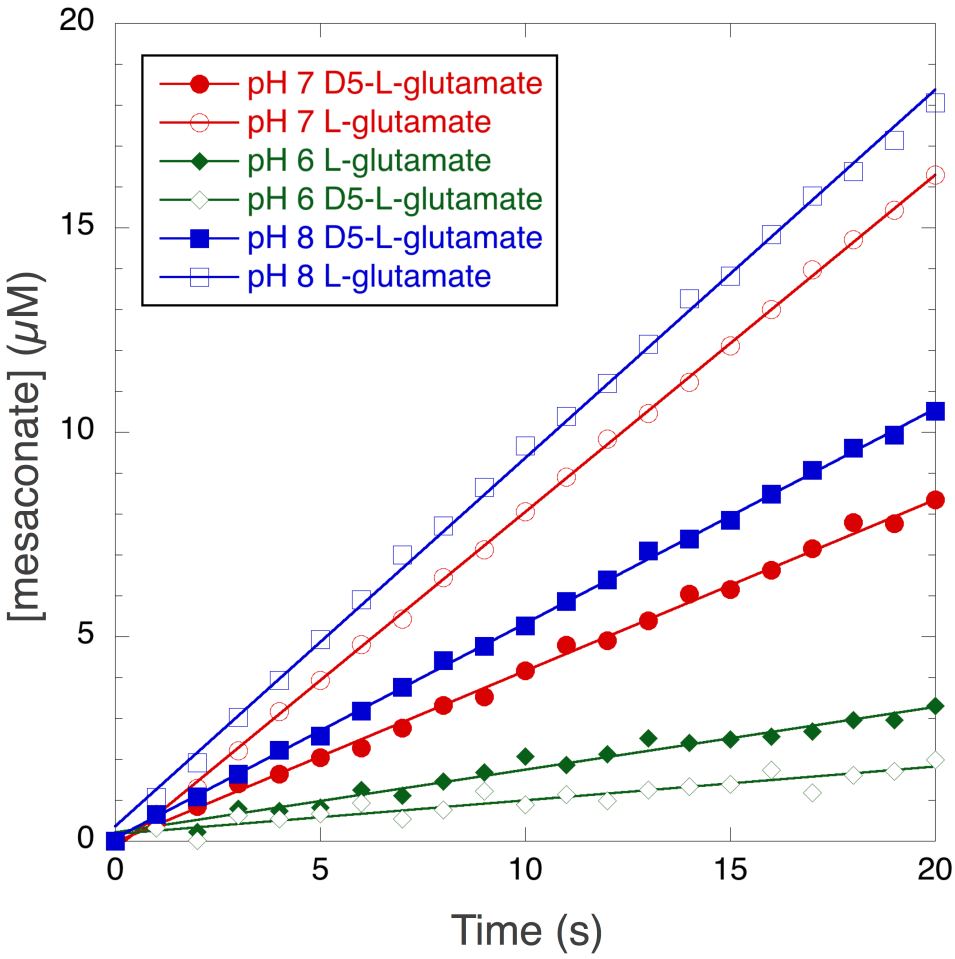

Figure 47. Determination of the Deuterium Kinetic Isotope Effect on V_{max} for Glutamate Mutase at Various pH. k_{cat} was determined from initial velocity plots for OptGlmES with saturating concentrations of *L*-glutamate. The symbols represent the reactions of unlabeled (open symbol) or D_5-*L*-glutamate (filled symbol).

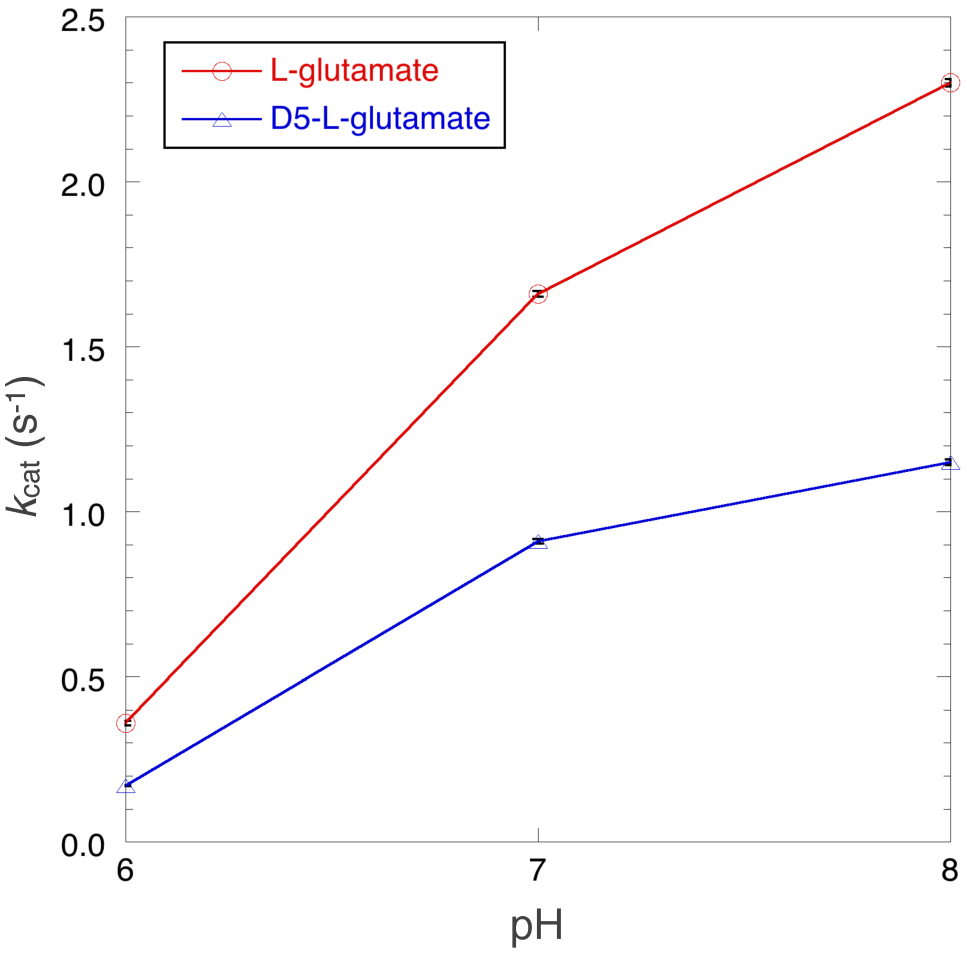

Figure 48. k_{cat} **of Glutamate Mutase at Various pH Using Saturating Concentrations of D_5 and Proteated *L*-Glutamate**. Rate data was averaged over at least 9 trials.

pH	Isotope	k_{cat} (s^{-1})	$^{D}V_{max}$
6	Proteum	0.36±0.01	2.1±0.1
	^{2}H	0.166±0.002	
7	Proteum	1.66±0.01	1.83±0.02
	^{2}H	0.909±0.007	
8	Proteum	2.30±0.01	2.00±0.02
	^{2}H	1.15±0.01	

Table 8. OptGlmES Vmax Deuterium Kinetic Isotope Effect at Various pH. Conditions for V_{max} used 6 mM substrate in 100 mM potassium phosphate at pH 8.0. The error associated with the data is reported as its standard error.

3.3.2. Magnetic Field Dependence on V_{max} and k_{cat}/K_M. Since glutamate mutase shares its initial chemical step with ethanolamine ammonia lyase (AdoCbl homolysis coupled to substrate hydrogen abstraction),[5] a static magnetic field was used in the range that Harkin and coworkers reported an observed effect,[174] 1,400±15% Gauss. Magnetic field effects on V_{max} and $^{D}V_{max}$ were determined as described in the previous sections. Assays were first conducted without any permanent magnets around the cuvette holder using 6 mM labeled and unlabeled substrate. Subsequently, permanent magnets were assembled around the cuvette holder ensuring the center of the magnetic field intersected with the center of the cuvette. The diameter of the magnets fully encompassed the size of the cuvette ensuring the entire cuvette was within the field. Assays were then repeated using 6 mM of each substrate.

There are two ways to measure V_{max}/K_M. One way is to arrive at the parameter indirectly, deriving both V_{max} and K_M separately by fitting the observed d[P]/dt vs. [substrate] to the Michaelis-Menten equation $d[P]]/dt = V_{max}[S]/(K_M + [S])$ using nonlinear methods. Alternatively, it can be measured directly because at sufficiently low substrate concentrations, the Michaelis-Menten equation reduces to $d[P]]/dt = V_{max}[S]/K_M$. Direct measurement introduces less error because the associated error is intrinsic to the measurement itself instead of having to propagate two different errors associated with measuring V_{max} and K_M separately. K_M for OptGlmES is about 0.6 mM. Therefore, using a substrate concentration of 0.2 mM gives a substrate concentration 3 times below K_M and provides a reasonable approximation to V_{max}/K_M conditions. The caveat is that, since a low substrate concentration must be used (relative to K_M), the concentration will change much faster than at V_{max} conditions.

Consequently, the initial rate will be linear for a much shorter time interval and greater care must be taken to ensure any measurements are made under steady-state conditions. To ensure this, it is very important to include in any rate calculation a change of 10% or less in substrate concentration. In this case, a 10% substrate depletion corresponds to a change in absorbance at 240 nm of 0.077 assuming ε_{240} = 3,850 $M^{-1}cm^{-1}$. Therefore, a maximum absorbance change of 0.077 was only included in rate data calculations in order to satisfy the experimental conditions. Despite spanning a range of less than 0.1 AU, a good linear fit was observed for that data as evidenced by the greatest standard error being ~ 3%. The kinetic parameters for OptGlmES in the absence or presence of an external magnetic field are shown in Table 9. Under the conditions used, V_{max} and k_{cat}/K_M, as well as their deuterium kinetic isotope effects, are invariant with magnetic field.

		V_{max} Conditions		k_{cat}/K_M Conditions	
	Isotope	$k_{cat}(s^{-1})$	$^{D}V_{max}$	k_{cat}/K_M ($s^{-1}mM^{-1}$)	$^{D}k_{cat}/K_M$
(-) MF	Protium	2.86±0.02	2.24±0.04	0.888±0.006	2.6±0.1
	^{2}H	1.27±0.02		0.34±0.01	
(+) MF	Protium	3.01±0.01	2.27±0.03	0.870±0.011	2.6±0.1
	^{2}H	1.32±0.01		0.34±0.01	

Table 9. Magnetic Field Dependence on the Kinetics of Glutamate Mutase. Magnetic field (MF) dependence of k_{cat}, k_{cat}/K_M, and the respective deuterium isotope effects for glutamate mutase using deuterated and proteated *L*-glutamate. Conditions for V_{max} used 6 mM substrate and k_{cat}/K_M used 200 μM substrate in 100 mM tris-HCl at pH 8.0. The error associated with the data is reported as its standard error.

3.4. Discussion

Magnetic field effects in enzymatic reactions can only be observed if certain stringent requirements are satisfied.[209] Based on the current mechanistic information known for the AdoCbl-dependent enzymes mentioned here, the biochemical reasons for the observed difference in field sensitivity is unfortunately left to speculation. On

balance, it is not surprising that a magnetic field effect is not observed under saturating concentrations of substrate (Harkins[174] and Taoka[221] observed this as well). Typically, the mechanism for AdoCbl-dependent rearrangements ends with recombination to reform AdoCbl after the final hydrogen transfer from 5'-deoxyadenosine back to product radical regenerates the [cob(II)alamin-AdoCH$_2$•] radical pair (Figure 3).[5] However, recombination need not occur from the end of one catalytic cycle to the beginning of another.[226, 227] Under V_{max} conditions, the enzyme's rate becomes independent of substrate concentration as it always has substrate bound (*i.e.*, the rate it is limited by product release). Existing primarily as the enzyme-substrate complex, the enzyme bound [cob(II)alamin-AdoCH$_2$•] radical pair state is maintained and the radical pair does not have to recombine before the next cycle starts. Since [cob(II)alamin-AdoCH$_2$•] recombination is reported to be the magnetically sensitive step in EAL,[223] saturating concentrations of substrate would bypass that step in the mechanism.

A magnetic field effect is more likely to be observed on the kinetic parameter V_{max}/K_M and considering that the first step in the mechanism of all AdoCbl-dependent enzymes is the same (*i.e.*, homolytic cleavage of the Co-C bond in AdoCbl resulting in the formation of a [cob(II)alamin-AdoCH$_2$•] radical pair), it is interesting that neither bacterial nor human methylmalonyl CoA mutase (MMCM)[221] nor glutamate mutase (OptGlmES) shows a magnetic field at effect 1,400±15% Gauss on k_{cat}/K_M, the range reported for EAL.[174] Under conditions of low substrate relative to K_M, the rate is dependent on the concentration of substrate and, thus, on the ability to form the enzyme-substrate complex. Since free enzyme predominates, the [cob(II)alamin-AdoCH$_2$•] radical pair is able to recombine to AdoCbl after turnover.

To observe a magnetic field effect on an enzymatic reaction, any mechanistic steps that precede formation of the enzyme-substrate radical pair must be reversible.[209] In other words, the substrate must be able to dissociate from the Michaelis complex faster than it reacts to give products. One way to monitor this is by using primary kinetic isotope effects. If the rate at which substrate is converted to product is much faster than non-productive substrate dissociation (sticky substrate), then an isotope effect on hydrogen abstraction will either not be observed or be very small. MMCM and EAL have deuterium kinetic isotope effects of 4.2 and 6.8, respectively. Similarly, OptGlmES has a significant isotope effect of 2, indicating that glutamate is able to dissociate faster than it is converted to methylaspartase. Therefore, as in the case of MMCM,[221] this cannot be a reason for the lack of a magnetic field effect on glutamate mutase.

This discrepancy may result from the slightly different chemical environments to which the [cob(II)alamin-AdoCH_2•] radical pair is exposed. The AdoCbl-dependent family of enzymes can be sub-divided into two classes based on the way AdoCbl is bound in the active site.[15] The carbon skeleton mutases, such as methylmalonyl CoA[164] and glutamate[165] mutase, as well as the aminomutases[71, 201] belong to the class I sub-family. The corrin ring sits on top of an $\alpha_5\beta_5$ Rossman fold, with the lower 5,6-dimethylbenzimidazole (DMB) axial ligand buried in a pocket about 14 Å away from the central cobalt atom; the DMB ligand is replaced by an active site histidine residue that coordinates cobalt.[228] The eliminases, such as ethanolamine ammonia lyase,[167] and diol dehydrase[166] make up class II. In these enzymes, AdoCbl is bound with the DMB base still coordinated to cobalt. In this case, the coenzyme rests on the side of a β-sheet that is part of an α/β fold (Figure 49). Accordingly, it is no surprise that the

electron paramagnetic resonance (EPR) spectra of the mutases differ from that of the eliminases.

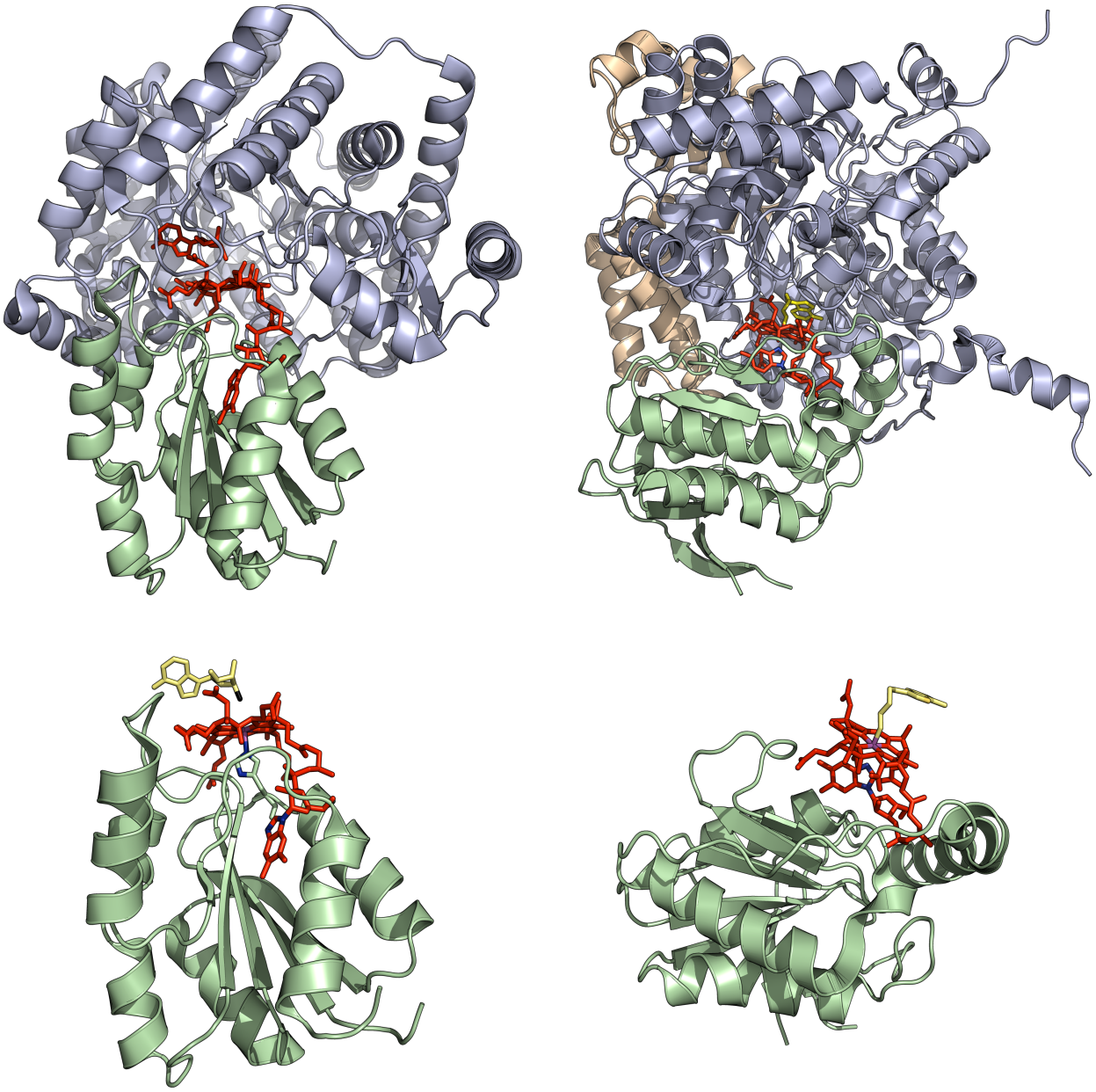

Figure 49. Structure of Glutamate Mutase and Diol Dehydrase. Left: Structure of glutamate mutase (PDB 1I9C) with AdoCbl bound in the "base-off" mode. Right: Structure of diol dehydrase (PDB 1EEX) with adenylpentanyl-cobalamin bound in the "base-on" mode. The B_{12}-binding subunit in green; the adenylpentanyl ligand for diol dehydratase and adenosyl ligand for glutamate mutase is in yellow; the cobalamin portion in red. For glutamate mutase, the bond between the ligand and cobalt is broken in the structure.

3.4.1. EPR of AdoCbl Elminases and Mutases. EPR spectroscopic studies on a variety of AdoCbl-dependent enzymes have confirmed the existence of paramagnetic intermediates characterized as an organic radical coupled to a low spin Co(II) center.[52, 202] Interestingly, despite similar homolytic reaction mechanisms, the nature of the coupling between the organic radical and the cob(II)alamin cofactor varies among the AdoCbl binding classes.[229]

The eliminases are characterized by a weak radical pair spin coupling.[63, 156, 157] In ethanolamine ammonia lyase,[230, 231] Zeeman interactions produce two signals: a broad doublet at 2.3 *g* characteristic of cob(II)alamin and a second doublet split by 140 Gauss at $g = 2$ characteristic of the substrate organic radical.[202] The organic radical's signal splitting arises from the through space, dipole-dipole interactions between the cob(II)alamin's *d* orbital radical and the organic *p* orbital radical weak exchange interaction of $K_{\alpha\beta} = 0.008$ cm^{-1}.[232, 233] Isotope labeling experiments have identified the organic radical as a mixture between substrate and product radical in EAL. Structural analysis of the electron signals revealed the organic radical to be 10 - 11 Å directly above the Co(II) center.[229, 230] A large rotation of the ribose sugar about the N-glycosidic bond moves the C5' carbon away from the cob(II)alamin and positions it within the substrate's van der Waals radius, accounting for the 10 - 11 Å separation between Co(II) and the substrate radical (Figure 50).

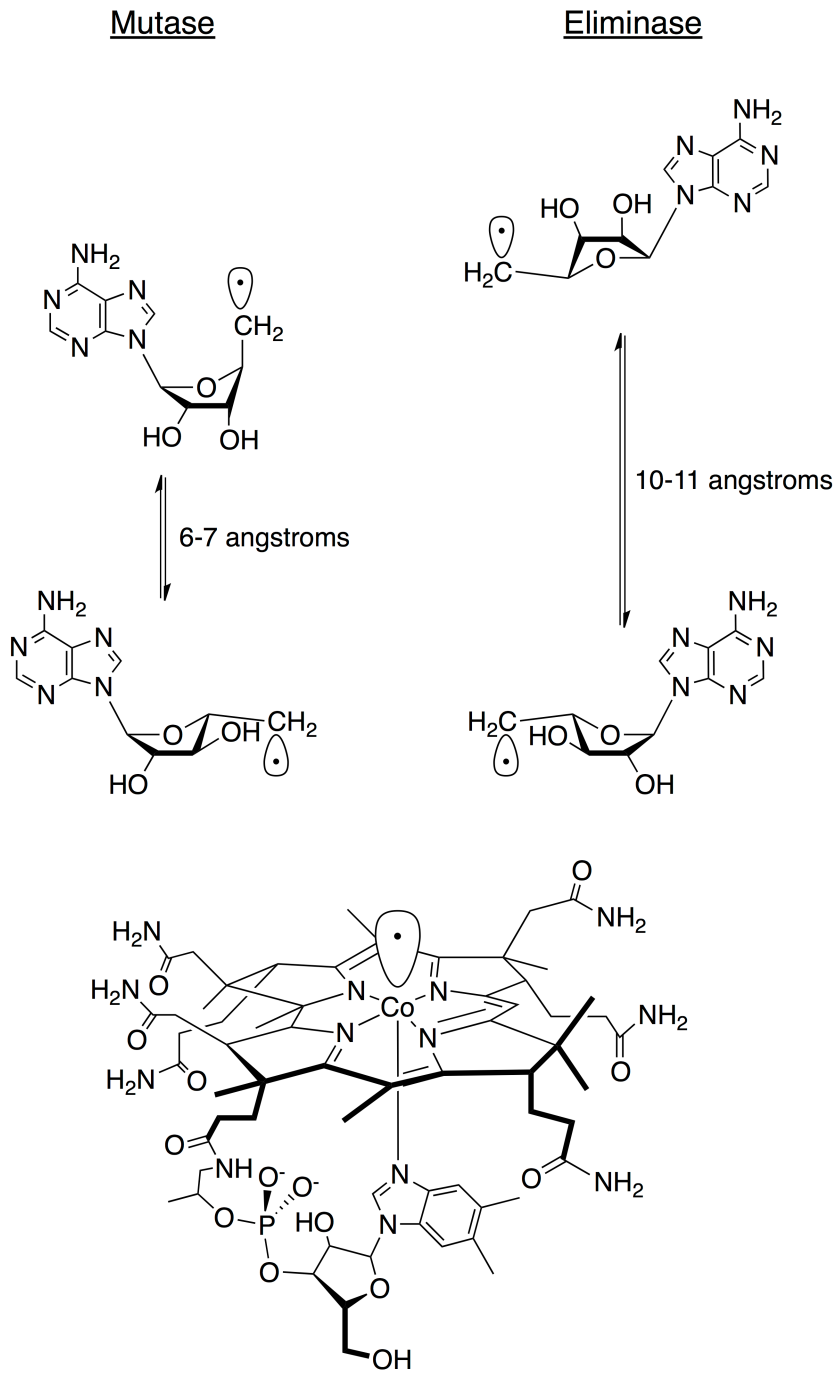

Figure 50. Different Trajectories of the 5'-Deoxyadenosyl Radical in AdoCbl-Dependent Enzymes. In glutamate mutase (left), simulations of its EPR spectra place the inter-radical distance between the substrate and cob(II)alamin to be approximately 6.6 Å. This distance can be bridged by a pseudorotation of the ribose ring that moves the 5'-carbon from an axial to an equatorial location, guiding the radical away from recombination and toward substrate radical generation. In the ethanolamine ammonia lyase (right), rotation about the N-glycosidic bond of the adenosyl moiety would allow the 5'-carbon of deoxyadenosine to move the required 10 - 11 Å between the position near the substrate and its original bound position with the cofactor.

In the case of the mutases,[234, 235] the EPR spectra are indicative of a strongly coupled spin system.[229] The spectrum is characterized by a single broad signal centered at a *g*-value of 2.1 with hyperfine splitting spaced at 55 Gauss.[202] The interaction is characterized as being dominated by an exchange interaction of $K_{\alpha\beta} > 0.1$ cm^{-1} with a *g*-value that is in between the values for isolated cob(II)alamin and an organic radical.[62] In this case, the inter-radical distance between substrate and cob(II)alamin was determined to be 6 - 7 Å, values were in excellent agreement with the positions of substrate and cofactor determined crystolographically.[236] In contrast to the large-scale glycosidic bond rotation in the eliminases, a simple pseudo-rotation of the ribose ring relocates the C5' carbon from its ground state axial position to an equatorial position that is primed for H-atom abstraction in the mutases (Figure 50). In glutamate mutase, isotopic substitution has identified the organic radical as the 4-glutamyl radical intermediate.[62]

3.4.2. Strong Spin-Spin Coupling in Glutamate Mutase Leads to an Overall Reduction in ISC. Energy must be released or absorbed by a radical pair for intersystem crossing to occur. Consequently, the rate at which ISC occurs strongly depends on a suitable mechanism being able to provide the necessary energy to bridge the gap between the singlet and triplet states (ΔE_{ST}).[209] In solution, radical pairs are free to diffuse apart decreasing the probability of geminate recombination. In the cage-like environment of an enzyme's active site, however, the degree to which the radical pair is held in close proximity can dramatically influence the energy required for ISC to occur. A radical pair maintained in close proximity will usually experience stronger coupling and require more energy than the hyperfine interaction is capable of providing

to bridge the ΔE_{ST} gap.[229] Therefore, in a close, strongly coupled system, an increase in ISC is energetically more difficult. Conversely, weakly coupled systems kept at a relatively large distance from each other (but still close enough to allow for the radical pair to maintain its spin correlation) tend to have small singlet to triplet energy gaps potentially allowing for more ISC. The following sections will discuss how an external magnetic field can modulate ISC and, thus, affect radical pair recombination in enzymatic systems.

3.4.3. An Applied Magnetic Field Will Reduce Hyperfine Induced Intersystem Crossing.[209, 214, 220, 221] Hyperfine coupling between the magnetic moments of an unpaired electron and a nearby nucleus will result in a "torque" capable of providing sufficient energy to flip the electron spin by the chemically-induced dynamic spin polarization mechanism. This will only occur in weakly coupled radical pairs where the ΔE_{ST} gap is relatively small (*i.e.*, $K_{\alpha\beta}$ is very close to zero). Furthermore, since ΔE_{ST} gap is modulated by the exchange interaction $K_{\alpha\beta}$ (Figure 44), this mechanism is feasible when the isotropic hyperfine coupling between the two radical centers is larger than the exchange between them. A zero external field results in $K_{\alpha\beta} = 0$, allowing the hyperfine coupling interactions to mix the S_0 and three degenerate $T_{0,\pm1}$ states. At equilibrium, the spin population will exist in a 25% singlet to 75% triplet distribution. Therefore, hyperfine coupling will thermodynamically drive a radical pair produced in the singlet state to undergo ISC to the triplet state. In an enzymatic system, this will promote a net forward flux in catalysis through the triplet state, since recombination is energetically unfavored from the triplet state. When a magnetic field is applied, the $T_{0,\pm1}$ degeneracy is lifted proportional to the field strength, decreasing the hyperfine induced

mixing of the S_0 and $T_{\pm1}$ states. Mixing is now only allowed between S_0 and T_0 as the $T_{\pm1}$ states are energetically out of reach. This enriches the radical pair population in the singlet state and leads to a reduction in singlet to triplet ISC. Consequently, radical pair recombination is increased.

Hyperfine coupling could explain the magnetic field dependent decrease in V_{max}/K_M observed for EAL. Since C-Co bond homolysis produces the spin-correlated [cob(II)alamin-AdoCH$_2$•] radical pair in the singlet state,[220] the reduction in V_{max}/K_M was attributed to a reduction in ISC.[174] In this case, ISC to the triplet $T_{\pm1}$ states are reduced by the Zeeman splitting, causing an increase in the singlet population which is free to recombine. An increase in recombination rate will decrease the forward flux to hydrogen abstraction. Since hydrogen abstraction is rate limiting in AdoCbl-dependent enzymes,[15] this will result in a decrease in V_{max}/K_M. EPR measurements established the hyperfine coupling between Co(II) and the organic radical to be 50 Gauss in glutamate mutase.[62] This is considerably smaller than the coupling of 140 Gauss reported for EAL.[232] The field strength range in which a magnetic field can affect ISC is proportional to the ability of the hyperfine coupling to bridge the ΔE_{ST} gap. Having an approximately 3-fold smaller coupling constant, it is possible the the field strength window in which glutamate mutase can experience a decrease in ISC is much smaller than in EAL so that in the field strength of 1,400±15% Gauss, ISC is not reduced in glutamate mutase.

It is possible that the magnetic field window to see an ISC reduction in glutamate mutase is narrower than in EAL, but another possibility is that glutamate mutase, having a strongly coupled radical pair, is unable to efficiently achieve ISC altogether. The

hyperfine mechanism relies on a relatively weak coupling interaction between the radical pair so that hyperfine interactions have the possibility to overcome the exchange interaction. The stronger the coupling, the larger the exchange integral is and the less likely hyperfine coupling can overcome it. As discussed previously, methylmalonyl-CoA mutase has a similar strongly coupled electron pair. Experiments on MMCM probed for field effects not only in 1,400 Gauss range done here for glutamate mutase, but on the entire range in which the hyperfine mechanism is established to operate (HFI reduced ISC typically occurs up to 1,000 Gauss).[172] Just as in glutamate mutase, no field effects were observed. If these strongly coupled systems cannot achieve ISC, there will be no equilibrium to funnel away from the triplet state in the first place and a magnetic field dependent decrease in ISC would not be observed.

3.4.4. The Level Crossing Mechanism Can Increase ISC in an Applied Magnetic Field. The exchange interaction modulates the interaction of two electrons only if they are within proximity of each other long enough for a fixed distance of ~ 10 Å to be established.[229] At this distance, coulombic repulsions between the electrons become significant and, to ensure the Pauli principle is maintained, electron coupling will become more prominent and the exchange energy $K_{\alpha\beta}$, which modulates electronic coupling, will be greater than zero. This will cause ΔE_{ST} to also be greater than zero, establishing an electronic preference for either the singlet or triplet state. If the exchange interaction between the electrons is twice as large as the energy provided by the HFI, hyperfine coupling will not be sufficient to overcome ΔE_{ST}.[209, 221] This will prevent ISC and conversion between the two states will not occur. The ΔE_{ST} gap for EAL or glutamate mutase is not known. However, the coupling constants for the radical

pair intermediates have been determined. The established value for $K_{\alpha\beta}$ between the 4-glutamyl and cob(II)alamin radicals in glutamate mutase is greater than 0.1 cm^{-1}.[237] In EAL, the exchange interaction between the EPR detected spin correlated radical pair is 0.008 cm^{-1}.[232, 233] Therefore, the electron spin-coupling between the radical pair in glutamate mutase is at minimum 12.5-fold larger than in EAL. Given that the inter-radical distance is in glutamate mutase is shorter than in EAL giving rise to a more strongly spin coupled system,[229] ISC between the singlet and triplet states in glutamate mutase may be much harder to achieve.

Assuming it is much harder for glutamate mutase to undergo ISC, there will be a greater population in the singlet state when compared to EAL since the radical pair after Co-C homolysis is born in the singlet state. Thus, the radical pair in glutamate mutase is predisposed to undergo a greater degree of recombination. But, how can a magnetic field shift the singlet-triplet equilibrium in EAL towards the singlet state so that forward catalysis through the triplet state is reduced? As mentioned previously, the triplet degeneracy is lifted such that $T_{\pm1}$ is separated from T_0 in equal but opposite directions. However, there may be a narrow region at the given inter-radical distance and magnetic field strength that the energy surface of S_0 and T_{-1} overlap promoting ISC (Figure 44).[172, 209] If the level crossing effect is the underlying mechanism for the observed magnetic field effect in EAL, then a field of ~ 1,000 - 1,800 Gauss is presumably optimized to allow S_0 and T_{-1} overlap at a distance of 10 - 11 angstroms. For glutamate mutase, however, an entirely different field strength may be necessary to provide this accessibility.

3.4.5. A Magnetic Field Can Increase Intersystem Crossing by Electron Spin Rephasing.[172, 209]

Whereas an external magnetic field diminishes ISC mediated by hyperfine coupling promoting geminate recombination, the spin rephasing or Δg mechanism acts to promote ISC and, thus, acts against geminate recombination. Instead of relying on the hyperfine interaction to provide the energy required for spin flipping, the Δg mechanism can promote ISC by simply rephasing the electron spin vectors.

In an applied magnetic field of strength B, the electrons net magnetic moment will precess about a defined axis at its Larmour frequency $v = g\mu_B B\hbar^{-1}$ (Figure 43). In a fixed magnetic field, μ_B, B, and $\hbar$ are constants and, thus, v is dependent on the g-value. Consequently, the precession rate can be written as $v = (g_\alpha - g_\beta)\mu_B B\hbar^{-1}$ when considering the coupling between a radical pair. Since the g-value is a function of the atomic nucleus associated with the electron, a homonuclear electron pair will have a Δg of zero and both electrons will precess at the same Larmour frequency. However, in the heteronuclear case of the Co(II)-organic radical pair Δg is nonzero. The frequency of precession for each electron will be different resulting in a system oscillating between the singlet and T_0 through a mixing of the S_0 and T_0 states (Figure 51). Electron spin evolution will only occur between S_0 and T_0 since the magnetic field has lifted the $T_{\pm1}$ degeneracy. The magnitude of Δg will, thus, have a direct impact on ISC rates. Harkins and Grissom found the magnetic field dependence of V_{max}/K_M in EAL to be biphasic. After 1,000 and 1,500 Gauss for proteated and perdeuterated substrate respectively, V_{max}/K_M begins to increase and plateaus between 2,000 - 2,500 Gauss.[174] Spin

rephasing becomes more significant at higher field strengths (typically above 1,000 Gauss)[172] and will, thus, increase ISC, ultimately increasing V_{max}/K_M.

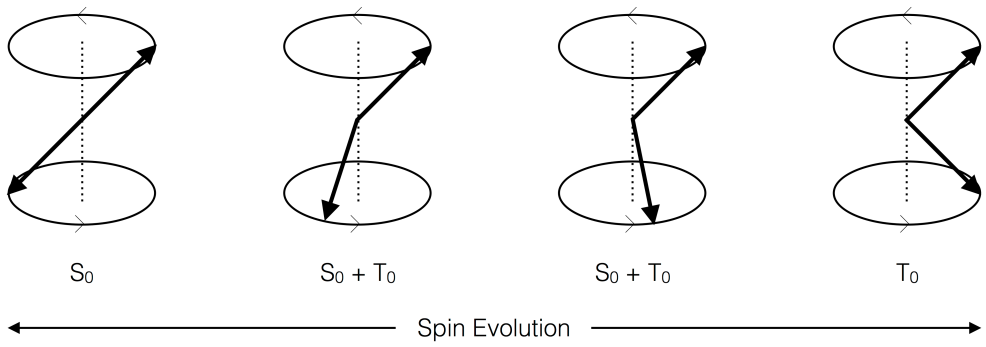

Figure 51. Vector Representation of Spin Evolution: The *Δg* Mechanism. A radical pair with sufficiently different *g*-values held in proximity long enough may experience spin rephasing of its electron vectors providing a mechanism for intersystem crossing to occur between the S_0 and T_0 states.

For ISC to occur, the radical pair must be held in close proximity for at least the length of time it takes for spin evolution to occur, which can be calculated from the *Δg* Larmour frequency equation. In EAL, the organic and cob(II)alamin radicals have discrete *g*-values of 2.00 and 2.3, respectively.[221] At 1,000 Gauss, the time required for spin evolution to rephase the S_0 and T_0 states is $v = 3.08 \times 10^{-10}$ s. This is within the timeframe required for ISC by spin rephasing to compete with radical separation or recombination. However, in the strongly coupled glutamate mutase system, the organic and cob(II)alamin radical's do not possess discrete *g*-values. Rather, EPR reports a single broad *g*-value suggesting that *Δg* is very close to zero.[62, 202] The spin vectors of the two unpaired electrons will, therefore, precess at similar rates and spin rephasing will not occur during the lifetime of the radical pair. Therefore, as in methylmalonyl-CoA mutase,[221] the spin-rephasing mechanism is unlikely to affect the ISC rates in glutamate mutase, resulting in radical pair recombination pathways that are insensitive to external magnetic fields.

CHAPTER 4‡

PROBING THE INHIBITION OF FARNESYL PYROPHOSPHATE SYNTHASE BY THE INTERFERON INDUCIBLE PROTEIN VIPERIN

4.1. Introduction

4.1.1. Initial Characterization of Viperin Suggests it Belongs to the Radical SAM Family of Enzymes. In response to viral infection, the innate immune system of mammalian cells triggers the release of type I interferon (IFN) cytokines which, upon binding to the type-I IFN receptor, results in the up-regulation of over 300 IFN stimulated genes (ISGs).[238-240] ISGs are crucial to the host's ability to ward off infection as evidenced in humans and mice deficient in type-I IFN that display an enhanced susceptibility to viral infection.[241] Although the antiviral response is increasingly well understood at the cellular and genetic level, the biochemical mechanisms by which ISGs limit viral replication remain unclear. One such ISG, viperin (Virus Inhibitory Protein, Endoplasmic Reticulum associated, INterferon inducible) is gaining interest because it is one of the few identified ISGs known to have direct antiviral activity against a number of pathogens that infect eukaryotic cellular based organisms including human immunodeficiency (HIV),[242] hepatitis C (HCV),[243, 244] and influenza [245, 246] viruses.[247-249]

‡ Paige Malec from the laboratory of Professor Robert Kennedy performed LCMS-MS analysis on the formation of 5'-deoxyadenosine from HEK293T cells.

The human homologue was initially identified in 2001 through studies on human cytomegalovirus (HCMV) in primary fibroblast cells where two cDNA fragments, designated cig5 and cig33 (cytomegalovirus inducible gene), were later discovered to form one transcript.[250] Sequence analysis reveals this 361-residue, 42 kDa protein to be highly conserved throughout vertebrate animals and comprises three domains (Figure 52).[247]

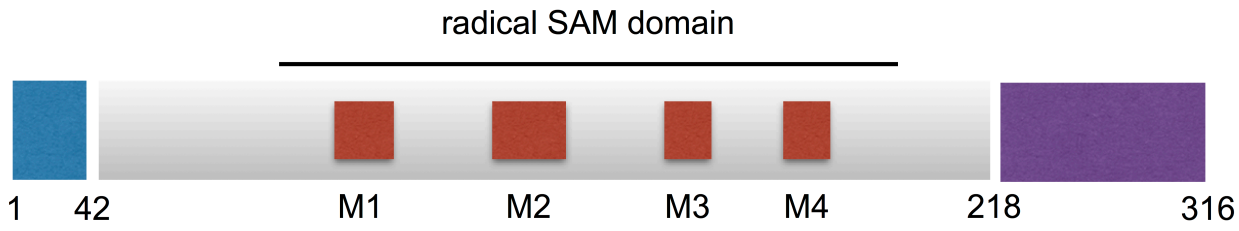

Figure 52. Schematic of Viperin Structure. Residues 1-42 contain the N-terminal amphipathic α-helix (blue). Residues 77-209 contain 4 conserved motifs, which make up the radical SAM domain (M1-M4, red). Residues 218-316 contain the conserved C-terminus (purple).

The first 42 N-terminal residues vary considerably among species but all contain an amphipathic helix that appears to be involved in binding to the cytosolic face of the endoplasmic reticulum (ER).[251] The amphipathic helix is essential for viperin's ability to limit the chikungunya virus (CHIKV), which is known co-localize with viperin on the ER.[252] Furthermore, viperin expression was found to inhibit the transport of soluble proteins across the ER, potentially limiting the transport of virally encoded and cellular proteins necessary for viral replication. Interestingly, the N-terminal α-helix expressed as a dsRed fusion protein was sufficient to significantly reduce secretion of soluble alkaline phosphatase as well as reduce its rate of ER-to-Golgi trafficking, suggesting it is essential for inhibiting protein secretion.[251] The N-terminal helix is also responsible for localizing the protein to lipid droplets and is crucial in viperin's ability to act as an

antiviral against HCV.[253] This domain appears to be dispensable for the enzyme's activity against HCV[254] the dengue virus (DENV).[255]

The C-terminal domain is highly conserved across species and may be important for the aggregation of ER bound viperin. Hinson and Cresswell demonstrated viperin self-associates independently of the N-terminal helix to form dimers, which are thought to bring opposing membranes of the ER together to form lattice-like crystalloid structure.[251] Its exact antiviral function remains unknown, yet its presence is important for viperin's activity against DENV.[255] In fact, it is so crucial to viperin's function against HCV that simple epitope tagging at the C-terminus leads to a complete loss of antiviral activity.[254] It is possible the C-terminal domain mediates viperin's interactions with its targets as it was shown to be important for viperin to interact with CIAO1, a key component of the cytosolic iron-sulfur protein assembly (CIA) machinery, during viperin's inhibition of vtick-borne encephalitis virus (TBEV).[256]

The central domain contains four motifs characteristic of radical *S*-adenosyl-*L*-methionine (SAM) enzymes, of which motif 1 contains the canonical CX_3CX_2C [4Fe-4S] cluster binding sequence. Radical SAM enzymes use a [4Fe-4S] cluster to chelate AdoMet and generate a highly reactive 5'-deoxyadenosyl radical (Ado•) intermediate by way of reductive cleavage of SAM's 5'-C-S bond.[26, 257] Ado• radical is then used abstract a hydrogen from the substrate; the common first step in a wide variety of challenging chemical transformations (Figure 53).[5]

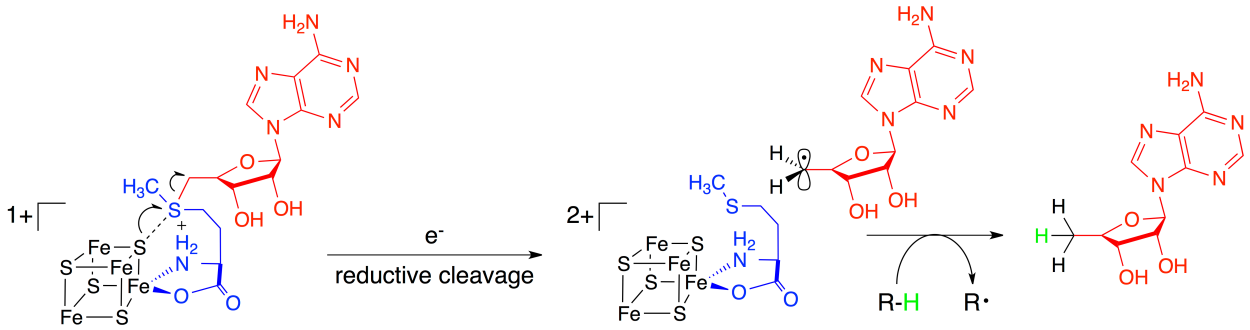

Figure 53. Generation of Substrate-Based Radicals by Radical SAM Enzymes. The key initiating step is the reductive cleavage of SAM into a 5′-deoxyadenosyl radical (Ado•). The highly reactive Ado• intermediate allows the substrate to be readily activated toward reaction through stereoselective H-atom abstraction.

This is perhaps the most unusual feature of viperin as radical SAM enzymes are notoriously sensitive to oxygen and, thus, once thought unlikely to function in aerobic organisms. However, this view is beginning to change as new studies elucidate possible strategies employed by aerobic organisms to combat oxidative degradation of the enzyme's iron-sulfur clusters.[5] Discovery of the oxygen-sensitive iron-sulfur protein Mocs1a[258] (a human homolog of the radical SAM enzyme MoaA involved in molybdopterin biosynthesis) and the recently characterized HMP-Synthase (a plant homolog of the radical SAM enzyme ThiC[259] that is involved in thiamin biosynthesis) demonstrate that radical SAM enzymes are able to function in aerobic metabolism.

Despite initial skepticism, there is now good immunological and biochemical evidence to suggest that viperin is indeed a radical SAM enzyme. Introduction of mutations into the radical SAM domain motifs impaired the enzyme's effectiveness against West Nile virus (WNV),[260, 261] HCV,[254] HIV,[242] DENV,[260] TBEV,[256] and Bunyamwera[262] virus *in vitro*. Spectroscopic studies on purified, N-terminally truncated viperin from heterologous expression in *E. coli* demonstrated viperin can bind a reducible [4Fe-4S]$^{+1}$ cluster that is able to coordinate SAM.[263, 264] Duschene and

Broderick showed that incubation of reduced viperin with SAM results in the reductive cleavage of SAM to produce 5'-deoxyadenosine, the classic radical SAM byproduct.[263] Furthermore, conformational analysis studies on viperin mutants in which the motif 1 cysteine residues were replaced with alanine suggest the mutants lack significant conformational integrity and lead to protein aggregates;[265] this may explain the lack of antiviral activity in the radical SAM domain mutants.

Type of Protein	Viperin Interacting Target	Mode of Action
Cellular Protein	Farnesyl pyrophosphate synthase (FPPS)[266]	Inhibits viral budding through lipid rafts by reducing cholesterol biosynthesis
	Mitochondrial trifunctional protein (MTP)[267]	Inhibits fatty acid metabolism after transport of viperin to mitochondrion by vMIA
	Vesicle associated membrane protein - associated protein A (VAPA)[268]	Unknown
	Interleukin-1 receptor-associated kinase 1 (IRAK 1)[269]	Binds both IRAK 1 and TRAF 6 to facilitate ubiquitination of IRAK 1 by TRAF 6
	TNF receptor-associated factor 6 (TRAF 6)[269]	Unknown
Viral Protein	hCMV / vMIA[267]	Recruits viperin to mitochondrian to inhibit MTP
	Dengue virus nonstructural protein 3[255]	Inhibits viral replication
	Hepatitis C nonstructural protein 5A[268]	Inhibits viral replication

Table 10. Proteins Identified to Interact with Viperin. Despite viperin being known to interact with a number of cellular and viral proteins none of these interactions have been characterized in any detail and in no case has the mechanism of inhibition been determined. The best-established target of viperin is farnesyl pyrophosphate synthase (FPPS).

The ability of viperin to interact with a variety of cellular and viral proteins highlights its important role in the innate immune response to viral infection (Table 10).[247, 270] However, none of these interactions have been characterized, and the enzyme has yet to be assigned an enzymatic function. So far, neither the substrate nor how the radical SAM activity of viperin relates to its antiviral activity has been established. The potential involvement of radical SAM chemistry in the mammalian antiviral response is completely unexpected, setting viperin apart from other radical SAM enzymes, and points to a new mechanism for the regulation of enzyme activity in eukaryotic cells.

4.1.2. Viperin Interacts with and Inhibits Farnesyl Pyrophosphate Synthase.[246-249, 271] With the observation that viperin-expressing cells limited the formation of plaque-forming units in influenza A infected cells 1,000-fold, Wang and coworkers set out to establish which step in the viral replication cycle is targeted by viperin.[246] Influenza A infection begins by binding of the virus to the cell surface receptor sialic acid. Upon endocytosis of the bound virus, the acidic endosomal environment triggers membrane fusion releasing the viral genome into the cytosol and makes its way into the nucleus. In the nucleus, the viral genome is replicated and mRNA, coding for proteins involved in viral capsid assembly, are synthesized. Viral mRNA enter the cytosol and viral protein synthesis begins. The two major viral proteins synthesized are the transmembrane glycoproteins hemagglutinin (HA) and neuraminidase (NA) that are directed to cholesterol rich plasma membrane subdomains known as lipid rafts, which serve as a platform for select cellular transmembrane proteins to concentrate in and promote cell-directed protein-protein interactions. Finally,

the matrix protein (M1) assists in formation of the nucleocapsid which then co-localizes with HA and NA on the lipid rafts for final assembly of the viral progeny.

Expression of viperin in HeLa cells led to an 80% reduction in released virus while not affecting the intracellular levels of M1 protein. When associated with lipid rafts, influenza HA is insoluble in the non-ionic detergent Triton X-100 at low temperatures. However, Wang and coworkers demonstrate it to be readily extracted into Triton X-100 in viperin-expressing HeLa cells. Furthermore, fluorescence recovery after photobleaching (FRAP) studies demonstrate viperin expression results in an elevated lateral mobility of HA as a consequence of increased membrane fluidity. These results are consistent with a model in which viperin disperses the tightly packed, orderly structure of a lipid raft and suggests viperin displays its antiviral activity against influenza A by impairing the viruses ability to bud from the plasma membrane.

To understand how viperin perturbs the structure of lipid rafts, Wang and coworkers identified the enzyme farnesyl pyrophosphate synthase (FPPS) as potential target for viperin using a yeast two-hybrid screen. FPPS catalyzes the condensation of geranyl pyrophosphate to isopentenyl pyrophosphate to yield farnesyl pyrophosphate, a key intermediate in the mevalonate pathway that leads to isoprenoid and cholesterol biosynthesis (Figure 54).[244, 272] Indeed, co-immunoprecipitation studies using mouse RAW264.1 macrophage cells treated with type-1 IFN confirm endogenous FPPS and viperin interact *in vivo*. Their interaction perhaps leads to inhibition of FPPS as viperin expression in HeLa cells led to a reduction in FPPS enzymatic activity of 20% and 50% after 24 h and 48 h, respectively. In a control experiment, the siRNA-mediated knockdown of FPPS led to a 10-fold decrease in the influenza A titer produced, as well

as a 50% reduction in the amount of viral protein released by infected cells. Not surprisingly, over-expression of FPPS reverses the effects of viperin's antiviral activity, restoring influenza's ability to egress from the cell. This observed inhibition elegantly supports viperin acting to block viral release from infected cells, as opposed to interfering with the early stages of replication. Inhibition of FPPS would block downstream production of cholesterol, a vital lipid raft precursor, and lead to an increase in membrane fluidity. Interestingly, Wang and coworkers showed the *in vitro* loading of exogenous cholesterol into viperin-expressing cells decreased the lateral mobility of HA in the plasma membrane.

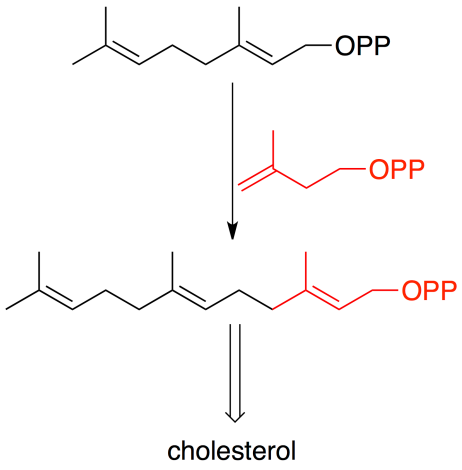

Figure 54. Reaction Catalyzed by Farnesyl Pyrophosphate Synthase (FPPS). This enzyme catalyzes the condensation of geranyl pyrophosphate with isopentenyl pyrophosphate to form farnesyl pyrophosphate, a key intermediate in the biosynthetic pathway leading to isoprenoids and cholesterol.

4.1.3. An Enzymological Approach to the Study of Viperin. In response to infection, the innate immune response induces the expression of many genes and regulates the activity of many cellular enzymes.[238-240] Understanding how the interferon stimulated gene viperin interacts with its protein targets will advance our knowledge of

how eukaryotic cells limit viral replication and prevent infection from spreading to other cells. Despite farnesyl pyrophsphate synthase (FPPS) being the currently best-established target for viperin, the mechanism by which its expression inhibits FPPS remains unknown. Consequently, understanding the biochemical underpinnings of radical SAM chemistry in the antiviral response of viperin is a primary objective. Establishing viperin's role in the innate immune response has primarily relied on cellular biology techniques to infer indirectly how the enzyme may be operating in the cell and evidence for its interaction with FPPS has amounted from *in vivo* studies.[246] However, there have been no studies to characterize these interactions on the molecular level. In this respect, an enzymology-based approach aimed at investigating the mechanism of viperin and its interaction with FPPS *in vitro* using recombinantly expressed proteins can provide a detailed mechanism of action on the molecular level lacking in a pure cell biology approach. To that end, this chapter describes studies on the interaction of viperin with FPPS using purified proteins *in vitro* with the goal of broadening our findings to study other proteins identified as targets of viperin.

4.2. Materials and Methods

4.2.1. Reagents. *S*-adenosyl-*L*-methionine was purchased from Sigma-Aldrich Co. as a *p*-toluenesulfonate salt. Isopentenyl (IPP) and geranyl (GPP) pyrophosphate were purchased from Isoprenoids, LC as their tri-ammonium salts. [4-^{14}C]-IPP was purchased from Perkin Elmer as its tri-ammonium salt. HEK293T cell line was purchased from ATCC. pcDNA3.1(+) mammalian expression vector was purchased from Invitrogen. Monoclonal 6x-His epitope tag antibody (HIS.H8) produced in mouse (IgG2b) was purchased from Thermo Scientific. Monoclonal Flag antibody

(M2) produced in mouse (IgG1) was purchased from Sigma-Aldrich Co. Monoclonal glyceraldehyde-3-phosphate dehydrogenase antibody (6C5) produced in mouse was purchased from EMD Millipore. Highly cross-adsorbed Alexa Fluor 647 mouse IgG (H+L) antibody produced in goat was purchased from life technologies. ProTEV Plus was purchased from Promega. All other materials were purchased from commercial suppliers.

4.2.2. Cloning of Viperin and FPPS.

4.2.2.1. *Cloning of viperin for bacterial expression in E. coli.* The gene encoding viperin (GenBank: AAL50053.1) was engineered to contain two unique Spe1 sites, allowing the removal of the N-terminal amphipathic alpha helix if necessary. This new construct was named M1Q/W2L-viperin. A naturally occurring Spe1 site (5'-A▼CTAGT-3') occurs between residues Q50 and L51. The first 6 residues of the wild-type viperin sequence (MWVLTP) lend itself to addition of a Spe1 site by simple point mutation of M1 to Q and W2 to L. Addition of a new start methionine yields the final M1Q/W2L-viperin sequence of MQLVLTP. Since the radical SAM domain begins at residue Y77, this design provides a simple strategy at generating truncated viperin. The gene for M1Q/W2L-viperin was codon-optimized for expression in *E. coli* with an N-terminal 6x histidine tag and purchased from GenScript sub-cloned into pET28 expression vector. A TEV protease cleavage site was included for optional removal of the histidine tag post purification. The sequence used for M1Q/W2L-viperin is shown in Figure 55. This yields a 383 amino acid protein with a predicted molecular weight of 44,630.31 Da.

```
atgggcagcagccatcatcatcatcatcacagcagcggcgagaatctttattttcagggc
 M  G  S  S  H  H  H  H  H  H  S  S  G  E  N  L  Y  F  Q  G
catatgcaactagtgctgaccccggctgcgttcgctggcaaactgctgagtgtgttccgt
 H  M  Q  L  V  L  T  P  A  A  F  A  G  K  L  L  S  V  F  R
caaccgctgtcgtcgctgtggcgttcgctggtgccgctgttttgctggctgcgtgcaacc
 Q  P  L  S  S  L  W  R  S  L  V  P  L  F  C  W  L  R  A  T
ttctggctgctggctacgaaacgtcgcaaacagcaactagtgctgcgcggtccggatgaa
 F  W  L  L  A  T  K  R  R  K  Q  Q  L  V  L  R  G  P  D  E
accaaagaagaagaagaagatccgccgctgccgaccacgccgacctcagttaactatcat
 T  K  E  E  E  E  D  P  P  L  P  T  T  P  T  S  V  N  Y  H
tttacgcgtcagtgtaattacaaatgcggcttttgtttccacaccgcgaaaacgtcgttc
 F  T  R  Q  C  N  Y  K  C  G  F  C  F  H  T  A  K  T  S  F
gtgctgccgctggaagaagcgaaacgtggtctgctgctgctgaaagaagccggcatggaa
 V  L  P  L  E  E  A  K  R  G  L  L  L  K  E  A  G  M  E
aaaattaacttttcaggcggtgaaccgttcctgcaggatcgcggtgaatatctgggcaaa
 K  I  N  F  S  G  G  E  P  F  L  Q  D  R  G  E  Y  L  G  K
ctggttcgtttttgcaaagtcgaactgcgcctgccgagcgtttctattgtctcaaacggt
 L  V  R  F  C  K  V  E  L  R  L  P  S  V  S  I  V  S  N  G
tcgctgatccgtgaacgctggtttcaaaattatggcgaatacctggatattctggccatc
 S  L  I  R  E  R  W  F  Q  N  Y  G  E  Y  L  D  I  L  A  I
agctgcgattctttcgacgaagaagtgaacgttctgatcggccgcggtcagggcaagaaa
 S  C  D  S  F  D  E  E  V  N  V  L  I  G  R  G  Q  G  K  K
aaccatgtcgaaaatctgcaaaaactgcgtcgctggtgtcgtgattaccgcgttgcattc
 N  H  V  E  N  L  Q  K  L  R  R  W  C  R  D  Y  R  V  A  F
aaaatcaactccgtgatcaaccgtttcaatgttgaagaagacatgaccgaacagattaaa
 K  I  N  S  V  I  N  R  F  N  V  E  E  D  M  T  E  Q  I  K
gctctgaacccggtgcgctggaaagtttttcaatgcctgctgatcgaaggtgaaaattgt
 A  L  N  P  V  R  W  K  V  F  Q  C  L  L  I  E  G  E  N  C
ggcgaagatgcgctgcgtgaagccgaacgcttcgtgattggtgacgaagaatttgaacgt
 G  E  D  A  L  R  E  A  E  R  F  V  I  G  D  E  E  F  E  R
ttcctggaacgccacaaagaagtcagttgcctggtgccggaatccaaccagaaaatgaaa
 F  L  E  R  H  K  E  V  S  C  L  V  P  E  S  N  Q  K  M  K
gatagctatctgatcctggacgaatacatgcgttttctgaattgtcgtaaaggccgcaaa
 D  S  Y  L  I  L  D  E  Y  M  R  F  L  N  C  R  K  G  R  K
gatccgagtaaatccattctggacgtcggtgtggaagaagcgatcaaattttctggcttc
 D  P  S  K  S  I  L  D  V  G  V  E  E  A  I  K  F  S  G  F
gatgaaaaaatgttcctgaaacgtggtggcaaatacatctggagcaaagccgacctgaaa
 D  E  K  M  F  L  K  R  G  G  K  Y  I  W  S  K  A  D  L  K
ctggattgg
 L  D  W
```

Figure 55. Sequence of M1Q,W2L-Viperin. The naturally occurring Spe1 site between Q50and L51 is shown along with the engineered one between Q2 and L3 are shown in red. The residues removed by Spe1 restriction digestion are shown in blue. The conserved CxxxCxxC iron-sulfur cluster-binding site of the radical SAM domain motif 1 is shown in orange.

4.2.2.2. *Cloning of truncated M1Q/W2L-viperin for bacterial expression in E. coli.* Truncated M1Q/W2L-viperin, in which residues L24-Q72 were removed, was created by standard molecular biology techniques through Spe1 restriction digestion of the M1Q/W2L-viperin pET28 plasmid and confirmed by sequencing. This yields a 334 amino acid protein with an expected molecular weight of 38,932.4 Da. Without considering the His tag and TEV site, residues L24-Q72 correspond to the removal of residues 3-50 of M1Q/W2L-viperin leaving 27 residues before the radical SAM domain (Figure 55).

4.2.2.3. *Cloning of FPPS for bacterial expression in E. coli.* The FPPS gene (GenBank: AAA52423.1) was codon-optimized for expression in *E. coli* with an N-terminal 6x HIS tag and purchased from GenScript sub-cloned into pET28 expression vector. A TEV protease cleavage site was included for optional removal of the histidine tag post purification. This yields a protein of 374 residues with a calculated molecular weight of 42,925.8 Da.

4.2.2.4. *Cloning of wild-type viperin and FPPS for mammalian expression in HEK293T.* Wild-type viperin encoding an N-terminal 3x FLAG tag (5'-DYKDHDGDYKDHDIDYKDDDDK-3') and FPPS encoding an N-terminal 6x HIS tag were cloned into pcDNA3.1(+) for transient expression in HEK293T cells using standard molecular biology methods. The genes for wild-type viperin and FPPS were obtained by PCR from the pET28 vectors described above. The Kozak consensus sequence (5'-GCCAAC-3') for efficient translation in eukaryotic cells was included in the PCR primers flanking the gene's start methionine. The final pcDNA3.1(+) constructs were confirmed by sequencing.

To clone wild-type viperin, the PCR primer hybridization sequence begun at V24 of M1Q/W2L-viperin and the original M1, W2 residues, along with the Kozak sequence and 3x FLAG tag were included in the primer overhang. Consequently, the TEV protease sequence and 6x HIS tag in M1Q/W2L-viperin was not included when transferred to pcDNA3.1(+). However, no modifications were necessary to clone FPPS with an N-terminal tag and, thus, was transferred to pcDNA3.1(+) with the TEV protease site.

4.2.3. Expression of Viperin and FPPS.

4.2.3.1. *Bacterial expression of M1Q/W2L-viperin and FPPS from E. coli.* Preparation of 1 L culture: 5 mL of sterile LB containing 50 µg/mL kanamycin was inoculated with BL21(DE3) *E. coli* cells containing the pET28 vector containing the appropriate gene. The cells were incubated at 37 °C with shaking at 240 rpm overnight. The next morning, the saturated 5 mL overnight was transferred to 1 L of sterile 2xYT media containing 50 µg/mL kanamycin. The 1 L culture was incubated at 37 °C with shaking at 150 rpm until the OD_{600} reached approximately 1.0 (5-6 h). The culture was chilled at 4 °C for 30 min and protein expression was induced by adding IPTG to a final concentration of 0.1 mM. The culture was further incubated at 18 °C with shaking at 150 rpm overnight (approx. 18 h). Cells were harvested by centrifugation at 5,000 rpm for 30 min at 4 °C. Cell pellet was stored at -80 °C until ready for use. Protein expression was confirmed by SDS-PAGE.

4.2.3.2. *Mammalian expression of wild-type viperin and FPPS from HEK293T.* Preparation of a 10 cm^2 dish from a 30-50% confluent culture: Dilute 3 µg pcDNA3.1(+) vector containing appropriate gene into 125 µL DMEM basal medium followed by the

addition of 9 µL FugeneHD transfection reagent. For co-transfections, dilute 3 µg DNA each into 125 µL DMEM followed by the addition of 18 µL FugeneHD transfection reagent. After incubation for 15 min at room temperature, add the mixture to the cell culture. Swirl the dish gently to uniformly distribute the DNA mixture and allow protein expression to proceed for 48 h in a humidified incubator containing a 5% CO_2 atmosphere. To harvest, aspirate the media, wash the cells with 10 mL D-PBS and lift the cells off the petri dish by re-suspending the cells in 2x 750 µL D-PBS. Collect each resuspension into a 1.5 mL eppendorf tube and centrifuge 1 min at 2,500 rpm to collect the cell pellet. Remove the supernatant and store the cell pellet at -80 °C until ready for use. Protein expression was confirmed by Western Blot (antiFlag 1:2,000; antiHIS 1:3,000; antiGAPDH 1:2,000; antiMouse 1:1,000). Typical cell pellet yield is ~ 50 µL.

4.2.4. Purification of Viperin and FPPS Expressed E. Coli.

4.2.4.1. *Purification of truncated M1Q/W2L-viperin from BL21(DE3) E. coli cells*. All steps were performed in a Coy chamber (O_2 <25 ppm) or under a nitrogen atmosphere using anoxic buffers unless otherwise noted. The cell pellet from a 6 L culture was resuspended in 100 mL lysis buffer (10 mM tris-HCl, 300 mM NaCl, 5 mM imidazole, 1 mM β-mercaptoethanol, 5mM dithionite to act as oxygen scavenger, 1 tablet/10 mL complete mini protease inhibitor tablet - Roche, 1 mg/mL lysozyme, benzonase nuclease, 10% glycerol, pH 8.0) and the suspension shaken for 30 min. Cell lysis completed by minimal sonication outside the Coy chamber. The lysate was taken back into the Coy chamber and allowed to briefly equilibrate with the anoxic environment prior to removal of the cell debris by centrifugation (17,000 rpm, 30 min, 4 °C). The supernatant loaded onto a super-loop connected to a 5 mL HIS-Trap (GE)

equilibrated in Buffer A (10 mM tris-HCl, 300 mM NaCl, 10 mM imidazole, 10% glycerol, pH 8.0) and the purification carried out by FPLC outside the Coy chamber with a flow rate of 1 mL/min (the column was kept at 10-15 °C by surrounding it with cold packs). The column was washed with Buffer A until the absorbance at 280 nm stabilized and the protein eluted with a linear gradient of 0-100% Buffer B (10 mM tris-HCl, 300 mM NaCl, 500 mM imidazole, 10% glycerol, pH 8.0) over 60 min at 1 mL/min. Elution fractions (15 total) were collected in 2.5 mL aliquots into vials followed by the addition of 500 uL of a 30 mM dithionite solution (C_f = 5 mM dithionite in 3 mL). Fractions containing truncated M1Q/W2L-viperin were pooled, centrifuged to remove precipitated protein, divided into 2mL aliquots, and stored at -80 °C until ready for reconstitution. Bradford analysis (which was used instead of the calculated extinction coefficient because the purified protein contained high levels of imidazole which would interfere with the A_{280} reading) established the enzyme stock to be 1 mg/mL (prior attempts to dialyze the pooled enzyme stock resulted in significant protein precipitation). Protein yield was ~ 4 mg/L culture.

4.2.4.2. *Purification of FPPS from BL21(DE3) E. coli cells.* FPPS was purified as described for truncated M1Q/W2L-viperin without the use of anoxic buffers, DTT, or Coy chamber. Elution fractions containing FPPS were pooled, concentrated and dialyzed 4x into 1 L of 10 mM tris-HCl, pH 8, 10% glycerol at 4 °C. Using a calculated extinction coefficient (average between the enzyme's oxidized and reduced states) of ε_{280} = 56,458 $M^{-1}cm^{-1}$, the final concentration was adjusted to 15 mg/mL, aliquoted and stored at -80 °C. FPPS (M_r 42,925.8 Da) was determined to be to > 95% as judged by SDS-PAGE. Protein yield was ~ 50 mg/L culture.

4.2.5. Reconstitution of Truncated M1Q/W2L-Viperin Purified from E. Coli.

Reconstitution was performed with slight modification of the protocol described by Duschene and Broderick.[263] All steps were performed in a Coy chamber (O_2 <25 ppm) using anoxic buffers unless otherwise noted. The following protocol is for ~ 2 mg of purified truncated M1Q/W2L-viperin. The day prior to reconstitution, an 8.3 mL PD-10 desalting column was equilibrated with copious amounts (~50 column volumes) of reconstitution buffer (10 mM tris-HCl, 300 mM NaCl, 10% glycerol, pH 8.0) in order to make the column as oxygen free as possible. The column was left to equilibrate overnight.

The truncated M1Q/W2L-viperin stock solution was slowly thawed on a cold pack and the u.v.-visible spectrum recorded using an anaerobic cuvette as a pre-reconstitution control. The protein was incubated with DTT (C_f = 5mM) for 20 min on the cold pack with gentle magnetic stirring. $FeCl_3$ (C_f = 150 uM, 6 equivalents) was added drop-wise to the stirring solution and incubate an additional 20 min. Na_2S (C_f = 150 uM, 6 equivalents) was added in one aliquot and stirred for 2 h on the cold pack. The cold pack was removed and stirred for an additional hour. EDTA (C_f = 2 mM) was added in one aliquot and stirred for 30 min to chelate any free iron and sulfide remaining in solution and solution diluted to 2.5 mL with reconstitution buffer (it is important not to exceed 2.5 mL as it is the limit for a PD-10 column). Load the reconstitution solution onto the PD-column and elute the protein. Elution aliquots were collected in 2 mL fractions. The first two fractions (dark reddish brown) were pooled and the u.v.-visible spectrum recorded using an anaerobic cuvette. The reconstituted protein was divided into 500 µL aliquots and stored at -80 °C. Since the desalting

column exchanges the truncated M1Q/W2L-viperin into reconstitution buffer, the concentration can now be determined using a calculated extinction (averaging the fully reduced and fully oxidized states) of ε_{280} = 42,712.5 $M^{-1}cm^{-1}$. Reconstituted protein yielded was typically ~ 26 μM (1 mg/mL).

4.2.6. Assays of Truncated M1Q/W2L-Viperin and FPPS.

4.2.6.1. *In vitro SAM cleavage assay*. The SAM cleavage assay was performed with slight modification of the protocol described by Duschene and Broderick.[263] Reagents were used in final concentrations of 78 μM reconstituted truncated M1Q/W2L-viperin, 5 mM DTT, 5 mM dithionite, 200 μM SAM, 10 mM tris-HCl at pH 8.0, 300 mM NaCl, and 10% glycerol in a total volume of 515 μL. The assay mixture was allowed to incubate at room temperature for 30 min prior to starting the reaction by the addition of SAM. The assay was allowed to age for 60 min at room temperature. The assay was quenched by heating at 95 °C for 10 min. The solution was chilled to 4 °C and precipitated proteins removed by centrifugation. The supernatant was decanted into a Microcon Ultracel YM30 spin column, and centrifuged at 13,000 rpm, 4 °C for 1 h to ensure all the solution passes through. The production of 5‘-deoxyadenosine was then analyzed by reverse phase HPLC.

4.2.6.2. *Detection of 5’-deoxyadenosine by HPLC*. 5‘-deoxyadenosine was analyzed by HPLC on a Vydac 201SP54 250 x 4.6 mm C_{18} reverse-phase column with a 5 μm particle size. 100 μL were injected onto the column (pre-equilibrated in Solvent A) using a 100 μL injection loop. 5‘-deoxyadenosine was eluted using a gradient of 0 - 5 min, 0 - 15% B; 5 - 10 min, 15 - 75% B; 10 - 11 min, hold 75% B, 11 - 15 min, hold 100% B, 15 - 20 min, hold 0% B at a flow rate of 1 mL/min.

5'-deoxyadenosine was detected by monitoring its absorbance at 260 nm (RT = 7.50 min) and confirmed by ESI-MS in the positive ion mode ($[M+H]^+$ = 252.1). The amount of 5'-deoxyadenosine produced was determined by peak integration and compared to a standard curve. *L*-tryptohan (40 ng/μL, RT = 9.95 min) was used as an internal standard. (Solvent A = 0.1% TFA in water, Solvent B = 0.1% TFA in acetonitrile).

4.2.6.3. *Radioactive FPPS assay.* Enzymatic activity was monitored through modification of a radioactivity-based assay described Kavanagh and coworkers.[273] Reagents were used in final concentrations of 4.7 nM FPPS (0.4ng/μL), 20 μM GPP, 18 μM IPP, 0.2 μCi/mL [4-C^{14}]-IPP (specific activity 10.8 Ci/mol), 5 μg/mL BSA, 2 mM DTT, 2 mM $MaCl_2$, 10% glycerol, 50 mM tris-HCl at pH 8.0 in a final volume of 800 μL. All reagents except enzyme were combined into a 1.5 mL eppendorf tube and equilibrated to 37 °C over 5 min. The assay, initiated by the addition of enzyme, was allowed to age and over the course of 15 min, 100 μL aliquots were quenched by addition into 200 μL of a 4:1 MeOH/HCl solution pre-equilibrated at 37 °C. The quenched solution was further incubated for 10 min at 37 °C, allowing for the selective hydrolysis of FPP to farnesol and nerolidol. The hydrolyzed FPP products were extracted into 400 μL ligroin and vortexed for 2 min. 200 μL of the ligroin layer was diluted into 4 mL scintillation cocktail and the absolute C^{14} content in decays per minute (DPM) of the extracted FPP hydrolysis products was then determined using the LS6500 Beckman liquid scintillation counter's factory installed quench curve.

4.2.7. Viperin and FPPS Pull-Down Assays.

4.2.7.1. *Pull-down assay with reconstituted truncated M1Q/W2L-viperin and FPPS purified from E. coli.* The 6x HIS tag was removed from FPPS using the TEV protease according to the manufacturer's instructions. All steps were performed in a Coy chamber (O_2 < 25 ppm) using anoxic buffers unless otherwise noted. In a 1.5 mL eppendorf tube, reconstituted truncated M1Q/W2L-viperin (64 µg, 1.6 nmol) was diluted into 50 µL buffer (10 mM tris-HCl at pH 8.0, 300 mM NaCl, 10% glycerol) containing 20 µL of buffer equilibrated Ni-NTA beads and incubated for 30 min at room temperature with shaking to allow binding of the protein to the resin. The resin was washed twice with 200 µL buffer to remove any unbound protein. FPPS (18 µg, 0.42 nmol) was then added to the resin in a final volume of 150 µL containing 1.5 mM imidazole and incubated for 30 min at room temperature with shaking. The suspension was centrifuged (14,000 rpm, 5 min) to pellet the resin and 30 µL of the supernatant was removed for analysis by SDS-PAGE. The resin was washed twice with 200 µL buffer. To elute, the resin was resuspended in 150 µL SDS-PAGE loading buffer [6% SDS (wt/vol), 3% mercaptoethanol (vol/vol), 15% glycerol (wt/vol), 0.025% Coomassie blue, 75 mM tris-HCl pH 7.0] and boiled for 2 min on the bench-top. Samples were analyzed by SDS-PAGE.

4.2.7.2. *Pull-down assay of wild-type viperin and FPPS expressed in HEK293T cells.* All steps were performed on ice or at 4 °C. Typically, HEK293T cells co-transfected with wild-type viperin and FPPS were resuspended in 500 µL lysis buffer containing tris-buffered saline, 1% Triton X-100, and 20 mM imidazole, pH 7.4 and lysed sonication. 25 µL Ni-NTA equilibrated in lysis buffer was added and the solution

incubated for 10 - 15 min at room temperature with shaking to allow the HIS-tagged FPPS to bind to the resin. The solution was centrifuged to pellet the resin and the supernatant (flow-through) removed carefully by pipette. The resin was washed 3x with 500 µL lysis buffer (60x resin volume). Bound protein was eluted by incubating the resing with 50 µL lysis buffer (2x resin volume) containing 500 mM imidazole for 5 min. The resin was separated by centrifugation and the supernatant decanted (elution). Samples were analyzed by Western Blot.

4.3. Results and Discussion

The studies described here take two complementary approaches to examining the mechanism by which viperin interacts with and inhibits FPPS as part of the innate immune response.[246] Pull-down and enzyme inhibition analyses will be used as tools to examine possible interactions between recombinantly expressed human viperin and FPPS, as well as probe the role reductive cleavage of SAM plays in the mechanism of inhibition *in vitro*. Secondly, using epitope-tagged constructs of viperin and FPPS transfected into mammalian HEK293T cells, the effect of viperin over-expression on the levels of 5'-deoxyadenosine *in vivo* as a marker for radical SAM activity was examined. Studying the enzymes under physiological conditions should ensure that any post-translational modifications necessary for their interaction are present. These studies represent the first steps to gaining a detailed understanding of the mechanism by which viperin inhibits FPPS and thereby delineate the apparently novel role for radical SAM chemistry in eukaryotic cells.

4.3.1. Initial Studies of Viperin and FPPS Expresed from Bacteria.

4.3.1.1. *Expression and purification of viperin and FPPS*. Both human viperin (M1Q/W2L-viperin) and FPPS were over-expressed in *E. coli* and purified as soluble proteins by Ni^{2+} affinity chromatography. Both enzymes migrated on an SDS-PAGE gel according to their calculated monomeric molecular weights of 39 kDa and 43 kDa for viperin and FPPS, respectively (Figure 56).

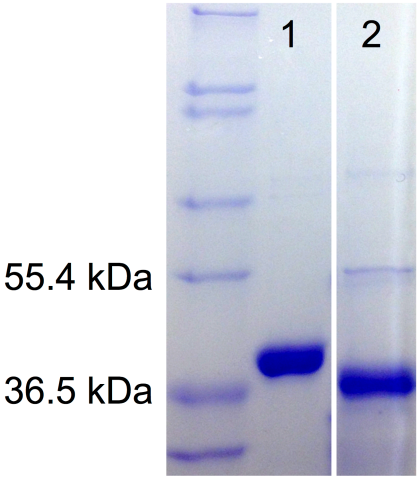

Figure 56. Purification of Bacterially Expressed FPPS and Truncated M1Q/W2L-Viperin. SDS PAGE of FPPS (lane 1) and N-terminal truncated viperin (lane 2). The proteins can be purifed > 95% to homogeneity in a single step by Ni^{2+} affinity chromatography.

For FPPS, its enzymatic activity was validated though modification of a radioactivity-based assay described Kavanagh and coworkers.[273] The assay is based on the selective, acid-catalyzed hydrolysis of the FPPS product farnesyl pyrophosphate (FPP) in acid at 37 °C to nerolidol and farnesol (Figure 57).

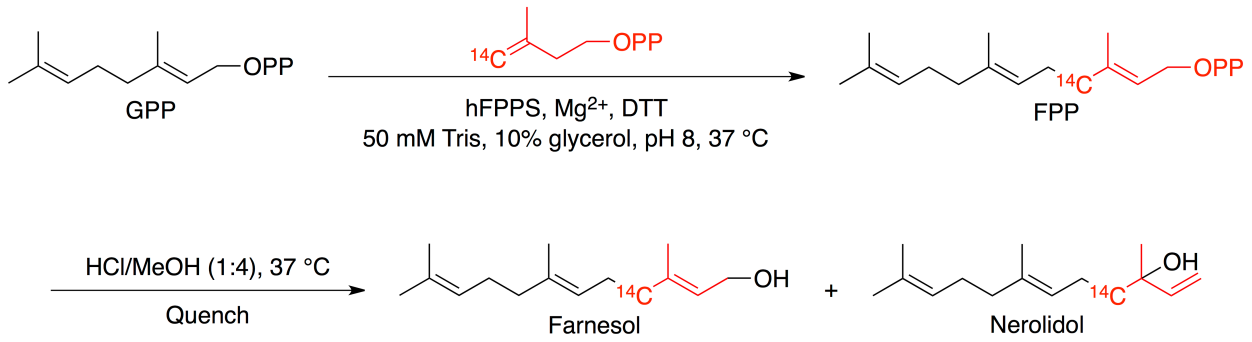

Figure 57. Design of FPPS Radioactive Assay. The assay follows formation of farenesyl pyrophosphate (FPP) from geranyl pyrophsophate (GPP) and ^{14}C labeled isopentenyl pyrophosphate (IPP) and is based on the selective, acid-catalyzed hydrolysis of FPP in acid at 37 °C to nerolidol and farnesol.

The hydrolysis products are ether-soluble and, thus, radioactivity incorporated into the product is recovered from the ether extract. The ^{14}C- isopentenyl pyrophosphate (IPP) substrate is stable in acid at 37 °C and even if some ^{14}C-IPP were hydrolyzed, it is not extracted into ether from the aqueous-ethanolic solution used to quench the reaction.[274] The rate at which ^{14}C is incorporated into products was determined by plotting the absolute DPM as a function of time for each quenched time point and fitting the data using Kaleidagraph's linear fit tool (Figure 58). The rate in nM/min of ^{14}C incorporation was determined by dividing the DPM by the known specific activity of the starting IPP and the volume of ether extract counted. From this, the rate constant for the production of FPP (k_{cat}) was calculated as 10.8±4% min^{-1} and is similar to literature reported values.[273, 275, 276]

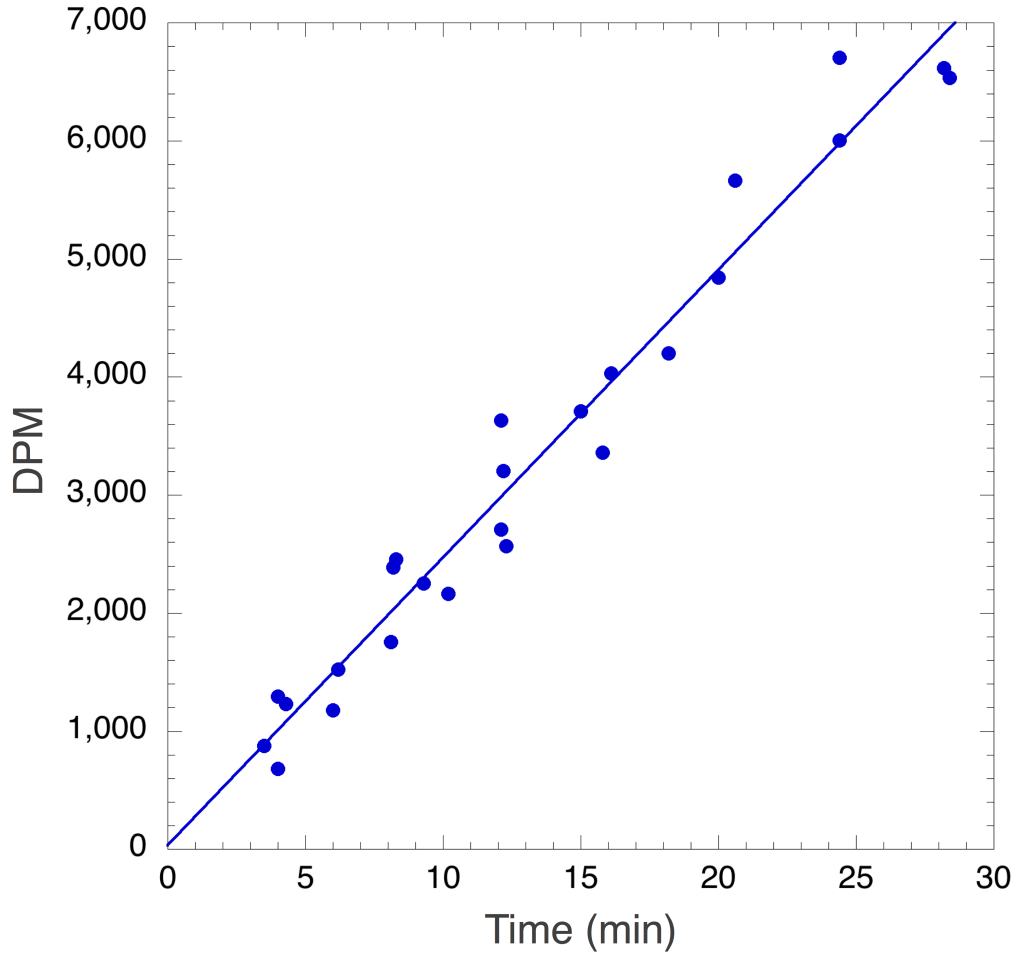

Figure 58. FPPS Activity Assay. The rate of ^{14}C incorporated into FPP from quadruplicate measurements was determined to be 243.4±9.7 DPM/min (r = 0.98, r^2 = 0.96).

Interestingly for viperin, only the truncated viperin lacking the N-terminal amphipathic α-helix could be purified because the full-length viperin constantly was found to not express (a similar result obtained by Shaveta and coworkers).[264] SDS-PAGE followed by western blot analysis failed to provide any evidence for viperin expression even in minute quantities as inclusion bodies. Furthermore, despite being codon-optimized for expression in *E. coli* and being cloned into a vector under control of the strong T7 *lac* promoter primed for high levels of expression, large sale preparations typically yielded only ~ 1 mg of truncated M1Q/W2L-viperin per gram of cell paste.

However, a high degree of protein precipitation was observed within minutes of purification. The observed precipitation may be related to viperin's ability to dimerize in solution. Viperin is known to bind to the ER by way of its N-terminal helix and aggregate to the extent of inducing dramatic changes in ER morphology, which are characteristic of a crystalloid ER. In solution, Hinson and Cresswell showed that viperin mutants lacking the N-terminal helix did indeed interact to form dimers.[251] However, preliminary size exclusion data suggests the extent of the dimerization is much lower than when bound to the ER and suggests the N-terminal helix is required for protein stability. Conversely, Hinson and Creswell demonstrated the N-terminal amphipathic α-helix still localizes to the ER but is not sufficient to cause crystalloid ER formation, suggesting the C-terminal and/or radical SAM domains are responsible for the formation of the high affinity dimers required for such drastic morphological changes.[251] The enzyme's predisposition to dimerize may be sufficiently strong that high concentrations of protein obtained during purification lead to aggregation and precipitation. Duschene and Broderick observed high levels of precipitation when concentrated to levels greater than 250 μM despite performing the entire purification under rigorous anaerobic conditions.[263] In either case, the N-terminal domain could have an impact on the overall protein stability.

4.3.1.2. *Viperin is capable of binding free iron and sulfide.*[263, 264] The truncated M1Q/W2L-viperin can be purified under aerobic conditions with retention of their iron-sulfur clusters as evidenced by the light reddish color of purified fractions. Furthermore, the UV–Vis absorption spectra for the isolated samples demonstrate broad ligand-to-metal charge transfer transitions characteristic of iron-sulfur clusters. Specifically, a

shoulder between 315 - 325 nm and a broad shoulder between 370 - 450 nm are both typical for proteins containing $[4Fe\text{-}4S]^{2+}$ clusters (Figure 59).

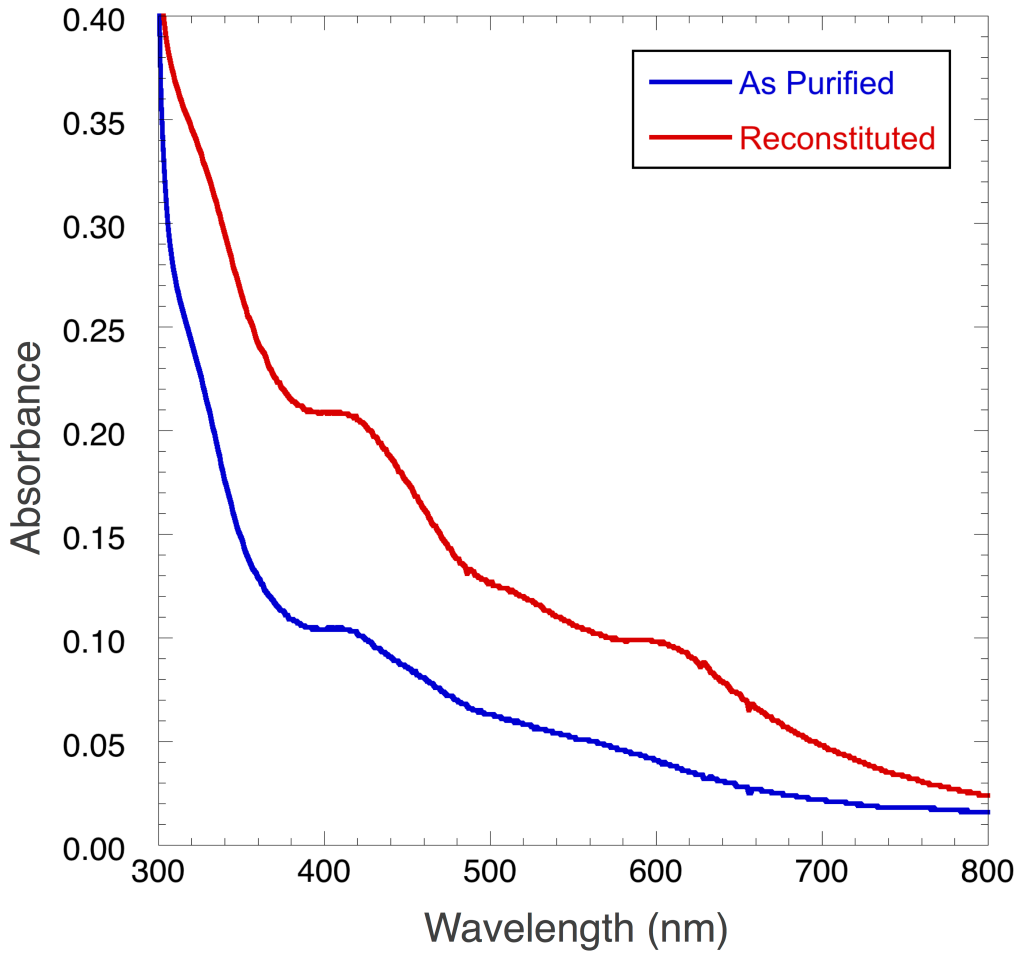

Figure 59. UV–Vis Spectroscopic Characterization of Viperin. U.V.-visible spectrum of viperin before (blue trace) and after (red trace) reconstitution of [4F-4S] cluster.

To protect the protein during aerobic purification, 5 mM dithionite was added to each fraction to act as oxygen scavenger. Reduction of the protein with dithionite bleaches the reddish color and results in a decreased intensity throughout the visible region, which is consistent with the reduction of a $[4Fe\text{-}4S]^{2+}$ cluster to a $[4Fe\text{-}4S]^{1+}$ cluster. Consequently, the 370 and 450 nm bands for the “as-purified spectrum” are weaker

than typical. Upon reconstitution, the protein became intensely dark, reddish brown at concentrations similar to the light reddish as purified sample (~ 1mg/mL, 26 μM). An additional band at 615 nm appeared upon reconstitution suggestive of $[2Fe\text{-}2S]^{2+}$ clusters present in the enzyme. The spectroscopic data is in agreement with previous viperin reconstitution studies and strongly suggests truncated M1Q/W2L-viperin binds an iron-sulfur cluster characteristic of radical SAM enzymes.

4.3.1.3. *Viperin cleaves SAM to 5'-deoxyadenosine in an uncoupled reaction.* The hallmark of a radical SAM enzyme is their ability to reductively cleave SAM and produce a 5'-deoxyadenosine (5'dA) radical.[5] The radical, generated on the 5'-carbon atom, typically abstracts a non-acidic hydrogen atom from the enzyme's substrate, generating 5'-deoxyadenosine as a byproduct. For most enzymes, reductive cleavage is heavily gated against radical formation in the absence of substrate, yet it is usually possible to observe a small degree of non-catalytic, uncoupled SAM cleavage.[48] Consequently, even in the absence of substrate the production of 5'-deoxyadenosine can be observed under reducing conditions.

To confirm truncated M1Q/W2L-viperin is indeed a radical SAM enzyme, we conducted a SAM cleavage assay in which SAM was incubated in the presence or absence of enzyme under reducing conditions. HPLC chromatographs of the assay products are shown in Figure 60.

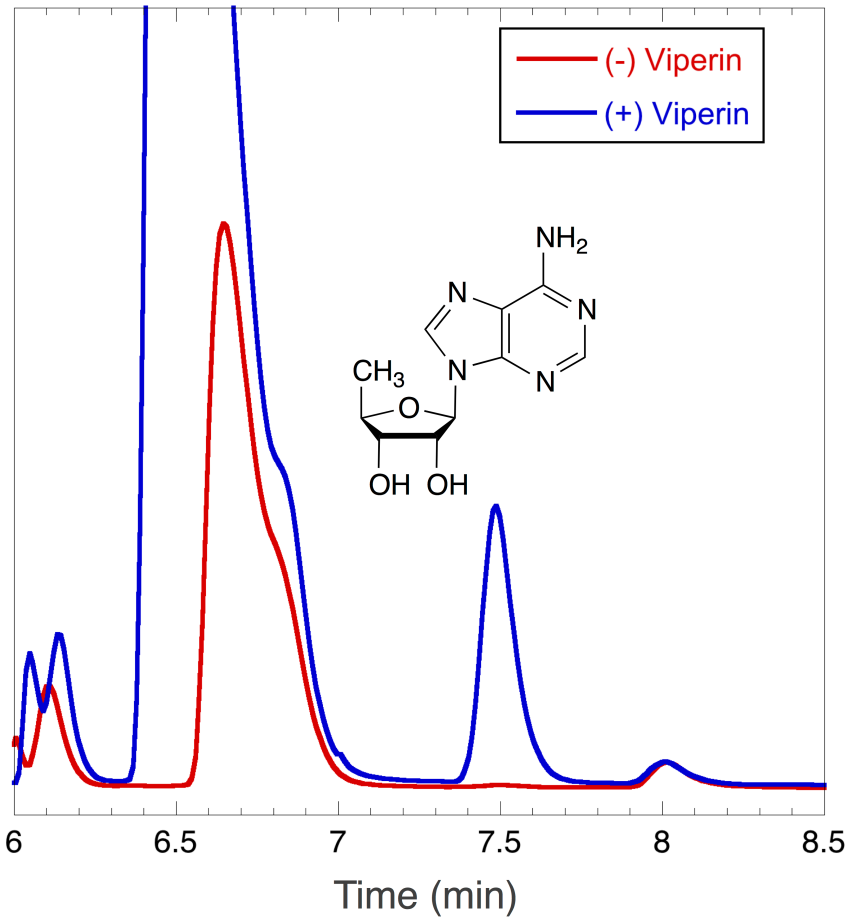

Figure 60. HPLC Analysis of SAM Cleavage Assay. HPLC trace demonstrating uncoupled formation of 5'-deoxyadenosine by reconstituted viperin (blue trace) and comparison with control reaction lacking enzyme (red trace).

Only in the presence of enzyme do assays containing SAM and reductant demonstrate production of 5'-deoxyadenosine. The cleavage product co-elutes at 7.5 min with a standard of 5'dA. The peak was collected and the identity of 5'dA confirmed by electrospray-ionization (ESI) mass spectrometry. In the positive ion mode, the peak collected at 7.5 min confirmed the presence of 5'-deoxyadenosine with a $[M+H]^+$ molecular ion peak of 252.1 m/z (Figure 61). From a calibration curve constructed from 5'-deoxyadenosine standards, it was determined that the amount of 5'dA produced in Figure 4.9 corresponds to less than one turnover and suggests only a small degree of uncoupling occurs.

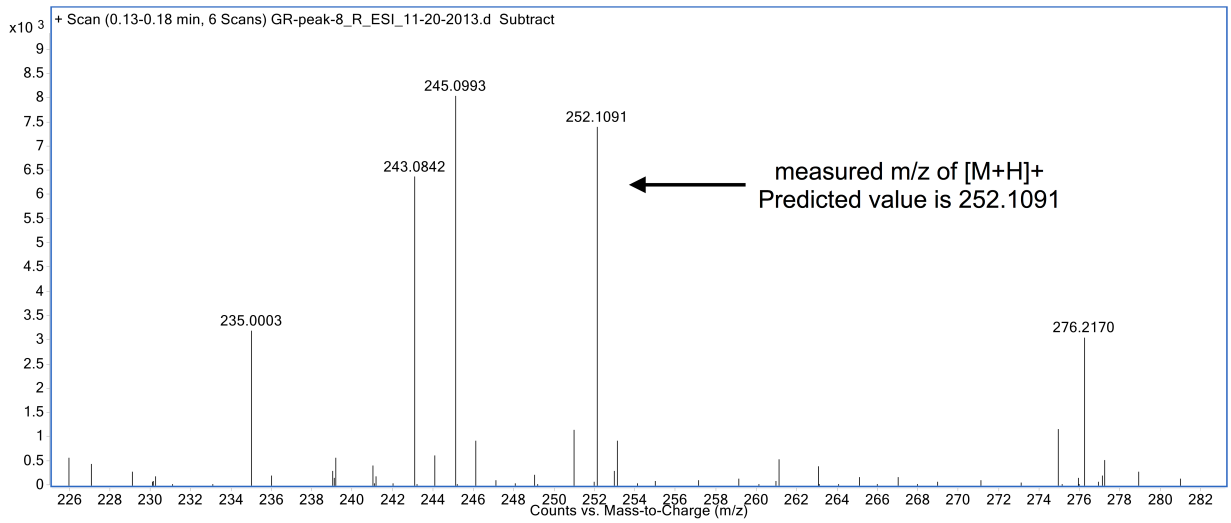

Figure 61. Mass Spectrum of 5'-Deoxyadenosine. The peak eluting at 7.5 min was collected and subjected to ESI-MS. 5'-deoxyadenosine production was confirmed by the presence of the 252.1 $[M+H]^+$ peak.

4.3.1.4. *FPPS inhibition assays*. Homology modeling of viperin indicates that it adopts a 6-stranded β/α "partial" barrel fold.[265] This fold is characteristic of radical SAM enzymes such as PFL activase and MoaA (Figure 62), which act on large substrates such as proteins and tRNAs.[257, 277]

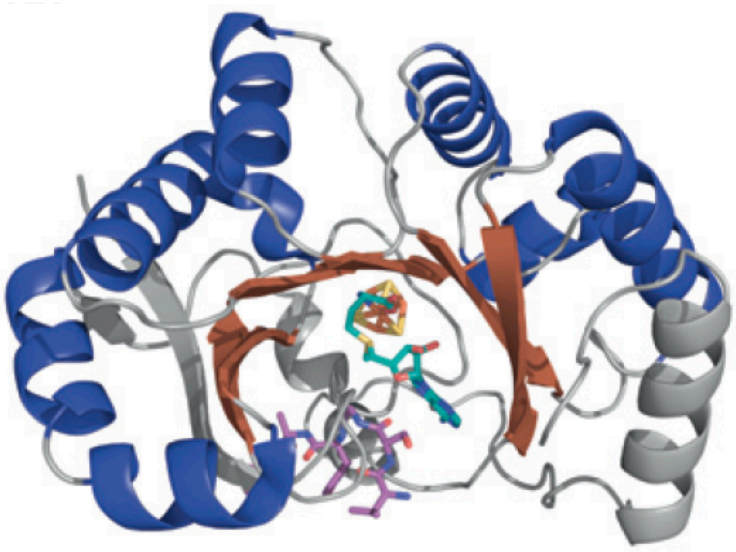

Figure 62. The Structure of the Radical SAM Enzyme Pyruvate Formate Lyase Activating Enzyme. PFL-activase belongs to a radical SAM subfamily known as glycyl radical enzymes and share a common 10-stranded β-barrel fold, with two sets of five-stranded sheets running antiparallel to each other. The active site, which contains the 4Fe-4S cluster, is located at the top of the partial barrel near the top of the enzyme's core.

For example, radical SAM enzymes are known to catalyze a wide range of modifications on proteins including oxidation of Ser and Cys residues to aldehydes, thiomethylation of Asp and the oxidation of Gly residues to glycyl radicals in enzymes such as PFL and BSS (Figure 63).[5, 23, 24, 257, 278, 279]

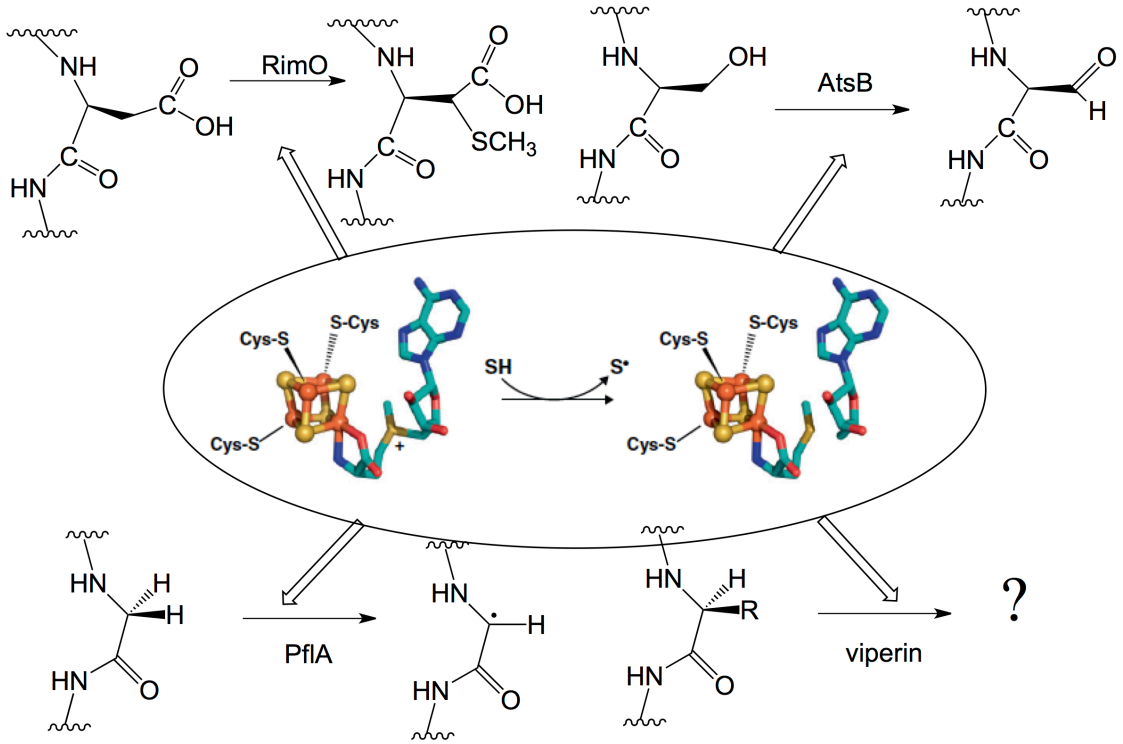

Figure 63. Protein Modifications Catalyzed by Radical SAM Enzymes. RimO is responsible for methylthiolation of the β-carbon of Asp88 of the ribosomal protein S12 in *E. coli* as a post-translational modification. AtsB catalyzes the oxidation of Ser72 on AtsA, an enzyme involved in the synthesis of a protein-derived formylglycine cofactor involved in sulfatase maturation. PflA activates pyruvate formate lyase, an enzyme involved in the anaerobic metabolism of glucose, by installing a catalytically essential glycyl radical on G^{734} of PFL through the direct and stereospecific abstraction of a hydrogen atom. The function of viperin remains unknown but, as a radical SAM enzyme involved in the antiviral response through interaction with various protein targets, it may function in a manner similar to other modifying radical SAM enzymes.

The case of the glycyl radical enzyme is particularly intriguing as these enzymes, which are known to only be expressed under strict anaerobic conditions, undergo rapid inactivation on exposure to air due to oxidative cleavage of the protein at the site of the radical (Figure 64).[280]

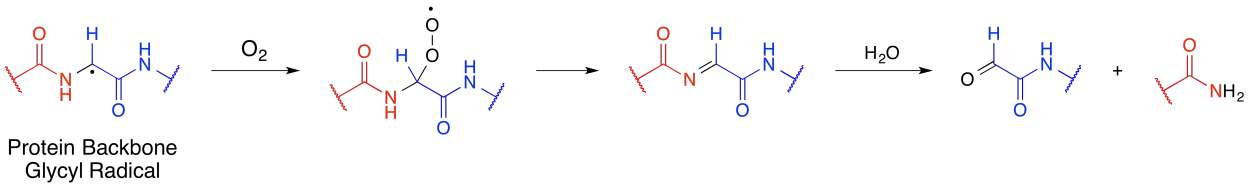

Figure 64. Proposed Mechanism for the Oxidative Decomposition of a Protein Backbone Glycyl Radical. Formation of a glycine C_α peroxy radical is proposed to undergo elimination of a superoxide radical. Subsequent hydrolysis of the resulting imine results in cleavage of the peptide bond.

Based on this homology, it is possible that viperin uses the transiently formed 5'-deoxyadensyl radical to install a modification on FPPS, which then leads to the observed inhibition of FPPS in viperin-expressing cells. The nature of the inhibition could manifest itself in either the context of cellular relocation or a simple degradation of the protein, possibly in a manner similar to the observed degradation of the glycyl radicals (*i.e.*, oxidative degradation leading to inactivation).

Ultimately, the goal is to determine whether viperin inhibits FPPS by simple non-covalent binding or by covalent modification of FPPS and gain insight into the interaction between viperin and FPPS at molecular-level. Based on the protein modification reactions catalyzed by other radical SAM enzymes, if viperin does inhibit FPPS directly, covalent modification seems the most likely mechanism of inhibition. Protein-modifying radical SAM enzymes consume SAM irreversibly as an oxidizing agent and, thus, require it in stoichiometric amounts. Therefore, during catalysis, the

5'-deoxyadenosine byproduct will be turned over stoichiometetrically as well. If FPPS acts as a true substrate for viperin, the amount of 5'-deoxyadenosine produced should be proportional to the concentration of FPPS in solution and this increase can be easily monitored by the HPLC. However, when the SAM cleavage assay was repeated in the presence of FPPS (equimolar to viperin), the amount of 5'-deoxyadenosine produced was similar to the uncoupled reaction. Addition of the FPPS substrates and magnesium (required for FPPS activity) also resulted in similar levels of 5'-deoxyadenosine. Even in experiments using an excess of 6-fold to 10-fold FPPS over viperin (or vice versa), the turnover number was at most 0.6 equivalents. This suggests FPPS does not act as a direct substrate for viperin, at least not in a way that involves radical SAM chemistry.

Wang and coworkers demonstrated that viperin expression in HeLa Tet-on cells inhibits endogenous FPPS enzymatic activity by 20% after 24 h and 50% after 48 h of viperin induction.[246] However, the mechanism by which this occurs remains unknown. Initial experiments were aimed at determining the effect of viperin on FPPS activity. To determine if the nature of the inhibition is only dependent on SAM, the k_{cat} of FPPS was measured in the presence of viperin. Typically, the FPPS assay is initiated by the addition of enzyme. However, for these inhibition studies, both enzymes were incubated together for ~ 10 min at 37 °C prior to initiating the reaction by the addition of GPP to begin the assay, which was performed in sealed vials under an argon gas inlet. Standard conditions for the FPPS assay in which viperin was omitted resulted in FPP production at a rate of 10.4±0.4 min^{-1}. Initial studies in which dithionite was omitted were aimed to directly compare with the standard FPPS assay and included truncated 100 nM viperin (21-fold excess over FPPS) and SAM (1 mM). Under these conditions,

the same value of k_{cat} = 10.4±0.4 min^{-1} was measured for FPPS. Both the control and the experiment assay consumed similar amounts of substrate with a maximum of 5% IPP conversion and 1% incorporation of radioactivity into FPP, ensuring the reaction is well within the steady-state. The formation of FPP remained linear over the 18 min the assay was performed. Conditions of 18 μM IPP and 20 μM GPP, 18x the reported K_M of IPP (1 μM) and 50x the reported K_M of GPP (0.4 μM), ensured conditions of V_{max} were satisfied. Statistically, under these conditions, there is no effect of viperin on the rate of hFPPS synthesis of FPP.

The redox state of the iron-sulfur cluster is important for viperin to be active. The *in vivo* conditions in which Wang and coworkers[246] found endogenous FPPS to be inhibited by viperin should provide adequate mechanisms to reduce the iron-sulfur cluster for SAM cleavage. Preliminary data demonstrates that addition of higher concentrations of reconstituted viperin (2 μM, 426-fold excess over FPPS) and the one-electron donor dithionite (2 mM) resulted in k_{cat} = 8.2±0.2 min^{-1}, suggesting FPPS activity was reduced by approximately 10% when considering the error associated with the measurement. Viperin activity was confirmed as a SAM cleavage assay was performed concomitantly and HPLC analysis revealed the enzyme did cleave SAM to yield 5'-deoxyadenosine.

It is important to note that detection of enzyme activity *in vitro* may require artificial conditions and, thus, may not provide a reliable indication of activity *in vivo*, in which enzyme and substrate concentrations are typically much lower. Thus, further experiments must be performed to confirm this result. For instance, an observed change in molecular weight can be highly informative as to the type of covalent

modification (methylation, oxidation, etc.). After the assays described above are quenched, FPPS can be subjected to liquid chromatography-ESI-MS in order to determine whether the molecular weight of either protein has changed. If a modification is indeed detected, follow up protein proteomic studies can then map its position onto FPPS. Knowledge of the modifications location would open the door to an array of informative enzymological studies. Point mutations at the modification site could identify the amino acids involved in viperin's recognition of FPPS. Furthermore, short peptides that mimic the modification site can act as FPPS substitutes, simplifying further kinetic studies. A similar approach was used for studying the interaction between PFL-activase and PFL. Once the location of the catalytically essential glycyl radical of pyruvate formate-lyase was identified to be G^{734}, synthetic peptide substrates containing the sequence surrounding G^{734} were used to analyze the recognition of PFL by PFL-activase kinetically,[8] as well as crystallographically.[281]

4.3.2. Expression of FPPS and Viperin in Mammalian Cells. A bacterial expression system is excellent for *in vitro* studies because it is able to provide large quantities of recombinant protein. However, both FPPS and viperin are human enzymes. Expression in *E. coli* introduces the risk of producing misfolded proteins and any post-translational modifications that may be necessary for activity or recognition will not be introduced. Neither of these are a cause of concern for FPPS as many kinetic and structure-activity relationship studies on lead compounds with clinical utility have been performed on the enzyme purified from recombinant bacteria.[282] However, this may be a problem for viperin about which little is known and a mammalian expression system will replicate the conditions under which the initial interaction[246] was identified. It

is also possible that viperin requires other mammalian proteins for its observed activity against FPPS, which would not have been identified in the original immunoprecipitation and inhibition studies. Consequently, studying the interaction of viperin with FPPS under a more physiological setting through expression in a mammalian cell line is important in establishing the nature of the interaction. Then, reversion to a bacterial expression system could provide the quantity of protein required for further mechanistic studies *in vitro*.

The co-precipitation of endogenous FPPS by viperin was performed in HeLa cells expressing full-length viperin,[246] whereas experiments demonstrating radical SAM activity through the uncoupled cleavage of SAM to 5'-deoxyadenosine were performed on the N-terminal-truncated viperin purified from recombinant *E. coli* cells.[263] Here, this discrepancy is expected to be resolved by co-transfection of the proteins in mammalian cells. For transient expression in mammalian cells, the pcDNA3.1 vector was used to construct epitope-tagged versions of viperin (FLAG) and FPPS (HIS), allowing the proteins to be orthogonally detected by fluorescent antibody staining, quantified by western blotting, and recovered by affinity chromatography. The genes were placed under control of the CMV promoter, which drives constitutive expression in HEK293T cells. Figure 65A demonstrates that transfection of these constructs into HEK293T cells resulted in both proteins being well expressed. Typically, transfection over 48 h in a 10 cm^2 dish yielded ~ 4 mg of protein per liter of culture.

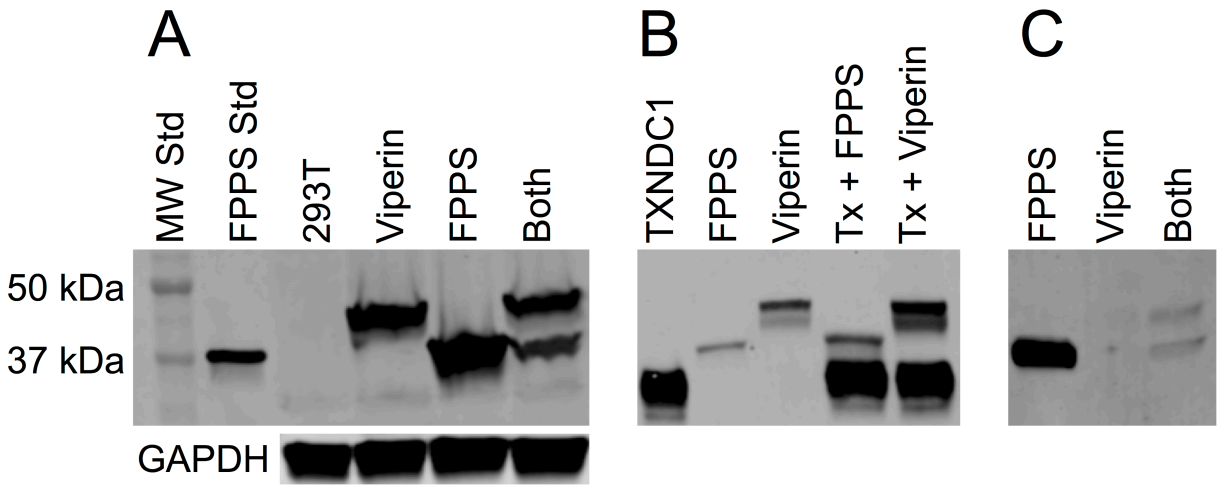

Figure 65. Expression of Viperin and FPPS in HEK293T Cells. (A) Expression of viperin and FPPS in HEK293T showing co-expression reduces FPPS. Cell lysates were stained with antibody to glyceraldehyde-3-phosphate dehydrogenase (GAPDH) to serve as loading control. (B) Controls showing co-expression of highly expressed TXNDC1 does not affect FPPS expression. (C) Pull-down of viperin by HIS-tagged FPPS co-expressed in HEK293T.

4.3.2.1. *Wild-type viperin reduces cellular levels of FPPS.* Initial expression trials demonstrated that FPPS is significantly reduced whenever it is co-expressed with viperin and this observation has proven reproducible over numerous trials. When equal amounts of DNA are used to co-transfect HEK293T cells, the concentration of FPPS is greatly reduced (~ 50% or greater after 48 h of transfection) compared to when the gene is expressed on its own. To ensure co-transfection was not simply interfering with the cell's protein synthetic machinery, control experiments were performed in which FPPS was co-expressed with TXNDC1 (Figure 65B), a highly expressed human thioredoxin gene. Co-expression with TXNDC1 resulted in no reduction in FPPS expression. This demonstrates that this observation is not simply an artifact of co-expression in which viperin out-competes FPPS for the transcription/translation machinery. Importantly, this observation agrees nicely with the result obtain by Wang

and coworkers, in which viperin expression in a HeLa Tet-on cell line led to a reduction in FPPS activity of ~ 50% after 48 h of doxycycline treatment.[246]

4.3.2.2. *Pull-down assays.* Co-immunoprecipitation studies demonstrated that endogenous FPPS interacts *in vivo* with IFN-induced viperin in mouse RAW264.1 cells.[246] Thus, it is possible that viperin inhibits FPPS by forming a non-covalent complex. To test this, pull-down assays were conducted in which viperin and FPPS were co-expressed in HEK293T cells. Preliminary results suggest that His-tagged FPPS pulls down co-expressed viperin in HEK293T cells (Figure 65C). Lysate from cells co-transfected with viperin and FPPS were incubated with Ni-NTA resin and extensively washed with buffer containing 20 mM imidazole to remove non-specifically bound proteins. FPPS was eluted with 500 mM imidazole and analyzed by western blotting. The blot was stained for both FPPS and viperin, suggesting that they bind in approximately a 1:1 complex. Clearly, the amount of FPPS in the elution is significantly reduced compared to a control in which the assay was conducted on HEK293T cells expressing only FPPS, suggesting FPPS expression was reduced. However, a complementary experiment in which the cell lysate was incubated with anti-FLAG (M2) affinity gel (Sigma) to determine if FLAG-tagged wild-type viperin pulls down FPPS was negative. Furthermore, a similar experiment on the bacterial constructs (performed under both aerobic and anaerobic conditions) in which TEV-cleaved FPPS was pulled down with His-tagged viperin demonstrated no observable interaction (Figure 66). It is important to note that for these experiments over-expression of *both* proteins is artificially driven by the vectors CMV promoter. The original experiment performed by Wang and coworkers was arguably a more physiologically relevant experiment. Mouse

RAW264.1 cells were treated with type-I IFN, which up-regulates viperin production *in situ.* Most importantly, IFN treatment not only up-regulates viperin but a host of other interferon-stimulated genes as well, any of which could potentially modulate viperin's recognition of FPPS.

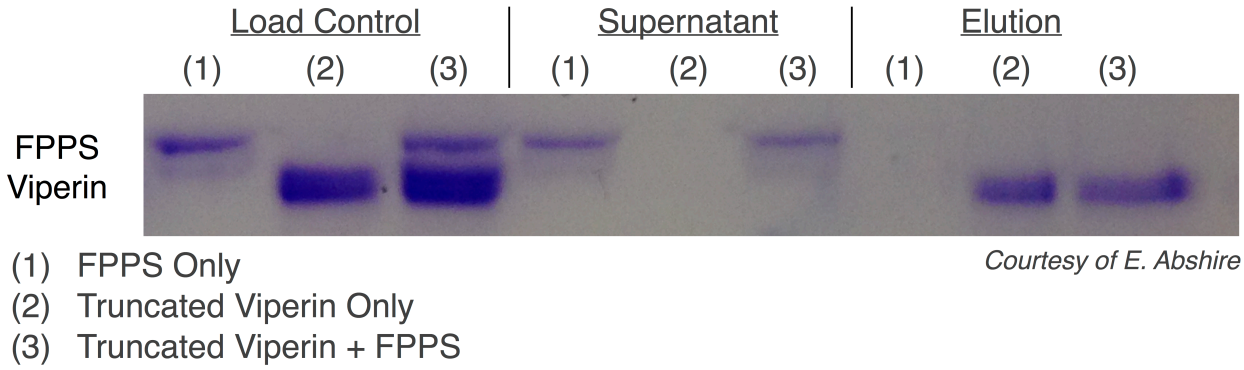

Figure 66. SDS-PAGE Analysis of Pull-Down Experiment Using Bacterially Expressed Viperin and FPPS. 1 µg of each enzyme was used as a loading control.

4.3.2.3. *Wild-type viperin cleaves SAM.* Studies on the bacterial constructs demonstrate that viperin catalyzes the uncoupled cleavage of SAM. However, it is crucial to establish whether viperin actually functions as a radical SAM enzyme *in vivo* in its interaction with FPPS. Preliminary results in which HEK293T extracts of cells expressing viperin were assayed in a similar manner to the bacterially-produced enzyme using HPLC to analyze 5'dA formation suggested that wild-type viperin did not cleave SAM to 5'-deoxyadenosine (cells from a 10 cm^2 dish were resuspended in 200 µL anoxic assay buffer including 1% Triton X-100 and lysed by sonication inside a Coy chamber). However, the limit of detection for 5'-deoxyadenosine by this method was ~ 2 µM, which is relatively high. Therefore, in collaboration with the Kennedy lab, the SAM cleavage assay was repeated and analyzed by slight modification of a

previously reported protocol developed to detect low molecular weight metabolites that provides a limit of detection of ~ 0.1 nM for 5'dA (Appendix A.5). There are currently no other known pathways for the generation of 5'-deoxyadenosine in eukaryotic cells and, thus, there is a minimal cellular background against which to detect this metabolite (trace amounts may be produced from the homolytic cleavage of adenosylcobalamin). SAM cleavage assays from viperin expressing cells, extracted in acetonitrile and subjected to benzoyl chloride derivatization followed by HPLC–tandem mass spectrometry, demonstrate viperin expressed in HEK293T cells is active in the uncoupled cleavage of SAM 5'-deoxyadenosine under reductive conditions (Figure 67).

This is the first result that demonstrates the wild-type, full-length, mammalian-expressed viperin displays radical SAM activity. The levels of 5'dA in viperin-expressing cells were 0.50±0.05 nM, which judging from typical levels of viperin expression in HEK293T cells, corresponds to less than one turnover. Interestingly, co-expression with FPPS did not increase the production of 5'dA. Cells co-transfected with *both* FPPS and viperin only made 5'dA to 0.49±0.03 nM, statistically the same to the amount as cells expressing viperin alone. Negative control cells without vector, as well as cells transfected with only FPPS, did not produce 5'dA.

Cells over-expressing viperin should produce elevated levels of 5'dA due both to the uncoupled reaction of SAM and to reaction with endogenous targets. Therefore, it is interesting that only when SAM was added to cell extracts containing viperin did uncoupled SAM cleavage occur (Figure 67). Presumably, expression in mammalian cells provides all the necessary post-translational modifications and cellular proteins for the interaction with FPPS to occur. These results mirror those obtained for the

bacterially produced enzyme in which the amount of 5'dA produced over 2 h corresponded to less than a turnover (uncoupled reaction) and similar levels of 5'dA were made when incubated with FPPS. As mentioned above, it is unlikely that any 5'-deoxyadenosine built up during the 48 h transfection period be depleted, as there are no known metabolic pathways for this metabolite (it is possible that it be secreted into the medium, which follow up experiments could detect using the Kennedy's HPLC-MS protocol). It is possible that other IFN-stimulated genes (which would not be present in this current vector based expression system) may be required for viperin to impose its antiviral effect on FPPS.

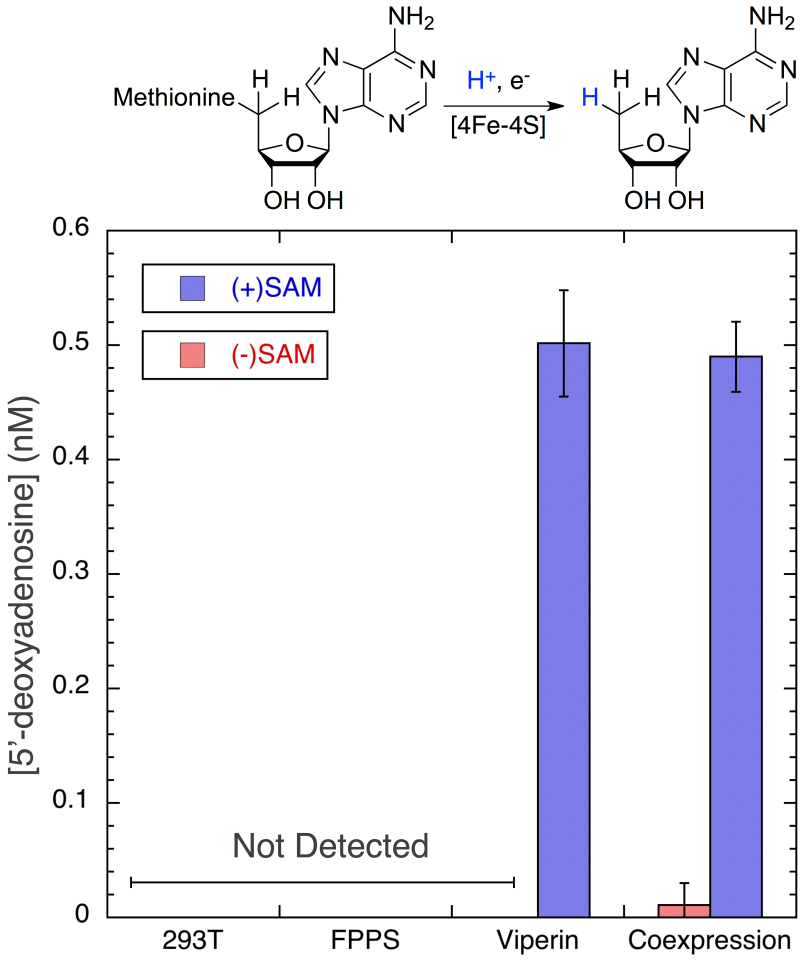

Figure 67. SAM Cleavage Assay from HEK293T Cell Lyasate. Formation of 5'-deoxyadenosine in SAM cleavage assays by viperin expressed in HEK293T cells.

CHAPTER 5

OUTLOOK AND FUTURE DIRECTIONS

5.1. Computation and Experiment as an Interdisciplinary Approach to Elucidating Enzyme Mechanism

Free radicals are important to biochemistry because they are able to catalyze reactions on otherwise un-reactive molecules.[1] For instance, ribonucleotide reductase catalyzes an essential reaction that is conserved across all organisms: the formation of deoxyribonucleotides that are then used to synthesize DNA. The enzyme is able to eliminate the hydroxyl group from the ribose 2'-carbon despite it not being activated toward reduction. The neighboring hydrogen atoms are not acidic and the -OH itself is a poor leaving group making acid-base and ionic chemistry unfeasible. Consequently, enzymes have evolved various mechanisms to generate reactive radical species that can be used for C-H bond activation.[2] In the case of class II ribonucleotide reductase, adenosylcobalamin is used to reversibly generate an active site cysteinyl radical which in turn abstracts the 3′-H adjacent to the site of reduction and activates the 2′-OH to become a good leaving group. However, free radicals are highly reactive species that once formed, rapidly react with whatever is available and, thus, must be produced in a controllable manner to avoid pernicious side-reactions. One way Nature controls radical formation is by "storing" them in a relatively weak bond an enzyme can break whenever it needs a radical initiator. Adenosylcobalamin serves as a radical reservoir by

producing a highly reactive adenosyl radical that is unmasked through homolysis of the cobalt–carbon bond and provides an elegant method of generating reactive radicals at the enzyme's active site in response to substrate binding.[5] Moreover, there are many reactions, both enzymic and non-enzymic, that proceed through radical mechanisms that could in principle be catalyzed by AdoCbl. Advances in our understanding of the principles by which these enzymes generate and control free radicals holds the prospect of re-designing them to catalyze a broader range of free radical chemistry.

Although the scope of the reactions catalyzed by AdoCbl-dependent enzymes is quite narrow, these well-understood mechanisms provide a good foundation for computational chemistry to probe many of the mechanistic questions that cannot easily be addressed by experiments. For instance, no experiment adequately explains the origin of the ~ 10^{12}-fold rate acceleration for AdoCbl homolysis or the remarkable ability of enzymes to stabilize radical intermediates. Radom and coworkers pioneered the computational analysis of AdoCbl reactions by using high-level computational approaches on small molecule models in which the protein is not considered.[283] Their studies, which probed the energetic feasibility of various mechanisms proposed for the 1,2 radical migrations, were the first to highlight the importance of electrostatic interactions in facilitating substrate radical rearrangements. They also found that the protonation state of the migrating group significantly influences reaction thermodynamics; suggesting that enzymes facilitate rearrangement reactions by either general acid–general base catalysis or hydrogen bonding interactions. The seminal work by Radom and coworkers allowed subsequent QM/MM studies on AdoCbl-dependent systems to use full enzyme structures in which electrostatic interactions

between coenzyme, substrate and protein are predicted to play a significant role in catalysis.[190]

Computational approaches play an increasingly important role in understanding the mechanisms of enzymes. Facilitated by increases in speed and the development of QM/MM methods that reliably model both the chemical reaction and the enzyme structure, computational modeling has greatly matured. It now provides an atomistic insight into the role of the protein during catalysis and produces mechanistic predictions that can be tested experimentally instead of merely rationalizing experimental results. In short, computational studies of AdoCbl reactions are of particular interest because the unusual nature of these rearrangements raises many mechanistic questions that cannot easily be addressed by experiments. For instance, modeling studies on the full structure of diol dehydrase led to a reevaluation of the metal requirements for the enzyme. It was generally accepted that K^+ was the only metal required by diol dehydrase. However, the metal-oxygen bond lengths determined from the crystal structure were much shorter than those calculated from the QM/MM model of diol dehydrase.[284, 285] To investigate this discrepancy, computational modeling was used to re-calculate the enzyme structure with *in silico* replacements of the K^+ ion with other metals.[286] After modeling structures with Na^+, K^+, Mg^{2+} and Ca^{2+}, only calcium resulted in metal–oxygen bond lengths that were in agreement with the crystallographic data. Subsequent biochemical experiments confirmed that Ca^{2+} is indeed required for activity (K^+ is still required for activity and is presumably bound at a separate metal site).[66]

The adenosylcobalamin dependent enzyme glutamate mutase, which catalyzes the difficult 1,2-rearrangement of glutamate's glycyl group with a non-acidic hydrogen,

has served as a paradigm for understanding how enzymes stabilize highly reactive radical species and harness them towards productive catalysis, a fundamental question that remains at the crux radical enzymology. Tritium isotope partitioning experiments aimed at measuring the hydrogen transfer between either glutamate or methylaspartate and the coenzyme found that one way glutamate mutase drives productive catalysis is by shaping the reaction free energy profile such that no single step is significantly rate limiting. Since the reaction catalyzed by glutamate mutase is fully reversible, the degree to which tritium is distributed from ^{3}H-labeled AdoCbl in the abstractable position depends on the relative heights of the energy barriers leading to product and substrate (Figure 68).[46] Rapid quench experiments found that tritium partitions in an almost 1:1 ratio between substrate and product, indicating that the activation energy for transfer of tritium from 5′-deoxyadenosine to glutamyl radical and methylaspartyl radicals are of equal height.[193]

Further insight into how AdoCbl-dependent enzymes stabilize radical species came from experiments that studied the kinetics of Co-C bond cleavage.[19] Homolysis of AdoCbl changes the oxidation state of the coenzyme from cob(III)alamin to cob(II)alamin and is accompanied by characteristic changes in the electronic spectrum of the coenzyme that can be monitored spectroscopically. The *holo*-enzyme exists predominantly in the cob(III)alamin state yet the addition of substrate leads to a rapid decrease in absorbance at 530 nm and an increase in absorbance at 470 nm.[33] During catalysis, radicals accumulate on enzyme during turnover indicating K_{eq} for radical formation is close to unity. This implies that adenosylcobalmin enzymes greatly stabilize radical intermediates toward product formation. A second way glutamate

mutase controls the reactivity of free radicals is by coupling the formation of one radical to another.[17, 19] Interestingly, significant kinetic isotope effects of 35 and 28 have been measured for Co-C cleavage using deuterated methylaspartate and glutamate substrates even though AdoCbl homolysis is formally not an isotopically sensitive step (Figure 69).[33]

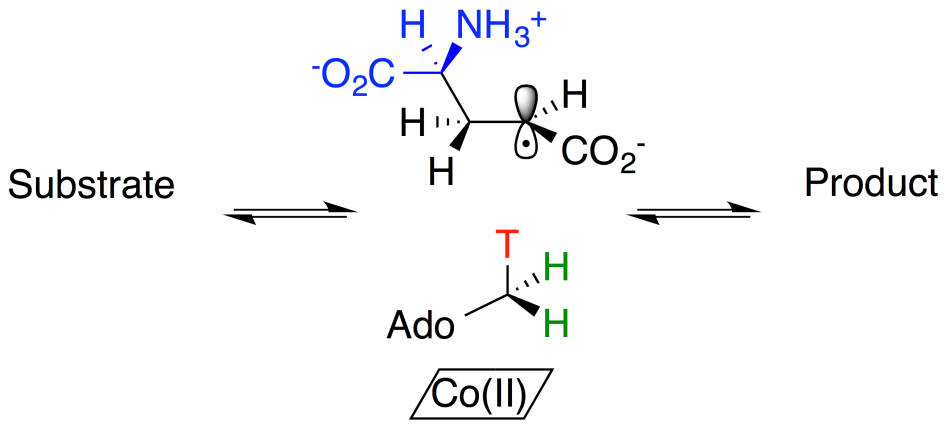

Figure 68. Tritium Partitioning Experiments Establish the Relative Energy Barrier Heights for Tritium Transfer between Coenzyme and Substrate Radical. The distribution of hydrogen isotopes between substrate and product from an enzyme bound intermediate depends on the relative energetic barrier heights of the catalyzed reaction. The reaction can either proceed forward onto product or reverse back to substrate once the substrate radical (illustrated here as glutamate) and tritiated 5'-deoxyadenosine are generated, incorporating tritium into either substrate or product. Rapid quench experiments on glutamate mutase that studies the reaction in both directions found that tritium partitions in approximately a 1:1 ratio between substrate and product, indicating the barrier heights for tritium transfer between glutamyl and methylaspartyl radical are of equal height.

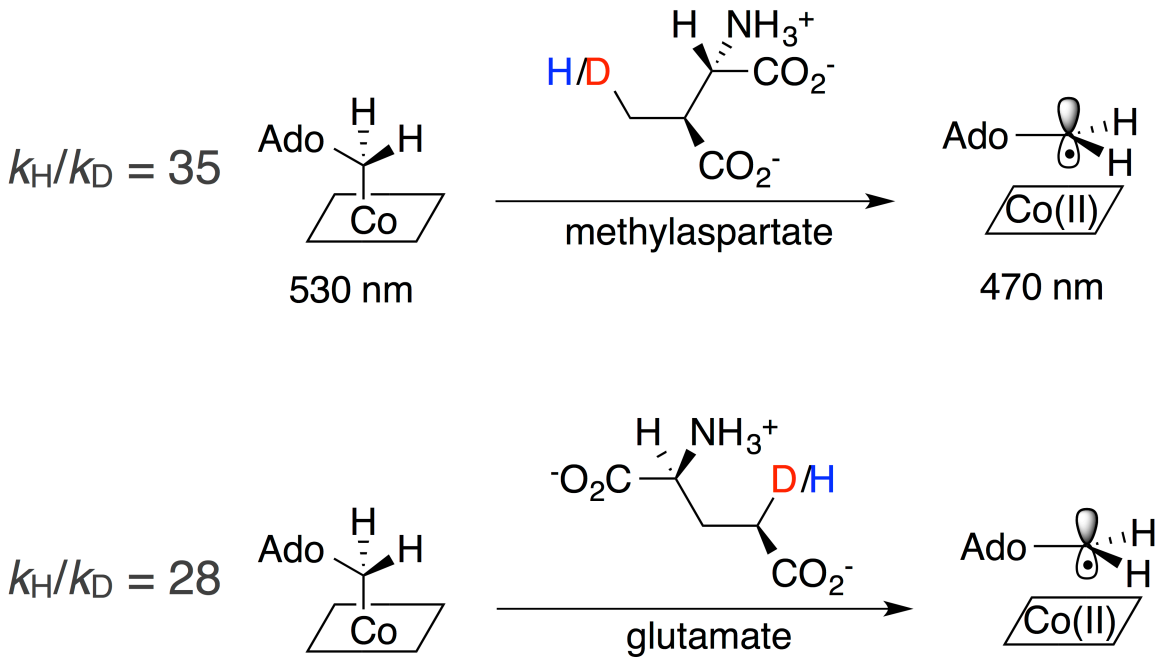

Figure 69. Cobalt-Carbon Bond Homolysis is Coupled to Hydrogen Abstraction in the Reaction Catalyzed by Glutamate Mutase. Co-C homolysis can be monitored spectroscropically as only the addition of substrate leads to a concomitant decrease in the 530 nm and increase in the 470 nm AdoCbl absorbance bands. There is a significant kinetic isotope effect on Co-C homolysis using deuterated substrates even though though it is not a formally isotopically sensitive step.

The first step in the mechanisms of all AdoCbl-dependent enzymes involves homolytic fission of the coenzyme. However, an important aspect of the mechanism for generating radicals is that the energetics of forming the 5'-deoxyadenosyl radical are extremely unfavorable since the bond dissociation energy of the Co-C bond is 32 kcal/mol and occurs at a rate of 10^{-9} s^{-1}. Yet, in response to substrate binding, enzyme bound AdoCbl readily undergoes homolytic cleavage at a rate of 10^{2} s^{-1}, corresponding to a 10^{11}-fold enhancement in rate over free solution.[5, 52] This creates a question specific to AdoCbl-dependent enzymes, *i.e.*, what does the enzyme [glutamate mutase] do mechanistically to lower the activation energy for homolysis? One possible explanation is the ground state destabilization theory, which proposes that substrate binding triggers a protein-induced distortion of the coenzyme that weakens the Co-C

bond sufficiently to promote homolysis.[42] Another theory proposes that the enzyme preferentially stabilizes the dissociated cob(II)alamin:5'-deoxyadenosyl radical pair state over the ground state (Figure 70).[191, 192] Although free radicals are electrically neutral species, experiment and computation point to the importance of electrostatic interactions between the protein, substrate and coenzymes in stabilizing radical intermediates. Consequently, active site charged residues are thought to preferentially stabilize the dissociated state over the associated state through electrostatic interactions with the adenosyl ribose ring.

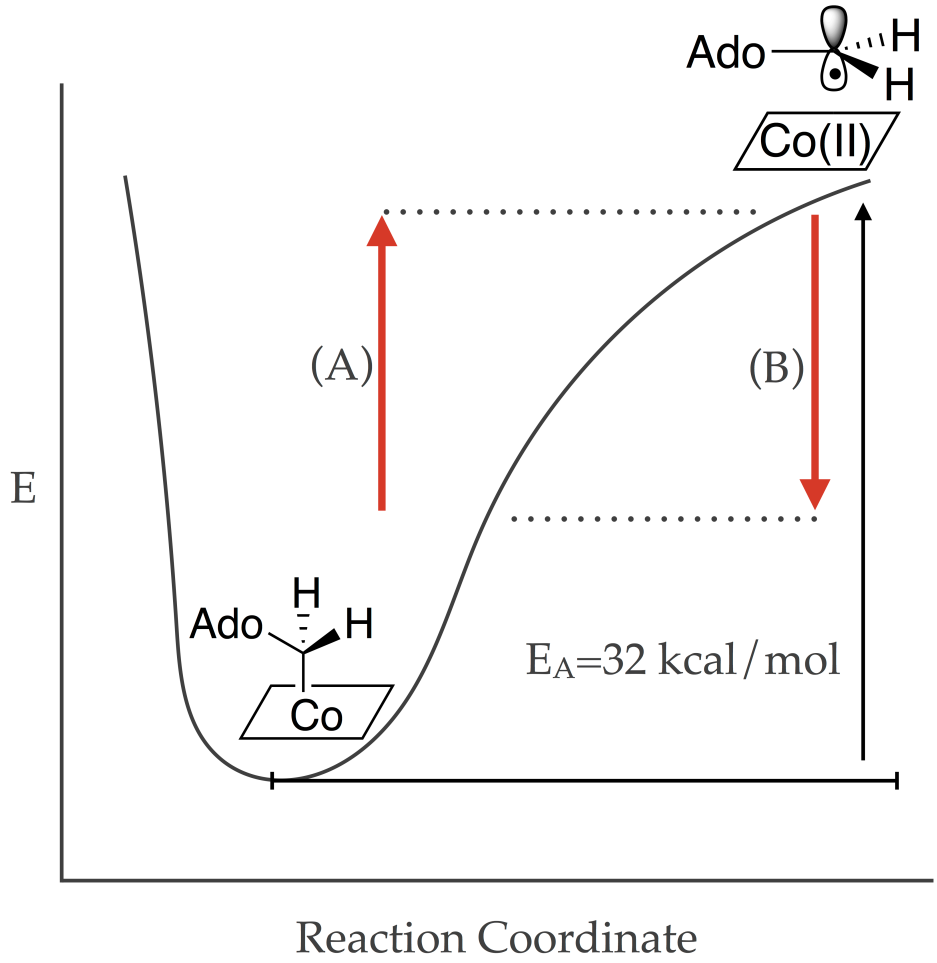

Figure 70. How Does Glutamate Mutase Activate AdoCbl Toward Co-C Bond Homolysis and Control the Adenosyl Radical Once Generated? A) Ground State Destabilization: Substrate binding triggers a protein-induced distortion of the coenzyme that weakens the Co-C bondsufficiently to promote homolysis. B) Stabilization of the Dissociated State: Active site charged residues preferentially stabilize the dissociated state over the associated state through electrostatic interactions with the adenosyl ribose ring.

Specifically, the residue Glu330 of glutamate mutase is conserved in the structures of all AdoCbl-dependent mutases. Computational[61, 191] and crystollographic[192] studies have proposed that Glu330 facilitates homolysis by stabilizing the dissociated state over the ground state by forming stronger hydrogen bonds with the ribose ring and forming an increased number of hydrogen bonds. Lys326 is not conserved but is the only other side-chain to directly interact with the ribose group, suggesting it is also important for catalysis. To test the theory of electrostatic stabilization, Chapter 2 describes the construction of a series of glutamate mutase variants at Lys326 and Glu330. In a targeted approach combining experiment with computational modeling (by Patrick von Glehn, Jeremy N. Harvey and Adrian J. Mulholland), the effect of mutation on catalysis was determined *in vitro* and on the structure and dynamics of the active site *in silico* with the goal of correlating changes in activity (determined experimentally) with changes to the structure of the active site (determined computationally).[287] Since mutation proved to be highly deleterious for enzymatic activity, the ability of the substrate to exchange tritium with the coenzyme was exploited to develop an extremely sensitive assay for AdoCbl cleavage and H-transfer. Spectroscopic characterization revealed that the mutants do not build up significant amounts of cob(II)alamin. This implies that the mutants destabilize the dissociated state such that radical pair recombination is much faster than homolysis. Under these conditions, the initial rate of tritium incorporation into AdoCbl reflects the rate of homolysis and hydrogen abstraction (coupled steps) so long as tritium exchange does not approach equilibrium. Mutation impaired the enzyme's ability to catalyze tritium exchange with the substrate by two to four orders of magnitude. Importantly, the amount of tritium incorporated by AdoCbl

was less than 4%, indicating that the exchange of tritium back to glutamate was negligible and the measurement indeed reflects the initial rate of tritium incorporation.

The wild-type and mutant enzymes were characterized *in silico* by molecular dynamics simulations of the enzyme−AdoCbl−substrate complex with AdoCbl modeled in the associated (Co−C bond formed) or dissociated [adenosyl radical with cob(II)alamin] state. No extensive changes to the peptide backbone or active site were observed over the course of the simulations, since RMSD values of backbone α-carbons relative to the crystal structure fell within the narrow range of 1−1.6 Å. This indicates that the enzymes are well-modeled by the simulation. The crystal structure represents an average of particular dynamic states that the enzyme samples over time. Accordingly, a variance in RMSD relative to the crystal structure does not indicate inaccuracy in the simulation; rather it reflects possible structural differences in the enzyme between the associated and dissociated states. Furthermore, neither adenosyl ribose ring conformation present in the crystal structure is representative of the associated state as the Co-C bond is broken in both. Therefore, modeling of the ground state is expected to include some variance in RMSD relative to the crystal structure.

The MD simulations were analyzed for the occurrence of hydrogen bonding configurations between the adenosyl -OH groups and Glu330 and Lys326. With the exception of the Glu330Ala mutation, which cannot hydrogen bond, the number and strength of hydrogen bonds between the residue at position 330 and the ribose moiety are significantly greater in the dissociated state of AdoCbl than in the associated state. Interestingly, the wild-type enzyme formed both more and shorter hydrogen bonds with the adenosyl -OH groups in both states than any of the mutant enzymes. Hydrogen

bonding between Lys326 and adenosyl -OH groups appears to be less important as the mean number of hydrogen bonds formed between Lys326 and adenosyl -OH groups during the simulations for the wild-type enzyme is smaller with no significant difference between the associated and dissociated states of AdoCbl. However, the low activity of the Lys326 mutants does appear to impair the ability of Glu330 to form hydrogen bonds with the ribose OH groups as the adenosyl 5′-carbon is much less well-positioned for hydrogen abstraction. These results confirm the theory of electrostatic stabilization in that the number and strength of hydrogen bonds between Glu330 and the ribose -OH are greater in the dissociated state of AdoCbl than in the associated state. This highlights the importance of the hydrogen bonds formed by this residue for catalysis. Even though these results support the electrostatic hypothesis, it is not the only factor necessary for efficient catalysis.

As in other enzymes, hydrogen tunneling, a phenomenon in which a particle crosses a barrier between reactants and products owing to its wave-like nature has emerged as a dominant mechanism by which the hydrogen atom moves between substrate and coenzyme.[153, 176] Since tunneling reactions occur when the reactant energy-well overlaps with the product energy-well, they are highly sensitive to changes in the donor-acceptor distance. Enzymes are believed to sample a variety of thermally equilibrated motions outside of the one-dimensional H-transfer reaction coordinate (*i.e.*, motions from the transferred particles environment) on a timescale equal to or faster than the experimental rate constant for the transfer event.[181, 288] For instance, as discussed in Chapter 2, the change in the secondary kinetic isotope effect for the formation of 5'-deoxyadenosine due to the primary kinetic isotope effect observed in

glutamate mutase is consistent with concerted motion in the transition state of the 5′-hydrogen atoms adjacent to the hydrogen that is transferred between substrate and coenzyme in a reaction that involves a large degree of quantum tunneling.[185] In a separate study, Defratyka and coworkers used a QM/MM model to study the molecular mechanism of H-transfer from coenzyme to substrate in the AdoCbl-dependent methylmalonyl CoA mutase reaction.[179] They modeled the tunneling reaction as an ensemble average of various reaction valleys by including multiple degrees of freedom outside of the progress coordinate for H-atom transfer. This multidimensional tunneling model predicted an intrinsic kinetic isotope effect that materially agreed with experiment.[153] The magnitude of the isotope effect was interpreted to arise from protein dynamics that decrease the distance over which the system tunnels to such a degree that the particle can bypass the saddle point along the reaction coordinate from reactant to product. This ensemble of sampled motions provides a mechanism for the enzyme to establish optimal donor-acceptor distances and the active site electrostatic interactions required to bring the potential energy surfaces of the reactants and products to a transiently degenerate state, allowing their wave functions to overlap and tunneling to occur.

The link between multidimensional protein dynamics and hydrogen tunneling efficiency is further illustrated by the dihydrofolate reductase catalyzed reaction.[181, 288] Stojkovic and coworkers found a correlation between the donor-acceptor distance and changes in the intrinsic kinetic isotope effect for the hydride transfer step in a series of active site mutants designed to modulate the donor-acceptor distance.[205] They attributed the increase in the temperature dependence of the intrinsic kinetic isotope

effect observed for the mutant enzymes to longer and broader distributions of the donor-acceptor distance with respect to the wild-type enzyme. Molecular dynamics simulations revealed that mutant enzymes with longer donor-acceptor distances possessed larger scale motions that produced a broader distribution of populations that could not reorganize to arrive at a tunneling ready state.

The work by Stojkovic and coworkers established that donor-acceptor distances are important to efficient hydrogen tunneling. Since AdoCbl-dependent enzymes are known to employ large degrees of quantum tunneling during H-atom transfer, the position of the adenosyl radical (acceptor) relative to the substrate (donor) appear to be important. Indeed, as discussed in Chapter 2, the mutant glutamate mutase enzymes (which were designed to modulate the donor-acceptor distance) were found to cause a progressive increase in the mean distance between the 5′-carbon of the adenosyl radical and the abstractable hydrogen of the substrate. This distance (determined computationally) was found to inversely correlate with the log*k* for tritium exchange (determined experimentally).[287]

The timescale of protein motions is important to consider when relating computational predictions to experimental observations. For instance, the molecular dynamics simulations in Chapter 2 were performed over 18 ns compared to the 10 ms it takes for a single turnover by glutamate mutase (considering a k_{cat} of 100 s^{-1}).[33] Enzymes constantly fluctuate between vast numbers of related conformations on a variety of different time scales, from large conformational changes that take 10^{-6} - 10^{-9} s, to local changes in configuration over 10^{-9} - 10^{-12} s.[288] Furthermore, both computational and experimental studies suggest that significant conformational changes accompany

Co-C bond cleavage with respect to the adenosyl's orientation,[192] internal conformation,[289, 290] and interactions with the active site,[190, 287] as well as large-scale changes to the enzyme conformation.[201, 291] These protein dynamics are believed to preferentially stabilize the dissociated adenosyl radical through enhanced H-bonding and carefully direct the 5'-adenosyl radical toward specific hydrogen abstraction from the substrate. It is therefore possible that an 18 ns simulation may not properly sample all the dynamic changes relevant to Co-C bond breaking between the associated and dissociated state of the coenzyme (since they occur on vastly different time scales). This could question the validity of the correlation considered in Chapter 2 between the mean positioning of the radical center on the adenosyl 5'-carbon relative to the abstractable hydrogen and the log*k* for tritium exchange. Because H-atom abstraction is kinetically coupled to Co-C homolysis, follow up computational studies were performed by Patrick von Glehn using enhanced (umbrella) sampling techniques to calculate the barrier heights to H-atom abstraction for the wild-type and mutant enzymes.[292] Interestingly, these were found to correlate with the experimentally determined log*k* for tritium exchange (r^2 = 0.89), substantiating the initial correlation. Still, modeling Co-C homolysis is devilishly difficult. Different computational studies have produced very different reaction profiles for Co-C bond breaking in enzymes (possibly due to the inability of properly capturing the relevant protein dynamics associated with Co-C homolysis).[155, 190, 191, 293] Clearly, since MD simulations show that significant conformational changes accompany Co-C bond breaking in the enzyme, sufficient conformational sampling is essential for an accurate computational representation of this event. More work is needed to assess how protein dynamics

influence the ability of enzymes to promote H-atom transfer in order to refine the current computational model.

Electrostatics alone are insufficient to explain the difference in activity between wild-type and mutant enzymes in glutamate mutase. The experiments considered in Chapter 2 show that Glu330Gln is more active than Glu330Asp. However, the neutral side-chain of Gln would be expected to form weaker hydrogen bonds with the ribose hydroxyl than the negatively charged Asp carboxylate. This is rationalized by showing through computation that hydrogen bonding between ribose and the shorter aspartate chain constrains the 5′-carbon so that it is, on average, 0.42 Å farther from the substrate than the glutamine mutant. Interestingly, the same activity trend was observed in ornithine aminomutase and methylmalonyl-CoA mutase when the equivalent glutamate residues were mutated to glutamine and aspartate.[196] Furthermore, various computational studies have examined aspects of the methylmalonyl-CoA mutase reaction and found that the enzyme strongly stabilizes the dissociated form of AdoCbl in the conformation that binds substrate, with changes in electrostatic interactions between substrate and protein appearing to play a significant role.[155, 294] It would also be interesting to pursue MD simulations of the mutations studied in both ornithine aminomutase and methylmalonyl-CoA mutase in a manner similar to those considered in Chapter 2.

In summary, combining computation with experiment in a targeted approach to elucidate enzyme mechanism has provided a powerful approach for gaining new atomic-level insights into reaction mechanism.[15] This approach allows the researcher to examine the structural features of an enzyme's active site that underpins catalysis in a

manner that is unavailable with either experimental observation or computation alone. The studies presented here provide an effective illustration of how computation may be used to direct experimental design. Understanding the origin of enzyme catalysis goes far beyond any academic significance. For instance, this approach may be applied to understand and optimize reactions of industrial importance. Present technology should allow for experiments that test the importance of protein–substrate interactions identified by QM/MM simulations (*e.g.,* by kinetic analysis of mutant enzymes and/or modified substrates), many of which are not obvious from simple inspection of the protein structures.

5.2. Towards a Mechanistic Understanding of the Antiviral Protein Viperin

Viperin (Virus Inhibitory Protein, Endoplasmic Reticulum associated, INterferon inducible) is an interferon-stimulated gene, which has direct antiviral activity against a number of DNA and RNA based pathogens that infect eukaryotic cellular-based organisms.[247-249, 270, 295] Despite viperin being shown to interact with a variety of cellular and viral based proteins (Table 10),[247] these have not been characterized and the protein has yet to be assigned an enzymatic function. The step at which viperin limits pathogen replication depends on the virus; for instance, viperin inhibits progeny particle budding during influenza A infection,[246, 271] prevents particle assembly and maturation during human cytomegalovirus infection,[250] and limits RNA genome replication in hepatitis C,[254] dengue,[255] and tick-borne encephalitis viruses.[256] Sequence analysis reveals this 361-residue protein (Mr 42,000) to be highly conserved throughout vertebrate animals and comprises three domains. First, the N-terminus contains an amphipathic helix that appears to be involved in binding to the cytosolic face of the

endoplasmic reticulum[251] and lipid droplets.[253] Next, the central domain contains four motifs characteristic to radical *S*-adenosyl-*L*-methionine (SAM) enzymes, including the canonical CX_3CX_2C [4Fe-4S] cluster-binding motif.[264] Previous reports (verified by studies discussed in Chapter 4) show that viperin can bind an iron-sulfur cluster and catalyzes the slow cleavage of SAM to 5'-deoxyadenosine under reductive conditions *in vitro*.[263] Radical SAM enzymes use the [4Fe-4S] cluster to chelate SAM and generate a highly reactive 5'-deoxyadenosyl radical intermediate through reductive cleavage of SAM's 5'-C-S bond. The 5'-deoxyadenosyl radical is then used to abstract a hydrogen atom from the substrate as a common first step in a wide variety of challenging chemical transformations.[23, 24] Finally, the C-terminus region is strongly conserved across species and is critical for antiviral activity against hepatitis C[254] and dengue[255] viruses. Although its function is not fully understood, it is thought to be involved in mediating viperin's activity by establishing protein-protein interactions with its targets (the C-terminal doman of radical SAM enzymes is responsible for binding their celluar substrates[26]).[247, 248]

Farnesyl pyrophosphate synthase (FPPS) is currently the best-established target for viperin. The enzyme catalyzes the condensation of geranyl pyrophosphate to isopentenyl pyrophosphate to produce farnesyl pyrophosphate, a key intermediate in isoprenoid and cholesterol biosynthesis.[282] Many viruses, such as influenza A, exploit cholesterol-rich lipid rafts in the cells membrane to assemble its progeny and bud from the cell. Inhibition of FPPS blocks downstream production of cholesterol, which leads to lipid raft dispersal, thus restricting viral replication.[271] Despite the antiviral response being well-understood at the cellular and genetic level, the biochemistry by which cells

regulate enzymes crucial to viral replication remain poorly understood, including the mechanism by which viperin inhibits FPPS. It is surprising that a radical SAM enzyme (such as viperin) participates in aerobic organisms, as this class of enzyme is highly susceptible to oxidative degradation.[5] Furthermore, the involvement of radical SAM chemistry in the mammalian antiviral response is completely unexpected and sets viperin apart from other radical SAM enzymes. In short, viperin represents a new paradigm for radical SAM enzymes in higher organisms and points to a new mechanism for the regulation of enzyme activity in eukaryotic cells. Consequently, elucidating the biochemical basis of radical SAM chemistry in the antiviral response is essential.

Chapter 4 considers how Wang and coworkers initially identified FPPS as a target for viperin through a yeast two-hybrid screen and established that expression of viperin inhibits endogenous FPPS in HeLa cells.[246] Presumably, viperin and FPPS interact to some degree in an over-expressing eukaryotic system. The results described in Chapter 4 support this interaction as evidenced by the observed decrease in FPPS concentration from viperin co-transfected HEK293T cells. Wang and coworkers further confirmed viperin's interaction with FPPS through co-immunoprecipitation studies. However, these were performed from interferon-induced mouse cells. Thus, if an interferon stimulated gene is required (*i.e.*, for viperin to bind FPPS strongly enough that it can pull down the protein), then the constitutive expression system used in Chapter 4 to over-express both proteins will not be able to reproduce the result. More importantly, how viperin specifically uses radical SAM chemistry remains unclear. It appears that any interaction viperin may have with FPPS in eukaryotic cells not induced by interferon is independent of viperin's ability to cleave

SAM. It only demonstrates cleavage if SAM is added post cell lysis and even then, it is still uncoupled. Interestingly, the amount of 5'-deoxyadenosine produced does not change when FPPS is present (*i.e.*, FPPS does not enhance viperin's ability to cleave SAM). Consequently, viperin's substrate remains unknown.

Mutagenic studies of viperin's CX_3CX_2C motif demonstrate that it is crucial for the enzyme to bind an iron-sulfur cluster in order for it to be functional against human immunodeficiency,[242] bunyamwera,[262] dengue,[260] hepatitis C[254] (although *in vivo* studies found the radical SAM domain to be dispensible)[244, 268] and West Nile[260] viruses, as well as in the ability of HCMV to co-opt viperin as a proviral host protein.[250, 267] Upadhyay and coworkers showed that viperin limits tick-borne encephalitis (TBEV) by inhibiting viral genomic RNA production and that the inhibitory effects are strictly dependent on the activity provided by the radical SAM domain.[256] Not only did they discover that radical SAM domain mutants completely loose their inhibitory activity and the ability to uptake iron, but also established viperin to interact with the cytosolic iron-sulfur protein assembly factor CIAO1 (a protein required for cytosolic iron-sulfur cluster assembly in human cells)[296] through immunoprecipitation studies. Expression of viperin into cells with a siRNA knockdown against CIAO1 significantly impaired the enzyme's ability to uptake iron and to suppress intracellular levels of viral RNA. Interestingly, the C-terminus of viperin was required for both the enzyme's interaction with CIAO1 and its ability to bind iron *in vivo*; various mutants lacking the extreme C-terminal W361 did not interact with CIAO1, did not uptake iron, and possessed no antiviral activity. Moreover, this C-terminal aromatic amino is also required for viperin's antiviral activity against the hepatitis C virus.[254]

The importance of viperin's radical SAM domain in effecting its enzymatic function is established. However, it is still necessary to determine if viperin actually functions as a radical SAM enzyme *in vivo* when considering its antiviral role in the cell (*i.e.*, reductive cleavage of SAM). Using multi-template homology modeling and molecular dynamics simulations, Haldar and coworkers developed a low-resolution model structure of viperin which predicted that removal of the iron-sulfur cluster would lead to destabilization of the enzyme's tertiary structure (leading to unfolding).[265] They confirmed their simulations through the spectroscopic characterization of various CX_3CX_2C to alanine variants, which resulted in a partially unfolded, conformationally unstable, and aggregation prone enzyme. In contrast to wild-type viperin, each of the cysteine mutants over-expressed in *E. coli* as inclusion bodies; which further supports that the removal of iron-sulfur cluster leads to protein destabilization. Consequently, it is not clear whether the loss of enzymatic function displayed by the viperin radical SAM domain mutants is directly related to the enzymes inability to act as a radical SAM enzyme or that mutation renders the enzyme unstable. Accordingly, Upadhyay and coworkers tried to find further evidence that the antiviral action of viperin is indeed based on the contribution of the enzymes radical SAM domain by modulating the intracellular levels of SAM in wild-type viperin expressing HEK293T Rex cells.[256] In one experiment, viperin expressing cells were treated with cycloleucine (an inhibitor of intracellular SAM synthesis) and infected with TBEV after 48 hours. Cycloleucine treatment resulted in a 4-fold rescue to the total TBEV RNA levels when compared to control cells that did not express viperin. In a second experiment, the intracellular levels of SAM were reduced by transiently transfecting HEK293T cells with viperin and a clone

encoding the SAM-cleaving enzyme SAMase. After 24 hours, the cells were infected with TBEV and, as expected, transfection of viperin substantially reduced levels of TBEV RNA. Consistent with the cycloleucine experiment, RNA levels of TBEV were completely restored in the cells co-expressing SAMase with viperin. The inclusion of SAMase had no influence over the viral titers recovered or over the expression levels of viperin. These results show that the mechanism by which viperin limits TBEV is indeed dependent on the enzymatic activity that is provided by the radical SAM domain. Further studies are needed to determine if viperin produces 5′-deoxyadenosine *in vitro* and whether this product is directly involved in limiting the synthesis of TBEV genomic RNA.

Even though many questions remain as to the nature of viperin's interaction with FPPS, Chapter 4 confirms that viperin is a radical SAM enzyme and suggests that its interaction with FPPS significantly lowers the levels of FPPS in co-transfected HEK293T cells. Likewise, Upadhyay and coworkers observed an analogous result, in which over-expressed FLAG-viperin strongly diminished levels of the tick-borne encephalitis envelope (E) protein in infected HEK293T cells.[256] It is unlikely that such modulation occurs at the level of RNA transcription or translation because both FPPS and viperin genes were expressed from CMV viral promoters. Moreover, no RNA or DNA-binding motifs are evident from the viperin's amino acid sequence. Still, viperin targets the RNA replication step of several flaviviruses and a mechanism involving mRNA targeting should not be excluded.[244, 254-256, 260, 268] Chapter 4 proposes a model in which viperin catalyzes the post-translational degradation of FPPS. Mutation of viperin's radical SAM domain needs to be studied in the context of influenza A infection and its interaction

with FPPS. Mutagenesis experiments may provide valuable insight into how viperin uses radical SAM chemistry to modulate the levels of FPPS.

Experiments described in Chapter 4 relied on the use of N-terminal epitope tags to probe viperin's interaction with FPPS. The choice of N-terminal tags was influenced by the work of Wang and coworkers, who used them to identify FPPS's interaction with viperin (through a yeast two hybrid screen). However, under these conditions, viperin and FPPS did not pull each other down. It is possible that the tag's location interferes with the interaction. This could be tested by switching the tag to the C-terminus or removing it all together using TEV protease. Furthermore, relying on epitope tags for detection limits the information that can be obtained about its degradation. If viperin directly degrades FPPS by cleaving the protein in a manner similar to the oxidative cleavage of glycyl radical enzymes, the use of a commercially available polyclonal antibody to FPPS is more appropriate. This type of antibody recognizes multiple epitopes of FPPS and allows the immunoprecipitation of any potential enzyme fragment, which can then be analyzed by LC-ESI-MS proteomics to determine the cleavage site.

Initial attempts to establish a time dependence for the rate at which viperin degrades FPPS involved the addition of viperin DNA at various times to cells already expressing FPPS. However, western blot revealed viperin was poorly transfected in cells already producing FPPS. This can be overcome by purifying the proteins from mammalian culture. Even though expression levels from such cells are typically much lower than those obtained from *E. coli*, proteins can routinely be expressed at 2 - 10 mg/L in HEK cells. The expression system described here routinely provides

expression levels of ~ 4 mg/L. Optimization of the culture and transfection conditions should then provide sufficient protein that can be purified from scale-up cell cultures. With pure protein, the time and concentration dependence of viperin on FPPS degradation may be established.

It is possible that viperin does not directly degrade FPPS but rather tags it for sequestration or degradation by other components of the cellular machinery through a covalent modification. The use of purified proteins from mammalian cells can aid in identifying any covalent modification made to FPPS through proteomic / LC-tandem MS studies. Alternatively, metabolic studies could determine if the metabolites in the mevalonate biosynthetic pathway change in response to viperin expression. Even though evidence from enzyme activity assays of cell lysates indicates that viperin expression diminishes FPPS activity,[246] it is far from clear whether this significantly affects the production of isoprenoids *in vivo*. If viperin truly inhibits FPPS, *in vivo* concentrations of upstream metabolites should increase whereas those downstream would decrease.

Further characterization of wild-type viperin is needed. ICP-MS of purified protein will allow the iron loading of viperin to be established. EPR will allow for characterization of the iron-sulfur cluster's interaction with SAM; a study that has not been performed on mammalian expressed, full-length viperin. Finally, a long-term goal is determining the crystal structure of viperin either on its own or in complex with FPPS, as well as its truncated analogues. Even though radical SAM enzymes are air sensitive, Chapter 4 demonstrates viperin to be tolerant to oxygen as aerobically purified enzyme from bacteria is able to retain some of its iron-sulfur clusters. Since, the crystal

structures of various radical SAM enzymes have been solved, there is a good chance that (if allowed to crystallize under anaerobic conditions) purified protein from mammalian cells can yield crystals that are able to diffract well.

It is important to know if there is a common mechanism by which viperin inhibits its targets despite the multiple functions ascribed to this enzyme based on virology studies. The goal of this effort is to understand the mechanism by which viperin interacts with FPPS and extend this knowledge to viperin's other, less understood targets (Table 10).[247] For instance, Seo and cowrkers showed that human cytomegalovirus (HCMV) infection resulted in viperin inhibiting the β-subunit of MTP (mitochondrion trifunctional protein),[267] a multienzyme complex comprised of two subunits which functions as an $\alpha_2\beta_2$ tetramer and catalyzes three out of the four reactions in the fatty acid β-oxidation pathway (a major route for the generation of cellular energy).[297, 298] Although viperin is known to inhibit HCMV when preexpressed in cells,[250] HCMV infection directly induces viperin expression and is able to facilate infection by co-opting the protein;[247, 267, 270] the HCMV encoded viral protein vMIA (viral mitochondrial inhibitor of apoptosis) binds viperin and transports it from the cytosolic face of the endoplasmic reticulum to the mitochondrion, signaled by an N-terminal mitochondrial localization epitope. Here, viperin interacts and inhibits MTP, dramatically reducing the cells ability to regenerate ATP. This is understood to weaken the actin cytoskeleton and facilitate viral cellular escape. Inhibition of MTP also appears to lead to up-regulation of lipid biosynthesis, which is needed for the viral envelope. Interestingly, it seems that interruption of ATP production is not dependent on vMIA as a viperin mutant in which the N-terminal amphipathic alpha helix was replaced with a

mitochondrial targeting sequence had the same effects on ATP generation and the actin cytoskeleton with no requirement for vMIA. Furthermore, viperin's iron-sulfur cluster binding motif is necessary for these effects (although it was not required for the interaction with MTP) suggesting radical SAM chemistry is mechanistically important. A similar approach to the one used for studying FPPS can be applied to the study of viperin's inhibition of MTP as its biochemical function is well established and easily assayed. The human enzyme can be stably purified from over-expressing *E. coli* cells as a soluble and active protein, allowing *in vitro* studies of its interaction with viperin.[299] Furthermore, the X-ray structure of an MTP homologue from *P. fragi* has been solved,[300] allowing for mechanistic studies to be interpreted in light of the enzyme's structure. Most importantly, Seo and coworkers demonstrated that viperin targeted to the mitochondria using a mitochindrial leader sequence had the same effect on MTP activity,[267] allowing viperin's inhibition of MTP to be studied in the absence of HCMV infection.

It is possible that viperin recognizes its targets through a conserved sequence motif. Bioinformatic analysis could then identify other unknown proteins that contain such a motif. Furthermore, if viperin is found to inhibit its targets through common modification, proteomic studies could then identify potential interacting partners. However, these techniques require a detailed understanding of the biochemistry pertaining to the identity of the recognition sequence, as well as the type of modification employed. Ultimately, these studies will advance the understanding the role interferon stimulated genes play in the antiviral response. It may also suggest new avenues for the design of antiviral therapeutics. If, in fact, viperin catalyzes a post-translational

modification of target proteins (once identified), this could be a signature amenable to proteomics profiling. If so, radical SAM-regulated enzymes could be identified in other cellular pathways. Understanding the role viperin plays in inhibiting the influenza A virus through its interaction with FPPS is the springboard for these efforts.

APPENDICES

Appendix A.1

Computational Methods

The Protein Data Bank structure of glutamate mutase (entry 1I9C) was used for all simulations; mutant structures were generated using the PyMol molecular graphics system, version 1.3 (Schrödinger, LLC). The Co−C bond is not formed in the crystal structure; however, minimization using a force field including a term for the Co−C bond followed by careful equilibration produced reasonable starting structures for simulation of the associated Co−C complex.

Histidine protonation states were determined by visual inspection of implied hydrogen bonds and pKa values estimated using PROPKA (Appendix A.2.). Some Asn and Gln residues were flipped to remove steric clashes as calculated using Molprobity. Where the calculated electron density in the crystal structure was indicative of more than one side-chain conformation, the conformation with the higher occupation number was chosen. In particular, there are two conformations of the adenosyl group, both of which have broken Co−C bonds. In only one of these conformations does the adenosyl group form hydrogen bonds with Glu330. This conformation was used as the starting structure for all simulations because it has the higher occupation number and because we believe it better resembles the dissociated state. The AmberTools 1.5 program 'tleap' was used to add hydrogen atoms. The protein was solvated in a water box with > 12 Å between the protein and the sides; sodium ions were added to neutralize the system.

The AMBER ff99SB force field was used; parameters for modeling cobalamin and adenosine groups were adapted from previously published parameters derived and

thoroughly tested against experimental structural data by other groups. The performance of the ff99SB force field has been shown to satisfactorily model hydrogen bonding, outperforming most semi-empirical quantum mechanics/molecular mechanics methods in reproducing some experimental properties, such as nuclear-magnetic resonance dipolar coupling constants.

Charges for the cobalamin, adenosyl, and glutamate substrate were calculated by the RESP fitting method at the HF/6-31G* level of theory using Gaussian09 and RED-IV by way of the RED server. Because of the known poor performance of the Hartree−Fock model in calculating properties of transition metals, the cobalamin charges close to the Co atom were refined by comparison with Mulliken charges calculated at the B3LYP/LACV3P* level with Jaguar 7.6 (Schrödinger, LLC). The positions of water and ions were optimized with 100 steps of steepest descent followed by 900 steps of conjugate gradient minimization. The whole system was then similarly optimized with restraints of 5 kcal mol^{-1} $Å^2$ on all α-carbons.

Energy minimizations were performed using the sander.MPI code in the AMBER11 package. Random velocities were assigned, and the system was heated to 300 K by 50 ps Langevin dynamics (collision frequency of 5 ps^{-1}) with α-carbon restraints applied; a 100 ps equilibration in the NPT ensemble at 300 K and 1 atm was performed with α-carbon restraints present followed by the gradual release of restraints after additional simulation over 50 ps. Eighteen nanosecond production runs were performed using Langevin dynamics (collision frequency of 5 ps^{-1}) at 300 K and 1 atm. All molecular dynamics (MD) simulations were performed with a 2 fs time step. The SHAKE algorithm was applied to constrain the length of all bonds involving hydrogen,

allowing a time step on a time scale similar to that of vibrations of bonds involving hydrogens to be used. Non-bonded interactions were not calculated between pairs of atoms separated by a distance greater than a cutoff of 10 Å. Periodic boundary conditions were used with a 130 Å × 100 Å × 110 Å orthorhombic box. The particle mesh Ewald (PME) method was applied to treat long-range electrostatic interactions. All MD simulations were performed using the pmemd.mpi code in the AMBER11 package. Analysis of the MD simulations was performed using the cpptraj module of AmberTools 1.5.

Appendix A.2

Histidine Protonation States Used In MD Simulations

Histidine protonation states were determined by visual inspection of implied hydrogen bonds and pK_a estimated using the program PROPKA. The histidine protonation states used in MD simulations are summarized below.

Histidine Protonation State	Chain	Residue Number
HID	A	16
HID	A	100
HID	B	14
HID	B	163
HID	C	16
HID	C	100
HID	D	14
HID	D	163
HIE	A	25
HIE	B	75
HIE	B	291
HIE	B	329
HIE	C	25
HIE	D	75
HIE	D	291
HIE	D	329
HIP	B	150
HIP	B	210
HIP	D	150
HIP	D	210

Appendix A.3

Parameters Obtained from the Fit to the Gamma Probability Density Function for the Distance Distribution Plots for Wild-Type and Mutant Glutamate Mutase Enzymes

As discussed in Chapter 2, data from MD simulations of the mutant and wild-type enzymes were analyzed to calculate the mean distance, $R_{(C5'-H)}$, between the 5'-carbon of the adenosyl radical and the abstractable hydrogen of the substrate in the dissociated state. The distances extracted from the simulations were binned and fitted to the gamma probability density function given below, from which the mean distance, $R_{(C5'-H)}$, was calculated.

Mutant	E330A	E330D	E330Q	K326M	K326Q	Wild-Type
kappa	10.69	4.46	22.18	15.50	16.97	5.45
theta	0.132	0.242	0.0516	0.0708	0.0880	0.0795
scaling (s)	0.0956	0.1025	0.1013	0.0909	0.0977	0.0991
offset (x_0)	2.072	2.179	1.657	2.013	1.874	2.188
mean	3.49	3.26	2.80	3.11	3.36	2.62
standard deviation	0.19	0.26	0.059	0.077	0.13	0.034

Appendix A.4

Normalized Distribution Plots of $R_{(C5'-H)}$ and Fits for Wild-Type and Mutant Glutamate Mutase Enzymes

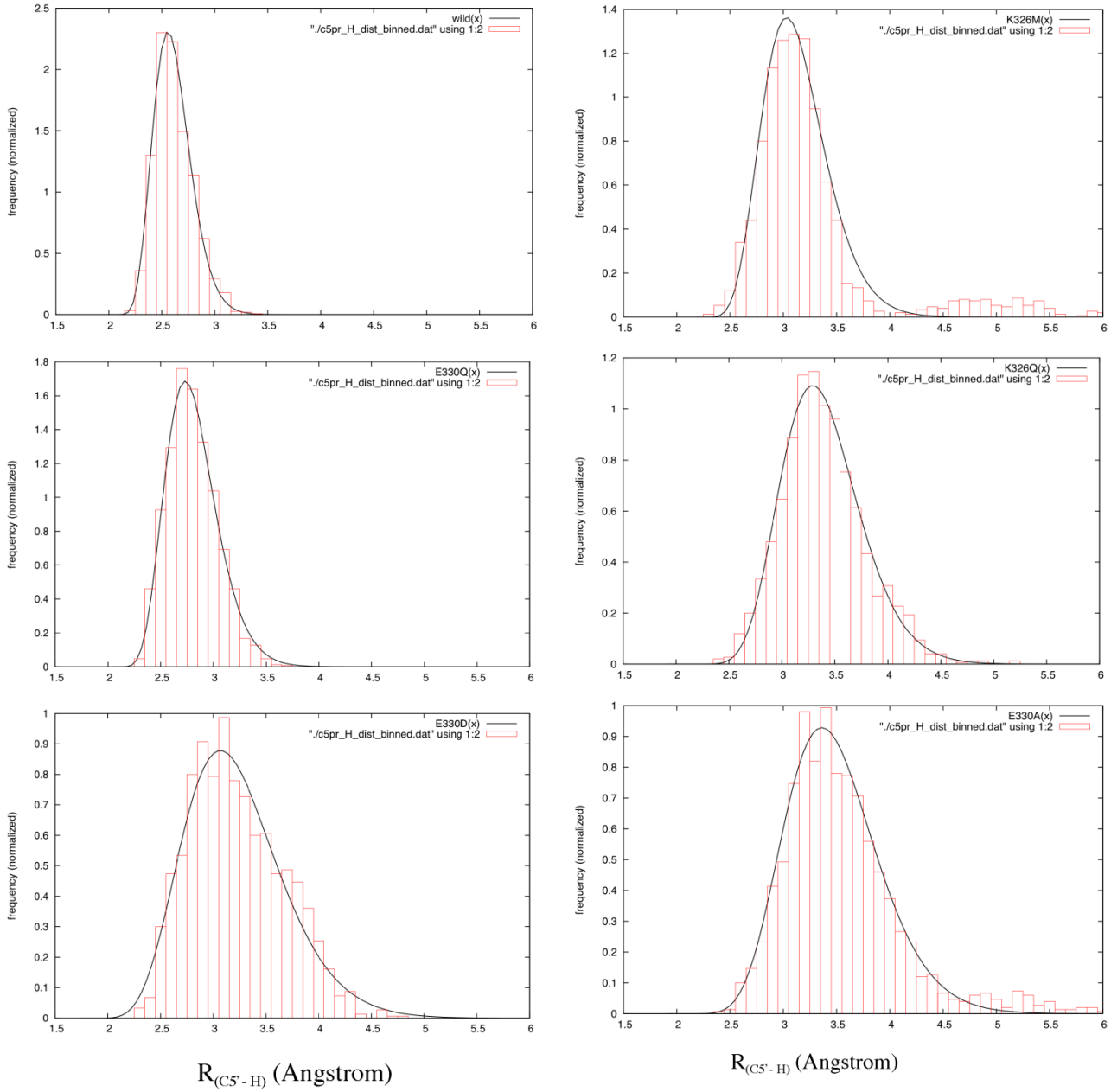

Appendix A.5

Benzoyl Chloride Derivatization and Liquid Chromatography–Mass Spectrometry of 5'-Deoxyadenosine

20 µL of the supernatant was benzoylated by sequential addition of 10 µL of 100 mM sodium carbonate, 10 µL of benzoyl chloride (2% in acetonitrile, v/v), and 10 µL of internal standards, with vortexing after each addition. Internal standards were prepared by benzoylating Ado, 3'dA, and 5'dA with 13C6 benzoyl chloride, followed by 100x dilution into 20% acetonitrile (v/v) containing 1% sulfuric acid.

A standard mixture of Ado, 3'-Ado, and 5'-Ado was prepared in water and diluted to create a calibration range of 5 - 1000 nM for Ado and 0.1 - 20 nM for 3'dA and 5'dA. Standards were derivatized as described above and calibration curves were prepared based on the peak area ratio of the standard to the internal standard by linear regression.

All samples were analyzed in triplicate using an Acquity HSS T3 C18 chromatography column (1 mm x 100 mm, 1.8 µm, 100 Å pore size) in a Waters nanoAcquity ultra performance liquid chromatograph interfaced to an Agilent 6410 triple quadrupole mass spectrometer. Mobile phase A was 10 mM ammonium formate with 0.15% (v/v) formic acid in water. Mobile phase B was acetonitrile. The flow rate was 100 µL/min, and the gradient used was as follows: Initial, 0% B; 0.01 min, 17% B; 0.50 in, 40% B; 2.99 min, 60% B; 3.00 min, 100% B; 3.99 min, 100% B; 4.00 min, 0% B; 5.00 min, 0% B.

The sample injection volume was 5 µL in partial loop injection mode. The auto-sampler was kept at ambient temperature, and the column was held at 27 °C.

Electrospray ionization was used in positive mode at 4 kV. The gas temperature was 350 °C, gas flow was 11 L/min, and the nebulizer was at 15 psi. Detection conditions for the doubly-labeled species by tandem mass spectrometry are as follows:

Species	Precursor (m/z)	Product (m/z)	Fragmentor (V)	Collision Energy (V)	Cell Accelerator (V)	Retention Time (min)
Bz-Ado	476	136	120	30	4	3.3
$^{13}C_6$Bz-Ado	488	136	120	30	4	3.3
Bz-3'dA	460	105	120	30	4	3.8
$^{13}C_6$Bz-3'dA	472	111	120	30	4	3.8
Bz-5'dA	460	105	120	30	4	4.1
$^{13}C_6$Bz-5'dA	472	111	120	30	4	4.1

Automated peak integration was performed using Agilent MassHunter Workstation Quantitative Analysis for QQQ, version B.05.00. All peaks were visually inspected to ensure proper integration.

REFERENCES

REFERENCES

1. Frey, P. A. (1990) Importance of Organic Radicals in Enzymatic Cleavage of Unactivated C-H Bonds, *Chemical Reviews 90*.
2. Booker, S. J. (2009) Anaerobic functionalization of unactivated C–H bonds, *Current Opinion in Chemical Biology 13*, 58-73.
3. Krebs, C., Fujimori, D., Walsh, C., and Bollinger, J. J. (2007) Non-heme Fe(IV)–oxo intermediates., *Accounts of Chemical Research 40*, 484-492.
4. Costas M, Mehn MP, Jensen MP, and Jr:, Q. L. (2004) Dioxygen activation at mononuclear nonheme iron active sites: enzymes, models, and intermediates, *Chemical Reviews 104*, 939-986.
5. Marsh, E. N. G., Patterson, D. P., and Li, L. (2010) Adenosyl Radical: Reagent and Catalyst in Enzyme Reactions, *Chembiochem 11*, 604-621.
6. Chandor-Proust, A., Berteau, O., Douki, T., Gasparutto, D., Ollagnier-de-Choudens, S., Fontecave, M., and Atta, M. (2008) DNA repair and free radicals, new insights into the mechanism of spore photoproduct lyase revealed by single amino acid substitution, *The Journal of biological chemistry 283*, 36361-36368.
7. Zhang, Q., and Liu, W. (2011) Complex biotransformations catalyzed by radical S-adenosylmethionine enzymes, *The Journal of biological chemistry 286*, 30245-30252.
8. Frey, M., Rothe, M., Wagner, A. F. V., and Knappe, J. (1994) Adenosylmethionine-dependent synthesis of the glycyl radical in pyruvate formate-lyase by abstraction of the glycine C-2 pro-S hydrogen atom. Studies of [2H]glycine-substituted enzyme and peptides homologous to the glycine 734 site., *Journal of Biological Chemistry 269*, 12432-12437.
9. Boal, A. K., Grove, T. L., McLaughlin, M. I., Yennawar, N. H., Booker, S. J., and Rosenzweig, A. C. (2011) Structural Basis for Methyl Transfer by a Radical SAM Enzyme, *Science 332*, 1089-1092.
10. Fujimori, D. G. (2013) Radical SAM-mediated methylation reactions, *Current Opinion in Chemical Biology 17*, 597-604.
11. Forouhar, F., Arragain, S., Atta, M., Gambarelli, S., Mouesca, J. M., Hussain, M., Xiao, R., Kieffer-Jaquinod, S., Seetharaman, J., Acton, T. B., Montelione, G. T., Mulliez, E., Hunt, J. F., and Fontecave, M. (2013) Two Fe-S clusters catalyze sulfur insertion by radical-SAM methylthiotransferases, *Nature chemical biology 9*, 333-338.

12. Wang, S. C., and Frey, P. A. (2007) S-adenosylmethionine as an oxidant: the radical SAM superfamily, *Trends in Biochemical Sciences 32*, 101-110.

13. Banerjee, R. (2003) Radical carbon skeleton rearrangements: Catalysis by coenzyme B-12-dependent mutases, *Chemical Reviews 103*, 2083-2094.

14. Arragain, S., Garcia-Serres, R., Blondin, G., Douki, T., Clemancey, M., Latour, J. M., Forouhar, F., Neely, H., Montelione, G. T., Hunt, J. F., Mulliez, E., Fontecave, M., and Atta, M. (2010) Post-translational modification of ribosomal proteins: structural and functional characterization of RimO from Thermotoga maritima, a radical S-adenosylmethionine methylthiotransferase, *The Journal of biological chemistry 285*, 5792-5801.

15. Marsh, E. N. G., and Melendez, G. D. R. (2012) Adenosylcobalamin enzymes: Theory and experiment begin to converge, *Biochimica Et Biophysica Acta-Proteins and Proteomics 1824*, 1154-1164.

16. Brown, K. L. (2005) Chemistry and enzymology of vitamin B-12, *Chemical Reviews 105*, 2075-2149.

17. Reed, G. R. (2004) Radical mechanisms in adenosylcobalamin-dependent enzymes, *Current opinion in chemical biology 8*, 477-483.

18. Matthews, R. G. (2009) Cobalamin- and Corrinoid-Dependent Enzymes, In *Metal Ions in Life Sciences*, pp 53-114.

19. Marsh, E. N. G., and Drennan, C. L. (2001) Adenosylcobalamin-dependent isomerases: new insights into structure and mechanism, *Current Opinion in Chemical Biology 5*, 499-505.

20. Hay, B. P., and Finke, R. G. (1987) Thermolysis of the Co-C Bond in Adenosylcorrins. Quantification of the Axial Base Effect in Adenosylcobalamin By the Synthesis and Thermolysis of Axial Base-Free Adenosylcobinamide - Insights Into the Energetics of Enzyme- Assisted Cobalt Carbon Bond Homolysis, *Journal of the American Chemical Society 109*, 8012-8018.

21. Frey, P. A., and Magnusson, O. T. (2003) S-Adenosylmethionine: a wolf in sheep's clothing, or a rich man's adenosylcobalamin?, *Chemical reviews 103*, 2129-2148.

22. Fontecave, M., Mulliez, E., and Ollagnier-de-Choudens, S. (2001) Adenosylmethionine as a source of 5'-deoxyadenosyl radicals, *Current opinion in chemical biology 5*, 506-511.

23. Jiarui Wang, Rory P. Woldring, Gabriel D.Romań-Meleńdez, Alan M. McClain, Brian R. Alzua, and E. Neil G. Marsh. (2014) Recent Advances in Radical SAM Enzymology: New Structures and Mechanisms, *ACS Chemical Biology 9*, 1929-1938.

24. Broderick, J. B., Duffus, B. R., Duschene, K. S., and Shepard, E. M. (2014) Radical S-Adenosylmethionine Enzymes, *Chemical Reviews 114*, 4229-4317.

25. Marsh, E. N. G., Huhta, M. S., and Patwardhan, A. (2004) S-adenosylmethionine radical enzymes, *Bioorganic Chem. 32*, 326-340.

26. Frey, P. A., Hegeman, A. D., and Ruzicka, F. J. (2008) The radical SAM superfamily, *Critical reviews in biochemistry and molecular biology 43*, 63-88.

27. Sofia, H. J., Chen, G., Hetzler, B. G., Reyes-Spindola, J. F., and Miller, N. E. (2001) Radical SAM, a novel protein superfamily linking unresolved steps in familiar biosynthetic pathways with radical mechanisms: functional characterization using new analysis and information visualization methods, *Nucleic acids research 29*, 1097-1106.

28. Christina Paraskevopoulou, Shirley A. Fairhurst, David J. Lowe, Peter Brick, and Onesti, S. (2006) The Elongator subunit Elp3 contains a Fe4S4 cluster and binds S-adenosylmethionine, *Molecular Microbiology 59*, 795-806.

29. N. Cecilia Martinez-Gomez, and Diana M. Downs. (2008) ThiC Is an [Fe-S] Cluster Protein That Requires AdoMet To Generate the 4-Amino-5-hydroxymethyl-2-methylpyrimidine Moiety in Thiamin Synthesis, *Biochemistry 47*, 9054-9056.

30. Krebs, C., Broderick, W. E., Henshaw, T. F., Broderick, J. B., and Huynh, B. H. (2002) Coordination of adenosylmethionine to a unique iron site of the [4Fe-4S] of pyruvate formate-lyase activating enzyme: a Mossbauer spectroscopic study, *Journal of the American Chemical Society 124*, 912-913.

31. Nathaniel J. Cosper, Squire J. Booker, Frank Ruzicka, Perry A. Frey, and Scott, R. A. (2000) Direct FeS Cluster Involvement in Generation of a Radical in Lysine 2,3-Aminomutase, *Biochemistry 39*, 15668-15673.

32. Padmakumar, R., and Banerjee, R. (1997) Evidence that cobalt-carbon bond homolysis is coupled to hydrogen atom abstraction from substrate in methylmalonyl-CoA mutase, *Biochemistry 36*, 3713-3718.

33. Marsh, E. N. G., and Ballou, D. P. (1998) Coupling of cobalt-carbon bond homolysis and hydrogen atom abstraction in adenosylcobalamin-dependent glutamate mutase, *Biochemistry 37*, 11864-11872.

34. Li Xia, D. P. B., E. Neil G. Marsh,. (2004) Role of Arg100 in the Active Site of Adenosylcobalamin-Dependent Glutamate Mutase, *Biochemistry 43*, 3238–3245.

35. Licht, S. S., Lawrence, C. C., and Stubbe, J. (1999) Thermodynamic and kinetic studies on cobalt-carbon bond homolysis by ribonucleotide triphosphate reductase: the importance of entropy in catalysis, *Biochemistry 34*, 1234-1242.

36. Chen, H. P., and Marsh, E. N. G. (1997) How enzymes control the reactivity of adenosylcobalamin: effect on coenzyme binding and catalysis of mutations in the conserved histidine- aspartate pair of glutamate mutase, *Biochemistry 36*, 7884-7889.

37. F.D.Saeva, B. P. M. (1984) Mechanism of one-electron electrochemical reductive cleavage reactions of sulfonium salts, *Journal of the American Chemical Society 106*, 4121–4125.

38. Glen T. Hinckley, P. A. F. (2006) Cofactor Dependence of Reduction Potentials for [4Fe-4S]2+/1+ in Lysine 2,3-Aminomutase, *Biochemistry 45*, 3219–3225.

39. Brooks, A. J., Fox, C. C., Marsh, E. N. G., Vlasie, M., Banerjee, R., and Brunold, T. C. (2005) Electronic structure studies of the adenosylcobalamin cofactor in glutamate mutase, *Biochemistry 44*, 15167-15181.

40. Chen, H. P., and Marsh, E. N. G. (1997) Adenosylcobalamin-dependent glutamate mutase: examination of substrate and coenzyme binding in an engineered fusion protein possessing simplified subunit structure and kinetic properties, *Biochemistry 36*, 14939-14945.

41. Dong, S. L., Padmakumar, R., Banerjee, R., and Spiro, T. G. (1999) Co-C bond activation in B-12-dependent enzymes: Cryogenic resonance Raman studies of methylmalonyl-coenzyme A mutase, *Journal of the American Chemical Society 121*, 7063-7070.

42. Huhta, M. S., Chen, H.-P., Hemann, C., Hille, C. R., and Marsh, E. N. G. (2001) Protein-Coenzyme interactions in adenosylcobalamin-dependent glutamate mutase, *Biochem. J. 355*, 131-137.

43. Frey, S. C. W. a. P. A. (2007) Binding Energy in the One-Electron Reductive Cleavage of S-Adenosylmethionine in Lysine 2,3-Aminomutase, a Radical SAM Enzyme, *Biochemistry 46*, 12889–12895.

44. Vey, J. L., and Drennan, C. L. (2011) Structural insights into radical generation by the radical SAM superfamily, *Chemical reviews 111*, 2487-2506.

45. Challand, M. R., Driesener, R. C., and Roach, P. L. (2011) Radical S-adenosylmethionine enzymes: mechanism, control and function, *Natural product reports 28*, 1696-1721.

46. Marsh, E. N. G. (2009) Insights into the mechanisms of adenosylcobalamin (coenzyme B-12)-dependent enzymes from rapid chemical quench experiments, *Biochemical Society Transactions 37*, 336-342.

47. Marsh, E. N. G. (2000) Coenzyme B12-dependent glutamate mutase, *Bioorganic chemistry 28*, 176-189.

48. Duschene, K. S., Veneziano, S. E., Silver, S. C., and Broderick, J. B. (2009) Control of radical chemistry in the AdoMet radical enzymes., *Current Opinion in Chemical Biology 13*, 74-83.

49. Kuo-Hsiang Tang, C. H. C., Perry A. Frey. (2001) Electron Transfer in the Substrate-Dependent Suicide Inactivation of Lysine 5,6-Aminomutase, *Biochemistry 40*, 5190–5199.

50. Nicolas H. Thomä, P. R. E., Peter F. Leadlay. (2000) Protection of Radical Intermediates at the Active Site of Adenosylcobalamin-Dependent Methylmalonyl-CoA Mutase, *Biochemistry 39*, 9213–9221.

51. Imlay, J. A. (2006) Iron-sulphur clusters and the problem with oxygen, *Molecular Microbiology 59*, 1073–1082.

52. Banerjee, D. P. a. R. (2009) Coenzyme B12-Catalyzed Radical Isomerizations, *Tetrapyrroles: Birth, Life and Death*, 330-342.

53. Buckel, W., and Golding, B. T. (2006) Radical enzymes in anaerobes, *Annual Review of Microbiology 60*, 27-49.

54. Gruber, K., and Kratky, C. (2002) Coenzyme B-12 dependent glutamate mutase, *Current Opinion in Chemical Biology 6*, 598-603.

55. Zerbe-Burkhardt, K., Ratnatilleke, A., Philippon, N., Birch, A., Leiser, A., Vrijbloed, J. W., Hess, D., Hunziker, P., and Robinson, J. A. (1998) Cloning, sequencing, expression, and insertional inactivation of the gene for the large subunit of the coenzyme B-12- dependent isobutyryl-CoA mutase from Streptomyces cinnamonensis, *Journal of Biological Chemistry 273*, 6508-6517.

56. Rohwerder, T., Breuer, U., Benndorf, D., Lechner, U., and Muller, R. H. (2006) The alkyl tert-butyl ether intermediate 2-hydroxyisobutyrate is degraded via a novel cobalamin-dependent mutase pathway, *Appl. Environ. Microbiol. 72*, 4128-4135.

57. Erb, T. J., Retey, J., Fuchs, G., and Alber, B. E. (2008) Ethylmalonyl-CoA Mutase from Rhodobacter sphaeroides Defines a New Subclade of Coenzyme B-12-dependent Acyl-CoA Mutases, *Journal of Biological Chemistry 283*, 32283-32293.

58. He, M., and Dowd, P. (1998) Mechanism of action of vitamin B-12. Ultrafast radical clocks provide no evidence for radical intermediates in cyclopropane models for the methylmalonyl-CoA to succinyl-CoA carbon skeleton rearrangement, *Journal of the American Chemical Society 120*, 1133-1137.

59. Susan Ashwell, A. G. D., Bernard T. Golding, Robyn Hay-Motherwell and Samson Mwesigye-Kibende. (1989) Model experiments pertaining to the mechanism of action of vitamin B12-dependent α-methyleneglutarate mutase, *J. Chem. Soc. Chem. Commun.*, 1483–1485.

60. Chih, H.-W., and Marsh, E. N. G. (2000) Mechanism of glutamate mutase: identification and kinetic competence of acrylate and glycyl radical as intermediates in the rearrangment of glutamate to methylaspartate, *J. Am. Chem. Soc. 122*, 10732-10733.

61. Rommel, J. B., and Kaestner, J. (2011) The Fragmentation-Recombination Mechanism of the Enzyme Glutamate Mutase Studied by QM/MM Simulations, *Journal of the American Chemical Society 133*, 10195-10203.

62. Bothe, H., Darley, D. J., Albracht, S. P., Gerfen, G. J., Golding, B. T., and Buckel, W. (1998) Identification of the 4-glutamyl radical as an intermediate in the carbon skeleton rearrangement catalyzed by coenzyme B12-dependent glutamate mutase from Clostridium cochlearium, *Biochemistry 37*, 4105-4113.

63. Toraya, T. (2003) Radical catalysis in coenzyme B-12-dependent isomerization (eliminating) reactions, *Chemical Reviews 103*, 2095-2127.

64. Sandala, G. M., Smith, D. M., Coote, M. L., Golding, B. T., and Radom, L. (2006) Insights into the hydrogen-abstraction reactions of diol dehydratase: Relevance to the catalytic mechanism and suicide inactivation, *Journal of the American Chemical Society 128*, 3433-3444.

65. Wetmore, S. D., Smith, D. M., Bennett, J. T., and Radom, L. (2002) Understanding the mechanism of action of B12-dependent ethanolamine ammonia-lyase: synergistic interactions at play, *Journal of the American Chemical Society 124*, 14054-14065.

66. Toraya, T., Honda, S., and Mori, K. (2010) Coenzyme B-12-Dependent Diol Dehydratase Is a Potassium Ion-Requiring Calcium Metalloenzyme: Evidence That the Substrate-Coordinated Metal Ion Is Calcium, *Biochemistry 49*, 7210-7217.

67. Stubbe, J. (2003) Radicals with a controlled lifestyle, *Chemical Communications*, 2511-2513.

68. Reichard, P. (2002) Ribonucleotide reductases: The evolution of allosteric regulation, *Archives of Biochemistry and Biophysics 397*, 149-155.

69. Wolthers, K. R., Rigby, S. E. J., and Scrutton, N. S. (2008) Mechanism of Radical-based Catalysis in the Reaction Catalyzed by Adenosylcobalamin-dependent Ornithine 4,5-Aminomutase, *Journal of Biological Chemistry 283*, 34615-34625.

70. Chen, H. P., Hsui, F. C., Lin, L. Y., Ren, C. T., and Wu, S. H. (2004) Coexpression, purification and characterization of the E and S subunits of coenzyme B-12 and B-6 dependent Clostridium sticklandii D-ornithine aminomutase in Escherichia coli, *European Journal of Biochemistry 271*, 4293-4297.

71. Berkovitch, F., Behshad, E., Tang, K. H., Enns, E. A., Frey, P. A., and Drennan, C. L. (2004) Locking mechanism preventing radical damage in the absence of substrate as revealed by the x-ray structure of lysine 5,6-aminomutase, *Proceedings of the National Academy of Sciences of the United States of America 101*, 15870-15875.

72. Tang, K. H., Mansoorabadi, S. O., Reed, G. H., and Frey, P. A. (2009) Radical Triplets and Suicide Inhibition in Reactions of 4-Thia-D- and 4-Thia-L-lysine with Lysine 5,6-Aminomutase, *Biochemistry 48*, 8151-8160.

73. Ballinger, M. D., Reed, G. H., and Frey, P. A. (1992) An organic radical in the lysine 2,3-aminomutase reaction, *Biochemistry 31*, 949-953.

74. W.M. Wu, S. B., K.W. Lieder, V. Bandarian, G.H. Reed, P.A. Frey,. (2000) Lysine 2,3-aminomutase and trans-4,5-dehydrolysine: characterization of an allylic analogue of a substrate-based radical in the catalytic mechanism, *Biochemistry 39*, 9561–9570.

75. W.M. Wu, K. W. L., G.H. Reed, P.A. Frey. (1995) Observation of a second substrate radical intermediate in the reaction of lysine 2,3-aminomutase—a radical centered on the beta-carbon of the alternative substrate, 4-thia-L-lysine,, *Biochemistry 34*, 10532–10537.

76. K.H. Tang, A. H., P.A. Frey,. (2002) Identification of a novel pyridoxal 5′-phosphate binding site in adenosylcobalamin-dependent lysine 5,6-aminomutase from Porphyromonas gingivalis, *Biochemistry 41*, 8767–8776.

77. Chirpich, T. P., Zappia, V., Costilow, R. N., and Barker, H. A. (1970) Lysine 2,3-aminomutase. Purification and properties of a pyridoxal phosphate and S-adenosylmethionine-activated enzyme., *J. Biol. Chem. 245*, 1778−1789.

78. Unkrig, V., Neugebauer, F. A., and Knappe, J. (1989) The free radical of pyruvate formate-lyase. Characterization by EPR spectroscopy and involvement in catalysis as studied with the substrate-analogue hypophosphite, *European journal of biochemistry / FEBS 184*, 723-728.

79. Atta, M., Mulliez, E., Arragain, S., Forouhar, F., Hunt, J. F., and Fontecave, M. (2010) S-Adenosylmethionine-dependent radical-based modification of biological macromolecules., *Current Opinion in Chemical Biology 20*, 684−692.

80. Lanz, N. D., and Booker, S. J. . (2012) Identification and function of auxiliary iron-sulfur clusters in radical SAM enzymes., *Biochim. Biophys. Acta, Proteins Proteomics 1824*, 1196−1212.

81. Esberg, B., Leung, H. C., Tsui, H. C., Bjork, G. R., and Winkler, M. E. (1999) Identification of the miaB gene, involved in methylthiolation of isopentenylated A37 derivatives in the tRNA of Salmonella typhimurium and Escherichia coli, *Journal of bacteriology 181*, 7256-7265.

82. Lei Li, D. P. P., Christel C. Fox, Brian Lin, Peter W. Coschigano, E. Neil G. Marsh. (2009) Subunit Structure of Benzylsuccinate Synthase, *Biochemistry 48*, 1284–1292.

83. L. Li, E. N. G. M. (2006) Mechanism of Benzylsuccinate Synthase Probed by Substrate and Isotope Exchange, *Journal of the American Chemical Society 128*, 16056 – 16057.

84. C. J. Krieger, W. R., S. P. J. Albracht, A. M. Spormann,. (2001) A Stable Organic Free Radical in Anaerobic Benzylsuccinate Synthase of Azoarcus sp. Strain T, *Journal of Biological Chemistry 276*, 12924–12927.

85. B. Leuthner, J. H. (1998) A two-component system involved in regulation of anaerobic toluene metabolism in Thauera aromatica, *FEMS Microbiol. Lett. 166*, 35–41.

86. Leuthner B, L. C., Schulz H, Hörth P, Haehnel W, Schiltz E, Schägger H, Heider J. (1998) Biochemical and genetic characterization of benzylsuccinate synthase from Thauera aromatica: a new glycyl radical enzyme catalysing the first step in anaerobic toluene metabolism, *Molecular Microbiology 28*, 615-628.

87. Ollagnier, S., Schmidt, P., Atta, M., and Mulliez, E. (1996) The free radical of the anaerobic ribonucleotide reductase from Escherichia coli is at glycine 681, *Journal of Biological Chemistry 271*, 6827–6831.

88. Himo, F. (2002) Catalytic mechanism of benzylsuccinate synthase, a theoretical study, *Journal of Physical Chemistry B 106*, 7688-7692.

89. Thorsten Selmer, A. J. P., Johann Heider. (2005) New glycyl radical enzymes catalysing key metabolic steps in anaerobic bacteria, *Biological Chemistry 386*, 981-988.

90. Eklund, H., and Fontecave, M. (1999) Glycyl radical enzymes: a conservative structural basis for radicals, *Structure 7*, R257-R262.

91. Himo, F. (2000) Stability of protein-bound glycyl radical: a density functional theory study, *Chemical Physics Letters 328* 270-276.

92. Selmer, T., Pierik, A. J., and Heider, J. (2005) New glycyl radical enzymes catalysing key metabolic steps in anaerobic bacteria., *Biological chemistry 386*, 981-988.

93. Duboc-Toia, C., Hassan, A. K., Mulliez, E., Ollagnier-de Choudens, S., Fontecave, M., Leutwein, C., and Heider, J. (2003) Very high-field EPR study of glycyl radical enzymes., *Journal of the American Chemical Society 125*, 38-39.

94. Parast, C. V., Wong, K. K., Lewisch, S. A., Kozarich, J. W., Peisach, J., and Magliozzo, R. S. (1995) Hydrogen exchange of the glycyl radical of pyruvate formate-lyase is catalyzed by cysteine 419., *Biochemistry 34*, 2393-2399.

95. Himo, F., and Eriksson, L. (1998) Catalytic mechanism of pyruvate formate-lyase (PFL). A theoretical study, *Journal of the American Chemical Society 120*, 11449-11455.

96. Wagner, A. F., Frey, M., Neugebauer, F. A., Schäfer, W., and Knappe, J. (1992) The free radical in pyruvate formate-lyase is located on glycine-734., *Proceedings of the National Academy of Sciences of the United States of America 89*, 996-1000.

97. Joachim Knappe, A. F. V. W. (2001) Stable glycyl radical from pyruvate formate-lyase and ribonucleotide reductase (III), *Advances in Protein Chemistry 58*, 277-315.

98. Serge Gambarelli, F. L., Dominique Padovani, Etienne Mulliez, Marc Fontecave. (2005) Activation of the Anaerobic Ribonucleotide Reductase by S-Adenosylmethionine, *Chembiochem 6*, 1960–1962.

99. Florence Luttringer, E. M., Bernard Dublet, David Lemaire, Marc Fontecave. (2009) The Zn center of the anaerobic ribonucleotide reductase from E. coli, *Journal of Biological Inorganic Chemistry 14*, 923-933.

100. Mikolaj Feliks, B. M. M., G. Matthias Ullmann. (2013) Catalytic Mechanism of the Glycyl Radical Enzyme 4-Hydroxyphenylacetate Decarboxylase from Continuum Electrostatic and QC/MM Calculations, *Journal of the American Chemical Society 135*, 14574–14585.

101. Selmer T, A. P. (2001) p-Hydroxyphenylacetate decarboxylase from Clostridium difficile. A novel glycyl radical enzyme catalysing the formation of p-cresol., *European journal of biochemistry / FEBS 268*, 1363-1372.

102. L. Lehtio, J. G. G., B. Kokona, R. Fairman, A. Goldman, . (2006) Crystal Structure of a Glycyl Radical Enzyme from Archaeoglobus fulgidus, *Journal of Molecular Biology 357*, 221 – 235.

103. J. R. O'Brien, C. R., C. Croux, L. Girbal, P. Soucaille, W. N. Lanzilot-Taga, M. E. (2004) Insight into the Mechanism of the B12-Independent Glycerol Dehydratase

from Clostridium butyricum: Preliminary Biochemical and Structural Characterization, *Biochemistry 43*, 4635–4645.

104. Marsh, E. N. G., Patwardhan, A., and Huhta, M. S. (2004) S-adenosylmethionine radical enzymes., *Bioorganic Chemistry 32*, 326-340.

105. Henshaw, T., and Cheek, J. (2000) The [4Fe-4S] 1+ cluster of pyruvate formate-lyase activating enzyme generates the glycyl radical on pyruvate formate-lyase: EPR-detected single turnover, *Journal of the American Chemical Society*, 8331-8332.

106. Broderick, J., and Duderstadt, R. (1997) Pyruvate formate-lyase activating enzyme is an iron-sulfur protein, *Journal of the American Chemical Society 119*, 7396-7397.

107. Buis, J. M., and Broderick, J. B. (2005) Pyruvate formate-lyase activating enzyme: elucidation of a novel mechanism for glycyl radical formation., *Archives of Biochemistry and Biophysics 433*, 288-296.

108. Walsby, C., Ortillo, D., Broderick, W., Broderick, J., and Hoffman, B. (2002) An anchoring role for FeS clusters: Chelation of the amino acid moiety of S-adenosylmethionine to the unique iron site of the [4Fe-4S] cluster of pyruvate formate-lyase activating enzyme, *Journal of the American Chemical Society 124*, 11270-11271.

109. Roach, P. L. (2010) Radicals from S-adenosylmethionine and their application to biosynthesis., *Current Opinion in Chemical Biology 15*, 1-9.

110. Krebs, C., Broderick, W. E., Henshaw, T. F., Broderick, J. B., and Huynh, B. H. (2002) Coordination of adenosylmethionine to a unique iron site of the [4Fe-4S] of pyruvate formate-lyase activating enzyme: a Mössbauer spectroscopic study., *Journal of the American Chemical Society 124*, 912-913.

111. Walsby, C., Hong, W., Broderick, W., Cheek, J., Ortillo, D., Broderick, J., and Hoffman, B. (2002) Electron-nuclear double resonance spectroscopic evidence that S-adenosylmethionine binds in contact with the catalytically active [4Fe-4S](+) cluster of pyruvate formate-lyase activating enzyme, *Journal of the American Chemical Society 124*, 3143-3151.

112. Grove, T. L., Radle, M. I., Krebs, C., and Booker, S. J. (2011) Cfr and RlmN Contain a Single [4Fe-4S] Cluster, which Directs Two Distinct Reactivities for S-Adenosylmethionine: Methyl Transfer by S(N)2 Displacement and Radical Generation, *Journal of the American Chemical Society 133*, 19586-19589.

113. Benitez-Paez, A., Villarroya, M., and Armengod, M. E. (2012) The Escherichia coli RlmN methyltransferase is a dual-specificity enzyme that modifies both rRNA and tRNA and controls translational accuracy, *Rna-a Publication of the Rna Society 18*, 1783-1795.

114. Grove, T. L., Benner, J. S., Radle, M. I., Ahlum, J. H., Landgraf, B. J., Krebs, C., and Booker, S. J. (2011) A Radically Different Mechanism for S-Adenosylmethionine-Dependent Methyltransferases, *Science 332*, 604-607.

115. McCusker, K. P., Medzihradszky, K. F., Shiver, A. L., Nichols, R. J., Yan, F., Maltby, D. A., Gross, C. A., and Fujimori, D. G. (2012) Covalent Intermediate in the Catalytic Mechanism of the Radical S-Adenosyl-L-methionine Methyl Synthase RlmN Trapped by Mutagenesis, *Journal of the American Chemical Society 134*, 18074-18081.

116. Landgraf, B. J., Arcinas, A. J., Lee, K. H., and Booker, S. J. (2013) Identification of an intermediate methyl carrier in the radical S-adenosylmethionine methylthiotransferases RimO and MiaB, *Journal of the American Chemical Society 135*, 15404-15416.

117. Leipuviene, R., Qian, Q., and Bjork, G. R. (2004) Formation of thiolated nucleosides present in tRNA from Salmonella enterica serovar Typhimurium occurs in two principally distinct pathways, *Journal of bacteriology 186*, 758-766.

118. Agris, P. F. (1996) The importance of being modified: roles of modified nucleosides and Mg2+ in RNA structure and function, *Progress in nucleic acid research and molecular biology 53*, 79-129.

119. Urbonavicius, J., Qian, Q., Durand, J. M., Hagervall, T. G., and Bjork, G. R. (2001) Improvement of reading frame maintenance is a common function for several tRNA modifications, *The EMBO journal 20*, 4863-4873.

120. Pierrel, F., Bjork, G. R., Fontecave, M., and Atta, M. (2002) Enzymatic modification of tRNAs: MiaB is an iron-sulfur protein, *The Journal of biological chemistry 277*, 13367-13370.

121. Hernandez, H. L., Pierrel, F., Elleingand, E., Garcia-Serres, R., Huynh, B. H., Johnson, M. K., Fontecave, M., and Atta, M. (2007) MiaB, a bifunctional radical-S-adenosylmethionine enzyme involved in the thiolation and methylation of tRNA, contains two essential [4Fe-4S] clusters, *Biochemistry 46*, 5140-5147.

122. Pierrel, F., Douki, T., Fontecave, M., and Atta, M. (2004) MiaB protein is a bifunctional radical-S-adenosylmethionine enzyme involved in thiolation and methylation of tRNA, *The Journal of biological chemistry 279*, 47555-47563.

123. Anton, B. P., Saleh, L., Benner, J. S., Raleigh, E. A., Kasif, S., and Roberts, R. J. (2008) RimO, a MiaB-like enzyme, methylthiolates the universally conserved Asp88 residue of ribosomal protein S12 in Escherichia coli, *Proceedings of the National Academy of Sciences of the United States of America 105*, 1826-1831.

124. Lee, K. H., Saleh, L., Anton, B. P., Madinger, C. L., Benner, J. S., Iwig, D. F., Roberts, R. J., Krebs, C., and Booker, S. J. (2009) Characterization of RimO, a new member of the methylthiotransferase subclass of the radical SAM superfamily, *Biochemistry 48*, 10162-10174.

125. Arragain, S., Handelman, S. K., Forouhar, F., Wei, F. Y., Tomizawa, K., Hunt, J. F., Douki, T., Fontecave, M., Mulliez, E., and Atta, M. (2010) Identification of eukaryotic and prokaryotic methylthiotransferase for biosynthesis of 2-methylthio-N6-threonylcarbamoyladenosine in tRNA, *The Journal of biological chemistry 285*, 28425-28433.

126. Kowalak, J. A., and Walsh, K. A. (1996) Beta-methylthio-aspartic acid: identification of a novel posttranslational modification in ribosomal protein S12 from Escherichia coli, *Protein science : a publication of the Protein Society 5*, 1625-1632.

127. Atta, M., Arragain, S., Fontecave, M., Mulliez, E., Hunt, J. F., Luff, J. D., and Forouhar, F. (2012) The methylthiolation reaction mediated by the Radical-SAM enzymes, *Biochimica et biophysica acta 1824*, 1223-1230.

128. Young, A. P., and Bandarian, V. (2013) Radical mediated ring formation in the biosynthesis of the hypermodified tRNA base wybutosine, *Current Opinion in Chemical Biology 17*, 613-618.

129. Suzuki, Y., Noma, A., Suzuki, T., Senda, M., Senda, T., Ishitani, R., and Nureki, O. (2007) Crystal structure of the radical SAM enzyme catalyzing tricyclic modified base formation in tRNA, *Journal of Molecular Biology 372*, 1204-1214.

130. Young AP, B. V. (2011) Pyruvate is the source of the two carbons that are required for formation of the imidazoline ring of the 4-demethylwyosine, *Biochemistry 50*, 10573-10575.

131. Perche-Letuvée, P., Kathirvelu, V., Berggren, G., Clemancey, M., Latour, J.-M., Maurel, V., Douki, T., Armengaud, J., Mulliez, E., Fontecave, M., Garcia-Serres, R., Gambarelli, S., and Atta, M. (2012) 4-Demethylwyosine Synthase from Pyrococcus abyssi Is a Radical-S-adenosyl-l-methionine Enzyme with an Additional [4Fe-4S]+2 Cluster That Interacts with the Pyruvate Co-substrate, *Journal of Biological Chemistry 287*, 41174-41185.

132. Mahanta, N., Fedoseyenko, D., Dairi, T., and Begley, T. P. (2013) Menaquinone Biosynthesis: Formation of Aminofutalosine Requires a Unique Radical SAM Enzyme, *Journal of the American Chemical Society 135*, 15318-15321.

133. Kuo, M. S., Yurek, D. A., Coats, J. H., and Li, G. P. (1989) Isolation and identification of 7,8-didemethyl-8-hydroxy-5-deazariboflavin, an unusual cosynthetic factor in streptomycetes, from Streptomyces lincolnensis, *Journal of Antibiotics 42*, 475-478.

134. Decamps, L., Philmus, B., Benjdia, A., White, R., Begley, T. P., and Berteau, O. (2012) Biosynthesis of F-0, Precursor of the F-420 Cofactor, Requires a Unique Two Radical-SAM Domain Enzyme and Tyrosine as Substrate, *Journal of the American Chemical Society 134*, 18173-18176.

135. Mulder, D. W., Boyd, E. S., Sarma, R., Lange, R. K., Endrizzi, J. A., Broderick, J. B., and Peters, J. W. (2010) Stepwise FeFe -hydrogenase H-cluster assembly revealed in the structure of HydA(Delta EFG), *Nature 465*, 248-U143.

136. Driesener, R. C., Duffus, B. R., Shepard, E. M., Bruzas, I. R., Duschene, K. S., Coleman, N. J. R., Marrison, A. P. G., Salvadori, E., Kay, C. W. M., Peters, J. W., Broderick, J. B., and Roach, P. L. (2013) Biochemical and Kinetic Characterization of Radical S-Adenosyl-L-methionine Enzyme HydG, *Biochemistry 52*, 8696-8707.

137. Kuchenreuther, J. M., Myers, W. K., Stich, T. A., George, S. J., NejatyJahromy, Y., Swartz, J. R., and Britt, R. D. (2013) A Radical Intermediate in Tyrosine Scission to the CO and CN- Ligands of FeFe Hydrogenase, *Science 342*, 472-475.

138. Nicolet, Y., Martin, L., Tron, C., and Fontecilla-Camps, J. C. (2010) A glycyl free radical as the precursor in the synthesis of carbon monoxide and cyanide by the FeFe -hydrogenase maturase HydG, *Febs Letters 584*, 4197-4202.

139. Kuchenreuther, J. M., Myers, W. K., Suess, D. L. M., Stich, T. A., Pelmenschikov, V., Shiigi, S. A., Cramer, S. P., Swartz, J. R., Britt, R. D., and George, S. J. (2014) The HydG Enzyme Generates an Fe(CO)(2)(CN) Synthon in Assembly of the FeFe Hydrogenase H-Cluster, *Science 343*, 424-427.

140. Benjdia, A., Heil, K., Barends, T. R., Carell, T., and Schlichting, I. (2012) Structural insights into recognition and repair of UV-DNA damage by Spore Photoproduct Lyase, a radical SAM enzyme, *Nucleic acids research 40*, 9308-9318.

141. Yang, L., Lin, G., Liu, D., Dria, K. J., Telser, J., and Li, L. (2011) Probing the reaction mechanism of spore photoproduct lyase (SPL) via diastereoselectively labeled dinucleotide SP TpT substrates, *Journal of the American Chemical Society 133*, 10434-10447.

142. Yang, L., Nelson, R. S., Benjdia, A., Lin, G., Telser, J., Stoll, S., Schlichting, I., and Li, L. (2013) A Radical Transfer Pathway in Spore Photoproduct Lyase, *Biochemistry 52*, 3041-3050.

143. Hanzelmann, P., and Schindelin, H. (2004) Crystal structure of the S-adenosylmethionine-dependent enzyme MoaA and its implications for molybdenum cofactor deficiency in humans, *Proceedings of the National Academy of Sciences of the United States of America 101*, 12870-12875.

144. Hanzelmann, P., Schwarz, G., and Mendel, R. R. (2002) Functionality of alternative splice forms of the first enzymes involved in human molybdenum cofactor biosynthesis, *The Journal of biological chemistry 277*, 18303-18312.

145. Hanzelmann, P., and Schindelin, H. (2006) Binding of 5'-GTP to the C-terminal FeS cluster of the radical S-adenosylmethionine enzyme MoaA provides insights into its mechanism, *Proceedings of the National Academy of Sciences of the United States of America 103*, 6829-6834.

146. Hover, B. M., Loksztejn, A., Ribeiro, A. A., and Yokoyama, K. (2013) Identification of a Cyclic Nucleotide as a Cryptic Intermediate in Molybdenum Cofactor Biosynthesis, *Journal of the American Chemical Society 135*, 7019-7032.

147. Mehta, A. P., Hanes, J. W., Abdelwahed, S. H., Hilmey, D. G., Hanzelmann, P., and Begley, T. P. (2013) Catalysis of a New Ribose Carbon-Insertion Reaction by the Molybdenum Cofactor Biosynthetic Enzyme MoaA, *Biochemistry 52*, 1134-1136.

148. Mehta, A. P., Abdelwahed, S. H., and Begley, T. P. (2013) Molybdopterin Biosynthesis: Trapping an Unusual Purine Ribose Adduct in the MoaA-Catalyzed Reaction, *Journal of the American Chemical Society 135*, 10883-10885.

149. Warncke, K. (2005) Characterization of the product radical structure in the Co-II-product radical pair state of coenzyme B-12-dependent ethanolamine deaminase by using three-pulse H-2 ESEEM spectroscopy, *Biochemistry 44*, 3184-3193.

150. Bender, G., Poyner, R. R., and Reed, G. H. (2008) Identification of the Substrate Radical Intermediate Derived from Ethanolamine during Catalysis by Ethanolamine Ammonia-Lyase, *Biochemistry 47*, 11360-11366.

151. Mansoorabadi, S. O., Padmakumar, R., Fazliddinova, N., Vlasie, M., Banerjee, R., and Reed, G. H. (2005) Characterization of a succinyl-CoA radical-cob(II)alamin spin triplet intermediate in the reaction catalyzed by adenosylcobalamin-dependent methylmalonyl-CoA mutase, *Biochemistry 44*, 3153-3158.

152. Yoon, M., Patwardhan, A., Qiao, C. H., Mansoorabadi, S. O., Menefee, A. L., Reed, G. H., and Marsh, E. N. G. (2006) Reaction of adenosylcobalamin-dependent glutamate mutase with 2-thiolglutarate, *Biochemistry 45*, 11650-11657.

153. Chowdhury, S., and Banerjee, R. (2000) Evidence for quantum mechanical tunneling in the coupled cobalt-carbon bond homolysis-substrate radical generation reaction catalyzed by methylmalonyl-CoA mutase, *Journal of the American Chemical Society 122*, 5417-5418.

154. Bandarian, V., and Reed, G. H. (2000) Isotope effects in the transient phases of the reaction catalyzed by ethanolamine ammonia-lyase: Determination of the number of exchangeable hydrogens in the enzyme-cofactor complex, *Biochemistry 39*, 12069-12075.

155. Li X, Chung LW, Paneth P, and K., M. (2009) DFT and ONIOM(DFT:MM) studies on Co-C bond cleavage and hydrogen transfer in B12-dependent methylmalonyl-CoA mutase. Stepwise or concerted mechanism?, *Journal of the American Chemical Society 131*, 5115-5125.

156. Schepler KL, D. W., Sands RH, Fee JA, Abeles RH. (1975) A physical explanation of the EPR spectrum observed during catalysis by enzymes utilizing coenzyme B12, *Biochimica et biophysica acta 397*, 510-518.

157. Buettner GR, C. R. (1977) EPR determination of the Co(II)-free radical magnetic geometry of the “doubleT” species arising in a coenzyme B-12-enzyme reaction, *Biochim. Biophys. Acta 480*, 495–505.

158. Licht S, G. G., Stubbe J. (1996) Thiyl radicals in ribonucleotide reductases, *Science 271*, 477-481.

159. Michel C, A. S., Buckel W. (1992) Adenosylcobalamin and cob(II)alamin as prosthetic groups of 2-methyleneglutarate mutase from Clostridium barkeri, *European journal of biochemistry / FEBS 205*, 767-773.

160. Zelder O, B. W. (1993) On the role of two different cobalt(II) species in coenzyme B12-dependent 2-methyleneglutarate mutase from Clostridium barker, *Biol. Chem. Hoppe-Seyler 374*, 85–90.

161. Zhao Y, A. A., Kunz M, Such P, Retey J. . (1994) Electron Paramagnetic Resonance Studies of the Methylmalonyl-CoA Mutase Reaction - Evidence for Radical Intermediates using Natural and Artificial Substrates as well as the Competitive Inhibitor 3-Carboxypropyl-CoA, *European journal of biochemistry / FEBS 225*, 891–896.

162. Padmakumar R, B. R. (1995) Evidence from Electron Paramagnetic Resonance Spectroscopy of the Participation of Radical Intermediates in the Reaction Catalyzed by Methylmalonyl-coenzyme A Mutase, *The Journal of biological chemistry 270*, 9295–9300.

163. Gerfen GJ, L. S., Willems J-P, Hoffman BM, Stubbe J. . (1996) Electron paramagnetic resonance investigations of a kinetically competent intermediate formed in ribonucleotide reduction: Evidence for a thiyl radical-Cob(II)alamin interaction, *J. Am. Chem. Soc. 118*, 8192–8197.

164. Mancia, F., Keep, N. H., Nakagawa, A., Leadlay, P. F., McSweeney, S., Rasmussen, B., Bosecke, P., Diat, O., and Evans, P. R. (1996) How coenzyme B12 radicals are generated: the crystal structure of methylmalonyl-coenzyme A mutase at 2 A resolution, *Structure 4*, 339-350.

165. Reitzer, R., Gruber, K., Jogl, G., Wagner, U. G., Bothe, H., Buckel, W., and Kratky, C. (1999) Structure of coenzyme B_{12} dependent enzyme glutamate mutase from *Clostridium cochlearium*, *Structure 7*, 891-902.

166. Masuda, J., Shibata, N., Morimoto, Y., Toraya, T., and Yasuoka, N. (2000) How a protein generates a catalytic radical from coenzyme B-12: X-ray structure of a diol-dehydratase-adeninylpentylcobalamin complex, *Struct. Fold. Des. 8*, 775-788.

167. Shibata, N., Tamagaki, H., Hieda, N., Akita, K., Komori, H., Shomura, Y., Terawaki, S., Mori, K., Yasuoka, N., Higuchi, Y., and Toraya, T. (2010) Crystal Structures of Ethanolamine Ammonia-lyase Complexed with Coenzyme B-12 Analogs and Substrates, *Journal of Biological Chemistry 285*, 26484-26493.

168. M. Yamanishi, M. Y., T. Tobimatsu, H. Sato, J. Matsui, A. Dokiya, Y. Iuchi, K. Oe, K. Suto, N. Shibata, Y. Morimoto, N. Yasuoka, T. Toraya, . (2002) The crystal structure of coenzyme B12-dependent glycerol dehydratase in complex with cobalamin and propane-1,2-diol, *European Journal of Biochemistry 269*, 4484–4494.

169. Chen, D. W., Abend, A., Stubbe, J., and Frey, P. A. (2003) Epimerization at carbon-5 ' of (5 ' R)-[5 ',H-2]adenosylcobalamin by ribonucleoside triphosphate reductase: Cysteine 408-independent cleavage of the Co-C5 ' bond, *Biochemistry 42*, 4578-4584.

170. Jones, A. R., Woodward, J. R., and Scrutton, N. S. (2009) Continuous Wave Photolysis Magnetic Field Effect Investigations with Free and Protein-Bound Alkylcobalamins, *Journal of the American Chemical Society 131*, 17246-17253.

171. Jones, A. R., Hay, S., Woodward, J. R., and Scrutton, N. S. (2007) Magnetic field effect studies indicate reduced geminate recombination of the radical pair in substrate-bound adenosylcobalamin-dependent ethanolamine ammonia lyase, *Journal of the American Chemical Society 129*, 15718-15727.

172. Grissom, C., and Natarjan, E. (1997) Use of Magnetic Field Effects to Study Coenzyme B12-Dependent Reactions, *Methods in Enzymology 281*, 235-247.

173. Grissom, C. B. (1995) Magnetic Field Effects in Biology: A Survey of Possible Mechanisms with Emphasis on Radical-Pair Recombination, *Chemical reviews 95*, 3-24.

174. Harkins, T., and Grissom, C. (1994) Magnetic field effects on B12 ethanolamine ammonia lyase: evidence for a radical mechanism, *Science 263*, 958-960.

175. Yoon, M., Kalli, A., Lee, H. Y., Hakansson, K., and Marsh, E. N. G. (2007) Intrinsic deuterium kinetic isotope effects in glutamate mutase measured by an intramolecular competition experiment, *Angewandte Chemie-International Edition 46*, 8455-8459.

176. Yoon, M., Song, H. T., Hakansson, K., and Marsh, E. N. G. (2010) Hydrogen Tunneling in Adenosylcobalamin-Dependent Glutamate Mutase: Evidence from Intrinsic Kinetic Isotope Effects Measured by Intramolecular Competition, *Biochemistry 49*, 3168-3173.

177. Doll, K. M., Bender, B. R., and Finke, R. G. (2003) The first experimental test of the hypothesis that enzymes have evolved to enhance hydrogen tunneling, *J. Am. Chem. Soc. 125*, 10877-10884.

178. Doll, K. M., and Finke, R. G. (2003) A Compelling Experimental Test of the Hypothesis That Enzymes Have Evolved To Enhance Quantum Mechanical Tunneling in Hydrogen Transfer Reactions: The Neopentylcobalamin System Combined with Prior Adocobalamin Data, *Inorg. Chem. 42*, 4849-4856.

179. Dybala-Defratyka, A., Paneth, P., Banerjee, R., and Truhlar, D. G. (2007) Coupling of hydrogenic tunneling to active-site motion in the hydrogen radical transfer catalyzed by a coenzyme B-12-dependent mutase, *Proceedings of the National Academy of Sciences of the United States of America 104*, 10774-10779.

180. Kohen, A. (2003) Kinetic isotope effects as probes for hydrogen tunneling, coupled motion and dynamics contributions to enzyme catalysis, *Progress in Reaction Kinetics and Mechanism 28*, 119-156.

181. Nagel, Z. D., and Klinman, J. P. (2006) Tunneling and dynamics in enzymatic hydride transfer, *Chem. Rev. 106*, 3095-3118.

182. Schramm, V. L. (2001) Transition state variation in enzymatic reactions, *Current Opinion in Chemical Biology 5*, 556-563.

183. Cheng, M.-C., and Marsh, E. N. G. (2005) Isotope effects for deuterium transfer between substrate and coenzyme in adenosylcobalamin-dependent glutatmate mutase, *Biochemistry 44*, 2686-2691.

184. Cheng, M.-C., and Marsh, E. N. G. (2004) Pre-steady state measurement of intrinsic secondary tritium isotope effects associated with the homolysis of adenosylcobalamin and the formation of 5'-deoxyadensosine in glutamate mutase, *Biochemistry 43*, 2155-2158.

185. Cheng, M. C., and Marsh, E. N. G. (2007) Evidence for coupled motion and hydrogen tunneling of the reaction catalyzed by glutamate mutase, *Biochemistry 46*, 883-889.

186. Huskey, W. P., and Schowen, R. L. (1983) Reaction Coordinate tunneling in hydride transfer reactions, *J. Am. Chem. Soc. 105*, 5704-5704.

187. Brooks, A. J., Vlasie, M., Banerjee, R., and Brunold, T. C. (2004) Spectroscopic and computational studies on the adenosylcobalamin-dependent methylmalonyl-CoA mutase: Evaluation of enzymatic contributions to Co-C bond activation in the Co3+ ground state, *Journal of the American Chemical Society 126*, 8167-8180.

188. Robertson, W. D., Wang, M., and Warncke, K. (2011) Characterization of Protein Contributions to Cobalt-Carbon Bond Cleavage Catalysis in Adenosylcobalamin-Dependent Ethanolamine Ammonia-Lyase by using Photolysis in the Ternary Complex, *Journal of the American Chemical Society 133*, 6968-6977.

189. Jensen, K. P., and Ryde, U. (2009) Cobalamins uncovered by modern electronic structure calculations, *Coordination Chemistry Reviews 253*, 769-778.

190. Sharma, P. K., Chu, Z. T., Olsson, M. H. M., and Warshel, A. (2007) A new paradigm for electrostatic catalysis of radical reactions in vitamin B-12 enzymes, *Proceedings of the National Academy of Sciences of the United States of America 104*, 9661-9666.

191. Jensen, K. P., and Ryde, U. (2005) How the Co-C bond is cleaved in coenzyme B-12 enzymes: A theoretical study, *Journal of the American Chemical Society 127*, 9117-9128.

192. Gruber, K., Reitzer, R., and Kratky, C. (2001) Radical shuttling in a protein: Ribose pseudorotation controls alkyl-radical transfer in the coenzyme B-12 dependent enzyme glutamate mutase, *Angewandte Chemie-International Edition 40*, 3377-+.

193. Chih, H.-W., and Marsh, E. N. G. (2001) Tritium partitioning and isotope effects in adenosylcobalamin-dependent glutamate mutase, *Biochemistry 40*, 13060-13067.

194. Madhavapeddi, P., and Marsh, E. N. G. (2001) The role of the active site glutamate in the rearrangement of glutamate to 3-methylaspartate catalyzed by adenosylcobalamin-dependent glutamate mutase, *Chem. Biol. 8*, 1143-1149.

195. Madhavapeddi, P., Ballou, D. P., and Marsh, E. N. G. (2002) Pre-Steady State Kinetic studies on the Gly171Gln Active Site Mutant of Adenosylcobalamin-dependent Glutamate Mutase, *Biochemistry 41*, 15802-15809.

196. Makins, C., Pickering, A. V., Mariani, C., and Wolthers, K. R. (2013) Mutagenesis of a Conserved Glutamate Reveals the Contribution of Electrostatic Energy to Adenosylcobalamin Co-C Bond Homolysis in Ornithine 4,5-Aminomutase and Methylmalonyl-CoA Mutase, *Biochemistry 52*, 878-888.

197. Barker H.A., R. V., Suzuki F., Iodice A.A. (1964) The Glutamate Mutase System. Assay And Properties, *Journal of Biological Chemistry 239*, 3260-3266.

198. Marsh, E. N. G. (1995) Tritium Isotope Effects in Adenosylcobalarnin-Dependent Glutamate Mutase: Implications for the Mechanism, *Biochemistry 34*, 7542-7547.

199. DESIRAJU, G. R. (1991) The C-H-O Hydrogen Bond in Crystals: What Is It?, *Accounts of Chemical Research 24*, 290-296.

200. Steiner, T. (2003) C-H-O Hydrogen Bonding in Crystals, *Crystallography Reviews 9*, 177-228.

201. Wolthers, K. R., Levy, C., Scrutton, N. S., and Leys, D. (2010) Large-scale Domain Dynamics and Adenosylcobalamin Reorientation Orchestrate Radical Catalysis in Ornithine 4,5-Aminomutase, *Journal of Biological Chemistry 285*, 13942-13950.

202. Banerjee R., R. S. W. (2003) The many faces of vitamin B12: catalysis by cobalamin-dependent enzymes, *Annual Review of Biochemistry 72*, 209–247.

203. Marsh, D. E. H. a. E. N. (1994) Adenosylcobalamin-dependent glutamate mutase from Clostridium tetanomorphum. Overexpression in Escherichia coli, purification, and characterization of the recombinant enzyme., *The Journal of biological chemistry 269*, 20425-20430.

204. Jeremy M Berg, J. L. T., Lubert Stryer. (2002) Free Energy Is a Useful Thermodynamic Function for Understanding Enzymes, *Biochemistry, 5th edition, W. H. Freeman & Company*, Section 8.2.

205. Stojkovic, V., Perissinotti, L. L., Willmer, D., Benkovic, S. J., and Kohen, A. (2012) Effects of the Donor-Acceptor Distance and Dynamics on Hydride Tunneling in the Dihydrofolate Reductase Catalyzed Reaction, *Journal of the American Chemical Society 134*, 1738-1745.

206. Donald Jung, M. M., and Donald Perrier. (1981) The “Ultra-Free” Ultrafiltration Technique Compared with Equilibrium Dialysis for Determination of Unbound Thiopental Concentrations in Serum, *Clinical Chemistry 27*, 166-168.

207. George K. Wolfer, J. a. W. B. R. (1987) Protocols for Use of Ultrafiltration in Determination of Free Ligand Concentration and of Complexity of Ligand/Protein Interactions, *Clinical Chemistry 33*, 115-117.

208. Ivan Y. Torshin, I. T. W. a. R. W. H. (2002) Geometric criteria of hydrogen bonds in proteins and identification of 'bifurcated' hydrogen bonds, *Protein Engineering 15*, 359-363.

209. Grissom, C. B. (1995) Magnetic field effects in biology: A survey of possible mechanisms with emphasis on radical-pair recombination., *Chemical Reviews 95*, 3-24.

210. Walleczek, J. (1995) Magnetokinetic effects on radical pairs: A paradigm for magnetic field interactions with biological systems at lower than thermal energy., *ACS Adv Chem Ser 250*, 395–420.

211. Brocklehurst B, and KA, M. (1996) Free radical mechanism for the effects of environmental electromagnetic fields in biological systems, *Int J Rad Biol 69*, 3–24.

212. Ulrich E. Steiner, and Ulrich, T. (1989) Magnetic field effects in chemical kinetics and related phenomena, *Chemical Reviews 89*, 51-147.

213. Chagovetz, A. M., and Grissom, C. B. (1993) Magnetic field effects in adenosylcob (III) alamin photolysis: relevance to B12 enzymes, *Journal of the American Chemical Society 115*, 12152–12157.

214. Brocklehurst, B. (2002) Magnetic fields and radical reactions: recent developments and their role in nature, *Chem. Soc. Rev. 31*, 301-311.

215. Khudyakov, I. V., Serebrennikov, Y. A., and Turro, N. J. (1993) Spin-orbit coupling in free-radical reactions: on the way to heavy elements, *Chemical reviews 93*, 537-570.

216. Turro, N. J. (1983) Influence of nuclear spin on chemical reactions: Magnetic isotope and magnetic field effects (A Review), *Proceedings of the National Academy of Sciences of the United States of America 80*, 609-621.

217. Turro, N. J., and Kraeutler, B. (1978) Magnetic isotope and magnetic field effects on chemical reactions. Sunlight and soap for the efficient separation of carbon-13 and carbon-12, *Journal of the American Chemical Society 23*, 7432–7434.

218. Charles B. Grissom, A. M. C. (1993) Magnetic Field Effects in Model B12 Enzymatic Reactions. The Photolysis of Methylcob(III)alamin, *Zeitschrift für Physikalische Chemie 1*, 181-188.

219. Turro, N. J., and Kraeutler, B. (1980) Magnetic field and magnetic isotope effects in organic photochemical reactions. A novel probe of reaction mechanisms and a method for enrichment of magnetic isotopes, *Accounts of Chemical Research 13*, 369–377.

220. Natarajan, E., and Grissom, C. B. (1996) The origin of magnetic field dependent recombination in alkylcobalamin radical pairs, *Photochemistry and Photobiology 64*, 286-295.

221. Taoka, S., Padmakumar, R., Grissom, C. B., and Banerjee, R. (1997) Magnetic field effects on coenzyme B12-dependent enzymes: Validation of ethanolamine ammonia lyase results and extension to human methylmalonyl CoA mutase, *Bioelectromagnetics 18*, 506-513.

222. Hore, P. J. (2012) Are biochemical reactions affected by weak magnetic fields?, *Proceedings of the National Academy of Sciences of the United States of America 109*, 1357-1358.

223. Harkins, T., and Grissom, C. B. (1995) The Magnetic Field Dependent Step in B12 Ethanolamine Ammonia Lyase Is Radical-Pair Recombination, *Journal of the American Chemical Society 117*, 566-567.

224. Taraban, M. B., Leshina, T. V., Anderson, M. A., and Grissom, C. B. (1997) Magnetic Field Dependence of Electron Transfer and the Role of Electron Spin in Heme Enzymes: Horseradish Peroxidase, *Journal of the American Chemical Society 119*, 5768-5769.

225. Harkins, T. T., and Grissom, C. B. (1995) The magnetic field dependent step in B12 ethanolamine ammonia lyase is radical-pair recombination, *Journal of the American Chemical Society 117*, 566-567.

226. Cleland, W. W. (1982) Use of Isotope Effects to Elucidate Enzyme Mechanisms, *CRC Critical Reviews in Biochemistry 13*, 385-428.

227. Bandarian V., and Reed, G. H. (2000) Isotope Effects in the Transient Phases of the Reaction Catalyzed by Ethanolamine Ammonia-Lyase: Determination of the Number of Exchangeable Hydrogens in the Enzyme-Cofactor Complex, *Biochemistry 39*, 12069-12075.

228. Marsh, E. N. G., and Holloway, D. E. (1992) Cloning and sequencing of glutamate mutase component S from Clostridium tetanomorphum. Homologies with other cobalamin-dependent enzymes, *FEBS Lett 310*, 167-170.

229. Reed, G. H., and Mansoorabadi, S. O. (2003) The positions of radical intermediates in the active sites of adenosylcobalamin-dependent enzymes, *Current Opinion in Chemical Biology 13*, 716-721.

230. Bandarian V, and GH., R. (2002) Analysis of the electron paramagnetic resonance spectrum of a radical intermediate in the coenzyme B12-dependent ethanolamine ammonia-lyase catalyzed reaction of S-2-aminopropanol, *Biochemistry 41*, 8580-8588.

231. Bandarian V, R. G. (1999) Hydrazine cation radical in the active site of ethanolamine ammonia-lyase: mechanism-based inactivation by hydroxyethylhydrazine, *Biochemistry 38*, 12394-12402.

232. Boas JF, H. P., Pilbrow JR, Smith TD. (1978) Interpretation of Electron Spin Resonance Spectra Due to Some B12-dependent Enzyme Reactions, *J Chem Soc Faraday Trans II 74*, 417–431.

233. SC, K. (2003) Spin-spin interaction in ethanolamine deaminase., *Biochimica et biophysica acta 1620*, 267-272.

234. Zelder O, B. B., Leutbecher U, Buckel W. (1994) Characterization of the coenzyme-B12-dependent glutamate mutase from Clostridium chochlearium produced in Escherichia coli., *European journal of biochemistry / FEBS 266*, 577-585.

235. Zhao Y, A. A., Kunz M, Such P, Retey J. (1994) Electron paramagnetic resonance studies of the methylmalonyl-CoA mutase reaction. Evidence for radical intermediates using natural and artificial substrates as well as the competitive inhibitor 3-carboxypropyl-CoA, *European journal of biochemistry / FEBS 225*, 891-896.

236. Reitzer R, G. K., Jogl G, Wagner UG, Bothe H, Buckel W, Kratky C. (1999) Glutamate mutase from Clostridium cochlearium: the structure of a coenzyme B12-dependent enzyme provides new mechanistic insights., *Structure Fold Des 7*, 891-902.

237. Bothe H, D. D., Albracht SP, Gerfen GJ, Golding BT, Buckel W. (1998) Identification of the 4-glutamyl radical as an intermediate in the carbon skeleton rearrangement catalyzed by coenzyme B-12-dependent glutamate mutase from Clostridium cochlearium, *Biochemistry 37*, 4105–4113.

238. Randall, R. E. G., S. (2008) Interferons and Viruses: An Interplay between Induction, Signalling, Antiviral Responses and Virus Countermeasures, *89*, 1-47.

239. Katze, M. G., He, Yupeng, Gale, Michael, . Viruses and interferon: a fight for supremacy, *Nature Reviews Immunology*.

240. Sen, G. C. (2001) VIRUSES AND INTERFERONS, *Annual Review of Microbiology 55*, 255-281.

241. U. Muller, U. S., L.F. Reis, S. Hemmi, J. Pavlovic, R.M. Zinkernagel, M. Aguet,. (1994) Functional role of type I and type II interferons in antiviral defense, *Science 264*, 1918-1921.

242. Nasr, N., Maddocks, S., Turville, S. G., Harman, A. N., Woolger, N., Helbig, K. J., Wilkinson, J., Bye, C. R., Wright, T. K., Rambukwelle, D., Donaghy, H., Beard, M. R., and Cunningham, A. L. (2012) HIV-1 infection of human macrophages directly induces viperin which inhibits viral production, *Blood 120*, 778-788.

243. Helbig, K. J., Lau, D. T. Y., Semendric, L., Harley, H. A. J., and Beard, M. R. (2005) Analysis of ISG expression in chronic hepatitis C identifies viperin as a potential antiviral effector, *Hepatology 42*, 702-710.

244. Wang, S., Wu, X., Pan, T., Song, W., Wang, Y., Zhang, F., and Yuan, Z. (2012) Viperin inhibits hepatitis C virus replication by interfering with binding of NS5A to host protein hVAP-33, *Journal of General Virology 93*, 83-92.

245. Tan, K. S., Olfat, F., Phoon, M. C., Hsu, J. P., Howe, J. L. C., Seet, J. E., Chin, K. C., and Chow, V. T. K. (2012) In vivo and in vitro studies on the antiviral activities of viperin against influenza H1N1 virus infection, *Journal of General Virology 93*, 1269-1277.

246. Wang, X., Hinson, E. R., and Cresswell, P. (2007) The Interferon-Inducible Protein Viperin Inhibits Influenza Virus Release by Perturbing Lipid Rafts, *Cell Host & Microbe 2*, 96-105.

247. Helbig, K. J. B., M. R. (2014) The Role of Viperin in the Innate Antiviral Response, *Journal of Molecular Biology 426*, 1210 - 1219.

248. Mattijssen, S. P., G. J. M. (2012) Viperin, a Key Player in the Antiviral Response, *Microbes and Infection 14*, 419-426.

249. Fitzgerald, K. A. (2011) The Interferon Inducible Gene: Viperin, *JOURNAL OF INTERFERON & CYTOKINE RESEARCH 31*, 131-135.

250. Chin, K. C., and Cresswell, P. (2001) Viperin (Cig5), an Ifn-Inducible Antiviral Protein Directly Induced by Human Cytomegalovirus, *Proceedings of the National Academy of Sciences of the United States of America 98*, 15125-15130.

251. Hinson, E. R., and Cresswell, P. (2009) The N-terminal amphipathic alpha-helix of viperin mediates localization to the cytosolic face of the endoplasmic reticulum and inhibits protein secretion, *Journal of Biological Chemistry 284*.

252. Terk-Shin Teng, e. a. (2012) Viperin restricts chikungunya virus replication and pathology, *The Journal of clinical investigation 122*, 4447–4460.

253. Hinson, E. R., and Cresswell, P. (2009) The antiviral protein, viperin, localizes to lipid droplets via its N-terminal amphipathic α-helix, *Proceedings of the National Academy of Sciences 106*, 20452-20457.

254. Dong Jiang, Haitao Guo, Chunxiao Xu, Jinhong Chang, Baohua Gu, Lijuan Wang, Timothy M. Block, and Guo, J.-T. (2008) Identification of Three Interferon-Inducible Cellular Enzymes That Inhibit the Replication of Hepatitis C Virus, *Journal of Virology 82*, 1665–1678.

255. Helbig KJ, C. J., Calvert JK, Wati S, Clarke JN, et al. (2013) Viperin Is Induced following Dengue Virus Type-2 (DENV-2) Infection and Has Anti-viral Actions Requiring the C-terminal End of Viperin, *PlOS Negl Trop Dis 7*, e2178.

256. Upadhyay AS, and al., e. (2014) Viperin is an iron-sulfur protein that inhibits genome synthesis of tick-borne encephalitis virus via radical SAM domain activity, *Cellular Microbiology 16*, 834-848.

257. Vey, J. L., and Drennan, C. L. (2011) Structural Insights into Radical Generation by the Radical SAM Superfamily., *Chemical Reviews ASAP*.

258. Hanzelmann, P. H., H. L.; Menzel, C.; Garcia-Serres, R.; Huynh, B. H.; Johnson, M. K.; Mendel, R. R.; Schindelin, H. (2004) Characterization of Mocs1a, an Oxygen-Sensitive Iron-Sulfur Protein Involved in Human Molybdenum Cofactor Biosynthesis., *J. Biol. Chem. 279*, 34721-34732.

259. Coquille, S. R., C.; Mehta, A.; Begley, T. P.; Fitzpatrick, T. B.; Thore, S. (2013) High-Resolution Crystal Structure of the Eukaryotic HMP-P Synthase (ThiC) from Arabidopsis Thaliana., *J. Struct. Biol. 184*, 438- 444.

260. Jiang, D., and al., e. (2010) Identification of Five Interferon-Induced Cellular Proteins That Inhibit West Nile Virus and Dengue Virus Infections, *Journal of Virology 84*, 8332-8341.

261. Szretter, K. J., Brien, J.D., Thackray, L.B., Virgin, H.W., Cresswell, P., and Diamond, M.S. (2011) The interferon-inducible gene viperin restricts West Nile virus pathogenesis, *Journal of Virology 85*, 11557–11566.

262. Carlton-Smith, C., and Elliott, R. M. (2012) Viperin, MTAP44, and Protein Kinase R Contribute to the Interferon-Induced Inhibition of Bunyamwera Orthobunyavirus Replication, *Journal of Virology 86*, 11548-11557.

263. Broderick, K. S. D. a. J. B. (2010) The antiviral protein viperin is a radical SAM enzyme, *FEBS Lett 584*, 1263–1267.

264. Goyal Shaveta, Jiahai Shi, Vincent T.K. Chow, and Song, J. (2010) Structural characterization reveals that viperin is a radical S-adenosyl-L-methionine (SAM) enzyme, *Biochemical and Biophysical Research Communications 391*, 1390–1395.

265. Shubhasis Haldar, Simantasarani Paul, Nidhi Joshi, Anindya Dasgupta, and Chattopadhyay, K. (2012) The Presence of the Iron-Sulfur Motif Is Important for the Conformational Stability of the Antiviral Protein, Viperin, *PLoS ONE 7*, e31797.

266. Wang, X., Hinson, E. R., Cresswell, P. (2007) The Interferon-Inducible Protein Viperin Inhibits Influenza Virus Release by Perturbing Lipid Rafts, *Cell Host & Microbe 2*, 96-105.

267. Seo, J. Y., Yaneva, R., Hinson, E.R., and Cresswell, P. (2011) Human cytomegalovirus directly induces the antiviral protein viperin to enhance infectivity, *Science 332*, 1093–1097.

268. Helbig, K. J., et al. . (2011) The antiviral protein viperin inhibits hepatitis C virus replication via interaction with nonstructural protein 5A, *Hepatology 54*, 1506–1517.

269. Tatsuya Saitoh, e. a. (2011) Antiviral Protein Viperin Promotes Toll-like Receptor 7- and Toll-like Receptor 9-Mediated Type I Interferon Production in Plasmacytoid Dendritic Cells, *Immunity 34*, 352–363.

270. Seo, J.-Y., Yaneva, R., Cresswell, P. (2011) Viperin: A Multifunctional, Interferon-Inducible Protein That Regulates Virus Replication, *Cell Host & Microbe 10*, 534-539.

271. Freed, A. A. W. a. E. O. (2007) Influenza Virus Not cRAFTy Enough to Dodge Viperin, *Cell Host & Microbe 2*, 71-72.

272. Kellogg, B. A., and Poulter, C. D. (1997) Chain elongation in the isoprenoid biosynthetic pathway, *Current Opinion in Chemical Biology 1*, 570-578.

273. Kavanagh, K. L., and et. al. (2006) The molecular mechanism of nitrogen-containing bisphosphonates as antiosteoporosis drugs, *Proceedings of the National Academy of Sciences of the United States of America 103*, 7829-7834.

274. Holloway, P. W., Popjak, G.,. (1967) The purification of 3,3-dimethylallyl- and geranyl-transferase and of isopentenyl pyrophosphate ismomerase from pig liver, *Biochem. J. 104*, 57-70.

275. Ding, V. D.-H., and et. al. (1991) Purification and characterization of recombinant human farnesyl diphosphate synthase expressed in Escherichia coli, *Biochemical Journal 275*, 61-65.

276. Barnard, G. F., and Popjak, G. (1981) Human liver prenyltransferase and its characterization, *Biochimica et biophysica acta 661*, 87-99.

277. Shisler, K. A., Broderick, J. B.,. (2012) Emerging Themes in Radical Sam Chemistry, *Current Opinion in Structural Biology 22*, 701-710.

278. Davidson, V. L., Liu, A. (2012) Tryptophan Tryptophylquinone Biosynthesis: A Radical Approach to Posttranslational Modification, *Biochim. Biophys. Acta-Proteins and Proteomics 1824*, 1299-1305.

279. Fluehe, L. M., M. A.,. (2013) Radical S-Adenosylmethionine Enzyme Catalyzed Thioether Bond Formation in Sactipeptide Biosynthesis, *Curr. Opin. Chem. Biol. 17*, 605-612.

280. Leuthner, B., Leutwein, C., Schulz, H., Hörth, P., Haehnel, W., Schiltz, E., Schägger, H., and Heider, J. (1998) Biochemical and genetic characterization of benzylsuccinate synthase from Thauera aromatica: a new glycyl radical enzyme catalysing the first step in anaerobic toluene metabolism., *Molecular Microbiology 28*, 615-628.

281. Vey, J. L., Yang, J., Li, M., Broderick, W. E., Broderick, J. B., and Drennan, C. L. (2008) Structural basis for glycyl radical formation by pyruvate formate-lyase activating enzyme, *Proceedings of the National Academy of Sciences of the United States of America 105*, 16137-16141.

282. Manoj K. Dhar, A. K. a. S. K. (2013) Farnesyl pyrophosphate synthase: a key enzyme in isoprenoid biosynthetic pathway and potential molecular target for drug development, *New Biotechnology 30*, 114-123.

283. Sandala, G. M., Smith, D. M., and Radow, L. (2010) Modeling the Reactions Catalyzed by Coenzyme B-12-Dependent Enzymes, *Accounts of Chemical Research 43*, 642-651.

284. Kamachi, T., Doitomi, K., Takahata, M., Toraya, T., and Yoshizawa, K. (2011) Catalytic Roles of the Metal Ion in the Substrate-Binding Site of Coenzyme B-12-Dependent Diol Dehydratase, *Inorganic Chemistry 50*, 2944-2952.

285. Kamachi, T., Toraya, T., and Yoshizawa, K. (2007) Computational mutation analysis of hydrogen abstraction and radical rearrangement steps in the catalysis of coenzyme B-12-dependent diol dehydratase, *Chemistry-a European Journal 13*, 7864-7873.

286. Kamachi, T., Takahata, M., Toraya, T., and Yoshizawa, K. (2009) What is the Identity of the Metal Ions in the Active Sites of Coenzyme B-12-Dependent Diol Dehydratase? A Computational Mutation Analysis, *Journal of Physical Chemistry B 113*, 8435-8438.

287. Gabriel D. Romań-Meleńdez, P. v. G., Jeremy N. Harvey, Adrian J. Mulholland, and E. Neil G. Marsh. (2014) Role of Active Site Residues in Promoting Cobalt−Carbon Bond Homolysis in Adenosylcobalamin-Dependent Mutases Revealed through Experiment and Computation, *Biochemistry 53*, 169−177.

288. Kohen, J. P. K. a. A. (2013) Hydrogen Tunneling Links Protein Dynamics to Enzyme Catalysis, *Annual Review of Biochemistry 82*, 471-496.

289. Brown, K. L., and Marques, H. M. (2001) Molecular modeling of the mechanochemical triggering mechanism for catalysis of carbon-cobalt bond homolysis in coenzyme B-12, *J. Inorg. Biochem. 83*, 121-132.

290. Brunk, E., Kellett, W. F., Richards, N. G. J., Rothlisberger, U. (2014) A Mechanochemical Switch to Control Radical Intermediates, *Biochemistry (Mosc.) 53*, 3830– 3838.

291. Mancia, F., and Evans, P. R. (1998) Conformational changes on substrate binding to methylmalonyl CoA mutase and new insights into the free radical mechanism, *Structure 6*, 711-720.

292. Glehn, P. v. (2014) Modelling the Reactivity of Glutamate Mutase and Heme Dioxygenase Enzymes (Doctoral Dissertation) University of Bristol, 187 pages.

293. Bucher, D., Sandala, G. M., Durbeej, B., Radom, L., Smith, D. M. (2012) The Elusive 5′-Deoxyadenosyl Radical in Coenzyme-B12-Mediated Reactions, *Journal of the American Chemical Society 134*, 1591–1599.

294. Kwiecien, R. A., Khavrutskii, I. V., Musaev, D. G., Morokuma, K., Banerjee, R., and Paneth, P. (2006) Computational insights into the mechanism of radical generation in B-12-dependent methylmalonyl-CoA mutase, *Journal of the American Chemical Society 128*, 1287-1292.

295. Kaitlin S. Duschene, J. B. B. (2012) Viperin: a radical response to viral infection, *BioMol Concepts 3*, 255–266.

296. Oliver Stehling, e. a. (2013) Human CIA2A-FAM96A and CIA2B-FAM96B Integrate Iron Homeostasis and Maturation of Different Subsets of Cytosolic-Nuclear Iron-Sulfur Proteins, *Cell Metabolism 18*, 187-198.

297. Eaton, K. B. a. (2004) Mitochondrial β-oxidation, *European journal of biochemistry / FEBS 271*, 462-469.

298. S. Eaton, e. a. (2000) The mitochondrial trifunctional protein: centre of a β-oxidation metabolon?, *Biochemical Society Transactions 28*, 177-182.

299. Benjamin Fould, e. a. (2010) Structural and Functional Characterization of the Recombinant Human Mitochondrial Trifunctional Protein, *Biochemistry 49*, 8608–8617.

300. Ishikawa, M., et. al. (2004) Structural basis for channelling mechanism of a fatty acid beta-oxidation multienzyme complex., *EMBO J. 23*, 2745–2754.